

Center for Cognitive Interaction Technology
Kognitronik und Sensorik
Prof. Dr.-Ing. U. Rückert

Bidirectional UWB Localization with Rigorous Sectoral Evaluations

zur Erlangung des akademischen Grades eines

DOKTOR-INGENIEUR (Dr.-Ing.)

der Technischen Fakultät
der Universität Bielefeld

genehmigte Dissertation

von

Cung Lian Sang

Referent: Prof. Dr.-Ing. Ulrich Rückert
Korreferent: Prof. Dr.-Ing. Ulf Witkowski

Tag der mündlichen Prüfung: 15.12.2022

Bielefeld / December 2022
DISS KS / 26

This work is licensed under the Creative Commons Attribution 4.0 (CC BY 4.0) unless expressly stated otherwise.

<https://creativecommons.org/licenses/by/4.0/deed.en>

Printed on acid-free paper according to ISO 9706.

Acknowledgments

First and foremost, I would like to express my deepest gratitude to my supervisor Prof. Dr. -Ing. Ulrich Rückert for his guidance and endless support in both academic and non-academic matters throughout my doctoral study as well as for giving me the freedom to explore and develop ideas on my own research interest. I'm also thankful to Prof. Dr. -Ing. Ulf Witkowski for reviewing my dissertation and participating in my oral examination process. I also would like to express my appreciation to Prof. Dr. -Ing. Franz Kummert for chairing the examination committee and Dr. -Ing. Sebastian Wrede for being the examiner on the committee.

I gratefully thank Cordula Heidbrede for her numerous help and support in administrative and resident permit matters during my study period. I extend my gratitude to Michael Adams, Dr. -Ing. Marc Hesse, and Dr. -Ing. Timm Hörmann for their help, support, and encouragement since my very first day in the research group. I also express my thanks to Jonas Homburg and Dr. -Ing. Michael Thies for their support and valuable suggestions during the writing process of my dissertation. I would like to convey my appreciation to all of my coauthors in my academic publications during this study and each of my colleagues in the Cognitronics and Sensor Systems research group, CITEC, Bielefeld University for their countless support and help.

I would like to thankfully acknowledge Deutsche Akademische Austausch Dienst (DAAD) for their doctoral grant (June 2015 - September 2019) and Bielefeld University for their doctoral scholarship (October 2019 - September 2021) during my Ph.D. study.

I would like to express my sincere gratitude and appreciation to my wife and son, my parents, my sister, and my two brothers for their emotional support and love throughout my entire life. Without them, I will not be at this stage of my life today. Lastly, I would like to thank Almighty God for all my blessings.

Abstract

This dissertation addresses a bidirectional scheme of Ultra-Wideband (UWB)-based localization system, which is generally overlooked in the literature causing its potential overshadowed. The bidirectional scheme is one of the three design integration processes usually applied in UWB-based localization systems. The key property of the bidirectional UWB scheme is its ability to act as both navigation and tracking tasks within a single localization scheme. Conventionally, the perspective of navigation and tracking in wireless localization systems is treated separately, because distinct methodologies were typically required in the implementation process. The ability to combine two unique positioning perspectives (i.e., navigation and tracking) within a single scheme is, indeed, a paradigm shift in the way location-based services are observed in the literature. Much to the author's surprise, there are no well-documented books or research articles related to the bidirectional UWB localization system. Thus, this dissertation attempts to serve as a complement to the mentioned gap in the literature.

In this dissertation, the bidirectional UWB localization scheme was tackled by dividing the system implementation process into several sectors. Then, the methodologies applicable in each sector were rigorously evaluated in order to give the readers insightful knowledge, findings, and recommendations. Regarding this, the concept of the bidirectional UWB localization scheme and its implementation process were thoroughly explained by comparing it with the typical unidirectional schemes.

Concerning the ranging sector of the bidirectional UWB scheme, this dissertation demonstrated the misconception widely practiced in literature in terms of the two-way ranging technique. Moreover, the dissertation suggested a better method compared to the conventional one, which could be used as a baseline or de facto standard for comparing or bench-marking different two-way ranging schemes. The claim was supported by the experimental results rigorously evaluated by using analytical methods, numerical simulation, and real-world experimental data.

Moreover, the comprehensive benchmark of five location estimation algorithms for the bidirectional UWB localization system was conducted in the dissertation. The five algorithms were evaluated based on the Bayesian framework and the detailed implementation process was regarded as an important aspect because the literature is generally lacking it, especially for the use-case of the UWB technology. The evaluation results showed that the linear positioning algorithms gave excellent performance in scenarios such as static conditions under a direct path signal. In contrast, the nonlinear techniques appeared to be better at resisting abrupt changes during measurements as well as the scenarios in non-direct path signals.

Furthermore, the identification and mitigation of errors produced by non-direct path signals in UWB were addressed. Concerning this, a novel mitigation technique was proposed in the thesis whereas the feasibility of the identification process was evaluated using machine learning methods. The classification procedure was considered as a multi-class problem, which is opposed to the typical binary class approach in literature. The results showed that the machine learning techniques are very promising compared to the conventional ones for identification of the non-direct path signals in UWB localization.

Contents

1	Introduction	1
1.1	Contributions	2
1.2	Terminology	3
1.3	Outline of the Dissertation	3
2	UWB for Indoor Localization: Overview and State of the Art	5
2.1	Overview of Indoor Positioning and Navigation	6
2.1.1	Measurement and Location Estimation Techniques in IPS	6
2.1.2	Technologies of Indoor Positioning and Navigation in Excerpt	8
2.1.3	The Role of UWB Technology in IPS	11
2.2	Core Features of UWB Technology	14
2.2.1	Brief History and Regulations	14
2.2.2	Basic Definition of UWB	15
2.2.3	UWB signal Characteristics in Brief	16
2.2.4	Modulation Schemes for IR-UWB	17
2.2.5	UWB Standards and Trade Groups	19
2.2.6	Potential Applications of UWB Technology	23
2.3	UWB-based Localization Schemes	24
2.3.1	Three Topological Aspects in UWB Localization Schemes	24
2.3.2	Comparing the Features of Three UWB Systems	26
2.3.3	The Potentials of a Bidirectional UWB System	28
2.4	Implementation of a Bidirectional UWB System	30
2.4.1	Hardware Components	31
2.4.2	UWB Ranging or Distance Measurement Phase	31
2.4.3	Identification and Mitigation of the Ranging Errors	32
2.4.4	Location Estimation in UWB	32
2.4.5	Filtering Process	34
2.4.6	Multiplexing Method for bidirectional UWB System	34
2.5	Thematic Aspect of the Dissertation	35
2.6	Chapter Summary	36
3	Delving into the Ranging Process of a Bidirectional UWB System	37
3.1	Background and Motivation	39
3.1.1	Brief Introduction to Time-based Wireless Ranging	39
3.1.2	State of the Art TWR Methods	40
3.1.3	Conventional TOF Error Estimation Approach	44
3.1.4	Related Work	46
3.2	TOF Error Estimation Model (TEEM)	46
3.2.1	Problem Statement	47

3.2.2	Novel TOF Error-Estimation Model (TEEM)	49
3.2.3	Extended State-of-the-Art TWRs for TOF Error Estimation	50
3.3	Comparison of TWR Methods by Analytical Studies	53
3.3.1	Error-Model Classification in Three Types	53
3.3.2	Comparison of TWR Methods in Ideal Case (Type I)	54
3.3.3	Comparison of TWR Methods in Special Case (Type II)	54
3.3.4	Comparison of TWR Methods in Typical Case (Type III)	55
3.4	Simulation and Experimental Evaluation Results	56
3.4.1	Numerical Simulation Results	56
3.4.2	Experimental Evaluation Results	60
3.4.3	Results Summary for Type II and Type III using TEEM	68
3.5	Inspection of Ranging Error in TWR Techniques	68
3.5.1	Ranging Error due to NLOS Scenario in TWR	69
3.5.2	Ranging Error due to Multi-path Scenario in TWR	70
3.5.3	Ranging Error due to Closed LOS Scenario in TWR	73
3.6	Chapter Discussion and Conclusion	75
4	Benchmarking Position Estimation Algorithms for UWB Localization	79
4.1	Background and Motivation	80
4.1.1	Brief Background Knowledge of the Study	80
4.1.2	Motivation	81
4.1.3	State of The Art	83
4.1.4	Chapter Contributions	84
4.2	True-range Positioning Algorithms in UWB	85
4.2.1	Trilateration: Geometric Technique	85
4.2.2	Multilateration: Closed-form Least Squares	87
4.2.3	First-order Taylor Series: Non-linear Iterative Method	89
4.2.4	Standard Kalman Filter: Continuous Tracking Mechanism	91
4.2.5	Extended Kalman Filter: Recursive Positioning Technique	93
4.2.6	Unscented Kalman Filter: Statistical Positioning Method	94
4.3	Implementation of Bayesian-based Filters for IPS	96
4.3.1	Dynamic or Motion Model for UWB Localization	97
4.3.2	Measurement Model for UWB Localization	102
4.3.3	Integration of the Dynamic and Measurement Models	103
4.4	Comparative Experimental Evaluation Results	107
4.4.1	Experimental Setup	108
4.4.2	Performance Comparison based upon a Static Scenario	109
4.4.3	Performance Comparison based upon a pure LOS Scenario	110
4.4.4	Performance Comparison based upon a NLOS scenario	113
4.4.5	Qualitative Score and Computational Aspect	115
4.5	Chapter Discussion and Conclusion	117
5	Identification and Error Mitigation of Non-direct Path Signals in UWB	121
5.1	Background and Motivation	122
5.1.1	Problem Description	122

5.1.2	Motivation	124
5.1.3	State of the Art	125
5.1.4	Considered the Multi-class Approach and Contributions	129
5.2	A Generic NLOS Mitigation Technique for UWB	129
5.2.1	Formulation of the considered Mitigation Technique	130
5.2.2	Explanatory Integration Process of the Mitigation Technique . .	132
5.2.3	Exemplary Implementation on Closed-form Methods	133
5.3	Setup and Data Preparation for Identification Process	134
5.3.1	Experimental Setup	134
5.3.2	Data Labeling and Feature Extraction	136
5.3.3	Data Collection Process for Two Independent Test Scenarios . .	137
5.3.4	Data Preprocessing	138
5.4	Machine Learning Models for Identification of the Non-direct Path Signals	139
5.4.1	Naive Bayes Classifier	140
5.4.2	Support Vector Machine Classifier	140
5.4.3	Random Forrest Classifier	140
5.4.4	Light Gradient Boosting Machine Classifier	141
5.4.5	Multilayer Perceptron Classifier	141
5.5	Experimental Evaluation Results	142
5.5.1	Performance Comparison based on Accuracy and F1-Score . . .	143
5.5.2	Comparative Analyses based on ROC Curve	144
5.5.3	Evaluation of the Results Using Confusion Matrix	146
5.5.4	Computational Time Comparison	148
5.5.5	Detailed Summary of the Classification Results	150
5.6	Chapter Discussion and Conclusion	151
6	Conclusion and Outlook	155
Lists		159
Abbreviations		159
Figures		163
Tables		167
Bibliography		169
References		169
Author's publications		185
Co-supervised Work		186
Appendices		189
A	Derivations of AltDS-TWR in TEEM	189
A.1	Derivation of AltDS-TWR in TEEM for Type I Case	189
A.2	Derivation of AltDS-TWR in TEEM for Type II Case	190
A.3	Derivation of AltDS-TWR in TEEM for Type III Case	191
B	Detailed Tables: Ranging Errors due to close LOS and MP Conditions . .	192
C	Detailed Classification Results: Confusion Matrices and ROC curves . .	193

1 Introduction

Location information is a fundamental human need because many of our decisions in daily life are influenced by the knowledge of our location. Suppose that the supports from positioning systems (e.g. satellite-based positioning system, digital interactive map, etc.) are suddenly disappeared in our modern life for some fictitious catastrophic reasons, it would be really hard to imagine our daily lives nowadays. It is undeniable that we heavily rely on the location information in many aspects of our lives including transportation, logistics, industrial asset tracking, environmental monitoring, medical services, robotics, etc. Global Navigation Satellite System (GNSS) such as Global Positioning System (GPS) from the US, Galileo from EU, GLONASS from Russia, BeiDou from China, etc. has been hugely impacted on the world we live now. However, GNSS systems are basically insufficient and in some cases unusable in indoor environments, because the radio waves were blocked by physical barriers, such as multi-floors storage, walls, furniture, etc.. Moreover, the indoor environments are generally crowded with closely located dense objects, which are movable including people as well as fixed ones. Those make it impossible to achieve the direct Line-of-Sight (LOS) between the target device and the base station or satellite, which plays the central part in the location estimation process of the GNSS. Another crucial fact is that almost all of the applications in indoor environments generally require the mean accuracy at the decimeter level [140, 142], which cannot be achieved by currently available surveillance rate GNSS.

Therefore, alternative technologies specifically designed to meet the requirements of indoor environments, a.k.a Indoor Positioning System (IPS), have been profoundly sought for many years. As a result, there are remarkably large numbers of IPS in literature and many others are still under research to emerge (Chapter 2.1). Among them, the Ultra-Wideband (UWB) technology, which is the primary focus of this dissertation, has been regarded as one of the most promising IPS [7]. Even within the UWB-based IPS, there are mainly three system implementation processes as concisely discussed in Chapter 2.3. The dissertation was devoted to one specific implementation process among the mentioned three types of UWB-based localization systems. Specifically, the implementation of a bidirectional UWB-based localization scheme is rigorously addressed in this dissertation. The intention is to give the readers a clear view of the implementation process with concrete and rigorous analyzes from different perspectives so that newcomers, as well as experts in the fields, will achieve some insight knowledge after reading each corresponding chapter presented in the dissertation.

Surprisingly, the bidirectional UWB scheme specifically addressed in this dissertation, i.e., one out of the three topological schemes in UWB (Chapter 2.3), was usually overlooked, and its potential in the field was overshadowed in literature. The key feature of the bidirectional scheme is the ability to provide both navigation and tracking scenarios (see the terminology in section 1.2) within a single platform, which has the

ability to serve as the generic solution provider for diversified indoor application areas. In simple terms, the nature of navigation and tracking in a localization system is fundamentally very different from each other. Therefore, the two scenarios generally need to implement separately. The ability to combine the mentioned two unique natures into a single core system is, in fact, a paradigm shift in the way localization systems are observed in literature. The reason is that it opens up a diverse field of application areas in the GNSS-denied indoor environments by banding the navigation and tracking system as one common process. Therefore, the dissertation pinpointed the potentials of the bidirectional UWB localization system. Moreover, there are no well-documented books or research articles that address each available methodologies in the implementation flow of UWB-based localization systems. This dissertation attempts to fulfill the mentioned gap of the UWB-based localization in literature. Regarding this, the implementation process of the bidirectional UWB localization system was divided into several sectors (i.e., ranging part, location estimation phase, error identification and mitigation section, etc.). Then, the rigorous evaluations of different methodologies typically applied in each divided sector were carried out in the dissertation. The aim is to give the readers insightful knowledge, findings, and recommendations in each sector of the implementation process in UWB-based positioning and navigation system (i.e., a bidirectional UWB-based localization system in this dissertation).

1.1 Contributions

To the best of the author's knowledge, this dissertation can be served as one of the earliest written documents in a complete form that clarifies the overall concept of bidirectional UWB-based localization scheme in literature, i.e., apart from the brief description given in our previous work [175]. Besides, parts of the ideas and concepts presented in this dissertation were previously published as academic papers in international conferences [172, 175], workshop [171], and as journal articles [130, 177]. Thus, the main contributions made in this dissertation are as follows:

- This dissertation itself is one of the first written documents that specifically explained and addressed the bidirectional UWB-based localization system.
- There was a misconception in UWB-based Two-Way Ranging (TWR) process (i.e., Symmetric Double-Sided Two-Way Ranging (SDS-TWR) was conventionally regarded as a de facto standard for comparing the performance of TWR methods since its inclusion in IEEE 802.15.4-2011 standard [33]). Our previous work in [172] was one of the earliest that pointed out the pitfalls of SDS-TWR. Regarding this, the analytical model described in this dissertation (Chapter 3.2) and proposed in our previous work [130, 172] demonstrated a systematic flaw of SDS-TWR and suggested a better TWR method for UWB ranging system namely Alternative Double Sided Two-Way Ranging (AltDS-TWR). Accordingly, AltDS-TWR was adopted as the default double-sided TWR technique for UWB in the latest amendment of IEEE 802.15.4z-2020 standard [98]. It can be stated that our work was involved in one of the driving forces to this amendment.

- The literature generally lacks the proper implementation steps for Bayesian-based location estimation algorithms, especially in the use-cases of UWB. This, in turn, leads to confusion in the system integration process among many practitioners. Chapter 4.3 disclosed the implementation of the Bayesian-based algorithm in detail so that newcomers in the field can easily understand and implement it.
- The feasibility of identifying the non-direct path signals in UWB ranging systems as a multi-class problem was validated in this dissertation using machine learning methods (Chapter 5), i.e., in contrast to the typical binary classification approaches and the close-form techniques.
- A novel generic mitigation technique applicable in a multi-class problem for UWB-based localization system was proposed in this dissertation (Chapter 5.2).
- Majority of the essential source codes and research data utilized for presenting results in this dissertation were provided publicly as an open source.

1.2 Terminology

For clarity, the core terminologies used in this dissertation are defined as follows:

- **Positioning** refers to the determination of a specific location of an object based upon the known reference points or landmarks regardless of its velocity [79].
- **Navigation** refers to the guidance of a moving object to reach a certain dedicated target location by providing a position and/or velocity information to the said object with respect to known reference points [79].
- **Tracking or surveillance** differs from navigation in the sense that the position and velocity information are obtained by a central server or a third party.
- **Localization** is the determination of a position for a given object within a certain network or known reference points [24]. In this dissertation, localization is used as a general terminology for a positioning system that is capable of either navigation or tracking as well as both perspectives mentioned above.

1.3 Outline of the Dissertation

In general, the contents of the chapters discussed in this dissertation are self-contained to a considerably large extent. In general, the majority of the chapters in the dissertation (Chapter 3, 4, and 5) can be read independently, i.e., in conjunction with the Chapter 2 indeed. This implied that a sequential reading of the whole dissertation is not necessary in order to understand the discussed contexts (Chapter 3 to Chapter 5). Though, that might help some readers a better understanding of the overall concepts. Moreover, the diagrammatic expression regarding the particular focuses of the chapter based on the entire big picture was given at the beginning of each chapter (Chapter 3, 4, and 5). The main goal is to remind the readers where the current discussion in the

chapter belongs to which parts of the big picture. That being said, the dissertation was organized and structured as in the following.

In Chapter 2, the state of the art IPS was firstly described by giving brief explanations for each available technologies in literature (Chapter 2.1). Then, the core features of UWB technology for the use-case of indoor localization system was explained (Chapter 2.2). The particular focus was made on describing the regularization and standardization of UWB signal as well as the data communication flow used in all available UWB standards by the time of writing this dissertation. There are three types of topology regarding UWB-based localization scheme and the three topologies are compared by highlighting the potentials of a bidirectional scheme (Chapter 2.3). As this dissertation is all about bidirectional UWB system, the overall implementation process of it was explicitly described in Chapter 2.4. After that, the thematic aspect of the whole dissertation in terms of block diagram was depicted (Chapter 2.5).

Chapter 3 specifically addressed the ranging phase of a bidirectional UWB system. Regarding this, the overview and background knowledge were addressed in Chapter 3.1. An error estimation model for TWR based on our previous work has been explained in Chapter 3.2. The core motivation was to demonstrate the misconception widely practiced regarding TWR technique in literature. Accordingly, rigorous comparative analyses of four widely known TWR techniques were addressed using analytical formulation (Chapter 3.3), numerical simulation (Chapter 3.4.1), and experimental real-world data evaluation (Chapter 3.4.2). Additionally, the inspection of ranging error in TWR techniques has been studied (3.5). Then, the chapter closes with a discussion and conclusion, which were based on the evaluation results (Chapter 3.6).

Chapter 4 corresponded for addressing the positioning phase of a bidirectional UWB system by rigorously benchmarking the location estimation algorithms applicable in UWB. The chapter started with the motivation behind the comparative study of the positioning algorithms and state-of-the-art evaluation process (Chapter 4.1). Then, basic theories of the location estimation algorithms bench-marked in the chapter were explained (Chapter 4.2). All the algorithms were evaluated based on the Bayesian framework. Accordingly, the detailed implementation process of the said Bayesian-based system for UWB localization was expressed in a way that newcomers in the field can easily understand it (Chapter 4.3). Indeed, such an implementation process is generally lacking in literature to the best of the author's knowledge. Then, the interpretations of the experimental results were described in Chapter 4.4, which was followed by the discussion and concluding remarks of the chapter.

In Chapter 5, the identification and mitigation process of non-direct path signal was specifically addressed. A generic mitigation technique for UWB has been proposed in Chapter 5.2. Machine learning algorithms (Chapter 5.4) were evaluated for the identification process and the corresponding measurement setups and data pre-processing methods were explained in Chapter 5.3. The evaluation results based on the experimental real-world data were presented in Chapter 5.5, which was again followed by the discussion and conclusion remarks (Chapter 5.6).

Finally, the concluding remarks and summary regarding the whole dissertation were addressed in Chapter 6, in which the author's perspective regarding the outlook of UWB-based localization system as well as the IPS as a whole was also discussed.

2 UWB for Indoor Localization: Overview and State of the Art

Since many centuries ago, people tried different methods to solve the problem of location estimation in unknown places. The subject of determining the position of stars by using the triangulation method was one example that explains how positioning was of great interest in ancient times [68]. As time went by, a lot of efforts and research have been conducted in these fields, and we were witnessed with several major advances throughout history. The most obvious example is the GNSS. Nowadays, we have reached sufficient accuracy for navigation systems inside the whole world thanks to the GNSS. This makes the GNSS become the de facto standard for positioning, navigation, and localization systems in outdoor environments. Nevertheless, there are still ongoing efforts to make a more precise, reliable, and ubiquitous system in the field of GNSS.

The main challenge for GNSS is that it cannot be observed with sufficiently and reliably in indoor environments (i.e. inside buildings). This is because the radio signal propagation in indoor environments is, in general, obstructed by a lot of obstacles which cause several multi-paths and signal blockage situations. This makes it impossible to achieve the direct LOS between the mobile device and the base station or satellite, which is the central part of the location estimation process in GNSS as already mentioned in Chapter 1. Similarly, GNSS systems suffer from signal attenuation and distortion in application areas such as underground mining, deep sea mining, under-water exploration, etc. [140]. For that reason, numerous dedicated techniques based on a multitude of diverse technologies have been proposed for localization system in GNSS-deprived areas (Section 2.1). Among available technologies for IPS in literature, UWB has been regarded as one of the most promising systems. One of the core reasons is the ability of UWB to provide a decimeter-level accuracy. In fact, there are three types of UWB-based localization system, and the dissertation was devoted to one specific implementation among the three in order to give more insightful details to the readers. In addition, this chapter corresponds to wrapping up the sectional focuses addressed in each chapter of the whole dissertation defined in Section 2.5.

Accordingly, the chapter is structured as follows: Section 2.1 gave the state of the art IPS by giving brief explanations for each available technology from the perspective of measurement and positioning techniques. Then, the properties of UWB technology for the use-case of indoor localization was discussed in Section 2.2 followed by the brief comparison of three typologies available in the UWB-based IPS. As this dissertation addressed a specific topology namely bidirectional UWB system among the three, the generic implementation process was explicitly described in Section 2.4. Finally, the thematic aspect of the whole dissertation was explained in Section 2.5 and the summarized discussion regarding the chapter is given in Section 2.6.

2.1 Overview of Indoor Positioning and Navigation

The technological progress in outdoor localization system has shaped our lives in a great deal of goodness in recent years. Meanwhile, the research on indoor localization is also steadily improving. It is expected that similar trends of outdoor localization for indoor scenarios will be witnessed in the coming near future [40]. Indeed, indoor localization is crucial because it is the place where people spend more than 80% on average of their lives according to the report in [117]. However, the indoor environments are very challenging for location estimation based on wireless communication and signal processing perspective because several objects in the environment have impacts differently on the measurement. As a result, a large variety of technologies have been proposed specifically for IPS in recent years. This leads to the situation where there is no a de facto standard for IPS or even an approach compared to its counterpart the outdoor scenario likes GNSS-based system.

Therefore, this section categorized the mentioned technologies for IPS in terms of the signal or data measurement and the underlying positioning techniques in Section 2.1.1. Subsequently, the technological perspectives for each of the IPS were separately explained in Section 2.1.2, which was followed by the role of UWB technology in IPS.

2.1.1 Measurement and Location Estimation Techniques in IPS

This section addresses the brief overview of IPS from the perspective of measurement and positioning techniques. In general, all the available technologies in IPS were built upon these two fundamental techniques. Figure 2.1 depicted the block diagram of general IPS based on the perspective of measurement and positioning techniques. By no means, this is not the only way to classify the IPS. Indeed, IPSs were classified in several ways, especially in survey literature [58, 142] such as device-free vs. device-based system [219], passive vs. active approach [160] and so on.

In general, the localization process of all IPS can be categorized into two phases namely the signal measurement phase and the positioning phase (Figure 2.1) [34, 130]. The techniques used in the former phase correspond to provide the information such as distances between two nodes in range-based IPS and the received signal strengths in range-free methods [142]. In the later phase, the actual location of the interested nodes was determined by the IPS based on the knowledge gained from the former case (i.e., the ranging phase) and by using relevant positioning algorithms.

For the signal measurement phase in IPS, six techniques can be basically defined based on the survey papers in the field [142, 222](the upper part of Figure 2.1). However, only four techniques are commonly applied in practice when jointly deployed with the technologies utilized in IPS namely Time-of-Arrival (ToA), Time Difference of Arrival (TDoA), Angle-of-Arrival (AoA), and Received Signal Strength (RSS) techniques. For the sake of brevity, the excerpts of signal measurement techniques in IPS are described in this section as follows and details can be found in the cited references:

1. **ToA technique:** measures the arrival time of radio or audio signal sending from a transmitting device by recording the absolute time instant at its receiving

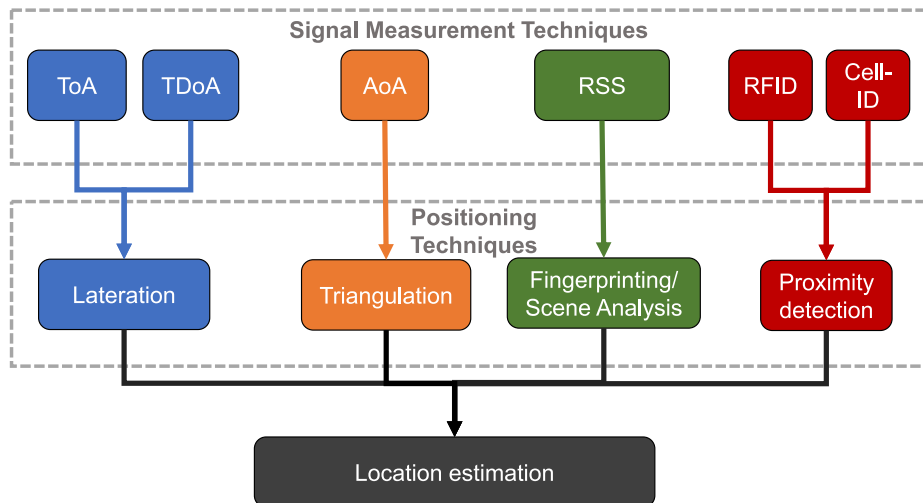


Figure 2.1: Block diagram regarding the overview of the signal measurement and positioning techniques in IPS. The image was inspired by the work in [222] and it was modified from it.

node. In cooperation with the exact time instant from the transmitting device, ToA techniques can be used to estimate the distance between the mentioned two transceivers by calculating their Time-Of-Flight (TOF) based on the known propagation speed of the signals (i.e., the speed of light in the air for the radio wave and 343 m/s for sound wave using air as propagation medium) [33, 98]. In ToA, the two transceiver devices are not necessary to be in a synchronized clock (see more details about ToA in chapter 3). The bidirectional UWB localization system addressed in this dissertation used the ToA in the ranging phase.

2. **TDoA technique:** is somewhat similar to ToA but a bit different in measurement perspective. TDoA requires at least two reference devices and a target mobile device to estimate the difference of distances among them (i.e., distances between target and references). This is accomplished by calculating the difference of signal arrival time at the reference devices by using hyperbolic function [198, 230]. In TDoA, a clock synchronization at the reference devices is mandatory.
3. **AoA technique:** generally estimates the position of a target device by observing the angular direction measured at a reference device, which is typically equipped with directional antennas or antenna arrays in radio-based system [146]. The mentioned direction is usually calculated based on the phase difference of the arriving angles in each element of the antenna array.
4. **RSS technique:** uses the measured power presented in the received signal of a radio wave to compute the distance between the transmitter and receiver according to the path loss formula or Friis's equations [59]. The nice thing about RSS technique is that the signal strength can be easily extracted in any existing radio frequency-based systems such as Wi-Fi, Bluetooth Low Energy (BLE), UWB, etc without the need to use any additional hardware. In general,

the received power level is getting smaller as the distance increases. However, the accuracy of the RSS-based system can be deficient easily due to shadowing effects, multi-path, Non-Line-of-Sight (NLOS), the orientation of the device, etc.

5. **Other measurement techniques:** do exist for localization purpose including Round-trip Time of Arrival (RTOA) and Channel State Information (CSI). Though they are rarely used in IPS [142]. Besides, a proximity detection based positioning algorithm can be applied in Radio-frequency identification (RFID) and Cell-ID-based 5G technology for broadband cellular networks. Moreover, hybrid methods such as a combination of ToA, AoA and RSS techniques on fingerprint-based positioning algorithm was also applied in IPS [222].

Regarding the positioning techniques in IPS, it is possible, in general, to categorize them into four namely the Lateration method, the triangulation, the fingerprinting, and proximity detection methods (Figure 2.1). Often the time, the positioning techniques are closely tied with the underlying location technologies (see Section 2.1.2) used in the IPS. For the ToA and TDoA signal measurement techniques, the Lateration method was commonly used as its positioning algorithm (Figure 2.1). Generally speaking, a Lateration is known as Trilateration when three distances are used in its location estimation process whereas it is called as Multilateration if more than three distances are involved in the mentioned localization process. Indeed, Lateration method can also be indirectly obtained from other location-based algorithmic patterns such as iterative and/or recursive approaches, state-space method, etc. (c.f. chapter 4). Similarly, the angulation method is commonly applied for dealing with the IPS-based technologies that use AoA technique in its distance measurement phase.

Besides, there exists a fingerprinting technique (a.k.a scenes analysis in some papers) as a location estimation algorithm for the technologies that use the RSS in the distance estimation phase (Figure 2.1). Fingerprinting technique is widely used in the Wi-Fi and BLE-based technologies, i.e. the current most influential IPS in literature. Fingerprinting estimates the location of a mobile device by looking for the closest match in a pre-collected fingerprint database, also known as a radio (or) coverage map. The core advantage of the fingerprinting technique is that it can exploit and naturally mitigate the multi-path effects within the pre-collected environments to produce quite a high accuracy. However, the disadvantages include time-consuming and tedious processes of offline data collection for the fingerprint database and maintenance of the produced radio map. Moreover, the environmental changes within the radio map, e.g. the removal or misplacement of the furniture in the measured database, can cause a strong effect on the accuracy of the overall IPS. Proximity detection as a location estimation algorithm was rarely used in IPS compared to the other three techniques, and they are mentioned here for the sake of a complete picture.

2.1.2 Technologies of Indoor Positioning and Navigation in Excerpt

This section briefly describes the technological perspectives of available IPS in literature. For the sake of brevity, while attempting to cover the whole IPS landscape as much as possible, the excerpt for each IPS technology was presented by using a maximum of

four sentences omitting the technical details. The cited references in each presented technology gave such specific information. Thus, the technologies for IPS are briefly expressed in an abstract level as follows [5, 116, 139, 140, 142, 203, 221, 222]:

1. **WiFi-based IPS:** is the most popular technology in the field of indoor localization because it is the default technology in Wireless Local Area Network (WLAN) as well as its availability in the modern smartphone [144, 218]. WiFi, based on the IEEE 802.11 standard for WLAN, operates on the 2.4 GHz and 5.0 GHz using typical channel bandwidths of 20 MHz, 40 MHz, and 80 MHz. The main applied signal measurement technique is RSS method (i.e. CSI is still in its early stage and ToA and AoA are seldom used) and the most applied positioning technique is Fingerprinting method (i.e. Lateration is usable but rare) [14, 144]. The core challenge in WiFi-based IPS is that the radio frequency signals are suffered from several sources of disturbance and alternation in the indoor environment while most of the WiFi-based IPSs rely on the existing infrastructures, which are mainly deployed for communication purposes instead of a localization [142, 225].
2. **BLE-based IPS:** is the second most popular technology, after the WiFi-based system, in indoor positioning and navigation system. BLE generally operates on 2.4 GHz with 2 MHz bandwidths and uses frequency hopping technique for data communication [57, 101]. For signal measurement method, RSS is mostly utilized similar to the WiFi technology and Fingerprinting technique is the most commonly applied location estimation method in BLE-based IPS [161]. In general, the achievable accuracy in BLE is normally higher than the WiFi though the coverage area of BLE is quite small, i.e. usually less than 20 m.
3. **Light-based IPS:** uses a light source (such as Light-Emitting Diode (LED)s for Visible light communication (VLC), Infra-red (IR) LEDs or IR lasers for IR-based system) to transmit data at the transmitter and photo-detector (i.e. for VLC), and IR photo-diode or an IR camera are typically used in the receiver [136]. As a signal measurement technique, RSS, ToA, and TDoA methods are generally used in light-based IPS whereas Lateration (for VLC and IR laser system) and angulation (for IR-camera system) technique are usually applied as the positioning method [4, 10]. Most of the light-based IPSs require LOS situation (i.e., otherwise the accuracy suffers significantly) and they are acknowledged to be in the early stage of development in the field [2, 136, 142].
4. **Computer Vision-based IPS:** typically uses the visual odometry technique (i.e., estimating the position of target based on the associated camera images) (or) Vision-based Simultaneous Localization and Mapping (SLAM) (i.e., SLAM is also applicable in laser, sonar, and odometry data other than Vision) to estimate the location of interesting objects within the Field of View (FoV) of the applied cameras [8, 115]. There are generally two approaches namely device-based and device-free systems: the former uses markers or printed QR codes to locate the target objects whereas the latter typically utilized the information gathered from several cameras in the environment for location estimation [1, 95]. The main challenges in Vision-based IPS include the occlusion of objects, lighting

conditions, computational cost, shadows from other objects, etc [1, 9]. Vision-based localization system has several future potentials in IPS wheres its current applications mainly lie in autonomous driving and visual reality fields [142].

5. **Sound-based IPS:** relies on acoustic signal (i.e., based on ultrasound or audible frequencies) to acquire the information necessary for location estimation of objects in indoor environments [183, 205]. In the signal measurement phase, the ToA, TDoA, and RSS techniques are typically applied in sound-based IPS depending on the concrete system setup. Accordingly, Lateration or Fingerprinting techniques are usable as positioning algorithms. In general, LOS condition is mandatory in sound-based IPS and the accuracy can also be varied due to the changes in temperature and humidity in the environment as those can impact the speed of sound in its communication medium (i.e., air) [142].
6. **Magnetic Field-based IPS:** uses the changes in strengths of magnetic fields measured by a measuring device to estimate the position of intended targets [42, 158]. To accomplish this, a database that records several variations of the magnetic field strengths for the intended environment is necessary to be created, and Fingerprinting algorithm can be used to compute specific location estimations of the targets [88, 151]. The strengths of the magnetic field can be affected by moving objects that contain ferromagnetic materials and electronic devices. As a result, the estimated location accuracy can be deteriorated [129].
7. **Inertial Measurement Unit (IMU)-based IPS:** uses measurement data gathered from multiple sensors (typically three: namely accelerometer, gyroscope, and magnetometer) to estimate the location of the interested object using Dead Reckoning (DR) and sensor fusion techniques [145, 157]. DR, a.k.a Pedestrian Dead Reckoning (PDR) for pedestrian target, is a method that estimates the current position of a moving target based on the previously known location (usually called as a fix) and the estimate of its incorporated measurements from the mentioned three sensors regarding the motion of the target [102, 104]. IMU-based IPS commonly suffers from cumulative errors, but can be reduced if the current estimation is not too far away from the last known fix [3].
8. **UWB-based IPS:** typically uses impulse radio technology [211] for location estimation, in which the technology inherently possess properties such as large bandwidth, high time resolution, and low power consumption due to a very short pulse, robustness against multi-path, ability to penetrate walls, high data rate due to large bandwidth, etc [72, 170]. For the signal measurement technique, the most commonly applied methods in UWB-based IPS are ToA and TDoA (i.e., AoA and RSS are seldom used due to higher complexity and poorer performance issue compared to the other two methods) whereas the Lateration method is the common choice for its positioning algorithm [126, 175, 198]. The coverage area (i.e., typically less than 60 m) and the cost were usually reported as the main hurdle in UWB system. However, it is expected that the recent incorporation of the UWB chip into smartphones by Apple and Samsung will further boost the technical progress and system use-case of UWB in IPS.

9. **Other Technologies in IPS:** do exist and their contributions to the field are enormously important though they were seldom addressed in detail in the literature. It is expected that new technologies specifically for IPS may still emerge in the near future and the list is, by no means, complete, rather the most commonly used ones. For brevity, the rest of technologies applicable in IPS can be named as: RFID-based IPS and near field communication based IPS [71], positioning algorithms built upon the Fifth Generation (5G) or Sixth Generation (6G) cellular network [202], radio technology such as Zigbee and Radar [143, 196], pseudolite system which is designed to produce GPS signal into its deprived areas [7], hybrid systems (a.k.a signal of opportunity approach) that attempt to combine several technologies into one common framework [143], etc.

2.1.3 The Role of UWB Technology in IPS

The most commonly applied technologies in IPS to date are Wi-Fi and BLE-based system [116, 142] as previously mentioned in above. One of the main reasons why the mentioned two technologies are so popular in IPS is that they are, by default, available on modern smartphones. Though the IPS are diversified into many technical approaches as discussed in Section 2.1.2, the IPS based on the radio wave technology [116], i.e. wireless communication system, are generally more prominent in practice and academic research compared to the other approaches. For instance, the LOS condition is not mandatory for location estimation in radio waves-based systems compared to the light and sound-based systems. Similarly, major challenges faced in the Vision-based system such as occlusion, lighting conditions, and shadows of objects are not counted as issues at all in radio-based positioning systems.

The interesting fact is that the most popular technology in IPS namely Wi-Fi and BLE are, indeed, rooted from the wireless communication technology similar to the outdoor de facto standard GNSS or GPS-based system. It can be stated that the tremendous success of wireless-based positioning systems in outdoor environments (i.e. GPS and GNSS) has more or less several inspirations on the technical investigation process for IPS. Apart from the Wi-Fi and BLE, one of the most viable and potential wireless technologies for IPS is UWB. Therefore, this section addresses the technological trend of radio frequency-based IPS from the perspective of academic publications and focuses the role of UWB technology in IPS.

UWB has been intensively explored for the use-case of location service in the last two decades and showed several crucial achievements in terms of location accuracy, data transfer rate, immunity to multi-path, capable of penetrating walls and other materials typically used in indoor environments, etc. compared to other available radio-based technologies dedicated to IPS. For brevity, Figure 2.2 (a) illustrates the comparison of technological trends regarding WiFi, BLE, and UWB in academic publications within the last decades based on the WoS database, one of the most renounce information archives for many academic disciplines. The graph showed that the interest in the three technologies was on an upward trend during the last decade. It can also be seen that WiFi has been addressed more frequently than UWB and BLE since 2013 (Figure 2.2). However, it should be noted that the presented graph was based on the name of

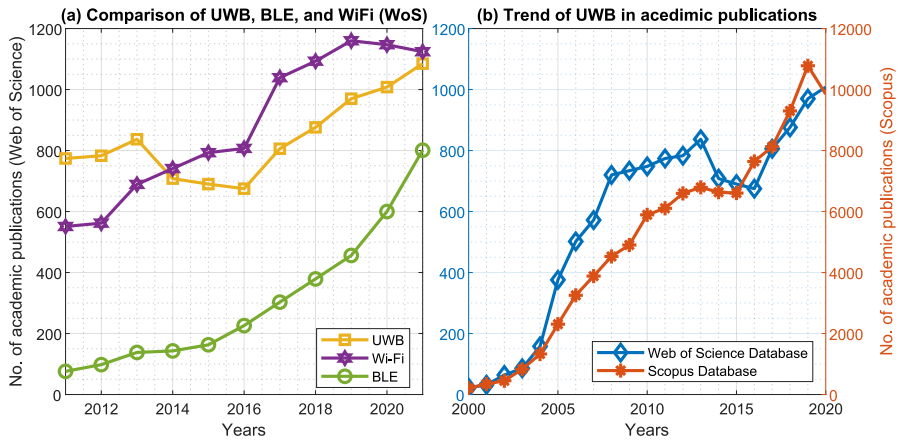


Figure 2.2: Illustration of the trend of technologies in academic publications: (a) comparison of UWB, WiFi, and BLE in academic publications during the last decade based on the Web of Science (WoS) database, (b) UWB technology in academic publications from 2000 to 2020.

technologies used in the academic publications, which were not specifically targeted for the use-case of positioning systems. Additionally, the first integration of BLE technology on consumer electronic devices was begun only in 2009.

Regarding UWB technology, Figure 2.2 (b) depicted the trend in academic publications based on the WoS and Scopus databases in the last 20 years. Since the first approval of UWB signal to be used in the unlicensed frequency band between 3.1 GHz and 10 GHz by Federal Communications Commission (FCC) in the USA, the interest on the technology was sharply risen until 2013 (Figure 2.2). There were a couple of years that the interest on technology seemed a bit of declination (somewhere around in 2015) and then it is remarkably climbed up again since 2016 to date. The author would emphasize that the second wave of interest on UWB technology has been greatly boosted by the availability of UWB hardware in the market manufactured by Decawave (Qorvo) in 2013 as well as other vendors such as Ubisense.

For a better comparative analysis based on an abstract level point of view, Figure 2.3 demonstrated the spider chart for four radio-frequency based positioning technologies in terms of eight important features. The presented properties in the figure are crucial for system deployments, technical choices for the integration process, assessment of the technology, and its applications in practice. The presented scores marked with 0 to 5 (i.e., 0 is the worst and 5 is the best) in Figure 2.3 are based on the typical reported data as well as information given in the survey papers [7, 140, 142] and data-sheets of the vendors [44]¹. The ideal case in the figure represents the best achievable score in each presented category. Moreover, GPS was utilized as a baseline system in the presentation since it is the state-of-the-art de facto standard for wireless positioning systems in outdoor environments (Figure 2.3).

It is exciting to see that UWB technology stands out to be very efficient in every aspect except for the property regarding the availability on modern smartphones and

¹<https://www.decawave.com/technology1/>

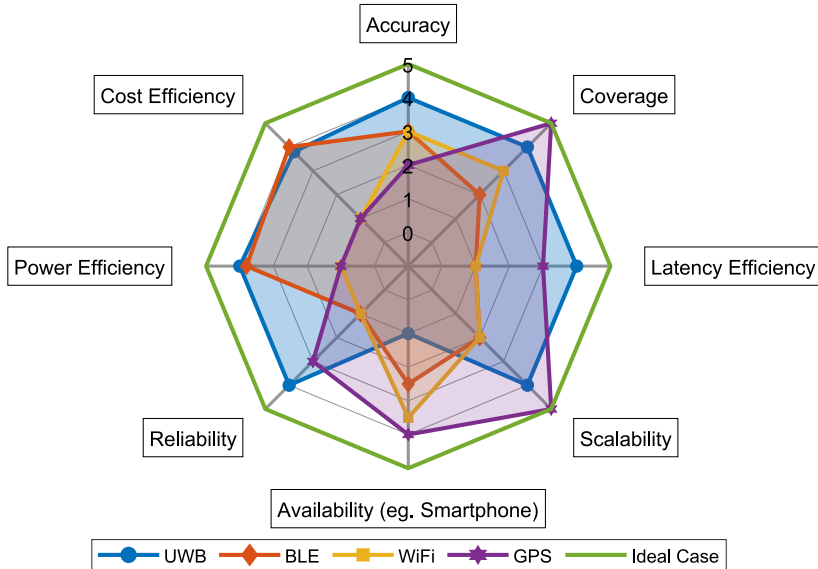


Figure 2.3: Spider chart comparison for four radio frequency-based positioning technologies in terms of eight core features. The information score represented with 1 (worst) to 5 (best) on the image are based on the typical reported data in survey papers and data-sheets of the vendors.

existing infrastructures compared to WiFi and BLE (Figure 2.3). In specific, UWB outperformed BLE and WiFi with great margins in terms of accuracy, latency efficiency (i.e., the processing time needed to provide each location data at a given time), reliability (i.e., the ability to provide location data in consistent manners), coverage area, and scalability (Figure 2.3). Compared to GPS, the UWB also showed a better performance with regard to the accuracy, latency efficiency, and reliability. Regarding power and cost efficiencies, it is notable that UWB is comparable to BLE technology, which is regarded as one of the most power efficient and low-cost devices in IPS next to the RFID devices. Based on these observations, we can conclude that UWB technology will be emerged as one of the key technologies for indoor environments in the near future, which also has the potential to surpass other viable existing technologies in IPS. Even in the current state, UWB technology was the core choice for IPS if accuracy is the main concern in the system deployment and application [139, 142].

Concerning the availability of the UWB technology in modern smartphones, Apple implemented its first UWB chip on its iPhone 11 in 2019². Subsequently, Samsung has also integrated UWB chip on its Galaxy S21 series and Galaxy Z Fold3 5G model³. To date, many companies from different industries are on the progress of integrating the UWB technology into their products [35]. It is expected that a lot of other vendors will start to use the UWB technology in consumer electronic devices in the near future. This will surely boost the rise of UWB in diverse application areas not specifically to the positioning use-cases in the near future.

²<https://www.apple.com/ca/iphone-11/specs/>

³<https://insights.samsung.com/2021/08/25/what-is-ultra-wideband-and-how-does-it-work-3/>

2.2 Core Features of UWB Technology

In this section, the core features of UWB technology are addressed in a short and abstract view so that readers without prior knowledge in the field can understand. Therefore, the in-depth theoretical details are omitted and only the necessary concepts for practical implementation of the UWB technology are tackled in an essay manner. For the readers who need more details in theory regarding UWB technology, the author would refer to read the books in [72, 154, 156, 170] and the papers in [70, 134, 212].

2.2.1 Brief History and Regulations

The term UWB was first used in a study undertaken for accurate ranging in radar applications by the US Defense Advanced Research Projects in 1990 [66]. However, the core idea of UWB signal by generating very short pulses was not new. The first UWB signals in history were generated by Heinrich Rudolf Hertz while conducting his experiments in 1887 [210]. It is noteworthy that the first radio in history realized by Guglielmo Marconi in his early wireless communications using spark gap transmissions in the late 1890s was actually based on the UWB technology. However, the dawn of UWB arrived for several years as the emphasis and interest on wireless communication systems were shifted into the Narrow-band (NB) systems, where a carrier is generally necessary for a signal transmission. The interest on UWB was started again only in the 1990s due to the improvement in digital signal processing and the introduction of impulse radio in time hopping system [210, 211].

The development of the UWB technology intensified when FCC in the US announced in 2002 that the frequency band between 3.1 GHz and 10.6 GHz can be applicable for the unlicensed operation of UWB under a certain restriction of Effective Isotropic

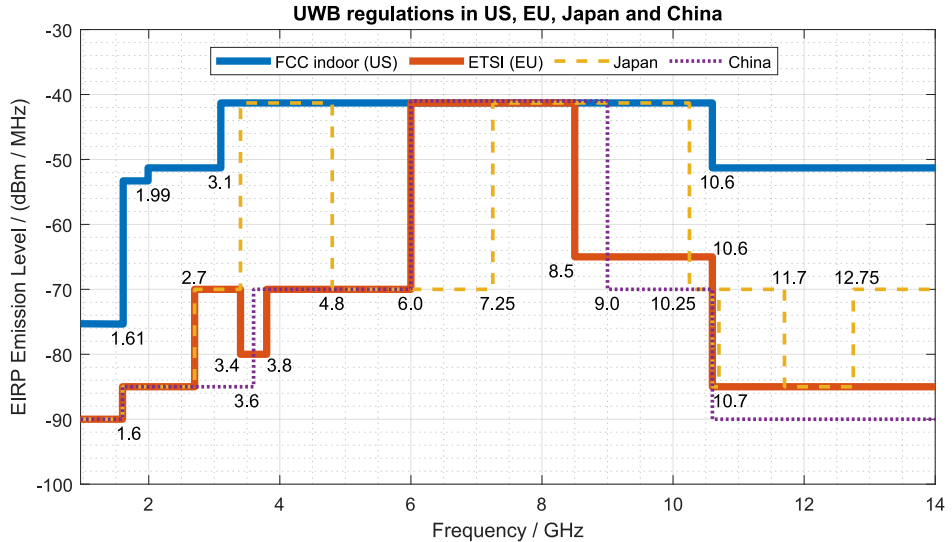


Figure 2.4: Illustration of UWB spectrum mask regulation in US, EU, Japan, and China. The representation style of four regulatory bodies on an image was inspired by the work in [230].

Radiated Power (EIRP) [154]. Subsequently, other countries such as European Union (EU), Japan, China, Canada, Russian Federation, etc. approved similar regulations on UWB operation. For demonstration purpose of spectrum restriction in different countries, Figure 2.4 illustrates the comparison of EIRP mask for UWB regulated by four regulatory bodies namely FCC in US, European Telecommunications Standards Institute (ETSI) in EU, Japan, and China. The detailed spectrum restriction of UWB for the rest of the countries in the world can be found in [32, 48].

It is interesting to see that the four presented regulators has a common maximum permissible EIRP in UWB with -41.3 dB m at the frequency spectrum between 7.25 GHz and 8.5 GHz (Figure 2.4). To be more specific, the maximum allowable UWB emission power in China is -41 dB m (i.e., 0.3 dB m greater than other three illustrated regulatory bodies). Indeed, the maximum allowable EIRP for UWB in other countries not listed in Figure 2.4 is roughly the same (-41.3 dB m) in that specific interval of the frequency spectrum (i.e. 7.25 GHz to 8.5 GHz).

Moreover, it should be highlighted that the frequency spectrum between 6.0 GHz and 8.5 GHz is generally allowed to use the maximum EIRP for UWB in US, EU, China and the rest of the world except for Japan according to [32] (Figure 2.4). To avoid the inference and to ensure the coexistence with other radio technologies such as BLE operated in 2.4 GHz frequency band and Wi-Fi operated in 2.4 GHz and 5 GHz , the permissive power of UWB is restricted with remarkably low in that specific regions especially in EU, Japan, and China compared to US (Figure 2.4).

2.2.2 Basic Definition of UWB

In general, UWB refers to a radio technology that takes advantage of having a very large bandwidth on a frequency spectrum with a very low energy level compared to its counterpart conventional NB signals. For the illustration purpose, Figure 2.5 compared the Power Spectrum Density (PSD) of UWB and NB in frequency domain. Historically, the first concrete definition of UWB was specified by FCC in 2002 [210], and it is generally accepted by default in UWB-based regulations and standards in many disciplines. According to the FCC, a signal is defined as an UWB if it possesses either an absolute bandwidth greater than (or) equal to 500 MHz (i.e. based on the measurement of -10 dB) or a fractional (relative) bandwidth greater than 20% (i.e. 0.2). The mentioned absolute bandwidth (BW) and the fraction bandwidth B_f for UWB signal can mathematically be defined as follows (Figure 2.5) [154]:

$$BW = f_H - f_L$$

$$B_f = \frac{BW}{f_C} = \frac{2(f_H - f_L)}{f_H + f_L} \quad (2.1)$$

where f_H and f_L are the upper and lower frequencies of the signal, BW is the absolute bandwidth, and B_f is the frictional bandwidth respectively.

In theory, the large bandwidth utilized in UWB signals can cause interference with other existing radio-based communication systems. Therefore, the regulatory bodies as discussed previously enforce very strict restrictions on the UWB emissions (i.e. EIRP) in

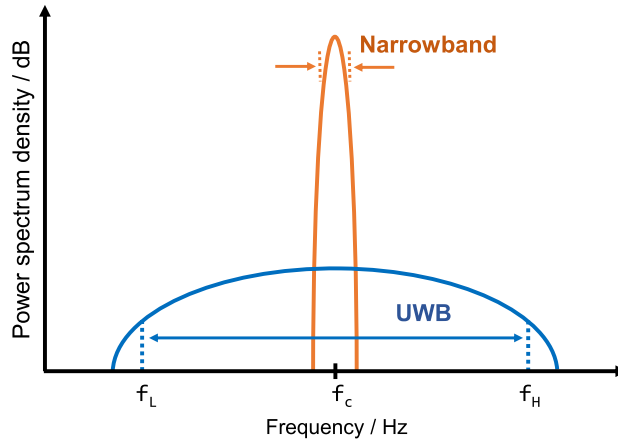


Figure 2.5: Power Spectrum density of UWB vs. NB signals in frequency domain [30, 50]. UWB is defined as absolute bandwidth $BW \geq 500$ MHz or fractional bandwidth $B_f > 0.2$. The representation of the image was inspired by the one depicted in [164].

order to avoid interference and ensure the coexistence in harmony with existing radio technologies (Figure 2.4). This allows the UWB technology the ability to coexist with other radio technologies such as BLE, Wi-Fi, and cellular communications without any interference in the same applicable environments.

2.2.3 UWB signal Characteristics in Brief

The use of large bandwidth in wireless communication systems enables several benefits due to its natural characteristics [209, 210]. The five main advantages of UWB are highlighted in this section. First, UWB provides high channel capacity, i.e., the maximum data rate that information can be reliably transmitted over a wireless channel, due to its high bandwidth. Second, decimeter level ranging accuracy, i.e. extremely accurate wireless distance measurement for positioning system, is achievable because of the high temporal resolution due to very short pulses in UWB. This is crucial for time-stamping the signal arrival time at the receiver. Third, the low transmission power (i.e., less than -41.3 dBm) in UWB enables immunity to interference, resistance to jamming, and coexistence with other NB wireless systems. Fourth, UWB provides robustness to multi-path effects and propagation fading due to the short time duration of the UWB pulses' transmission. This short temporal time allows the arrival time of the UWB pulses at the receiver to be easily split up and filtered out as necessary compared NB systems. Finally, UWB signal has the ability to penetrate obstacles such as walls and other materials by using the lower frequency components part of its signal. Though, it should be noted that the signal can be attenuated, delayed or even dispersed when it propagates through the mentioned obstacles.

Despite its promising characteristics mentioned above, the generation and processing of UWB signal are challenging and this section briefly discussed the common state-of-the-art techniques. In general, UWB signal generation can mainly be divided into two: (i)Impulse Radio Ultra-Wideband (IR-UWB) approach and (ii) multi-band UWB

technique. A good resource of UWB signal generation can be found at the chapter 2 of the Ph.D. dissertation in [230] whereas more concrete detail in [72, 156].

- **IR-UWB:** transmits information by using very short pulses, which are in the order of nanoseconds. These extremely short pulses in time domain enable a large bandwidth in the frequency domain that could be spread up to several GHz. The typical pulse shapes used in IR-UWB are the family of Gaussian pulses [230]. The good thing about IR-UWB signal is that it can be directly generated from the base-band Gaussian pulses without using carrier signal or frequencies.
- **Multi-band UWB:** divides the whole available UWB spectrum (e.g. 3.1 – 10.6 GHz in US) into multiple smaller sub-bands with each contains a minimum of 500 MHz bandwidth. This enables the available spectrum to be used efficiently by switching the mentioned sub-bands for different devices. Regarding the modulation technique for multi-band UWB, many types can be adopted though the most popular one is Orthogonal Frequency Division Multiplexing (OFDM) technique and is usually named as the multi-band OFDM.

In recent years, the focus of UWB research has been shifted into the IR-UWB. In general, IR-UWB system posses more significant advantages compared to the multi-band systems in terms of simplicity in design, potentially lower cost and lower power consumption, and the ability to generate UWB pulses from the base-band signal (i.e., no carrier signal is separately necessary for UWB channel model). This enables the IR-UWB to support many basic modulation schemes discussed in the next section. Due to these characteristics, IR-UWB was regarded as very attractive in many system aspects and was adopted in Institute of Electrical and Electronics Engineers (IEEE) 802.15.4 standard in 2002. The amendments and regulations regarding IR-UWB are constantly updated, and it is currently the most applied UWB-based technology in practice and commercial markets. Therefore, the overview of IEEE 802.15.4 standard and its defined operational flow for the wireless channels are briefly described in Section 2.2.5.

2.2.4 Modulation Schemes for IR-UWB

Modulation is a process of encoding information to be transmitted (e.g. a digital signal representing a sequence of binary digits) into its carrier frequency. It should be noted that the base-band signal itself can be used as the carrier frequency in the case of IR-UWB system as previously mentioned. In this section, only the necessary concepts of the modulation are described in a short and concise way for a better understanding of the UWB technology. The complex technical details and theories are omitted since those can be easily found in academic books and publications. For the readers who need a concrete theoretical concept, the author would refer to the book in [187] for general modulation techniques in wireless communication channels and the books in [72, 156] for UWB specific signal modulation techniques. In short, there are, in general, four modulation schemes for UWB-based signal processing (see the visual demonstration of each concept in Figure 2.6) as follows [156]:

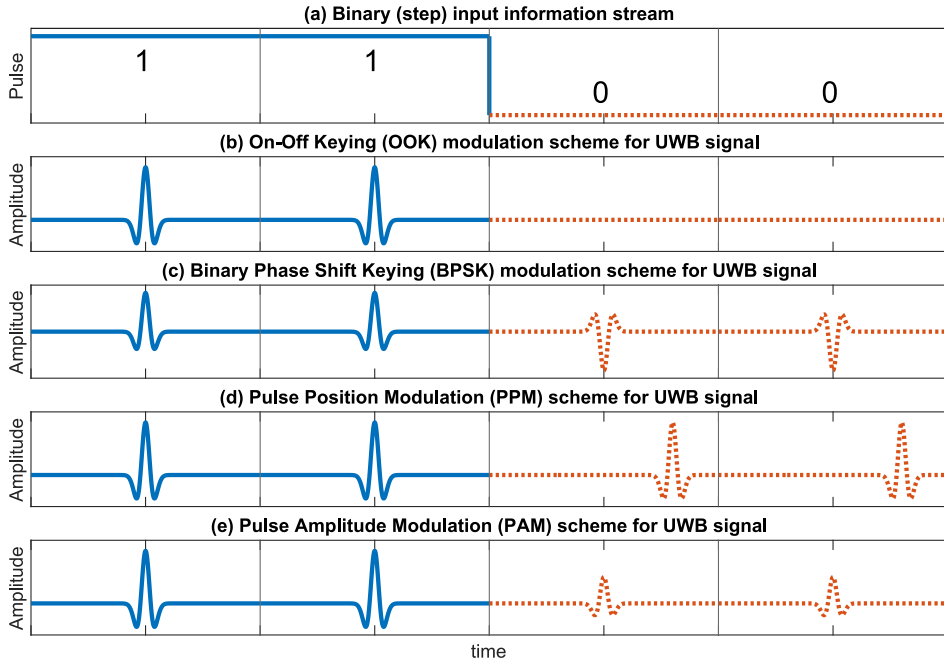


Figure 2.6: Demonstration of four typical modulation techniques used in UWB system. The UWB pulse shape used in the Figure is based on the Gaussian doublet waveform.

1. **On-Off Keying (OOK) modulation scheme:** conveys the digital information based on the presence (i.e., logical 1) or absence (i.e., logical 0) of binary data stream in its input waveform (Figure 2.6 (b)). In simple terms, the UWB pulses are transmitted via wireless channel in OOK scheme only when the digital information includes logical ‘1’. Otherwise, no signal transmission is conducted meaning the binary information is encoded with a logical ‘0’.
2. **Binary Phase Shift Keying (BPSK) modulation scheme:** uses two phases, which are separated with 180° to each other, to represent information encoded in its carrier frequency (Figure 2.6 (c)). In basic terms, the phase of BPSK is shifted by 180° if the binary information to be sent via wireless channel includes logical ‘0’. Otherwise, there is no phase shifting in the modulation of BPSK, i.e. for information encoded with logical ‘1’.
3. **Pulse Position Modulation (PPM) scheme:** encodes information to be transmitted via wireless channel by shifting the position of specific pulse occurrence in time (e.g. shift occurs when binary information includes logical ‘0’) as depicted in Figure 2.6(d). In other words, the UWB pulse is shifted in time whenever ‘0’ from the binary information stream is to be sent by the PPM scheme. In contrast, no pulse shifting is performed in the modulation when logical ‘1’ is to be sent.
4. **Pulse Amplitude Modulation (PAM) scheme:** encodes information to be transmitted via wireless channel by varying the amplitudes in accordance with the sample values of the message (i.e. binary data in UWB) signal. In simple terms,

the information in PAM scheme is encoded by varying different signal amplitudes for each binary digit. For instance, the logical ‘0’ has different amplitude than its counterpart logical ‘1’ for binary-coded information data (Figure 2.6 (e)).

For a better understanding of the concept through visual representations, Figure 2.6 demonstrated the discussed four modulation schemes for UWB signal by using a sample binary step data stream with values [1, 1, 0, 0] as the input information message to be sent via the wireless channel. The UWB pulse shape used in Figure 2.6 is based on the Gaussian doublet waveform, which is the second derivation of the Gaussian pulse typically used to generate the IR-UWB radio signal in practices. The figure illustrated a single modulation scheme for IR-UWB system. For multiple access schemes, time-hopping codes or direct sequence codes are generally utilized in IR-UWB system along with one of the modulation schemes discussed in this Section [156]. Noted that the modulation generally occurs in the Physical Layer (PHY) of the UWB system and it is typically applied in both the synchronization and data slot areas of the PHY frame transmission process in IEEE 802.15.4 standard (see more details in Section 2.2.5.3).

2.2.5 UWB Standards and Trade Groups

This section briefly discusses the UWB related standard called IEEE 802.15.4, which is actively specified by the IEEE (i.e. the current active version is IEEE 802.15.4z-2020 for UWB by the time writing this dissertation). The IEEE 802.15.4 standard is generally regarded as the foundational technical standard for mass production and interoperability of the UWB technology and its applications. Moreover, the trade group formed for the use-case of UWB and other available standards, which are mainly built upon the IEEE 802.15.4 standard, are briefly described in this section.

2.2.5.1 IEEE standards for UWB

The first attempt to create UWB related standard in IEEE was initiated in 2002 as part of an amendment for the IEEE 802.15.3 standard, namely IEEE 802.15.3a. The attempt was unsuccessful due to selection procedure issues for adopting UWB architectures. In consequence, the IEEE 802.15.3a task force group⁴ was also disbanded by the IEEE standards Association⁵ in 2006. The earlier 802.15 standard model was an important step for the understanding of UWB channels and was established to be useful for the new standard related to UWB high-data rate communications [61].

In 2007, IEEE 802.15.4a was specifically defined for UWB related channels as a part of the amendment to IEEE 802.15.4-2006 standard. The mentioned amendment was successfully merged into the release of the IEEE 802.15.4-2011 standard. It should be noted that an alphabet at the end of the name of the IEEE standard (e.g. IEEE 802.15.4a) means an amendment to the previously defined standard, and the name of the entire IEEE standard is usually accompanied by the specified year at the end (e.g. IEEE 802.15.4-2006). The specification defined in IEEE 802.15.4-2011 played a

⁴<https://www.ieee802.org/15/pub/TG3a.html>

⁵<https://standards.ieee.org/>

Table 2.1: Summarized list of UWB related standards in IEEE

Standards	802.15.3a	802.15.4a	802.15.4-2011	802.15.4-2015	802.15.4z
Years	2002	2007	2011	2015	2020

very crucial role in the rise of UWB technology in the research community as one of the most influential UWB chips in the field manufactured by Qorvo (formerly Decawave), namely DW1000 chip, was created upon this standard.

IEEE 802.15.4-2015 standard, that superseded the IEEE 802.15.4-2011, was released by IEEE standard association in 2015. However, there was not much alternation about UWB within the standard. It should be noted that IEEE 802.15.4 standard, in general, is responsible bodies for the technical specifications in all technologies usable in low-rate wireless personal area networks including UWB technology. In general, IEEE 802.15.4 standard specifies the PHY and Medium Access Control (MAC) layers. In 2020, the IEEE 802.15.4z standard, the most current amendment to IEEE 802.15.4-2015 as the time of writing this dissertation, was specified particularly for UWB technology in order to enhance its PHY layer. Table 2.1 provides the summarized list of the UWB-related standards specified by the IEEE.

2.2.5.2 Other Standardization Bodies

In fact, there are standardization bodies other than the IEEE that focus to specify the development process and interoperability of the UWB technology. A good overview of those standard bodies can be found in [35]. However, the defined standards on those bodies are mainly concerned about the application layers of UWB in general. In terms of the Open Systems Interconnection model (OSI model), the standardization of those bodies focuses only on the network layer and above (namely the network, transport, session, presentation, and application layers). In the nutshell, the mentioned standardization bodies generally use either the IEEE 802.15.4z standard or the more completed version of the IEEE 802.15.4 standard in their PHY and MAC layers.

In brief, there are four main standards at the time of writing this dissertation that specified the UWB application layers [35]. **FiRa Consortium** defined specific layer called **common service management layer** on top of the PHY and MAC layers of the IEEE 802.15.4z standard. The aim is to allow interoperability between the FiRa devices during the deployment process and in applications. Similarly, **Apple** defined the protocol called **nearby interaction accessory protocol** that controls the UWB ranging between the Apple device and its connecting accessories. Moreover, cross-industry organization named **Car Connectivity Consortium** specified the **Digital Key 3.0** standard that uses UWB for hand-free location-aware key-less access for cars. Unlike the mentioned three standards, **omlox standard** (<https://omlox.com/home>) aims to combine different location-based technologies (e.g. UWB, BLE, RFID, Wi-Fi, and GPS) into the common framework. For the interoperability among different technologies, omlox standard defines a middle-ware called **omlox hub** on top of each executable base technology. The white paper that demonstrated the use-case of omlox standard for virtual reality application can be found in [168].

2.2.5.3 Description of Data Communication Flow in IEEE 802.15.4 Standard

To the best of the author's knowledge, IEEE standard association is the only active standardization group for specifying the PHY and MAC layers of UWB based technology. The rest of the standard bodies generally builds upon the IEEE standard as already mentioned above. Therefore, this section briefly explains the operational flow of IEEE 802.15.4 standard. Figure 2.7 illustrates the frame format of PHY and MAC layer, which is used for data communication between wireless devices in IEEE 802.15.4 standard. In short, the wireless data communication was performed by transmission and reception of the frames depicted in Figure 2.7.

Regarding the PHY layer of UWB data communication in IEEE 802.15.4 standard, the frame format can be divided into three parts (light blue color in Figure 2.7). Those three are the synchronization header, the physical header, and the data parts. First, the synchronization header is composed of the preamble and Start of Frame Delimiter (SFD). The preamble sequences are used in UWB receiver to detect whether there exists an UWB signal transmission from the transmitter and acknowledge the data communication types such as data rate. The standard defines several specific preamble codes for different configuration (see details in [33, 96]). The SFD is a unique sequence of symbol data that signifies the end of a preamble sequence and the start of PHY header in the data frame. For precise ranging in UWB system, accurately time-stamping of this critical switched moment is crucial and the UWB hardware available in the market is usually capable of doing it automatically within the chip. The standard defines separate lengths of SFD sequences in order to support distinct data rates for various configurations in the UWB devices. Second, the PHY header is responsible for specifying which modulation schemes should be used for the data part of the frame with assignable data rates. The standard typically defines various modulations applicable in UWB, and it is likely that amendment and extension can occur based on the requirements of the application (e.g., IEEE 802.15.4z has already attempted to amend for the use-case of high rate PHY layer for UWB). Third, the data slot in the frame format of the PHY layer in IEEE 802.15.4 standard was generally occupied by its upper layer, which is the MAC layer in the case of UWB-based localization system (Figure 2.7).

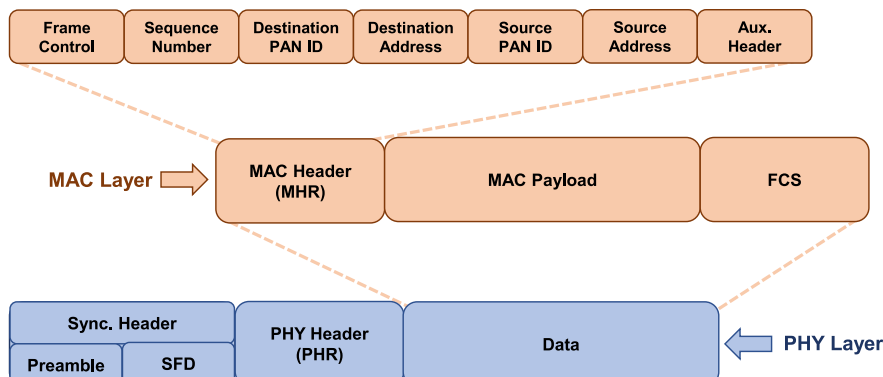


Figure 2.7: Overview of the PHY and MAC layers frame structure in IEEE 802.15.4 standard specifically defined for wireless personal area networks including UWB technology [45, 97].

Regarding the MAC layer of UWB data communication in IEEE 802.15.4 standard, the frame can be again split into three parts namely the MAC header, MAC payload, and Frame Checking Sequence (FCS) (light orange color in Figure 2.7). First, the MAC header is responsible for controlling the data flow between the UWB hardware and its wireless channel (Figure 2.7). The MAC header is further divided into seven parts, of which four of them correspond to the source and destination addresses of the communicated UWB devices and their corresponding Personal Area Network (PAN) identifiers. The sequence number field in the MAC header is typically used to match or validate transmitted data frames for further processing such as data acknowledgment, data re-transmission, etc. Basically, the sequence number should be incremented by 1 after each successful data transmission process. The frame control field in the MAC header is critical for configuring the types of frames (e.g., broadcast, acknowledgment, data, MAC commands, etc.). Second, the MAC payload slot in the frame format of the MAC layer in IEEE 802.15.4 standard is again reserved for its upper layers, which is in many cases the application layer (Figure 2.7). For instance, the information related to the ranging data of UWB signal is usually loaded directly onto this MAC payload slot in several location-based system integration processes [201, 230]. Third, the FCS in the footer of MAC layer frame is responsible for detection and correction of the transmission errors in wireless channel using Cyclic Redundancy Check (CRC). In other words, the FCS is used to detect accidental changes due to the imperfection of the wireless channel during the data transmission. Provided errors are detected in the course of the data transmission process, correction can be performed arithmetically up to a certain limit in order to avoid data corruption.

2.2.5.4 UWB-based Trade Groups

The coexistence with other wireless technologies is one of the greatest challenges and it is currently accomplished by restricting the spectrum mask of the UWB emission power by regulatory bodies across the world as described in Section 2.2.1. This sometimes limits the mass production of UWB based hardware and chips across the globe for certain frequency bands and in consequence, it further limits the interoperability in some particular cases. Therefore, the industry trade groups are usually formed in order to promote the adoption of UWB technology and to influence the decision-making of the regulation, standardization, and multi-vendor inter-operation processes.

Throughout the history of UWB technology, the first trade group namely **WiMedia Alliance**⁶ was founded in 2002 with the core members being Samsung and Alereon. The **WiMedia Alliance** adopted the IEEE 802.15.3a standard, which had not ended up to a successful adaptation into the core IEEE standard association as explained in Section 2.2.5.1. Consequently, the trade group was dissolved in the later years and its existence has gradually vanished.

In December 2018, **UWB Alliance**⁷ was officially launched by a group of technology companies, and its members are actively growing. The three main missions of UWB

⁶<https://www.wimedia.org/en/index.asp>

⁷<https://uwb alliance.org/>

alliance are: (i) persuading the beneficial rule-making process for UWB technology in US and EU, (ii) strategically building multi-radio coexistence solutions, and (iii) promoting an international standard for UWB that can interoperate among multi-vendors. The UWB alliance adopted the IEEE 802.15.4z standard and is actively involved in the amendment process of the mentioned standard.

In addition, the UWB related standards provided by **FiRa Consortium** and **omlox** has been sponsored and heavily backed by hundreds of leading technology companies that use or intended to use the UWB technology in their products, chip manufacturers that produce the UWB chips, and many market leaders in the field. Therefore, FiRa consortium and omlox are also included as part of the trade groups in this section. It is expected that the mentioned two standards will play an important role in promoting the wider use-case of the UWB technology into diverse fields of the consumer markets.

2.2.6 Potential Applications of UWB Technology

In general, UWB technology can be applied in three main areas: (i) data communication system in Wireless Sensor Network (WSN), (ii) location-based precise navigation and tracking systems in GNSS-deprived environments, a.k.a Real-time locating system (RTLS), and (iii) UWB-based short-range radar [7]. This dissertation is devoted to the use-case of UWB localization system. Hence, the potential applications of UWB in location-aware systems are briefly highlighted in this section by citing verifiable references for each use-case demo in literature. Therefore, those potential application areas of UWB technology are coarsely summarized as follows:

- Access tracking and localization of objects in crowded area such as hospital, shopping malls, airport, museum, industrial workplaces, etc. (e.g. in [204])
- Navigation and localization of objects in logistics using robotic engineering in factory environment (e.g. use-case in [200])
- Contact tracing and social distancing (e.g. use-case in [150])
- Player statistics and sport analytic in indoor sports (e.g. use-case in [60])
- Tracking, monitoring, and locating of tools and assembly parts in complex factory environments (e.g. use-case in [69, 123])
- Search and rescue missions (e.g. use-case in [125])
- Monitoring human health parameters in healthcare (e.g. use-case in [73])
- Location services for Unmanned Ariel Vehicle (UAV) in GNSS-deprived area (e.g. use-case in [152, 169, 214])
- Behavioral detection and localization of animals (e.g. use-case in [207])
- Hand-free access control to vehicle using UWB as a digital key for cars in BMW⁸
- Tracking assembling process of cars in automotive industry environments (e.g. use-case demo in BMW⁹ at Regensburg, German)

Besides the above-mentioned list, it is expected that the integrating of UWB chip inside the smartphones will definitely boost its applications into a new dimension in the near future. Examples include finding lost belongings, reminders of left behind properties, assets tracking in more diverse areas, factory automation systems, etc.

⁸<https://www.bmw.com/en/innovation/bmw-digital-key-plus-ultra-wideband.html>

⁹<https://ubisense.com/vehicle-assembly/>

2.3 UWB-based Localization Schemes

There are, in general, three (wireless) topologies or system implementation aspects in UWB-based indoor positioning and navigation systems. To the best of the author's knowledge, the earliest description of the said three topologies was defined in [72], in which the UWB network systems were categorized as: (i) Network-based system (i.e., GPS-like system), (ii) Handset-based systems (i.e., inverted GPS-like system), and (iii) Hybrid-systems (i.e., a combination of the referred two systems). Based on the mentioned categories, this section define the integration process of UWB technology into three topologies (Section 2.3.1). Surprisingly, we found out that only two of the three topologies (i.e., GPS-like and its inverted systems) are widely studied and addressed in academic publications whereas the information regarding the remaining one (i.e., Hybrid-system) was left out as unnoticed. Therefore, this section re-introduces the overlooked topology, which is named as a bidirectional UWB localization system in this dissertation, and highlights its potential in IPS (Section 2.4). In fact, the whole dissertation was wrapped around the implementation process of the mentioned bidirectional UWB-based localization system.

2.3.1 Three Topological Aspects in UWB Localization Schemes

According to UWB-based system integration processes in academic publications and industrial projects, the UWB systems can be divided into three categories: (i) the UWB system that imitates the GNSS scheme, i.e., GPS-like system, (ii) the UWB system that uses the inverted approach of the GNSS scheme, and (iii) the UWB system that combines the advantages of the two mentioned schemes in single system integration.

In a GNSS-like system as from the first case, a self-navigation scenario for a non-stationary mobile node (hereinafter referred to as tag) can be accomplished in a given space provided that the tag has prior knowledge regarding the exact location of the reference nodes or landmarks (hereinafter referred to as anchors). In this scheme, anchor nodes are placed at the fixed known locations within the areas, where the positions of objects are intended to be observed. Similar to the GNSS system, the anchor nodes are responsible for transmitting the UWB signals in a periodic way in this kind of UWB system. Upon passively receiving the sent UWB signals from the known anchors, the tag device is capable of self-navigation relative to the mentioned fixed location of anchor nodes. In terms of system integration process in UWB technology, the first GNSS-like approach for UWB-based localization system was addressed in [126]. Subsequently, this approach has been explored and used in several academic projects [36, 78, 87, 178, 229]. The mentioned GNSS-like UWB system integration approach is termed as a **unidirectional Active Anchor System (AAS)** in this dissertation. It is defined as unidirectional because the wireless communication between the anchor and tag is only in one direction. Moreover, the term active anchor denotes that the transmission of UWB signals are performed by the anchor nodes whereas the tags are responsible only for receiving tasks. The visual representation of the concept regarding the unidirectional AAS UWB localization system is given in the left image of Figure 2.8. In the unidirectional AAS system, the ranging phase (Section 3), i.e. measuring the distances

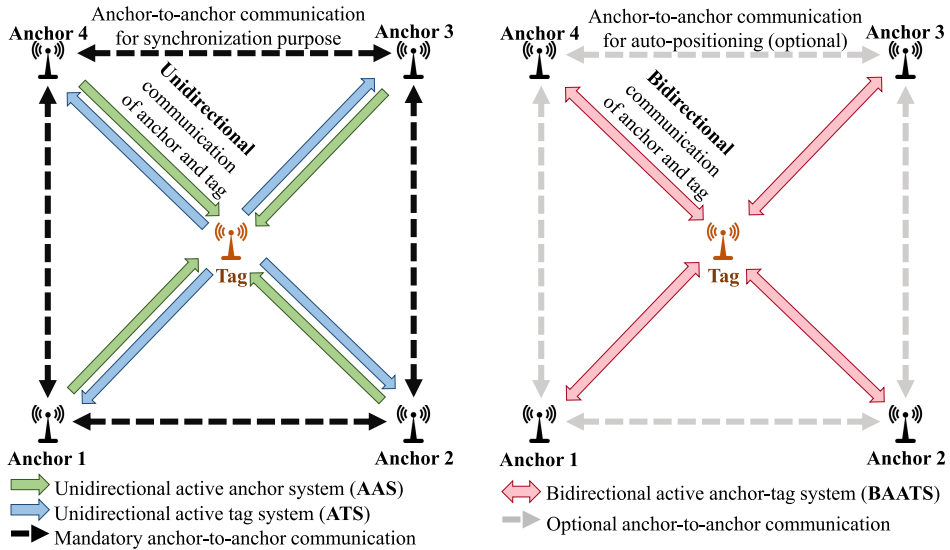


Figure 2.8: Illustration of visual comparison among the three topologies for UWB-based system integration namely the AAS, ATS, and BAATS.

between anchors and tag, is usually based on the TDoA technique [87]. For the location estimation algorithm, the Multilateration method is commonly used in AAS [230].

In contrast to the GNSS-like system integration process as described above, the inverted approach has been widely used in the UWB-based localization system. In the mentioned inverted system, the tags devices utilized in the UWB system are, in turn, responsible for transmitting the UWB signal whereas the anchor nodes are accountable for receiving the sent signal and computing the location estimation of the tag based on the sent UWB pulse. This approach is termed as an **unidirectional Active Tag System (ATS)** in this dissertation. Similar to the previous one, unidirectional refers to the one-way data communication, in which the sender is a tag and the receivers are anchors. The active tag means the UWB pulse transmission is performed by the tag whereas the anchor nodes passively listen for further processing in the ATS. The first integration of UWB-based unidirectional ATS was implemented at academic publication in [236]. Later, the approach has been extensively explored and studied in [78, 198, 201, 204]. In an unidirectional ATS, TDoA technique is the common measurement method and the Multilateration algorithm is the core positioning technique akin to the AAS [236]. Correspondingly, the unidirectional ATS can be used in a tracking scenario where the central server on the anchors' side is capable of tracking the motion of all available tags within its coverage area of the system. Figure 2.8 illustrates the visual representation of unidirectional ATS in contrast to the AAS approach. The figure also shows that the only difference between the two systems is the direction of the data transmission flow. However, the mentioned difference ignites totally different applicable scenarios (e.g. tracking vs navigation) and several opposing system parameters (Section 2.3.2).

Unlike the above-mentioned two unidirectional approaches, a bidirectional architecture for UWB-based localization scheme can be constructed as well by combining the

benefits from the two unidirectional systems into one common platform. This enables a promising paradigm shift in UWB-based localization system from the perspective of topological concepts as the scheme allows both navigation and tracking capabilities under a single localization system. In other words, the applications of UWB technology regarding the navigation and tracking scenario can be commonly integrated by using a single platform. In this dissertation, the mentioned scheme is namely as Bidirection Active Anchor-Tag System (BAATS) for simplicity. The term bidirectional in BAATS refers to the two-way communication between anchors and tags. In addition, both the tag and anchor nodes are necessary to be active, i.e., data transmission is necessary to perform by both the tag and anchors size. The first demonstration of UWB localization system similar to BAATS was presented by Qorvo (formerly Decawave) in their commercially available UWB development kits called TREK100 and MDEK1001 [47]. To the best of the author's knowledge, however, there is no prior work in literature that specifically addressed the bidirectional concept in UWB-based localization systems except for our previous work in [175]. Instead, it was always regarded as a by-product. Therefore, a BAATS system using two-way signal communication between the anchors and tags (Chapter 3) was specifically addressed in this dissertation. Figure 2.8 (the image on the right) illustrates the said BAATS system for UWB-based localization.

Moreover, there are, indeed, a few set-ups that are different from the typical system implementation process described in this section. One such approach is the use of a single anchor for UWB localization in which the system needed cooperation from IMU units as an additional resource [26]. In addition, the unidirectional AAS and ATS systems can also be designed to support the bidirectional localization system by using a two-steps approach. In such a two-stages case, a secondary wired or wireless technology (e.g BLE) is mandatory for exchanging the last updated location data estimated by the UWB between the two parties (i.e. the server/anchor and tag sides). In simple terms, the position of the targeted mobile tag is estimated based on the UWB technology by either the tag itself (i.e., for a navigation scenario in AAS system) or the anchors (i.e. for the tracking scenarios in the) in the first stage. The second stage corresponds to exchanging the positioning data to the other parties by means of a wired or wireless technology other than the UWB in this case. In this dissertation, the two-stages approach is disregarded due to the increased complexity in implementation as it requires cooperating with other suitable technology. Therefore, the bidirectional UWB system that can perform both the navigation and tracking scenarios within a single platform is promoted as a promising and attractive solution for many diverse location-based applications and addressed in this dissertation (Section 2.4).

2.3.2 Comparing the Features of Three UWB Systems

The general comparison of features regarding the presented three system implementation aspects of UWB-based localization namely AAS (i.e. GNSS-like system), ATS (i.e. inverted GNSS-like system), and BAATS is given in Table 2.2. The well-known GNSS system setup is used as a reference here for the purpose of explaining the implementation aspects of UWB-based localization system. Concerning the ranging phase in UWB, the two unidirectional AAS and ATS setups are traditionally based on the TDoA technique

Table 2.2: Summarized feature comparison of three UWB-based localization topologies

Properties	UWB-based Localization Systems		
	AAS [78, 87, 126, 229]	ATS [78, 198, 204, 236]	BAATS [47, 175]
System setup	GNSS-like	inverted GNSS-like	mixture of both
Ranging method	TDoA	TDoA	ToA
Clock sync.	mandatory	mandatory	unnecessary
Localization approach	navigation purpose only	tracking purpose only	navigation and tracking purposes
Availability of position data	only at the Tag devices	only at the Anchor (server)	both at Tag and Anchor (server)
Signal direction	unidirectional	unidirectional	Bidirectional
System-wide energy usage	very low	low	medium
No. of Tags	unlimited	limited	highly limited
No. of Anchors	limited	limited	highly limited
Signal transmitter	active Anchors	active Tags	active Anchors-Tags

while the ToA method is typically used in the bidirectional BAATS. In general, the TDoA-based unidirectional systems (i.e., AAS and ATS) need expensive and complex clock synchronization setups among the anchor nodes in order to achieve accurate location estimations due to clock drift errors. However, this is not the case for the ToA-based bidirectional system as the issues related to clock drifts can be effectively eliminated by using the TWR scheme in the ranging phase (more details in Chapter 3).

Due to the nature of unidirectional, information can be transferred in one-way, which is from a transmitter to a receiver, in AAS and ATS. As a result, there are limitations in the system use-case of the unidirectional AAS and ATS based on where the location data is available in the system (e.g., anchors vs. tags). For a GNSS-like unidirectional AAS, the transmitters in the system are anchors whereas the receivers are the tag devices. This corresponds that the AAS can be used as a navigator or in the navigation scenario because the estimated location data of the system is available only at the tag device. In contrast, the unidirectional ATS can be used in a tracking scenario where the location information is available at the anchors' side or the central server in the system. Unlike the mentioned two unidirectional approaches, the bidirectional BAATS is flexible to be used in both the navigation and tracking purposes in applications as the location information is available at both the tags and anchors (central server) of the system.

In terms of system-wide energy consumption, the AAS topology is very efficient and considerably lower than the ATS and BAATS mainly because only the anchor nodes are responsible for transmitting UWB signal. As a matter of fact, the highest energy in UWB hardware is typically evident in the data transmission process compared to the receiving and idle cases [44, 230]. In general, the number of anchor nodes necessary to be used in UWB localization system including AAS is relatively fewer

than its counterparts the number of tags in the system. In addition, there is no limit for the number of tags in GNSS-like AAS for the use-case of navigation purposes. In contrast, the scalability of the number of tags in ATS is limited due to the possible signal collisions within the same environments. Similarly, the number of allowable tags is highly limited in BAATS due to the requirements of its multiplexing scheme for multiple access. In terms of the allowable anchor nodes, all the UWB-based localization schemes have limitations. The constraint in the TDoA-based unidirectional systems are due to the synchronization procedure mandatory in the system implementation whereas the bidirectional ToA-based scheme is due to the multiplexing process.

In summary, the two main advantages of AAS topology are the unlimited number of tags supported in the system and its very low system-wide energy consumption. However, the AAS can be used only in a navigation scenario which limits its application areas, especially in indoor environments. To fill the gap with the tracking scenario, the ATS setup was risen up recently and applied in many UWB-based localization system [78, 198, 204, 236]. Generally speaking, there are no substantial benefits in ATS except for its applicable tracking scenario in the localization system compared to the AAS. The core disadvantage of the two unidirectional systems (AAS and ATS) is the requirement of system-wide clock synchronization for accurate location estimation. In contrast to the unidirectional TDoA-based systems, the bidirectional ToA-based BAATS has a considerable benefit in its flexible applicable areas as the system can be used as both a navigator and tracker at the same in a single scheme.

2.3.3 The Potentials of a Bidirectional UWB System

As already mentioned above, the bidirectional UWB localization system (i.e., BAATS) is considerably flexible in its application areas due to its ability usable in both navigation and tracking scenarios within a single uniform scheme. From the perspective of applied UWB-based localization system integration approach, the capability of both navigation and tracking scenarios in a single platform is, in fact, a paradigm shift in the field as previously it was addressed under separate categories. In other words, BAATS is flexible to act as either a navigation scheme or tracking scenario under the same system setup without changing the underlying implementation processes. As a result, the bidirectional scheme opens a paradigm shift in a diverse field of application areas, which are unaddressed previously by incorporating the navigation and tracking scenario under a common single system.

The current state-of-the-art system implementations in UWB-based wireless localization emphasize only the accuracy of positioning information. Hence, the data payload section of the MAC layer (Section 2.2.5.3), where sensor data and other information can be transmitted on it depending on the available resource space, were commonly ignored and not used at all in unidirectional AAS and ATS [78, 87, 126, 229, 236]. Instead, the data payload section of the MAC layer was used only for essential timestamps to be used for the location estimation process in those systems. The main reason is that the strict requirement of synchronization in unidirectional approaches necessitates a fixed and constant data frame processing time during the communication between UWB devices. In contrast, the bidirectional BAATS shows that it has the capability to transmit

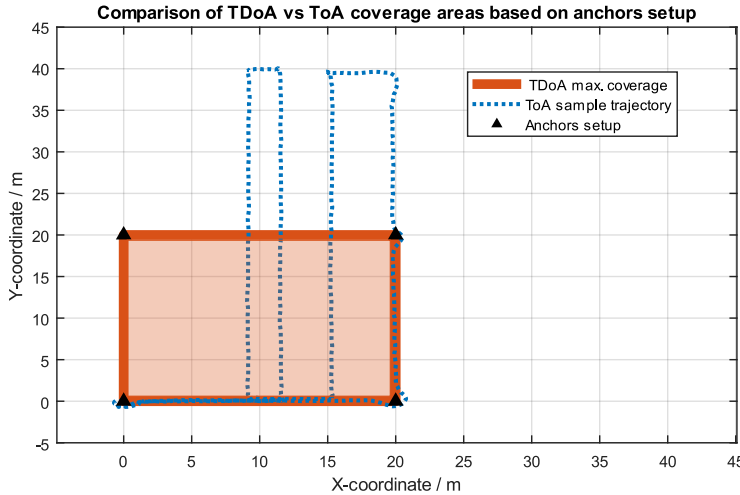


Figure 2.9: Illustration of the coverage areas comparison for the TDoA- vs. ToA-based UWB localization systems for accurate positioning under the same anchors' setup.

both actual information such as sensor data in WSN as well as the required data for location estimation within one system without losing its accuracy in the localization process. This can be accomplished due to the freedom of strict synchronization in the system. This fact is critical because it shows the potential of UWB technology, which can be used not only as the well-known precise location-based service producer but also as a typical sensor in WSN.

As already mentioned several times, the clock synchronization is not necessary in BAATS compared to the TDoA-based systems due to its usage of a two-way communication scheme in its ranging phase (see more details about the topic in Chapter 3). This fact is also very crucial because clock inaccuracies in localization systems cause serious problems and are troublesome in system integration and applications. In general, no device is truly accurate in constantly keeping its time and the natural drift between two communicating devices will still lead to issues as time goes on even if they are perfectly synchronized at the beginning. This is particularly very challenging for time synchronization protocols designed to be applied in wireless communication systems and the research on this area is still active to date. The bidirectional scheme simplifies the requirement of clock synchronization by using two-way ranging methods.

Moreover, ToA-based BAATS topology shows substantial benefits in system-wide coverage areas compared to its counterpart TDoA-based AAS and ATS. This comparative indication is usually overlooked in literature when promoting the TDoA-based scheme. For demonstration purposes, Figure 2.9 illustrated the trajectory of a ToA-base system measured from the real-world experimental data in order to compare with its counterpart the TDoA-based system. Under the same anchor setup as depicted in Figure 2.9, the maximum coverage area for the TDoA-based system is highlighted with the orange color whereas the trajectory of the measurement data from ToA-based bidirectional system is shown with a dotted line. The ToA sample data used in the figure were extracted from the real-world experiments in sport hall (see more details

about the data collection process in chapter 4). Figure 2.9 proved that the location of objects can still be accurately localized in the ToA-base bidirectional system even in a situation such as the targets are not necessarily inside the perimeter of the four anchors. On the contrary, the positioning data outside the four anchors' perimeter cannot be determined with high accuracy in TDoA-based unidirectional systems. One possible example use-case of the illustrated ToA-scheme is a transporter machine in a large factory that follows the worker who carries the UWB tag autonomously so that objects can be loaded on it without the need for a human driver. In the said exemplary application, all the UWB anchor nodes in the localization scheme can be set up on the autonomous vehicle itself to localize the tag, i.e. the worker in the example. Here, the anchor nodes allocated on the vehicle itself are also continuously moving along with the transporter machine, which can't be accomplished in TDoA-based systems.

2.4 Implementation of a Bidirectional UWB System

Motivated by the potentials of the bidirectional UWB system discussed in Section 2.3.3 and its lack of documentation about the methodology in literature, this dissertation is devoted to the bidirectional localization scheme of UWB technology. Figure 2.10 depicted the overview block diagram of a complete system set-up for ToA-based BAATS for UWB localization. In brief, the bidirectional UWB localization scheme can be regarded as a complete system if the mandatory four main blocks colored with light green in the figure are established. The four blocks correspond to the UWB hardware components, the ranging phase of the system, the location estimation phase, and the multiplexing process. In addition, there are optional blocks that are crucial for the enhancement of the system to improve the quality of the UWB localization scheme (light orange color in Figure 2.10). The two optional blocks in the figure correspond to the identification and mitigation process of the ranging error, and filtering of the output location data. Each block in Figure 2.10, i.e. the implementation process in a bidirectional UWB localization, are shortly described in the next subsections.

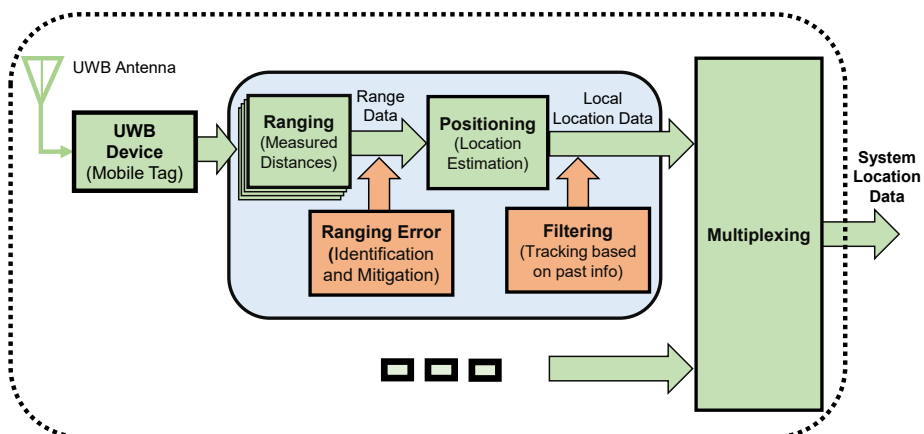


Figure 2.10: Block diagram representation of a bidirectional UWB-based localization system

2.4.1 Hardware Components

Basically, the UWB device is composed of four main components: (i) the antenna, which is used for transmitting and receiving the UWB radio signal, (ii) the UWB chip specified in accordance with a standard such as IEEE 802.15.4, which is used for precise time-stamping, UWB signal processing, configuration of the UWB channel, data rate, emission power as well as other suitable parameters based on the intended application, (iii) the Microcontroller Unit (MCU), which is typically used to control the data communication flow in the UWB chip, and (iv) high precision oscillator, which is used to provide a local clock to the MCU for tasks like defining precise timestamps in UWB localization. It should be noted that the underlying hardware components for the BAATS, AAS, and ATS are generally the same though more precise oscillators are fundamentally demanded in TDoA-based system due to its strict requirement of clock synchronization within the system.

Nowadays, several UWB chips are manufactured by many companies around the world, and they are available at quite a low cost in the electronic markets. Among them, the current leading manufacturers of UWB chip are Decawave (at present under Qorvo), Ubisense, Bespoon, and NXP. In addition, smartphone companies such as Apple and Samsung have already integrated UWB chips into their products and it is expected that the exponential growth of UWB chips will be evident in the near future.

2.4.2 UWB Ranging or Distance Measurement Phase

The careful choice of a ranging methodology for UWB localization is crucial because it determines whether the applied final scheme becomes a unidirectional or bidirectional system. In other words, a particular UWB-based localization scheme can be identified as either a unidirectional or bidirectional system by looking at the applied technique in the ranging phase. Generally speaking, the ranging techniques for UWB-based localization

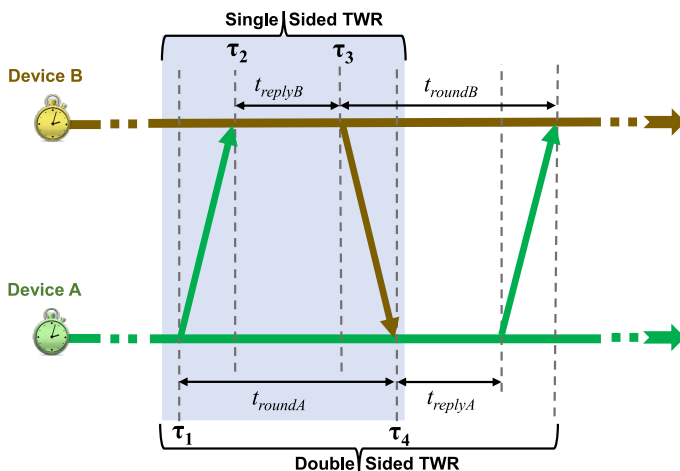


Figure 2.11: Illustration of two-way ranging method usable for both distance measurement phase in BAATS as well as node synchronization process in TDMA scheme (shaded area). The image was reproduced with minor changes from [175] (©2019 IEEE. Reprinted, with permission.).

systems are closely tied up with its signal measurement techniques (or) topological configurations such as TDoA, ToA, AoA and RSS [222]. Unidirectional UWB systems in literature are built upon the TDoA techniques [126, 198, 229] whereas the bidirectional systems are fundamentally based on the ToA technique.

Figure 2.11 illustrates two basic ranging schemes for bidirectional UWB system namely Single-Sided Two-Way Ranging (SS-TWR) and Double-Sided Two-Way Ranging (DS-TWR) respectively. The defined TWR corresponds under the category of ToA-based ranging methodology for a bidirectional UWB system. There are, indeed, several ranging schemes regarding TWR techniques as well as a misconception in literature. Therefore, the rigorous analysis specifically for TWR schemes are examined in chapter 3 and clarified the misconception typically made in academic publications. In brief, we found out that the AltDS-TWR technique was the most reliable and consistent TWR method available in the literature (see chapter 3 for more details). Therefore, the bench-marking of position estimation algorithms addressed in chapter 4 applied the AltDS-TWR as its ranging technique for the BAATS. For the readers who are interested in the validation process regarding the choice of AltDS-TWR as well as the misconception in TWR, the author would refer to read chapter 3 of this dissertation, where the verification was specifically carried out analytically, numerically, and experimentally.

2.4.3 Identification and Mitigation of the Ranging Errors

The ranging errors identification and mitigation process is generally not a mandatory aspect in the implementation of BAATS (light orange color in Figure 2.10). Instead, they are crucial for enhancing the location-related solutions provided by the UWB-based system. In simple terms, a localization system will work fine without it. However, the performance of the system in terms of accuracy will degrade substantially in case non-direct path signals are involved in the UWB measurements. This is a very typical scenario in practice due to the fact that the propagation time of UWB signal is normally delayed by the NLOS and Multi-path (MP) conditions. As a result, the estimated ranges are elongated compared to the actual true ones.

Generally, the measured ranges in UWB are affected by errors due to NLOS and MP conditions. The mentioned ranging errors can be identified and corrected before further processing in the positioning phase in order to enhance the overall system performance. The identification process of the mentioned ranging errors is, in fact, very challenging due to the nature of wireless signal processing and the field is still novice under active research. Lately, machine learning methods are seen as attractive solutions for solving the mentioned identification and mitigation problems for UWB-based localization system. Therefore, the whole chapter 5 is devoted to rigorously addressing the identification process of the ranging errors due to NLOS and MP condition for bidirectional UWB-based localization system using machine learning approaches.

2.4.4 Location Estimation in UWB

The determination of a position in the bidirectional UWB localization system relies on the measured distances between anchors and tags in the ranging phase as well as a

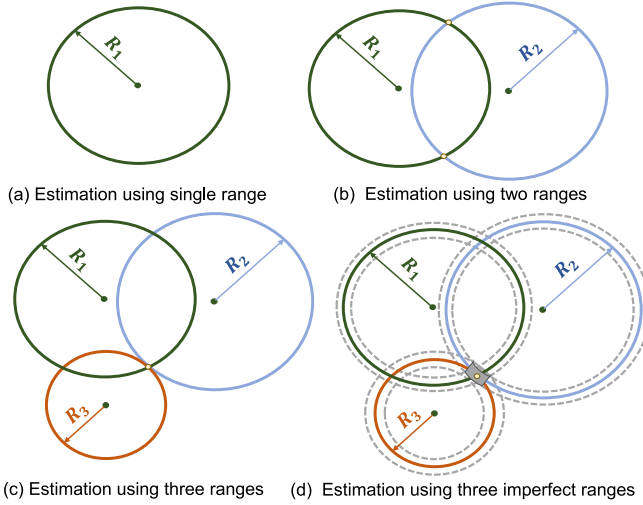


Figure 2.12: Demonstration of location estimation procedure in UWB-based localization system by using measured ranges between anchors and tags in 2D space.

dedicated positioning algorithm. In general, at least three ranges are necessary to locate a position of a target tag in two-dimensional (2D) space whereas at least four ranges are mandatory for three-dimensional (3D) space. Figure 2.12 demonstrates the fundamental of Lateration technique in 2D space, which is widely utilized in range-based positioning algorithms. In fact, the more complex location estimation methods (chapter 4) given in the literature are generally built upon the basic understanding of the illustrated concept in the figure. In brief, the Lateration technique is called Trilateration if the system uses three ranges to get the position of a tag in 2D space whereas it is called Multilateration when more than three ranges are used.

Fundamentally, the position of a tag could be anywhere around a circle in 2D space suppose that only a single range between an anchor and a tag is available to the system (Figure 2.12 (a)). The plausible position of a tag is reduced into two points at the intersection of two circles if two ranges (i.e. distances between two anchors and a tag) are obtainable in the system (Figure 2.12 (b)). Eventually, the exact position of a tag can be determined in 2D space at the intersection point of three circles by using three ranges (i.e., distances between three anchors and a tag) as depicted in Figure 2.12 (c). However, the mentioned intersection of circles at a single point can only be achievable in an ideal case where all the measured ranges are perfectly aligned with error-free. In practice, the estimated ranges are effected by measurement noises such as NLOS and MP conditions, and as a result, the circles will not intersect at a single point (Figure 2.12 (d)). Instead, an overlapping area regarding the position of a tag typically occurs. Therefore, statistical positioning techniques are becoming attractive in UWB-based localization to overcome the mentioned overlapping areas.

Accordingly, there are several location estimation algorithms for UWB-based localization systems. Specifically, for ToA-based BAATS, the position estimation algorithms for UWB system can be divided into three types: (i) geometric approach (for instance using the Trilateration method), (ii) close-form least square approach (for instance us-

ing Multilateration method), and (iii) statistical approach (for instance using Bayesian framework). Chapter 4 rigorously addressed the benchmarking of the mentioned three types of location estimation algorithms in order to help the practitioners in the field the right choice of a positioning algorithm for a certain application.

2.4.5 Filtering Process

The optional filtering process depicted with orange color in Figure 2.10 is a crucial statistical tool for dealing with the uncertainty in the estimated location data produced by the positioning algorithms. The reason is clear because, on the one hand, no localization system works well in all situations. On the other hand, the measured ranges used by the location estimation algorithms in UWB systems are imperfect as stated before. The filtering process gives the optimized solution in the mentioned imperfect world. In addition, the filtering process can also be used for multi-sensor fusion aspects based on the system requirements. Among other filtering processes, the Bayesian techniques are particularly attractively and widely used in WSN-based location services including the UWB-based localization system [64]. For instance, the Bayesian framework that made use of Kalman filter was applied for the system implementation process of UWB-based localization in [175, 230].

In short, the filtering part is mainly acquired for tracking scenarios in the localization system by incorporating the past accumulated information into the current location estimation. The core methodology in the field is Bayesian-based state-space models. In fact, the filtering process and the positioning algorithm are usually tied up together, especially for localization purposes. Therefore, chapter 4 rigorously addresses the implementation details of the cooperated positioning algorithm and filtering process for the bidirectional UWB localization system.

2.4.6 Multiplexing Method for bidirectional UWB System

Multiplexing is a methodology that combines multiple individual outcomes into a single system output over a shared medium. The aim of multiplexing is to share limited resources within a system without signal collisions or minimum losses during processing. From the topological perspective of UWB localization system, the multiplexing technique is mainly applied in ATS [201, 204] and BAATS [47, 175] system setups. On the contrary, the AAS works well without the need for multiplexing as the location estimation is conducted for a single navigator device.

To the best of the author's knowledge, the only multiplexing method applied in UWB-based localization systems is Time Division Multiple Access (TDMA) technique. The other multiplexing approaches namely frequency and code divisions are not used at all specifically in UWB system. The core reason may be due to the high temporal resolution produced by IR-UWB technology which is practically very attractive for TDMA scheme. In short, TDMA is a simple multiplexing technique for a system where power efficiency (e.g., no idle listening) and guaranteed real-time message delivery without collisions are required within a bounded system latency. The drawbacks, however, are that the unused

time slots will be wasted and a network-wide synchronization is required. Nevertheless, the accurate node synchronization in the TDMA scheme is quite straightforward to implement, especially when a two-way message exchange scheme is available as in the case of the bidirectional UWB system.

One simple algorithm for synchronization nodes within the TDMA scheme in order to eliminate the jittering effects is the *timing-sync protocol* [67]. The basic formula for synchronization in the protocol is as follows based on the shaded area in Fig. 2.11:

$$\Delta e = \frac{(\tau_2 - \tau_1) - (\tau_4 - \tau_3)}{2} \quad (2.2)$$

where Δe represents the clock drift between the two nodes, τ_1 and τ_4 are the transmitted and received timestamps of node A respectively, and τ_3 and τ_2 are the transmitted and received timestamps of node B respectively.

By knowing the drift between two nodes (i.e., Δe in Equation (2.2)), it is plausible for the clock of node A to correct its own clock by adjusting it so that it is synchronized with the clock of node B (shaded area of Fig. 2.11). In case the two nodes are already in the same clock domain, Δe will become zero. Noted that Δe can be positive or negative depending on the clock of one node leading the other.

2.5 Thematic Aspect of the Dissertation

In the previous section, the overall system implementation process for ToA-based bidirectional UWB localization scheme was described, and its corresponding phases are briefly discussed. Along the way, it is noticeable that some parts in the systems are kind of accomplished in full potential thanks to the tremendous works in research and industrial UWB communities. Therefore, much more works on those areas are not necessary from the perspective of a system implementation process for the practitioners. For instance, the in-depth research on the circuitry of the UWB chip is becoming less deserving as those are available at quite a low cost in the market nowadays and can be directly used in the intended products and projects. Likewise, there is basically not much choice in multiplexing method except for TDMA in UWB-based localization system as already mentioned above.

At the same time, there exist unanswered research questions, perplexing in the choice of ranging and position techniques, and in some cases even a misconception in UWB system implementation. Moreover, there is no well-documented books or research articles that addressed each available methodologies in different sector of the implementation flow. Therefore, this dissertation rigorously addresses the mentioned gap in literature specifically for the bidirectional UWB localization system. Figure 2.13 expresses the thematic aspect of the bidirectional UWB positioning scheme addressed in this dissertation by highlighting with color. The thematic aspect can be subdivided into four sectional parts namely the ranging process, the location estimation phase, the filtering process, and the NLOS identification and mitigation part of the system.

In this dissertation, each of the above-mentioned sectional parts for bidirectional UWB system (Figure 2.13) are rigorously evaluated by addressing in a dedicated chapter for

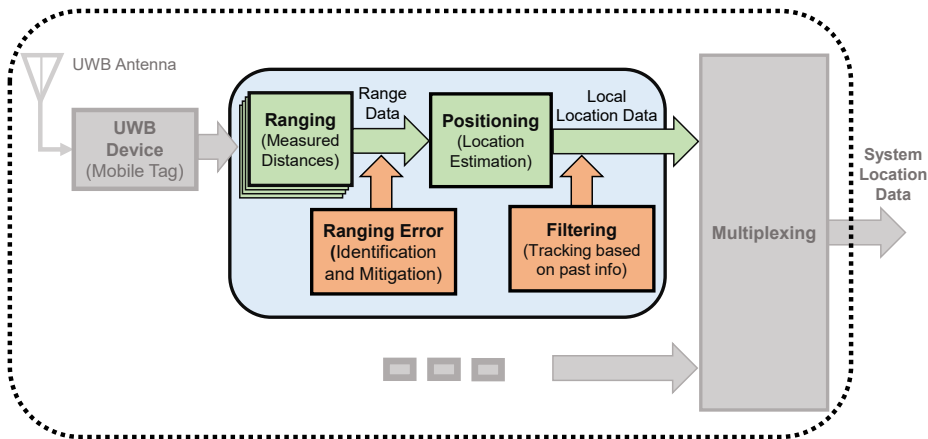


Figure 2.13: Highlight of the addressed thematic aspect in this dissertation.

each process. Basically, the location estimation algorithm and the filtering processes in UWB system implementation can be tied up together as already mentioned previously. Therefore, the ranging part from the bidirectional UWB system was rigorously evaluated and addressed in chapter 3, and the positioning and filtering aspects in Chapter 4. Similarly, the identification and mitigation of non-direct path signals for bidirectional UWB-based localization system were addressed in chapter 5.

2.6 Chapter Summary

In summary, the chapter started by introducing the overview of indoor positioning and navigation in Section 2.1, in which the general signal measurement techniques and positioning algorithms are described. In addition, the state-of-the-art location-based technologies for IPS are briefly explained and the role of UWB technology in an indoor environment was highlighted. Then, it was followed by reporting the fundamental and core features of UWB technology in Section 2.2. It was focused on providing the readers with a basic understanding of the technology in terms of system integration and implementation process. As such the section touched on the general regulations of UWB in different countries, typical modulation schemes applicable in UWB, and the main standardization bodies that drive the current success of UWB technology in the commercial market and academic research areas. Specifically, the data communication flow in PHY and MAC of the IEEE 802.15.4 standard, i.e. the basic frame format for currently all available UWB-related standards, was also concisely explained.

The three topologies of UWB-based systems were discussed, and their features are compared in Section 2.3. Among the three systems, the bidirectional aspect of the UWB system was generally overlooked in the literature. Therefore, the potential of the bidirectional aspect in UWB was highlighted followed by the whole implementation process. Indeed, this dissertation was devoted to the bidirectional UWB-based localization system. Accordingly, the sectional focuses addressed in each chapter in the dissertation were illustrated as a thematic aspect in Section 2.5.

3 Delving into the Ranging Process of a Bidirectional UWB System

This chapter addresses the ranging phase of a bidirectional UWB localization system by delving into the methodologies for the distance measuring process. Ranging phase is one of the two core foundations (i.e., ranging and location estimation phases) in all location-aware wireless positioning systems, including UWB technology. In specific, the comparative analysis of TWR technique in UWB-based wireless localization system was rigorously analyzed in this chapter. Figure 3.1 illustrates the block diagram concerning the sectional focus of the chapter in reference to the complete big picture of the bidirectional UWB localization system.

In general, TWR technique is the primary choice for measuring the distance between two wireless transceiver nodes when clock synchronization is unavailable. Moreover, TWR methods play an important role in a bidirectional UWB-based localization system, in which the system could be used as both a navigator and tracking purposes in a single platform as already described in previous chapters. There are several TWR techniques with different properties in literature (Section 3.1.2). To qualify the most appropriate TWR method for a specific scenario or application, a mathematical model is usually defined in order to give a comparative result. For TWR methods, the TOF error-estimation model was defined in the IEEE 802.15.4-2011 standard [33].

The TOF error estimation model specified in IEEE 802.15.4-2011 assumes that the only dominant error in TWR technique is due to clock drifts [33]. This assumption is incomplete in many ways (see more details in Section 3.2). In consequence, the

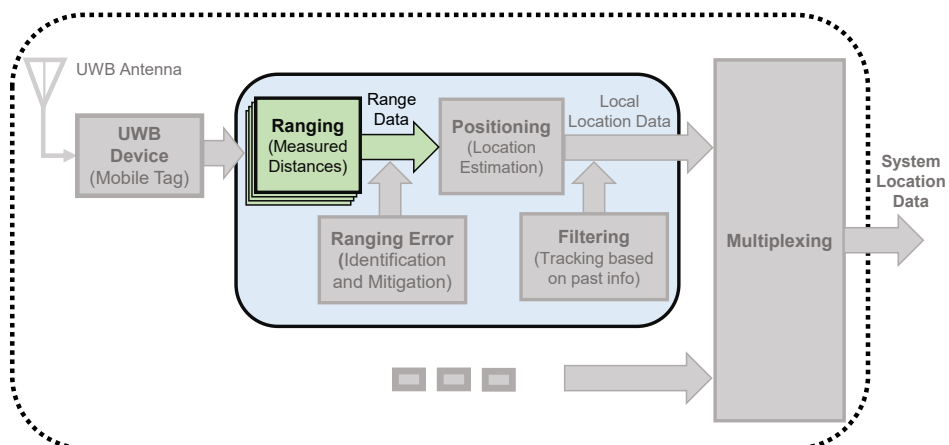


Figure 3.1: Description of the sectional focus in the chapter which is the ranging phase

comparative results achieved from the model are often the time inadequate to express a clear distinction among different TWR methods. This is typically true especially when similar TWR techniques are needed to examine in the analysis [149]. This motivates us to revise the existing error estimation model for TWR methods. This chapter expressed the Time-of-flight Error Estimation Model (TEEM), which was proposed in our previous work [130, 172]. TEEM was designed to specify clear distinctions among different TWR methods in terms of their performances. Specifically, the chapter focuses on the comparative analysis of different TWR methods available in the literature in terms of the ranging accuracy as their performance metrics using TEEM.

TEEM is an extended version of the existing TOF error estimation model for TWR methods defined in the IEEE 802.15.4-2011 standard. Correspondingly, TEEM completely holds the properties of the existing clock drift error model described in the mentioned standard. Nevertheless, TEEM is able to distinguish the performance difference between very similar TWR methods, which is simply unachievable in the mentioned existing model. Using TEEM model, the comprehensive analyses of four TWR methods were evaluated analytically, numerically, and experimentally using real-world data in this chapter. This implied that the analytical outcomes achieved from TEEM were validated with numerical simulation as well as experimental evaluation results. Besides, the pitfalls of the commonly used TWR method called SDS-TWR was demonstrated using TEEM. Because of its highly accurate performance on clock-drift error reduction when reply times are symmetric, SDS-TWR is the most highlighted TWR method in UWB-based localization systems in the literature. In fact, SDS-TWR even became a de-facto standard for many comparative analyses in literature. We argued that an AltDS-TWR originally proposed in [149], outperforms the mentioned de-facto standard SDS-TWR. The argument was verified with both numerical simulation and experimental evaluation results. Our findings suggested that AltDS-TWR should be a baseline model compared to the widely used SDS-TWR for benchmarking and comparing the TWR techniques.

The core ideas presented in this chapter were already published in our previous works [130, 172]. In [172], we proposed the concept for an analytical error model for two-way ranging methods. The verification of the concept is established using simulation results. The extended version of the analytical methods in [172] was addressed in [130]. In [130], we verified TEEM with both numerical and experimental evaluation results. In this chapter, TEEM model is revised and an errata regarding Assymmetric Double-Sided Two-Way Ranging (ADS-TWR) was corrected. Moreover, a clearer and more detailed description of the concept regarding TEEM model itself and the evaluation of different TWRs using the mentioned model were carefully organized in this chapter.

The chapter is organized as follows: In Section 3.1, the overview of TWR methods, the conventional TOF error-estimation approach, and related work are addressed. Then, the foundation of the proposed TEEM is established in Section 3.2, in which the analytical comparison for TWR methods using the proposed TEEM and conventional TOF error estimation approach was examined. The evaluation results based on numerical simulations (3.4.1), experimental assessments (3.4.2) and a summarized discussion (3.4.3) were presented in Section 3.4. Moreover, the experimental Study of Ranging Errors in TWR methods are analyzed in Section 3.5. The chapter discussion and final conclusions are given in Section 3.6.

3.1 Background and Motivation

This section expresses the role of TWR methods in UWB-based localization systems by reasoning why TWRs are crucial for a bidirectional scheme (Section 3.1.1), the basic four types of TWR methods from which other available TWRs in literature were deriving (Section 3.1.2), and the conventional approach for TOF error estimation in TWR methods (Section 3.1.3). Besides, the motivation behind novel TEEM proposed in our previous works is also portrayed in this section.

3.1.1 Brief Introduction to Time-based Wireless Ranging

The fundamental of a wireless localization system is typically composed of two main phases namely (i) the ranging (distance measurement) phase and (ii) the positioning (target location estimation) phase [34]. In the former case, the aim is to measure the estimated distances between transceivers using ranging techniques such as ToA, TDoA, AoA, RSS, etc. When the ranging information from sufficient devices within a specific network is achieved, the actual position of the target device is estimated in the latter case. Therefore, the positioning phase corresponds to the determination of the estimated real-time position of the target device using the knowledge of the above-mentioned ranging phase and positioning algorithms.

As already mentioned in the previous chapter, the TDoA-based ranging system require a synchronized clock to determine the distances between transceivers. This constraint forces the localization system to have a network-wide clock synchronization in TDoA-based system implementation. In the absence of the aforementioned clock synchronization, TWR is the most commonly used technique in a time-based wireless ranging system. However, TWR methods suffer a longer ranging time compared to the TDoA-based wireless ranging protocols because the TWR techniques need at least two times message delivery to get a single ranging unit (Section 3.1.2).

This section describes the state-of-the-art TWR methods and conventional TOF error estimation model for the wireless ranging methodology in UWB. Indoor localization systems with ranging accuracy of the decimeter level are an active research trend in recent years. Basically, the distance between two transceivers in wireless communications can be determined by the equation $d = T_{tof} \cdot c$. Where, d is the distance between



Figure 3.2: Illustration of measuring a signal's TOF in wireless communications.

two wireless transceivers, T_{tof} is the duration of a signal's propagation time between the transmitter and receiver in free space and c is the speed of light ($2.9979 \cdot 10^8$ m/s).

In general, the TOF (T_{tof}) is a signal's traveling time between transceivers in a certain medium such as air, vacuum, etc. In practice, the T_{tof} can be achieved by computing the difference between two timestamps extracted from the transceivers' devices, which are the signal's departure timestamp at the transmitter (τ_{ATx}) and the signal's arrival timestamp at the receiver (τ_{BRx}) (Figure 3.2). Obviously, the two transceivers need to have a synchronized clock. In other words, the two transceivers should be in the same clock domain to extract the mentioned TOF (Fig. 3.2). When this synchronization process is unavailable or unable to achieve in a time-based localization system, TWR is the primary choice for measuring distance in wireless transceivers.

In TWR techniques, a set of time periods or intervals is utilized to compute the distance between two transceivers, i.e., a signal round-trip-time likes $t_{round} = 10\ \mu s$ and a reply time likes $t_{reply} = 4\ \mu s$ (Section 3.1.2). This is in contrast to distance estimation using direct timestamps as illustrated in Fig.3.2. The reason is that the time interval (i.e. a period of a certain time) within a certain device is the same for the interval in another device even if the two devices have different clock domains. However, the device's clock in the real physical world drifts away even if it is perfectly tuned in the initial state due to the imperfections of clock oscillators [216]. These clock drifts create small errors in determining the mentioned time interval to be used for distance estimation in TWR. Eliminating these small errors is crucial especially when the application requires centimeter-level accuracy. The reason is that the TOF error of 1 ns in time corresponds to approximately 30 cm errors of distance estimation in TWR method [33]. In consequence, several proposals for TWR methods have been made in literature to minimize this inaccuracy in ranging due to clock drifts. The coming next section (Section 3.1.2) addresses the basic four types of TWR methods, from which other available TWRs in literature were basically derived.

3.1.2 State of the Art TWR Methods

As already mentioned in Section 3.1.1, a single transmission of a signal is sufficient in the one-way ranging system to estimate the TOF when clock synchronization between the devices exists in the network (Fig. 3.2). In the lack of before-mentioned clock synchronization, an exchange of more signals between the devices is required in wireless communications to extract the estimated TOF [33, 97]. This is where the TWR methods play an important role in the wireless ranging systems.

In this section, the basics of different TWR methods used in time-based wireless localization systems were addressed. Concerning this, four TWR schemes were carefully chosen so that they can be represented as the most fundamental TWR methods in the literature. In principle, the rest of the TWR schemes (Section 3.1.2.5) described in the academic papers were built upon the expressed four TWR methods in this section, i.e., the remaining TWR are generally derived from these four techniques. The mentioned four TWR methods are the SS-TWR, SDS-TWR, AltDS-TWR, and ADS-TWR. The brief introductions to each scheme are explained in the forthcoming subsections.

3.1.2.1 (Simple) SS-TWR

SS-TWR is generally regarded as the basic scheme for all available TWR methods in literature. As described in Figure 3.3 (the shaded area), the operation of SS-TWR comprises measuring the round-trip delay of a signal in device A and a response (reply) time in device B. Hence, the round-trip time of the signal for SS-TWR [33, 86] is:

$$t_{roundA} = 2 T_{tof} + t_{replyB} \quad (3.1)$$

where $t_{roundA} = \tau_{ARx} - \tau_{ATx}$ is the true round-trip time of a signal measured at the local clock of Device A and $t_{replyB} = \tau_{BTx} - \tau_{BRx}$ is the true reply time of a signal measured at the local clock of Device B (Figure 3.3). τ_{ATx} and τ_{ARx} are the transmitted and received timestamps measured at Device A, and τ_{BTx} and τ_{BRx} are the transmitted and received timestamps measured at Device B, respectively.

In specific, the round-trip time of a signal (t_{roundA}) is measured within the local clock of device A by subtracting two timestamps, which are the transmitting timestamp of the initiator (τ_{ATx}) and the receiving timestamp from the responder (τ_{ARx}) as depicted in Figure 3.3). Similarly, the reply time (t_{replyB}) is achieved from the difference between two timestamps of the local clock in device B ($\tau_{BTx} - \tau_{RTx}$). Therefore, the TOF for the SS-TWR scheme can be expressed as:

$$T_{tof} = \frac{1}{2}(t_{roundA} - t_{replyB}) \quad (3.2)$$

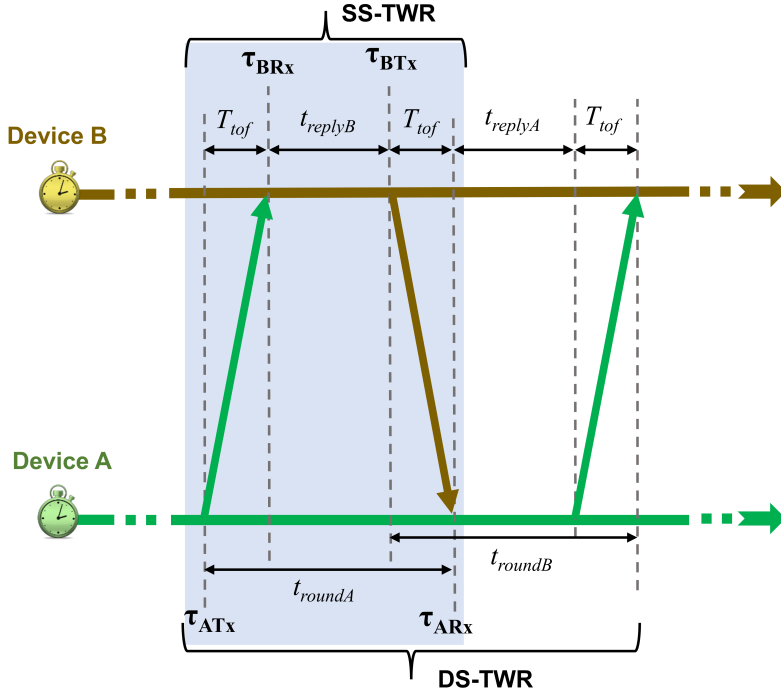


Figure 3.3: Illustration of single- and double-sided TWR methods. The image was reproduced with slight modification from [175] (©2019 IEEE. Reprinted, with permission.).

In practice, the estimated TOF possess errors due to the clock drifts in the finite crystal tolerance of the devices [33, 96, 97]. This error typically increases when the reply time in SS-TWR takes longer as it is verified in Section 3.4.

3.1.2.2 SDS-TWR

To compensate for the ranging error due to clock drifts in SS-TWR as defined in the previous subsection, the DS-TWR technique is conventionally utilized [98]. DS-TWR is an extension of SS-TWR in which two round-trip time measurements are used to give the estimated TOF value. There are several DS-TWR techniques and SDS-TWR is the most widely used DS-TWR in literature. The method is originally adopted in the IEEE802.15.4-2011 standard to demonstrate the DS-TWR technique [33]. The two round-trip times for the SDS-TWR [33, 86] (Figure 3.3) can be represented as:

$$t_{roundA} = 2 T_{tof} + t_{replyB} \quad (3.3a)$$

$$t_{roundB} = 2 T_{tof} + t_{replyA} \quad (3.3b)$$

where t_{roundA} and t_{roundB} are the real (true) round-trip times of a signal measured at Device A and B, respectively. t_{replyA} and t_{replyB} are the real (true) reply times or response times measured at Device A and B, respectively.

By combining Equation (3.3a) and (3.3b), the TOF for SDS-TWR can be defined:

$$T_{tof} = \frac{1}{4}((t_{roundA} - t_{replyA}) + (t_{roundB} - t_{replyB})) \quad (3.4)$$

In general, the ranging time for a single measurement in SDS-TWR or simply DS-TWR is approximately twice as long as the SS-TWR due to the additional response (reply) time as illustrated in Figure 3.3.

3.1.2.3 AltDS-TWR

The key restriction in the SDS-TWR method is that symmetrical response times are expected for the scheme. The AltDS-TWR method is built to resolve this constraint. In fact, the AltDS-TWR method [149] has the same basic concept as the SDS-TWR method from Section 3.1.2.2 of Equations (3.3a) and (3.3b) (Figure 3.3):

$$t_{roundA} = 2 T_{tof} + t_{replyB} \quad (3.5a)$$

$$t_{roundB} = 2 T_{tof} + t_{replyA} \quad (3.5b)$$

However, the AltDS-TWR method is accomplished by multiplying Equations (3.5a) and (3.5b), which is in contrast to combining the two equations in SDS-TWR, as:

$$t_{roundA} \cdot t_{roundB} = (2 T_{tof} + t_{replyB}) \cdot (2 T_{tof} + t_{replyA})$$

The T_{tof} for AltDS-TWR scheme, which was originally introduced in [149], is obtained by simplifying the equation as follows:

$$T_{tof} = \frac{t_{roundA} \cdot t_{roundB} - t_{replyA} \cdot t_{replyB}}{t_{roundA} + t_{replyA} + t_{roundB} + t_{replyB}} \quad (3.6)$$

The comprehensive derivation of the formula is given in the original paper of AltDS-TWR [149]. The goal of AltDS-TWR is to reduce the errors in the range estimation even for very long response delays in the presence of uncorrected clock frequency offset. In fact, the formulation of AltDS-TWR method was adopted to demonstrate the DS-TWR scheme in the IEEE 802.15.4z-2020 standard [98], which is the latest amendment by the time of writing this chapter. This implied that SDS-TWR method (i.e., included in IEEE 802.15.4-2011 standard [33]) was replaced with the AltDS-TWR in the amendment for the demonstration of the DS-TWR scheme.

3.1.2.4 ADS-TWR

The drawback of the Symmetric Doubled-Sided (SDS)- and AltDS-TWR methods is that the scheme requires at least three ranging messages of which two response times are included in the calculation of the distance. In general, the delay in reply time (typically in the order of microseconds) is relatively longer than the delay in the TOF (typically in the order of nanoseconds). The ADS-TWR was designed to improve the ranging latency of the aforementioned DS-TWR without the loss of the system performance [99]. Therefore, the round trip times for ADS-TWR (Figure 3.4) can be formulated as:

$$t_{roundA} = 2 T_{tof} + t_{replyB} \quad (3.7a)$$

$$t_{roundB} = 2 T_{tof} \quad (3.7b)$$

The T_{tof} for ADS-TWR can be obtained by adding Equations (3.7a) and (3.7b):

$$T_{tof} = \frac{1}{4}(t_{roundA} + t_{roundB} - t_{replyB}) \quad (3.8)$$

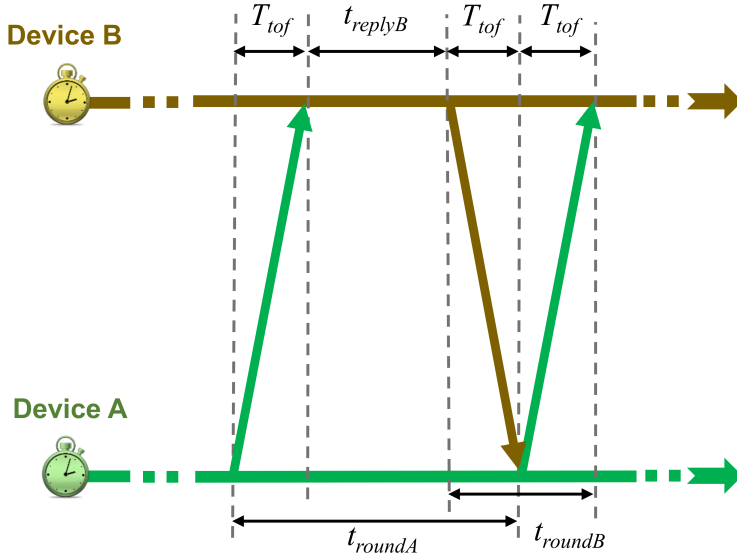


Figure 3.4: Illustration of the asymmetric double-sided TWR method.

In brief, the primary motivation behind the design of the ADS-TWR scheme is to minimize the operation of the ranging time while maintaining the same level of performance and efficiency as SDS-TWR or AltDS-TWR. In ADS-TWR scheme, Device A does not have a separate response time. Hence, the round trip time for Device B is equivalent to simply doubling the TOF, which is in the order of nanoseconds compared to the order of microseconds in reply time.

3.1.2.5 Further TWR Schemes in Literature

The most fundamental TWR techniques in UWB-based localization systems are described in Section 3.1.2.1 to 3.1.2.4. Indeed, there are several other TWR schemes in literature that are not presented in this section. However, the remaining TWR schemes are mainly derived from the presented TWR techniques given in this section. In general, more than three messages are necessary to exchange in the rest of TWR schemes, i.e apart from the TWR schemes presented in this section.

This section acknowledges the existence of other TWR techniques not specifically addressed in this chapter and their important contributions to the development of the field in each specific application area. However, the detailed schemes are not presented here because the author assumed that it is quite adequate to evaluate the general system performance of TWR based only on the presented four techniques. Moreover, there was a misconception in the earlier developments of TWR regarding the SDS-TWR method. Hence, SDS-TWR becomes kind of a de facto standard for bench-marking whenever a new TWR technique was developed [13, 114, 122, 127, 148, 149]. The pitfall of the SDS-TWR was demonstrated in our previous works [130, 172] and further analyses were made Section 3.4. As we'll see in Section 3.4, AltDS-TWR outperforms the SDS-TWR in many tested conditions. Therefore, the remaining extensions of the TWR schemes will likely be the same performance level of AltDS-TWR while requiring a longer ranging time because more message exchanges are obliged in the scheme. In consequence, AltDS-TWR was adopted as the demonstration of DS-TWR scheme in IEEE 802.15.4z-2020 standard [98].

As already mentioned before in above, the rest of TWR methods available in literature, which are excluded in this chapter, are: SDS-TWR with unequal reply-time method [127], TWR using estimated frequency offsets [148], SDS-TWR with multiple acknowledgments [114], asynchronous Double Two-Way Ranging (D-TWR) [122], burst-mode SDS-TWR [13], parallel DS-TWR [39], and passive extended DS-TWR [92]. Moreover, a network-based TWR technique was recently proposed in [233, 234] for the purpose of efficient ranging in a large-scale network to reduce the signal overhead produced by classical TWR algorithms. In addition to the use-case of estimating distances or TOF in wireless communications, TWR has also been commonly utilized in network-wide clock-synchronization algorithms for WSN [29, 53, 67, 128].

3.1.3 Conventional TOF Error Estimation Approach

In general, the TWR scheme addressed in this section eliminates the requirement of synchronization in wireless communication systems (Section 3.1.2) when estimating

the ranges(or) distances between transceivers. However, the frequency offset of a crystal oscillator utilized in the transceivers is imperfect in the real world. This is more particular when a low-cost oscillator is applied in the transceivers' hardware [33, 97]. This frequency offset introduces error in the time measurement of TOF resulting in errors to ranging accuracy of TWR methods. Typically, the unit for the frequency offset of a crystal oscillator is presented in parts per million (ppm) [96]. Hence, low-cost and low-quality crystal oscillators have large ppm ratings while a small ppm rating requires a high-quality oscillator that is, in general, more expensive for implementation. IEEE 802.15.4 standard specifies that an adequate rating for low-cost Wireless Personal Area Network (WPAN) devices to be ± 20 ppm [33].

As a consequence, the existing traditional TOF error-estimation technique described in IEEE 802.15.4-2011 standard is explicitly established on clock-drift error effects in TWR technique [33] (pp. 258–275). Based on the approach originally proposed in Reference [86] and approved in Reference [33], the fundamental model can be simplified in the following equations. The method was later widely practiced and studied in many research works [12, 13, 99, 122, 149]. The corresponding idea related to the traditional approach is shown in Figure 3.3. The formulation of the set of equations given in the following is inspired by the work in [149].

$$\hat{t}_{roundA} = (1 + e_A)t_{roundA} \quad (3.9a)$$

$$\hat{t}_{replyA} = (1 + e_A)t_{replyA} \quad (3.9b)$$

$$\hat{t}_{roundB} = (1 + e_B)t_{roundB} \quad (3.9c)$$

$$\hat{t}_{replyB} = (1 + e_B)t_{replyB} \quad (3.9d)$$

where \hat{t}_{roundA} and \hat{t}_{roundB} are the estimated round-trip times of Devices A and B, respectively. t_{roundA} and t_{roundB} are the real (true) round-trip times of Devices A and B, respectively. \hat{t}_{replyA} and \hat{t}_{replyB} are the estimated replied times of Devices A and B, respectively. t_{replyA} and t_{replyB} are the real (true) replied times of Devices A and B, respectively. e_A and e_B are the clock-drift errors introduced by Devices A and B, which are expressed in ppm, respectively.

It is conventionally assumed that the value of TOF is negligibly small compared to the reply times in TWR, i.e., $T_{t0f} \ll t_{replyA}$ or $T_{t0f} \ll t_{replyB}$. The reason is also obvious since the reply times in TWR are in the order of hundreds of microseconds up to several milliseconds [33] (Section 3.4). In contrast, the standard values of T_{t0f} in TWR are in the order of nanoseconds [33, 96].

The conventional TOF error estimation model defined in IEEE 802.15.4-2011 applies clock drifts as the only dominant error for analyzing the TOF errors among different TWR techniques [33]. However, the use-case of the mentioned conventional model is inadequate and imperfect, especially when the qualitative scores of closely related TWR methods are necessary to identify. For instance, the dilemma of specifying a distinguishable score between two similar TWR methods using the conventional model can be observed in [149]. This motivated us to explore a bit further in this area and ended up with the TEEM model proposed in this chapter (Section 3.2.2), which is, indeed, built upon the mentioned IEEE standard.

3.1.4 Related Work

To the best of the author's knowledge, there weren't too many papers that discussed the modification of the existing TOF error estimation besides the clock drift errors in TWR. In [132], an error analysis based on a linear algebra approach was performed for a cooperative positioning system that used GPS and TWR technique in the system implementation. The overall idea is interesting because the approach described in the paper can be used as a transition mechanism that bridges both the indoor and outdoor localization systems. In other words, the described system can be used as a seamless location system using UWB (indoor) and GPS (outdoor). However, the error analysis carried out in that work for the TWR scheme is too superficial and shallow. Firstly, the authors simply assumed that clock-drift errors are compensated just by using the SDS-TWR scheme, which is not true as we'll verify in Section 3.4. Secondly, the authors also assumed that the measurement errors are purely white Gaussian noises. The above-mentioned hypothesis is not sufficiently concrete enough to reveal the actual TOF error in the TWR method.

In addition, the error model and protocol exclusively for the Parallel Double-Sided Two-Way Ranging (PDS-TWR) scheme were presented in [39]. The authors outline two sources of error in TWR defined as the ranging phase and the localization phase, in which the presented model in the paper is devoted to the former case. Afterward, the discussion regarding the variation of ranging error upon symmetric and quasi-symmetric cases was examined. In their work, they proved that PDS-TWR is a better TWR method compared to the SDS-TWR scheme. However, it is unclear in which criteria the error are defined in their proposed model. To be specific, the error term is vaguely defined as the difference between a duration measured with the PHY of a node and a real duration (ppm). Moreover, the given error model described in the paper is not generic. In contrast, it is strictly designed only for the PDS-TWR scheme. In addition, the approach is also absolutely based on the concept that clock drifts are the dominant errors in the presented model.

3.2 TOF Error Estimation Model (TEEM)

Accordance with common practice specified in the IEEE 802.15.4-2011 standard [33], the clock drifts due to the frequency offset of the oscillator are the only dominant errors in TOF error-estimation for TWR technique. However, the mentioned model is inadequate for analyzing the qualitative performance scores among various TWR methods. For instance, the existing model cannot identify a clear performance difference between two closely related TWRs, i.e. SDS-TWR and AltDS-TWR. The evaluation results presented in [149] further confirmed the mentioned case. Besides, we found out that AltDS-TWR is robust and efficient even in case such as the delay gap (i.e., the level of asymmetry) between two reply times are relatively large (Section 3.4). The mentioned scenario cannot be explained using the aforementioned conventional clock-drift model. In contrast, the TEEM model, which is the presented methodology in this section, has the ability to clarify the mentioned issue with a clear indication.

In fact, TEEM for evaluation TOF errors in TWR methods is an extended version of the IEEE 802.15.4-2011 standard [33] (pp. 258–275). Regarding this, a delay in message delivery (Section 3.2.1), i.e. in addition to clock drifts, is considered as a crucial characteristic in TEEM. Indeed, this delay is critical and fundamental, because the impact of TOF error in TWR is influenced not only by clock drift in the oscillator but also by other error sources in the system [41, 67, 216]. Those sources of error include propagation time delay [41], transmission time delay, receiving time delay [216], etc. This implied that the mentioned delay is typically caused by the antenna, Printed Circuit Board (PCB), and other external and internal electronic components used in the implementation of the transceivers and the localization system itself.

Thus, this section is composed as follows: the problem statement and sketch of various error sources were outlined in Section 3.2.1. Then, the foundation of the set of equations regarding the presented TEEM model for TWR schemes were explained in Section 3.2.2. Subsequently, the extension of state of the art TWR methods for TOF error estimation based on TEEM model were formulated in Section 3.2.3. Finally, the analytical comparison of four TWR methods was examined in Section 3.3.

3.2.1 Problem Statement

As already mentioned several times in this chapter, TWR methods are great in distance estimation between two wireless transceiver devices without the need to use clock synchronization. However, clock-drift errors due to frequency offset in oscillators introduced errors in real-world measurement and degraded the ranging accuracy (i.e., indeed, it depends on the quality of the oscillator as well). Therefore, the IEEE 802.51.4-2011 standard specified the mentioned offset value of WPAN for practical used case as ± 20 ppm [33]. Consequently, the conventional TOF error approach, represented in IEEE 802.51.4-2011, specifically tackles clock drifts as the only dominant error source in wireless ranging process using TWR schemes.

However, the estimation of T_{t0f} in TWR scheme is fundamentally disturbed by numerous sources of possible delays that cause errors in time-based wireless communications [130, 172]. These delay sources can be categorized as follows:

- **Propagation Time Delay (PTD):** The propagation time generally means the duration of time taken for a transmitted signal or message to arrive at the destined receiver on a wireless channel [216]. PTD happens in two circumstances [41]: Firstly, when there is a barrier between transceivers that completely blocked or obstructed the direct path signal. In this case, only the reflected signals from the mentioned transmitter are able to reach to the receiver. Secondly, when the transmitted signal has to traverse through obstacles, in which the value of the refractive index differs based on the types of materials the signal travels through. In short, PTD happens when the signal propagation path from the transmitter has been obstructed by obstacles or reflected from nearby objects.
- **Transmission Time Delay (TTD):** This delay is mainly influenced by the time it takes to build a message at the application layer (software and implementation), the time it takes for a message to access the MAC layer depending on

the applied protocols, and the time it takes to send and receive the messages in the PHY layer [67, 216]. In brief, the TTD delay involves the delays produced by the physical antennas of the transceivers, the PCB design as well as all the electronic components utilized in the implementation of the system.

- **Receiving Time Delay (RTD):** Similar to TTD, this delay occurs in the receiving side of the transceivers due to the time taken for achieving a message at the PHY, MAC, and application layers [67, 216].
- **Preamble Accumulation Time Delay (PATD):** This delay mainly concerns with an UWB-based localization system that used coherent receivers [141]. PATD is the length of time needed for a coherent receiver to detect a specific preamble sequence and to discover the SFD sequence in the PHY layer [46]. PATD is normally affected by the occurrence of multi-path signals in the communications [25] and quick frame arrival time of the signal [33] when the measurement is conducted in a relatively short range [46]. The mentioned delay is more apparent in a scenario where the reflected signals of the transmitter reach the receivers within the chip period of the first path signal [25].

For simplicity without losing generality, it is possible to model the above-mentioned T_{tow} estimation error due to delays in wireless communications using a simple linear equation. By taking SS-TWR scheme as an example (Figure 3.3), the total delay within a single round-trip time of SS-TWR can be expressed as:

$$\begin{aligned}\Delta_{ABA} &= \sum_{i=1}^n (\text{AB_Delay}_i + \text{BA_Delay}_i) \\ &\approx 2 \cdot \sum_{i=1}^n \text{Delay}_i \\ &\approx 2 \cdot (\text{TTD} + \text{PTD} + \text{PATD} + \text{RTD})\end{aligned}\tag{3.10}$$

where Δ_{ABA} is the cumulative delay within a single round-trip-time of the transmitted signal in SS-TWR scheme, which is measured using the local clock of Device A (Figure 3.3). That implied that the mentioned total delay refers to the total time it takes for a signal, which is transmitted from Device A to B and returns to the original Device A. The *Delay* in the equation refers to one or more of the above-listed individual delays, namely TTD, PTD, PATD, and RTD. n in (3.10) represents the total number of possible delays concerning the round-trip delay error of the SS-TWR scheme. There is a constant ‘2’ in Equation (3.10) because two-way traveling routes of a signal are necessary for a single measurement in the SS-TWR scheme. In this particular case, the delays that occurred in the measurement for the first route (Device A to B), and for the second route (Device B to A) are assumed to be the same.

Concerning this, the absolute and relative errors of the total delay defined in Equation (3.10) for the single round-trip-time of SS-TWR (shaded area in Figure 3.3) can be defined as follow [91] (p. 62):

$$\epsilon = \text{estimated value} - \text{exact value} = \hat{t}_{roundA} - t_{roundA}\tag{3.11}$$

$$\xi = \frac{\text{absolute error}}{\text{exact value}} = \frac{\epsilon}{t_{\text{round}A}} = \frac{\hat{t}_{\text{round}A} - t_{\text{round}A}}{t_{\text{round}A}} \quad (3.12)$$

where ϵ and ξ are the absolute error and relative error of the cumulative delay (Δ_{ABA}).

Suppose the above-mentioned absolute error (ϵ) in the measurement process is only influenced by the cumulative delay (Δ_{ABA}) defined in (3.10), then the estimated round-trip-time for SS-TWR turns into $\hat{t}_{\text{round}A} = t_{\text{round}A} + \Delta_{ABA}$. If we substitute this value into Equation (3.12), the relative error for the cumulative delay within a single-round-trip time of SS-TWR can be defined as:

$$\xi_{ABA} = \frac{\Delta_{ABA}}{t_{\text{round}A}} \quad (3.13)$$

where ξ_{ABA} is the relative error of the total delay for SS-TWR scheme in a single-round-trip time of a transmitted signal, in which the value is measured at the local clock of Device A (shaded area in Figure 3.3). The relative error is a ratio (unit-less), which is sometimes defined as a percent error by multiplying the value with 100 %.

By definition, the relative error in (3.13) (ξ_{ABA}), i.e., the cumulative error within the round-trip time delay of SS-TWR scheme, is equal to zero if there is no delay ($\Delta_{ABA} = 0$) between the two transceivers as defined in Equation (3.10). Otherwise, the relative error (ξ_{ABA}) becomes the ratio obtained from the summation of all the relevant delays along the path of the signal's round-trip time and its actual value in the SS-TWR scheme.

In the same manner, the relative delay errors for the DS-TWR scheme can be defined. Since the DS-TWR (Figure 3.3 requires two round-trip times in their formulation (Section 3.1.2.2 and 3.1.2.3), two separate representation of relative errors are required to define namely ξ_{BAB} and ξ_{ABA} .

3.2.2 Novel TOF Error-Estimation Model (TEEM)

TEEM was proposed in our previous work [130, 172] to overcome the dilemmas caused by the conventional approach [33] (i.e, the model built specifically upon clock-drift error due to the oscillator's frequency offset). In consequence, TEEM can give a distinctive performance metric for TWR methods, which possess similar characteristics. Regarding this, TEEM composed of both the clock-drift error and the relative error due to a signal's round-trip time delay in TWR schemes as described in Section 3.2.1. The analytical formulas of TEEM concerning DS-TWR technique, in which SS-TWR is already included, are given in the following. This is in reference to Figure 3.3.

$$\hat{t}_{\text{round}A} = (1 + e_A + \xi_{ABA}) t_{\text{round}A} \quad (3.14a)$$

$$\hat{t}_{\text{reply}A} = (1 + e_A) t_{\text{reply}A} \quad (3.14b)$$

$$\hat{t}_{\text{round}B} = (1 + e_B + \xi_{BAB}) t_{\text{round}B} \quad (3.14c)$$

$$\hat{t}_{\text{reply}B} = (1 + e_B) t_{\text{reply}B} \quad (3.14d)$$

where ξ_{ABA} and ξ_{BAB} (as introduced in Section 3.2.1) are the relative error caused by the cumulative delays in the round-trip time of a signal measured at Device A or

B respectively. Similar to conventional approach (Section 3.1.3), e_A and e_B are the clock-drift errors (expressed in ppm) produced by Devices A and B respectively.

Since ξ_{ABA} and ξ_{BAB} correspond to the relative error of the (total) cumulative delay during a signal's round trip of a TWR scheme, their effects are sufficient to represent in the estimated round-trip time (\hat{t}_{roundA} Equation (3.14a) and \hat{t}_{roundB}) alone as given in Equations (3.14a) and (3.14c). Hence, similar to the conventional clock-drift error approach described in Section 3.1.3, the estimated reply time (\hat{t}_{replyA} and \hat{t}_{replyB}) can remain unchanged in Equations (3.14b) and (3.14d). The reason is that the delay affected to reply time has been already accounted for in the calculation when the cumulative delay of the round-trip-time was observed.

It should be pointed out that ξ_{ABA} and ξ_{BAB} in Equations (3.14a) and (3.14c) (Section 3.2.1), are entirely different parameters from the conventional clock-drift errors e_A and e_B , which are susceptible to the finite frequency offset of the oscillators' clock [33]. Indeed, ξ_{ABA} and ξ_{BAB} are the relative errors in TWR due to delays in the practical signal's measurement, which is in addition to the clock-drift error.

3.2.3 Extended State-of-the-Art TWRs for TOF Error Estimation

This section briefly gave the analytical expression regarding the extension of each evaluated four TWR techniques for TOF error estimation using TEEM [130, 172]. For the sake of clarification in contrast to conventional models, the analytical representations of each TWR method for the conventional approach [33] were also provided.

3.2.3.1 Extended SS-TWR Method for TOF Error Estimation

For the extension of the SS-TWR, the predicted value of TOF for the SS-TWR can be formulated based on the true theoretical value using Equation (3.2) as:

$$\hat{T}_{tof} = \frac{1}{2}(\hat{t}_{roundA} - \hat{t}_{replyB})$$

where \hat{T}_{tof} is the estimated value of TOF in the system.

Thus, the difference between the predicted TOF and the true TOF for SS-TWR can be analytically defined as:

$$\hat{T}_{tof} - T_{tof} = \frac{(\hat{t}_{roundA} - \hat{t}_{replyB})}{2} - \frac{(t_{roundA} - t_{replyB})}{2}$$

The equation is turned into the following by using Equations (3.14a) and (3.14d):

$$\hat{T}_{tof} - T_{tof} = \frac{1}{2}[(e_A + \xi_{ABA})t_{roundA} - e_B t_{replyB}]$$

Substituting t_{roundA} from Equation (3.1) provides:

$$\hat{T}_{tof} - T_{tof} = \frac{1}{2}[2T_{tof}(e_A + \xi_{ABA}) + (e_A - e_B + \xi_{ABA})t_{replyB}]$$

This drives the TOF error for SS-TWR into:

$$\hat{T}_{t_{of}} - T_{t_{of}} = T_{t_{of}}(e_A + \xi_{ABA}) + \frac{1}{2}(e_A - e_B)t_{replyB} + \frac{1}{2}\xi_{ABA}t_{replyB} \quad (3.15)$$

For the purpose of clarification, the TOF error based on the conventional method for SS-TWR using Equations (3.9a) and (3.9d) is:

$$\hat{T}_{t_{of}} - T_{t_{of}} = T_{t_{of}}e_A + \frac{1}{2}(e_A - e_B)t_{replyB} \quad (3.16)$$

Suppose $\xi_{ABA} = 0$ in (3.15), then the TEEM-based analytical model in Equation (3.15) broke down into the conventional model expressed in Equation (3.16). This explains that the TOF error achieved by using TEEM shares the basic characteristics of the conventional model defined in [33] regarding SS-TWR.

3.2.3.2 Extended SDS-TWR Method for TOF Error Estimation

In the same manner as expressed in Section 3.2.3.1, if Equation (3.4) is applied in the TEEM's Equations (3.14a)–(3.14d), and by substituting t_{roundA} and t_{roundB} with Equations (3.3a) and (3.3b), the TOF error between the predicted and the real value for SDS-TWR yields as follows:

$$\begin{aligned} \hat{T}_{t_{of}} - T_{t_{of}} = & \frac{1}{2}T_{t_{of}}(e_A + e_B + \xi_{BAB} + \xi_{ABA}) + \frac{1}{4}(e_A - e_B)(t_{replyB} - t_{replyA}) \\ & + \frac{1}{4}(\xi_{BAB}t_{replyA} + \xi_{ABA}t_{replyB}) \end{aligned} \quad (3.17)$$

For the purpose of clarification, the TOF error for the SDS-TWR method achieved from the conventional model using Equations (3.9a)–(3.9d) is:

$$\hat{T}_{t_{of}} - T_{t_{of}} = \frac{1}{2}T_{t_{of}}(e_A + e_B) + \frac{1}{4}(e_A - e_B)(t_{replyB} - t_{replyA}) \quad (3.18)$$

Akin to the aforementioned SS-TWR, Equation (3.17) turn into (3.18), in case no delay in message delivery for SDS-TWR is feasible, i.e., $\xi_{BAB} = 0$ and $\xi_{ABA} = 0$. This illustrates the backward compatibility of TEEM in SDS-TWR scheme.

3.2.3.3 Extended AltDS-TWR Method for TOF Error Estimation

By using Equation (3.6) and Equations (3.14a)–(3.14d) from TEEM, the TOF error between the predicted and true value for AltDS-TWR due to clock drifts and delay can be formulated as given below:

$$\begin{aligned} \hat{T}_{t_{of}} - T_{t_{of}} = & \frac{\hat{t}_{roundA} \cdot \hat{t}_{roundB} - \hat{t}_{replyA} \cdot \hat{t}_{replyB}}{\hat{t}_{roundA} + \hat{t}_{replyA} + \hat{t}_{roundB} + \hat{t}_{replyB}} \\ - & \frac{t_{roundA} \cdot t_{roundB} - t_{replyA} \cdot t_{replyB}}{t_{roundA} + t_{replyA} + t_{roundB} + t_{replyB}} \end{aligned} \quad (3.19)$$

By assuming $T_{t0f} \ll t_{replyA}$ (or) t_{replyB} (Section 3.3.1) and simplifying the equation, the TOF error for AltDS-TWR becomes:

$$\hat{T}_{t0f} - T_{t0f} \approx \frac{C_1 t_{replyA} t_{replyB}}{C_2 t_{replyA} + C_3 t_{replyB}} \quad (3.20)$$

where $C_1 = \xi_{BAB}(1 + e_A) + \xi_{ABA}(1 + e_B) + \xi_{BAB}\xi_{ABA}$, $C_2 = 2 + e_A + e_B + \xi_{BAB}$ and $C_3 = 2 + e_A + e_B + \xi_{ABA}$. The formula derivation of the equation is given in Appendix A.3. It is also publicly available in [173].

For the purpose of clarification, the TOF error regarding the conventional model from Equations (3.9a)–(3.9d) for the AltDS-TWR method [149] is:

$$\hat{T}_{t0f} - T_{t0f} = e_A \cdot T_{t0f} \text{ (or)} \quad \hat{T}_{t0f} - T_{t0f} = e_B \cdot T_{t0f} \quad (3.21)$$

Concerning this, the solution in Equation (3.20) equals zero if we assumed that there is no delay in message delivery, i.e., $\xi_{BAB} = 0$ and $\xi_{ABA} = 0$. This means that the theoretical true TOF error for AltDS-TWR in TEEM is related only to the actual T_{t0f} , similar to the same expression as in Equation (3.21). The core reason is that T_{t0f} is assumed to be negligible ($T_{t0f} \ll t_{replyA}$ (or) $T_{t0f} \ll t_{replyB}$) when Equation (3.20) is formulated [173], as the formula derivations for AltDS-TWR in three scenarios are given in appendices A.1, A.2, and A.3.

3.2.3.4 Extended ADS-TWR Method for TOF Error Estimation

For the extended ADS-TWR using TEEM, the TOF error can be defined as in the following if we substitute Equations (3.14a), (3.14c) and (3.14d) into Equation (3.8), and by replacing the t_{roundA} and t_{roundB} with Equations (3.7a) and (3.7b):

$$\begin{aligned} \hat{T}_{t0f} - T_{t0f} = & \frac{1}{2} T_{t0f} (e_A + e_B + \xi_{ABA} + \xi_{BAB}) + \frac{1}{4} (e_A - e_B) t_{replyB} \\ & + \frac{1}{4} \xi_{ABA} t_{replyB} + \frac{1}{4} \xi_{BAB} t_{ack} \end{aligned} \quad (3.22)$$

where, t_{ack} in Equation (3.22) corresponds to the processing time of sending the auto-acknowledgment signal specifically for the ADS-TWR method (Section 3.1.2.4). More precisely, the second round-trip-time in ADS-TWR (Equation (3.7b)) omitted the traditional reply time. Instead, a feature similar to auto-acknowledgment was applied in the scheme [99]. We stressed that t_{ack} is likely to be smaller than the traditional reply time in TWR according to the numerical evaluation results given in the original paper [99]. However, the verification of the condition in a practical environment cannot be done due to the lack of such feature in the available state of the art UWB hardware in the market at the time of writing this chapter.

For clarification purpose, the conventional TOF error for the ADS-TWR method using Equations (3.9a), (3.9c) and (3.9d) is:

$$\hat{T}_{t0f} - T_{t0f} = \frac{1}{2} T_{t0f} (e_A + e_B) + \frac{1}{4} (e_A - e_B) t_{replyB} \quad (3.23)$$

Similar to the aforementioned three TWR methods, Equation (3.22) will reduce to (3.23) if it is assumed that ξ_{ABA} and ξ_{BAB} are approximated into zero.

3.3 Comparison of TWR Methods by Analytical Studies

In this section, the comparative study of TOF error among different TWR methods was examined analytically. The analytical results achieved from this section were further investigated using numerical and experimental evaluation in Section 3.4. In order to give comprehensive results in the analytical study, three types of assumptions were defined and categorized for the evaluations in Section 3.3.1. Based on the defined assumptions, the comparative analyses of four TWRs were conducted for each assigned assumption in Section 3.3.2–3.3.4.

3.3.1 Error-Model Classification in Three Types

Three types of assumptions were established to evaluate the comparative analyses of TWR methods systematically and uniformly in this section as outlined in Table 3.1. The mentioned three assumptions as detailed in the subsequent paragraphs are: (i) Type I representing to an ideal case (Sections 3.3.2), (ii) Type II exemplifying to a special case (Sections 3.3.3), and (iii) Type III corresponded to a typical case (Sections 3.3.4) in the evaluation. In each of the mentioned three cases, T_{tof} is assumed to be negligible when its value is compared to the reply time (t_{replyA} and t_{replyB}) in accordance with the conventional realization [33], i.e., $T_{tof} \ll t_{reply}, t_{replyA}, t_{replyB}$. The reason is that the magnitudes of T_{tof} are in the order of nanoseconds, while the magnitudes of reply times are in the order of hundreds of microseconds to several milliseconds as mentioned before. The three types of assumptions (Table 3.1) are:

Type I Assumption: corresponds to an ideal case in the evaluation. In Type I, it is assumed that $T_{tof} \ll t_{reply}$, $e_A = e_B = e = 0$, and $t_{replyA} = t_{replyB} = t_{reply}$. In brief, the ideal case in Type I assume that firstly, there are no clock-drift errors in the distance measurement between two transceivers in UWB and secondly, the two reply times are symmetric or exactly the same in DS-TWR.

Type II Assumption: represents a special case in the evaluation. In Type II, it is assumed that $T_{tof} \ll t_{reply}$ and $t_{replyA} = t_{replyB} = t_{reply}$. In brief, the special case in Type II assumes that the clock-drift error does exist in the distance measurement between two transceivers. However, the reply times in DS-TWR are assumed to be symmetric or the same.

Type III Assumption: represents a typical case in the evaluation. In Type III, it is assumed that $T_{tof} \ll t_{reply}$ and $t_{replyA} \neq t_{replyB}$. In the typical case in Type III assumed that not only does clock-drift error exist in the distance measurement between the transceivers, but also the reply times DS-TWR are different or varied.

Table 3.1: Three types of assumption for TOF Errors Classification (©2018 IEEE. Reprinted, with permission, from [172]).

Types: Cases	Round-Trip Delay	Clock Drifts	Reply Time
Type I: Ideal	$\xi = \xi_{BAB} = \xi_{ABA}$	$e_A = e_B = 0$	$t_{replyA} = t_{replyB}$
Type II: Special	ξ_{BAB}, ξ_{ABA}	e_A, e_B	$t_{replyA} = t_{replyB}$
Type III: Typical	ξ_{BAB}, ξ_{ABA}	e_A, e_B	$t_{replyA} \neq t_{replyB}$

3.3.2 Comparison of TWR Methods in Ideal Case (Type I)

For the ideal case, it can be written as $\xi_{BAB} = \xi_{ABA} = \xi$, and $t_{replyA} = t_{replyB} = t_{reply}$ in accordance with the Type I assumption (Section 3.3.1). When the characteristics of Type I assumptions are applied in Equations (3.15), (3.17), and (3.20), the TOF error between the predicted and real value for three TWR methods namely SS-TWR, SDS-TWR, and AltDS-TWR are simplified as below:

$$\hat{T}_{t_{of}} - T_{t_{of}} \approx \frac{1}{2} \xi t_{reply} \quad (3.24)$$

On the contrary, the TOF error between the predicted and true value for ADS-TWR posses a slightly different formulation due to the auto-acknowledgment procedure in the second round-trip time, i.e., $t_{roundB} = 2 \cdot T_{t_{of}}$ (Figure 3.3) as follows:

$$\hat{T}_{t_{of}} - T_{t_{of}} \approx \frac{1}{4} \xi t_{reply} + \frac{1}{4} \xi t_{ack} \approx \frac{1}{2} \xi t_{reply} \quad (3.25)$$

With the exception of ADS-TWR, the TOF error for all three methods was approximated as provided in Equation (3.24). The proof of formula derivation regarding AltDS-TWR is given in Appendix A.1, which is also openly available in Reference [173]. Regarding ADS-TWR given in Equation 3.25, we further stressed that ξt_{reply} and ξt_{ack} are assumed to be the same in ideal case. Theoretically, the acknowledgment time (ξt_{ack}) will be shorter than the usual reply time (ξt_{reply}). Due to the lack of support in the auto-acknowledge procedure introduced by ADS-TWR in the current available UWB hardware in the market, the experimental evaluation based on real-world excluded the method (Section 3.4.2). Expectantly, the above-mentioned assumption regarding ADS-TWR could be fully resolved in the future.

3.3.3 Comparison of TWR Methods in Special Case (Type II)

For the special case, the TOF error between the predicted and actual value for different TWR methods can be expressed as in the following when the characteristics of the Type II assumption are applied to Equations (3.15), (3.17), (3.20), and (3.22):

The TOF error regarding SS-TWR turns into:

$$\hat{T}_{t_{of}} - T_{t_{of}} \approx \frac{1}{2} (e_A - e_B + \xi_{ABA}) t_{reply} \quad (3.26)$$

The TOF error regarding SDS-TWR becomes:

$$\hat{T}_{t_{of}} - T_{t_{of}} \approx \frac{1}{4} (\xi_{BAB} + \xi_{ABA}) t_{reply} \quad (3.27)$$

The TOF error regarding AltDS-TWR turns:

$$\hat{T}_{t_{of}} - T_{t_{of}} \approx \frac{K_A}{K_B} t_{reply} \quad (3.28)$$

where, $K_A = \xi_{BAB}(1 + e_A) + \xi_{ABA}(1 + e_B) + \xi_{BAB}\xi_{ABA}$ and $K_B = 4 + 2(e_A + e_B) + \xi_{BAB} + \xi_{ABA}$. Derivation of the formula is given in appendix A.2 [173].

The TOF error regarding ADS-TWR is:

$$\hat{T}_{t_{of}} - T_{t_{of}} \approx \frac{1}{4}(e_A - e_B + \xi_{ABA})t_{reply} + \frac{1}{4}\xi_{BAB}t_{ack} \quad (3.29)$$

In brief, the conclusion can be drawn by comparing Equation (3.26)–(3.29) that the SDS (3.27) and the Alternative Double-Sided (AltDS) (3.28) outperformed the Single-Sided (SS) (3.26) and ADS-TWR (3.29). More precisely, the TOF error concerning SDS (3.27) and AltDS (3.28) will be approximated into zero (null) if we assume that $\xi_{BAB} = 0$ and $\xi_{ABA} = 0$.

3.3.4 Comparison of TWR Methods in Typical Case (Type III)

For the typical case, the TOF error for the four TWR methods by applying the characteristics of Type III assumption in Equations (3.15), (3.17), (3.20) and (3.22) can be determined as in the following:

The TOF error regarding the SS-TWR turns into:

$$\hat{T}_{t_{of}} - T_{t_{of}} \approx \frac{1}{2}(e_A - e_B + \xi_{ABA})t_{replyB} \quad (3.30)$$

The TOF error regarding the SDS-TWR becomes:

$$\hat{T}_{t_{of}} - T_{t_{of}} \approx \frac{1}{4}(e_A - e_B)(t_{replyB} - t_{replyA}) + \frac{1}{4}(\xi_{BAB}t_{replyA} + \xi_{ABA}t_{replyB}) \quad (3.31)$$

The TOF error regarding the AltDS-TWR is:

$$\hat{T}_{t_{of}} - T_{t_{of}} \approx \frac{C_1 t_{replyA} t_{replyB}}{C_2 t_{replyA} + C_3 t_{replyB}} \quad (3.32)$$

where $C_1 = \xi_{BAB}(1 + e_A) + \xi_{ABA}(1 + e_B) + \xi_{BAB}\xi_{ABA}$, $C_2 = 2 + e_A + e_B + \xi_{BAB}$ and $C_3 = 2 + e_A + e_B + \xi_{ABA}$. The formula derivation is given in appendix A.3 [173].

The TOF error regarding the ADS-TWR becomes:

$$\hat{T}_{t_{of}} - T_{t_{of}} \approx \frac{1}{4}(e_A - e_B + \xi_{ABA})t_{replyB} + \frac{1}{4}\xi_{BAB}t_{ack} \quad (3.33)$$

It can be stated by analytically comparing Equations (3.30)–(3.33) that the AltDS-TWR method in Equation (3.32) outperformed the rest of the three evaluated TWRs and stands out to be the best choice for minimizing TOF errors in typical case (Type III). In specific, the TOF error for AltDS-TWR will be approximated into zero if we assumed that no delay errors were produced in the message delivery, i.e., $\xi_{BAB} = 0$ and $\xi_{ABA} = 0$. On the contrary, the TOF error for the other three TWRs still holds the non-zero values in their respective solutions.

3.4 Simulation and Experimental Evaluation Results

Based on the proposed TEEM, the evaluations of four core TWR methods were conducted in this section. The verification of the results are performed in both numerical simulation (Section 3.4.1) and experimental evaluation in indoor environments (Section 3.4.2). In addition, the systematic pitfalls of the most highlighted TWR techniques in the literature, namely SDS-TWR, was also demonstrated in this section. Conventionally, SDS-TWR is commonly used to illustrate the reduction of TOF error due to clock drifts in wireless ranging systems [33]. Concerning this, we argued that AltDS-TWR is more robust than SDS-TWR in all aspects under several tested conditions.

3.4.1 Numerical Simulation Results

This section explores the verification of the TEEM analytical model given in Section 3.3 for TWR schemes based on the numerical simulation results using Matlab. The parameters used in the simulations included the clock-drift errors (e_A and e_B), the reply time of the transceivers (t_{replyA} and t_{replyB}), and the cumulative relative error due to delays in the signal's round-trip time (ξ_{BAB} and ξ_{ABA}) in TWR scheme, as introduced in Section 3.2.1. Table 3.2 gives the numerical sample values for the aforementioned parameters utilized in the simulations. For the sake of simplicity, we assumed that the two relative errors due to delays (i.e., $\xi = \xi_{BAB} = \xi_{ABA}$) in the round-trip time of a signal are identical in the presented simulation results. In addition, a consistent random seed value for e_A and e_B was applied throughout the simulations. This allows the random generator in Matlab to produce a consistent sequence of random numbers for all evaluated TWR methods.

3.4.1.1 Simulation Results for Ideal Cases (Type I)

The ideal case is the most fundamental simplest condition in the evaluation process of TWR. Yet, the ideal condition is important because it is a reference case that usually defines how the systems under test are expected to behave in theory. The simulation results showed that the TOF errors for all TWRs in the ideal case grew constantly when the round-trip time delay (ξ) and the reply time (t_{reply}) in TWR were increased (Figure 3.5). Most importantly, the simulation result in Figure 3.5 showed that all TWR methods gave identical outcomes in the ideal case (Type I).

Table 3.2: Sample Values of the parameters used in the Numerical Simulations (©2018 IEEE. Reprinted, with permission, from [172]).

Parameters	Symbols	Range of Value	Unit
Relative delay error in round-trip time	$\xi = \xi_{BAB} = \xi_{ABA}$	0:0.025:5	ppm
Reply times in responder device	$t_{reply} = t_{replyB}$	0:5:1000	μs
Clock-drift error (pseudo-random)	t_{replyA} e_A, e_B	0 :11:2200 ± 20 as stated in 802.15.4-2011 [33]	μs ppm

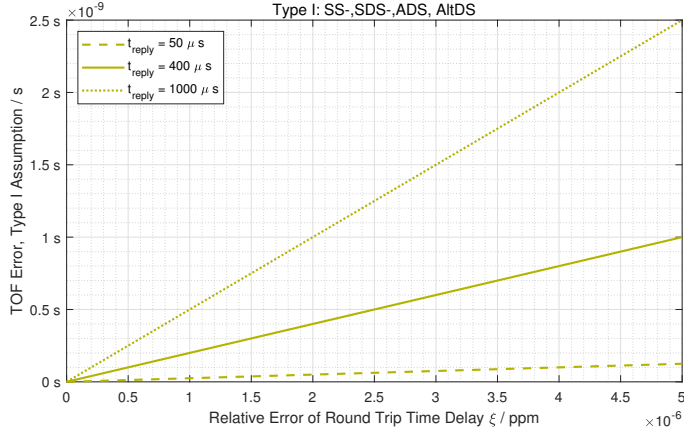


Figure 3.5: TOF error comparison using a Type I assumption (ideal case) as in Equation (3.24) and (3.25) (©2018 IEEE. Reprinted, with permission).

3.4.1.2 Simulation Results for Special Cases (Type II)

For the special case defined as Type II in Section 3.3.1, the comparative outcomes of simulation results for the evaluated four TWRs were given in Figure 3.6. The presented outcomes were based on two main parameters namely the relative error due to delay in round-trip time (ξ) and reply time (t_{reply}). In this particular simulation for Type II,

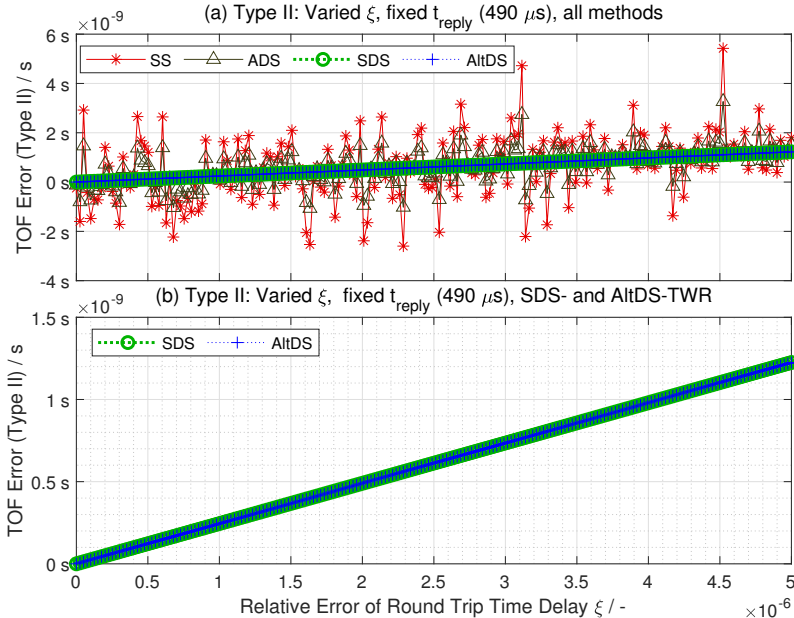


Figure 3.6: Comparison of TOF errors in Type II, (i.e., special case) assumption based on Equations (3.26)–(3.29). (a) TOF error vs. delay (ξ) for four TWRs; and (b) TOF error only for SDS-TWR and AltDS-TWR.

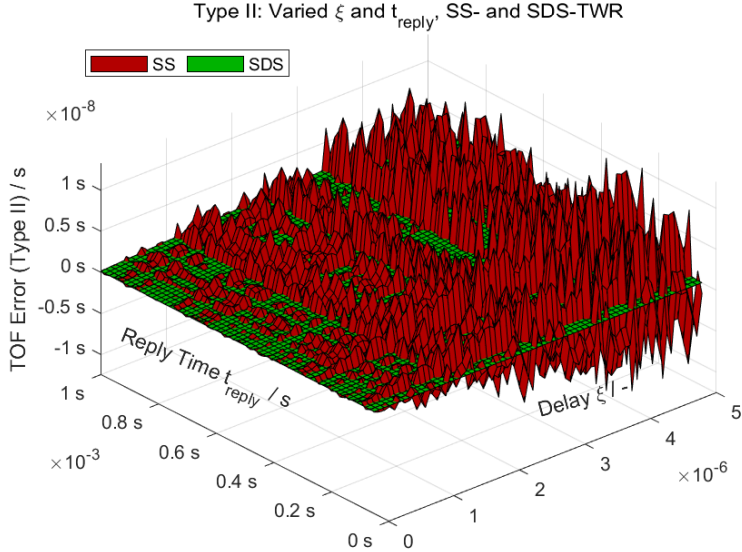


Figure 3.7: 3D representation of TOF error comparison for SS-TWR and SDS-TWR using 65 sample point of parameters defined in Table 3.2.

a constant reply time $t_{\text{reply}} = 490 \mu\text{s}$ was set in order to align with the experimental setup and evaluation presented in (Section 3.4.2). The crucial point in the simulation results of special case (Type II) was the numerical proof of AltDS-TWR method. As depicted in Figure 3.6 (b), AltDS-TWR preserved the exact same performance and score as the SDS-TWR method in the simulation results. In fact, the SDS-TWR has been well known for the base model in many bench-markings due to this unique characteristic and performance in the special case (Type II) when two reply times in DS-TWR schemes are symmetric [13, 114, 122, 127, 148, 149]. Regarding this, we stressed that there were absolutely no differences between the TOF error regarding SDS-TWR and AltDS-TWR in Type II according to the simulation results (Figure 3.6 (b)).

However, the SS-TWR and ADS-TWR showed significant TOF errors in the evaluation compared to AltDS-TWR and SDS-TWR (Figure 3.6 (a)). In contrast, both the AltDS-TWR and SDS-TWR were numerically stable regarding the TOF error estimation in the simulation (Figure 3.6 (b)). In general, the TOF error in all evaluated TWR was perpetually grown when we increased the parameters in the simulation, i.e., the reply time (t_{reply}) and the round-trip time delay (ξ) (Figure 3.6 and Figure 3.7).

In order to see the bigger picture of the special case (Type II) in TWR methods, the 3D graphical representation was given in Figure 3.7. In Figure 3.7, we chose SDS-TWR and SS-TWR as an exemplar for the worst and best cases scenario for the evaluation when the reply time (t_{reply}) and the round-trip time delay (ξ) were varied. Obviously, the SDS-TWR produced a kind of flat surface solutions in the evaluation while SS-TWR gave varying mountainous outcomes.

To give a further discussion for the special case (Type II) based on the value of parameters provided in Table 3.2, the simulation results showed that the TOF errors of

both the SDS-TWR and AltDS-TWR were less than 1 ns when $\xi < 3$ ppm and $t_{\text{reply}} < 650\mu\text{s}$ were applied. This refers to approximately 30 cm error in distance estimation in the real world. Moreover, it can be stated according to the simulation results that the parameter t_{reply} in Type II is flexible to vary up to 1 ms if the parameter ξ is allowed to decrease up to 2 ppm. This infers that the aforementioned ranging accuracy (30 cm) is unchanged. Conversely, decreasing t_{reply} in the simulation environments relaxes the increase of ξ without the loss of the overall system performance.

3.4.1.3 Simulation Results for Typical Cases (Type III)

For the typical case defined as Type III in Section 3.3.1, the simulation results regarding TOF errors for four evaluated TWR methods were presented in Figure 3.8. In fact, the Type III case is the most critical assessment in the chapter because the case exactly represents the implementation of TWR in the practical real world. As discussed earlier, the simulation results for the comparative analysis of the four TWR methods, when the reply time in Device A ($t_{\text{replyA}} = 840\mu\text{s}$) is greater than the reply time in Device B ($t_{\text{replyB}} = 400\mu\text{s}$) were given in Figure 3.8(a). Oppositely, Figure 3.8(b) presented the comparative outcomes of the four TWR, when the two reply times in Figure 3.8(a) were swapped in the opposite order ($t_{\text{replyA}} < t_{\text{replyB}}$). In addition, Figure 3.8(c) allowed a bigger gap between the two reply times (t_{replyA} and t_{replyB}) to show that the outcomes of TOF errors, particularly SDS-TWR, in a different point of view. Figure 3.8(c) highlighted the simulation results presented in Figure 3.8(a–c) specifically for the AltDS-TWR methods. The value of the parameters in simulation results were chosen to match with the set-up and experiments presented in Section 3.4.2.

Two crucial proofs were revealed in the simulation results of typical case (Figure 3.8). Firstly, the pitfalls of SDS-TWR was seen in the simulation results when the reply

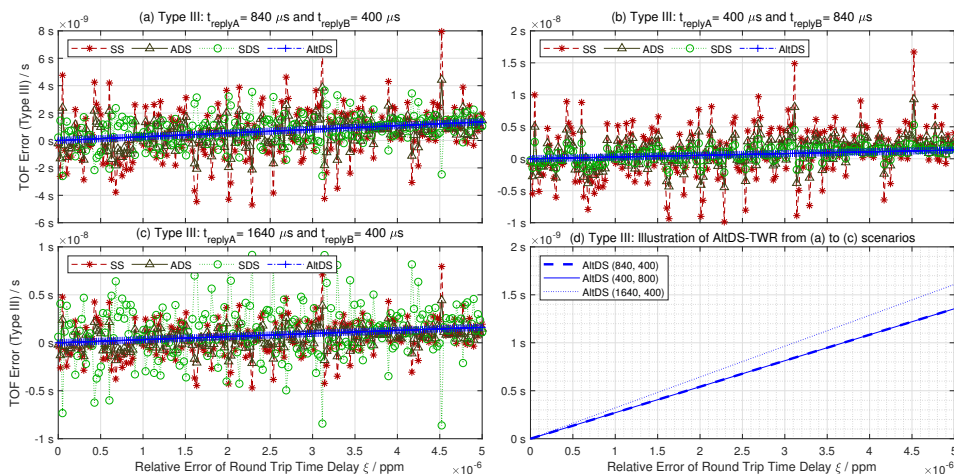


Figure 3.8: TOF error comparison between TWR methods using Type III assumption (typical case) as in Equations (3.30)–(3.33). (a) TOF error when $t_{\text{replyA}} > t_{\text{replyB}}$, (b) TOF error when $t_{\text{replyA}} < t_{\text{replyB}}$, (c) TOF error when $t_{\text{replyA}} = 1640\mu\text{s}$ and $t_{\text{replyB}} = 400\mu\text{s}$, and (d) TOF error for AltDS-TWR method in (a)–(c).

times (t_{replyA} and t_{replyB}) were asymmetric (Figure 3.8(a–c)). The severity of the TOF errors in SDS-TWR was more apparent especially when the gap between the reply times was large (Figure 3.8c). Secondly, the simulation results in Figure 3.8 showed that the AltDS-TWR was the only TWR in the evaluation that gave consistent numerical outcomes for the typical case (Type-III).

In summary, revealing the pitfalls of SDS-TWR was crucial because it was a de facto standard for TWR methods in the last decades [33] and it became the base model in several bench-marking [13, 114, 122, 127, 148, 149] as previously mentioned many times. By contrast, AltDS-TWR overcomes the error due to variation of reply times and it has the ability to provide accurate ranging even in asymmetric conditions as we proved in this section. Accordingly, AltDS-TWR was adopted in the amendment of IEEE 802.15.4z-2020 [98] standard to illustrate the default DS-TWR scheme for wireless ranging system, i.e. the replacement of SDS-TWR in IEEE 802.15.4-2011 [33].

It should be pointed out that the ADS-TWR and SS-TWR methods require only one-sided reply time (t_{replyB}). Hence, the magnitude of t_{replyB} determines their performance. Figure 3.8a showed that the ADS-TWR provided a lower TOF error compared to the SDS-TWR method when $t_{\text{replyB}} < t_{\text{replyA}}$. In reverse, the TOF errors of SS-TWR and ADS-TWR methods increased when $t_{\text{replyB}} > t_{\text{replyA}}$ as expected (Figure 3.8b). In both scenarios, the performance of the SDS-TWR method stays unchanged. The simulation results indicated that SDS-TWR outperformed both the SS-TWR and ADS-TWR with a large margin in this particular experiment (Figure 3.8b). However, the TOF error in SDS-TWR was severely increased and its performance was worse than SS-TWR and ADS-TWR, when the gap between reply times was relatively large (Figure 3.8c).

3.4.2 Experimental Evaluation Results

As previously reported in Section 3.4.1, two crucial findings using TEEM have been verified for TWR methods in UWB-based wireless ranging systems. The primary goal of this section was to prove the conclusions drawn from the simulation results conducted in Section 3.4.1 with the experimental evaluation results. The mentioned two findings in TWRs include the pitfalls of the SDS-TWR method in a typical case (Type III) defined in Section 3.3.1 and the robustness of AltDS-TWR.

In the experiments, the comparative analyses of three out of four TWR methods were conducted namely SS-TWR, SDS-TWR, and AltDS-TWR. ADS-TWR was excluded in experiments because the auto-acknowledgment mechanism (Figure 3.4), i.e., the instant reply time in Device A ($t_{\text{replyA}} = 0$), was not supported in the UWB hardware in the market at the time of writing this dissertation. The research data used for presenting the results in this section were made available publicly in [174].

This section was subdivided as follows: Section 3.4.2.1 explained the experimental setup, i.e., the data from that section was utilized to present the evaluation results in both Section 3.4.2 and Section 3.5 respectively. The goal of the experiments was clarified in Section 3.4.2.2, which was followed by the evaluation results of the comparative analysis regarding three TWRs at two specific scenarios (i.e., a special case in Section 3.4.2.3 and a typical case in Section 3.4.2.4 respectively). Figure 3.9 illustrated the test environments for all the experimental evaluations conducted in this chapter.

3.4.2.1 Setup and Data-Collection Process

Regarding the hardware used in the experiments, the device under test was composed of an UWB transceivers, the main MCU, and Universal Synchronous/Asynchronous Receiver/Transmitter (USART) interface for logging the data into Personal Computer (PC). We used a DWM1000 module [44] from Decawave for the UWB transceivers and the NUCLEO-L476RG, i.e., an STM32 development board from STMicroelectronics, for the main MCU. For the clock source of the MCU, the built-in High Speed Internal (HSI) (16 MHz) from the NUCLEO-L476RG was utilized in all of the evaluation results given in this chapter. This clarifies that no external oscillators were connected to the MCU of the evaluated device. As specified by the data-sheet in [192], the accuracy of the HSI in NUCLEO-L476RG is $\pm 1\%$ using the factory-trimmed RC oscillator.

Before starting the measurement campaigns, the aggregated antenna delay calibration for the UWB modules was conducted as specified by the procedure and algorithm instructed in the manufacturer application notes [43, 46]. In fact, the mentioned aggregated antenna delay in the evaluation refers to TTD and RTD as defined in Section 3.2.1. Hence, the TOF error estimation in the measurement was mainly affected by the error caused by the delay in PTD and PATD. It should be noted that all the presented results in Section 3.4.2 and 3.5 were measured in distance as opposed to TOF in the simulation results. The reason is that the references for the experiments were based on distances. In other words, the TOF value achieved from the ranging scheme was transformed into a distance by multiplying with the speed of light, which is 299,702,547 m/s in the air.

In the course of the measurement, we connected one of the two transceivers (Device A in Figure 3.3) to a PC in order to log the measurement data, which were arriving to PC from the MCU via USART port. The software provided for production testing of evaluation kit (EVK1000) by Decawave was run on the two transceivers. The

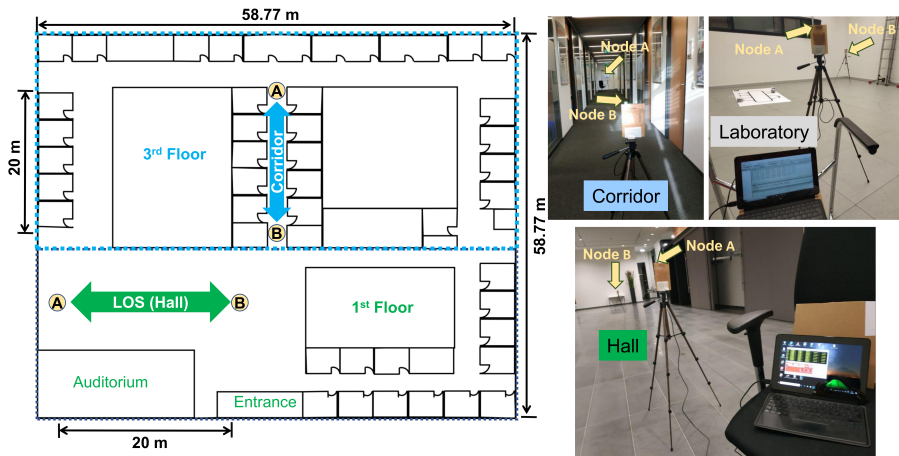


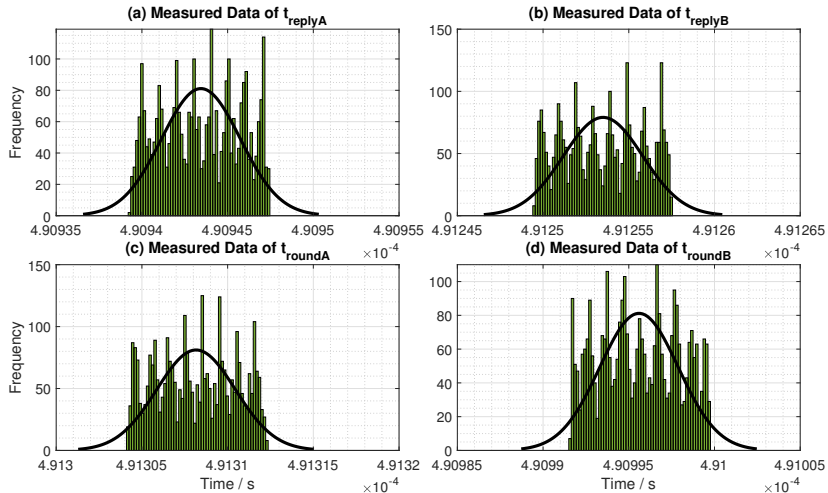
Figure 3.9: Test environments of the experimental evaluations: (a) overview of office floor plan for the LOS experiment in hall (green arrow) and the multi-path experiment in a corridor (sky-blue arrow), (b) fixed-distance experiment in the laboratory, LOS experiment in a hall (office environment), and multi-path experiment in a corridor (office environment).

Table 3.3: The configuration of UWB used in the evaluations.

Properties	Values
Data rate	6.8 Mbps
Channel	2
Center frequency	3993.6 MHz
Bandwidth	499.2 MHz
Pulse-repetition frequency (PRF)	16 MHz
Preamble code sequence index [33] (p.203)	3
Module name	DWM1000
Manufacturer	Decawave
Reported precision [44]	10 cm

software is available online on Decawave's website¹. The source code of the mentioned software was modified in order to extract the four parameters of time instances in DS-TWR (t_{roundA} , t_{roundB} , t_{replyA} , and t_{replyB}) during the measurement. The retrieved parameters were, then, individually logged into a PC and saved in separate files at each measurement. Afterward, the logged data regarding the above-mentioned time periods were processed with the TWR formulas given Section 3.1.2 using Matlab. This ensured that the evaluation results of each TWR were based on the exact same raw data (periods of time) from the measurement. For instance, only two of the four collected raw data from a file namely t_{roundA} and t_{replyB} was used to study SS-TWR while the entire four parameters from the same file were used for the study of SDS-TWR.

Table 3.3 gave the configuration of the UWB hardware module used for transceivers in all of the experimental evaluations. For all the experimental results reported in this dissertation, the antenna height of the UWB transceivers was always set to at least 1.06 m to ensure that the errors due to Fresnel zones were not affected in the


Figure 3.10: Sample measured data for the symmetry in the special case (Type II)

¹<https://www.decawave.com/software/>

3.4 Simulation and Experimental Evaluation Results

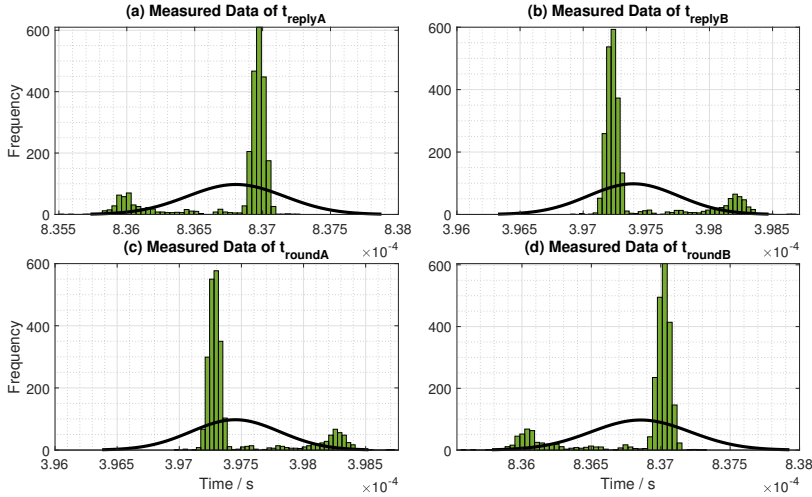


Figure 3.11: Sample measured data for the asymmetry in the typical case (Type III)

measurement. We used a laser distance meter, CEM iLDM-150 model², to measure the ground truth reference distances in the evaluation. The applied laser distance meter provides an accuracy of ± 1.5 mm according to the manufacturer.

For evaluating the special case (Type II) defined in Section 3.3.1, the hardware of the two UWB transceivers was carefully tuned until we achieved the equivalent (symmetric) two reply times. Figure 3.10 described the histogram of the mentioned symmetric replied time scenario (special case, or Type II) based on the sample data collected from one of our measurements. The figure illustrates the measured time periods for a single trial in the evaluation, in which the duration of the measurement lasted roughly around 5 min using an updated rate of 10 Hz. The mean values of the reply times are $t_{replyA} = 490.94 \mu\text{s}$ and $t_{replyB} = 491.25 \mu\text{s}$ (Figure 3.10 and Table 3.4). Indeed, all of the evaluation results presented in this chapter were based on the mentioned setting and reply time for the symmetry case (Type II).

For an asymmetric scenario for a typical case (Type III), Figure 3.11 demonstrated the histogram of the typical case using the sample data collected from one of our

Table 3.4: Sample reply time drawn randomly from each category (LOS, close LOS, and MP).

Cases	RMSE (μs)		Mean (μs)		STD (ns)		Data Spread (ns)		Sample Size
	$t_{replyA} - t_{replyB}$		t_{replyA}	t_{replyB}	t_{replyA}	t_{replyB}	t_{replyA}	t_{replyB}	
Special case (Type II)	0.31		490.94	491.25	2.29	2.32	8.17	8.00	2350
	0.28		490.97	491.25	2.30	2.32	8.47	8.00	2450
	0.26		491.0	491.25	2.34	2.34	9.14	8.00	2000
Typical case (Type III)	439.41		836.80	397.40	357.14	357.11	1754.5	1754.0	2350
	439.58		836.90	397.33	375.07	375.07	4451.3	4451.6	2450
	439.83		837.04	397.22	1369.1	1369.1	16,474.0	16,474.0	2000

²<http://www.cem-instruments.in/product.php?pname=iLDM-150>

measurements. Once again, the figure showed the measured time periods for the asymmetric case based on a single trial. The mean values of the reply times for Type III in this measurements are $t_{\text{replyA}} = 836.8 \mu\text{s}$, and $t_{\text{replyB}} = 397.4 \mu\text{s}$ (Figure 3.11 and Table 3.4). It should be pointed out that Figure 3.11 was just an exemplar for typical cases achieved from the default setup (out of the box) from Decawave's software. For evaluating the Type III scenario in Section 3.4.2.2, we further varied the reply times of one device from the two transceivers to analyze the performance differences between the SDS-TWR and AltDS-TWR. Moreover, the illustrated setting and reply times were used for evaluating the typical condition discussed in Section 3.5.

In summary, Table 3.4 provided the sample data of reply times randomly drawn from our measurements for Types II and III. The collected data were categorized in three scenarios namely LOS, close LOS and MP as expressed in three types for each in the table. We verified upon the evaluation that the magnitude of the difference (similarity) between the two reply times (t_{replyA} and t_{replyB}) was always less than $0.35 \mu\text{s}$ in average for the symmetry case (Type II). The defined similarity between reply times was annotated as Root Mean Square Error (RMSE) in Table 3.4.

3.4.2.2 Scope and Goals of the Experimental Evaluation

The experimental evaluation results reported in the upcoming sections aims to validate the outcomes achieved from simulation results given in the previous section regarding TWR methods. The emphasis was focused on the performance comparison between the AltDS-TWR and SDS-TWR (the de facto base model for TWR in literature). The findings in the simulation result pointed out that there are two crucial points, i.e., the pitfall of SDS-TWR and the robustness of AltDS-TWR. Therefore, this section aimed to validate the mentioned two outcomes achieved from the simulation with the experimental validation results. Firstly, it was aimed to demonstrate the pitfalls of SDS-TWR using experimental data instead of numerical values. Indeed, the fact has been already proved with simulation results in Section 3.4.1. Secondly, it was aimed to prove the efficiency of the AltDS-TWR method in a typical case (Type III) when reply times are varied using experimental results compared to other TWRs. Regarding this, different

Table 3.5: Evaluation results for variable reply times at fixed reference distance (5.494 m).

No. of Trials	RMSE (ms) Reply Time	RMSE (cm) Distance Error			Reply Time (ms)		Sample Size
		AltDS	SDS	SS	t_{replyA}	t_{replyB}	
1.	0.0003	3.44	3.44	18.40	0.4909	0.4913	2850
2.	0.24	2.74	2.27	15.16	0.64	0.40	2966
3.	0.74	3.51	8.87	15.76	1.14	0.40	2435
4.	1.24	3.63	15.58	15.145	1.64	0.40	2496
5.	1.74	3.50	22.27	14.56	2.14	0.40	2523
6.	2.24	3.72	28.60	14.51	2.64	0.40	2320
7.	2.74	3.50	34.33	13.97	3.14	0.40	2454
8.	3.24	3.51	39.17	13.55	3.64	0.40	2485
9.	3.74	3.59	44.40	13.40	4.14	0.40	2574
10.	4.24	3.51	50.75	13.39	4.64	0.40	2446

sets of experiments by varying the values of reply times in TWR were conducted at a static scenario in the laboratory environment. As opposed to the simulation, the clock drift error cannot be randomly generated and tuned in the experiments. Hence, we used the built-in high-speed internal oscillator from the main MCU in the experiments as described in Section 3.4.2.1.

A total of ten trials were conducted in order to specifically address the pitfall of SDS-TWR and the robustness of the AltDS-TWR. Table 3.5 provided the magnitude of the difference between two reply times (t_{replyA} and t_{replyB}) starting from 0.0003 (symmetry case) up to 4.2 ms (variable reply times case). In the evaluation, only one of the two reply times, specifically, t_{replyA} , was varied with different values to show various levels of asymmetry in the reply times. The variation was done in the experiment by manipulating the value of delays on the ranging software during evaluation (see Columns 6 and 7 from Table 3.5, denoted as “Reply Time (ms)”).

3.4.2.3 Evaluation Results for Special Case (Type II)

The special case was evaluated in the experiment for the three TWRs where the corresponding data were given in Trial 1 in Table 3.5. The primary goal was to prove experimentally how closely related the outcomes of the SDS-TWR and AltDS-TWR in Type II. The evaluation results showed that only very small errors occurred in SDS-TWR technique when the two reply times are exactly equal as the name symmetric is applied in the method itself (Trial 1 in Figure 3.12). For the purpose of better visualization of the reported results, Figure 3.12 expressed the experimental outcomes for special case (Type II) in two kinds of data representations namely box plots and empirical CDF. In both of the data representations, the results indicated that both AltDS-TWR and SDS-TWR had identical performance level in the symmetry case (Figure 3.12). In other words, AltDS-TWR is comparable to SDS-TWR in the symmetry case (Type II). The exact values of the presented results can also be seen in the first-row of Table 3.5.

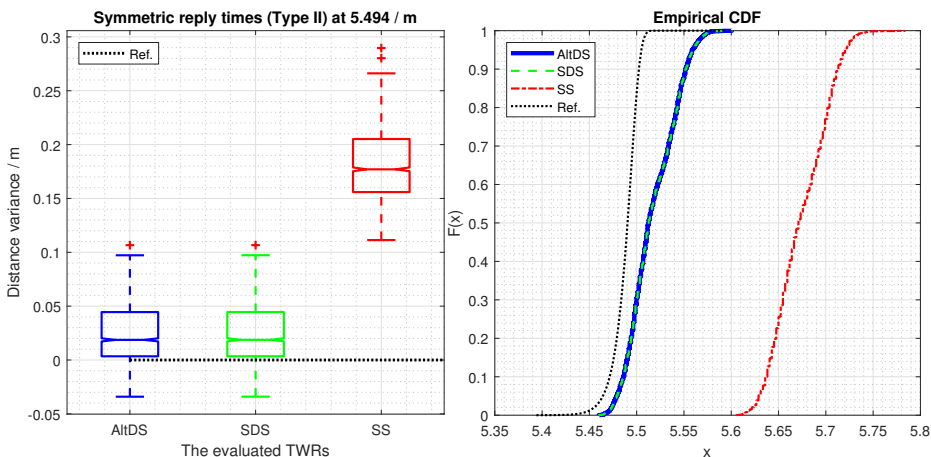


Figure 3.12: Evaluation results of three TWRs for the special case (Type II) using box plots and empirical Cumulative Distribution Function (CDF) measured at a static distance of 5.494 m

In specific, the RMSE in distance estimation for both AltDS-TWR and SDS-TWR was also equivalent in this particular experiment, with an exact value of 3.44 cm (the third and fourth columns of the first-row in Table 3.5). Similar findings for the special case (Type II) based on the simulation were already reported in Section 3.4.1.2. It is worth mentioning that it rarely happens to have a symmetric reply time in a real-world situation. In this particular experiment, we manually tuned the two reply times (t_{replyA} and t_{replyB}) until we achieved the approximately equal values (see the magnitude of difference between the two reply times ($t_{replyA} - t_{replyB}$)) in Table 3.5 (second column), which was 0.0003 ms in the symmetry case (first row). As expected, the experimental results showed that distance error using SS-TWR was significantly higher than both of AltDS-TWR and SDS-TWR (Figure 3.13).

3.4.2.4 Evaluation Results for Typical Case (Type III)

For the purpose of visualizing the evaluated three schemes, the first five trials from Table 3.5 were depicted in Figure 3.13. In the figure, it can be clearly seen that the box corresponding to SDS-TWR was drifting away from the reference as indexes of the trial numbers are increasing. In other words, Figure 3.13 was demonstrating the pitfall of SDS-TWR, frequently mentioned throughout this chapter. For the referencing purpose, the symmetry condition was also given again in Figure 3.13 (Trial 1). As shown previously, SDS-TWR gave a very small errors in distance estimation when the two reply times were exactly the same (Trial 1 in Figure 3.13 and Figure 3.14).

However, SDS-TWR encounters significant errors in the estimation of wireless distances when the symmetry in the reply time was broken down. The severity in the error of SDS-TWR increases in parallel when the difference between the reply time ($t_{replyA} - t_{replyB}$) were increasing (Figure 3.13, Figure 3.14 and Table 3.5). The evaluation results showed that the distance error even reaches up to 50.75 cm when the magnitude of difference between the two reply times ($t_{replyA} - t_{replyB}$) was raised to

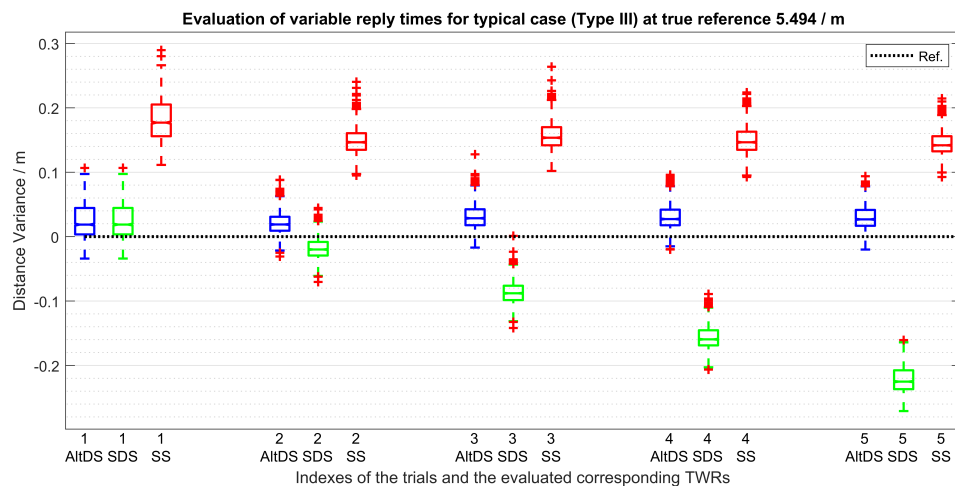


Figure 3.13: Variable reply times at fixed distance measurement.

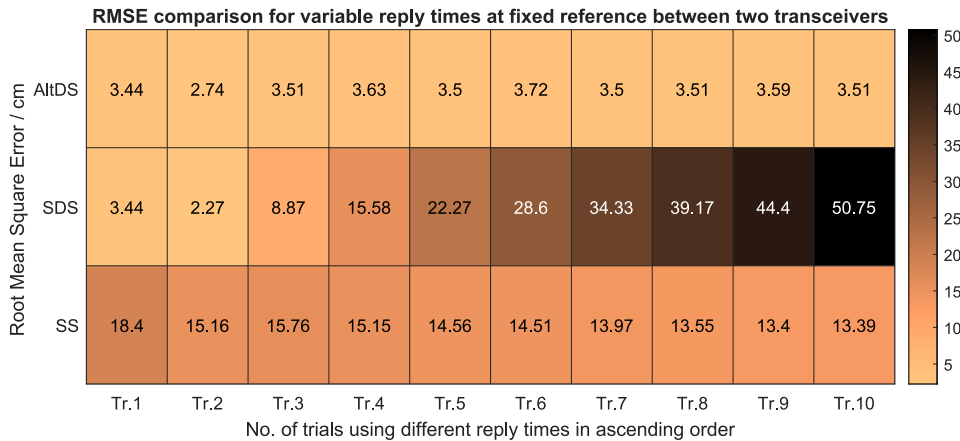


Figure 3.14: Variable reply times at fixed distance measurement.

until 4.24 ms (last row in Table 3.5 and last column in Figure 3.14). The monotonously increase of the estimation error in SDS-TWR clearly indicates that SDS is not a perfect technique to be used for a standardized benchmarking method as opposed to the widely used case in many papers during the past decade.

In contrast, we observed that AltDS-TWR technique was robust against the variation of the reply times (t_{replyA} and t_{replyB}) in wireless distance estimation using TWR. The consistency of AltDS-TWR across several evaluation trials were depicted in Figure 3.13 and Figure 3.14. The exact numerical values using RMSE as a decisive score were also provided in Table 3.5 and Figure 3.14. Regarding the distance error in the evaluation, the outcomes of RMSE for AltDS-TWR provided a consistent manner throughout the measurement (Figure 3.14). To give it with the exact value, the RMSE for AltDS-TWR ranges only to a small span between 2.74 cm to 3.72 cm (Figure 3.14) while a quite large span regarding the magnitude of difference between the reply times ($t_{replyA} - t_{replyB}$) was varied starting from 0.0003 ms to 4.24 ms (Table 3.5). The results clearly showed that the error produced by AltDS-TWR was quite small, reliable in all tested conditions, and consistent across a large range of variations.

The above-mentioned results proved the robustness and consistency of distance estimation regarding AltDS-TWR. Moreover, the results showed that AltDS-TWR technique should be a preferred method as a reference to be used in benchmarking of TWR techniques compared to the commonly used SDS-TWR technique. Regarding the SS-TWR, the results in Figure 3.13 and Figure 3.14 showed that consistent outcomes across the evaluated trials. This is because SS-TWR relies only on one reply time, namely, t_{replyB} (3.2), which was constant and did not change throughout the evaluation. In fact, only one reply time (t_{replyA}) was varied in the experiment and the one applied for SS-TWR (t_{replyB}) stayed unchanged throughout the evaluation (see the seventh column in Table 3.5). It is worth mentioning that SS-TWR also encountered severe errors in distance estimation similar to the SDS-TWR when the reply time namely t_{replyA} was varied (i.e., see the simulation results demonstrated in Section 3.4.1).

3.4.3 Results Summary for Type II and Type III using TEEM

In this section, we primarily focused on two basic TWR techniques. The aim was to reveal the pitfalls of SDS-TWR and the robustness of AltDS-TWR technique. In order to give comprehensive results, three types of cases were defined and examined. The results were validated with both simulation and experiments. SDS-TWR was the most highlighted TWR techniques and a de facto standard for bench-marking TWR in literature [13, 114, 122, 127, 148, 149]. However, there is a critical flaws in SDS-TWR technique that showed that the method was not good enough to be used as a gold standard for performance evaluation in TWR techniques. Additionally, we demonstrated the pitfall of the mentioned SDS-TWR based on numerical simulation and experimental evaluation results (Figure 3.14). The severity of the technique becomes more corrupting as the magnitudes of the difference between the two reply times increase (Figure 3.14). Moreover, we reminded the readers that the constraint on strict symmetry in reply times for SDS-TWR is hardly achievable in practice due to hardware constraints.

In contrast, we showed that AltDS-TWR was robust against the clock drifts and asymmetric reply times in several tested situations. In other words, the accuracy of AltDS-TWR was not affected by the variation of the reply times in TWR compared to SDS-TWR (Figure 3.14). This shows many important aspects in UWB localization in which both the positioning information and actual data from sensors can be processed simultaneously on a single wireless platform. Previous implementations focused only on the position accuracy and neglected the payload section of the MAC layer in UWB communication due to extra processing delay introduced by adding data on it. The evaluation results in Section 3.4.1 and Section 3.4.2 showed that the mentioned issue can be overcome by using AltDS-TWR technique as a ranging method.

3.5 Inspection of Ranging Error in TWR Techniques

In addition to the ranging errors due to the choice of methodologies in TWRs as previously discussed, the error in UWB-based wireless ranging occurred due to the non-direct path signal communication between transceivers (i.e., the presence of obstacles that block the LOS path between devices). In literature, the mentioned occurrences was typically classified as NLOS propagation and MP effects [177, 217]. Therefore, the issue typically introduces positive biases in the ranging performance and, in turn, affects the localization accuracy of the overall system. Moreover, our previous work in [130] reported that significant errors occurred in purely LOS scenarios for UWB if the measurement was conducted in a very closed range, especially when the coherent receivers are used in the transceivers.

The ranging error due to the NLOS propagation in wireless communications are well known and the effects are obvious to achieve in the measurements. Therefore, the study on NLOS identification and mitigation technique for UWB is heavily examined in the literature. Similarly, the ranging errors due to the MP effects are also regarded as crucial in some papers. However, only a few investigations were actually conducted. On the contrary, the ranging errors due to the closed LOS condition are rarely examined

and even mentioned in literature. The experimental results showed that the errors due to closed LOS are significant especially when the measurement was conducted in less than 1 m (close range). Hence, this section examined the mentioned three main causes of ranging errors in UWB using TWR techniques based on comprehensive experiments. The reported results for NLOS propagation were described in Section 3.5.1, MP effects in Section 3.5.2, and closed LOS case in Section 3.5.3 respectively.

Moreover, the aforementioned ranging errors are related to the various possible delays in UWB-based ranging schemes defined in Section 3.2.1. In order to give comprehensive results, the experimental data from four different scenarios were collected in indoor environments: (i) pure LOS (conducted in a Hall), (ii) MP conditions (conducted in Corridors), (iii) NLOS condition and (vi) close LOS scenario (conducted in laboratory). Regarding this, the error influenced by PTD can be validated in the MP scenario (Section 3.5.2), where the effects of PATD in the close LOS scenarios (Section 3.5.3). The summarized report of the three scenarios was given in Appendix B in which Table A.1 provided all the values in the experiments for the special case (Type II) and Table A.2 for the typical case (Type III) respectively.

3.5.1 Ranging Error due to NLOS Scenario in TWR

The experimental data regarding the NLOS scenario was collected in the laboratory in order to evaluate the effects of NLOS in UWB's ranging. During the data collecting process, the measurement was recorded for roughly three minutes in total for both Type II and Type III cases using the ground truth reference between the two transceivers at 2 m. As shown in Figure 3.15, the data collecting procedure was established in three parts during the mentioned 3 min (roughly). The pure LOS data were recorded in the first one minute. After that, the communication between the two transceivers during the measurement was blocked by a human subject for 1 min by standing up in the middle, i.e., 1 m away from each transceiver. Then, the blocking was removed again to achieve the pure LOS recorded data for the rest of the last 1 min. As already described in experimental setup (Section 3.4.2.1), the mean reply times during data collection were $t_{\text{replyA}} = 490.94 \mu\text{s}$ and $t_{\text{replyB}} = 491.25 \mu\text{s}$ for the symmetric (special) case (Type II), and $t_{\text{replyA}} = 836.80 \mu\text{s}$ and $t_{\text{replyB}} = 397.40 \mu\text{s}$ for the asymmetric (typical) case (Type III), respectively.

The evaluation results in Figure 3.15 indicated that a large error in distance estimation due to the NLOS propagation occurred in both cases of the two types in all of the evaluated TWRs. In specific, the average error reaches up to 40 cm within 2 m ground truth, which is quite enormous. The results also proved the reason why the effects of NLOS in UWB systems were the most heavily studied for high resolution location-based wireless communications. In this particular NLOS measurement, the propagation errors were due to the signal-traveling time that needs to penetrate the human body and/or the non-direct signals reflected from the small laboratory environment. Therefore, the identification and mitigation of NLOS techniques are absolutely mandatory for any application where NLOS scenarios are expected to exist. Regarding this, the machine learning based identification and mitigation of NLOS and MP conditions specifically for UWB ranging systems are addressed in chapter 5.

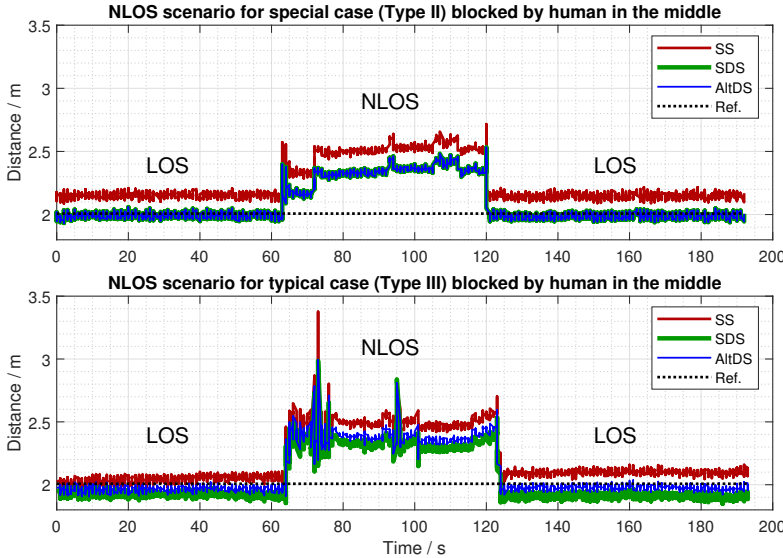


Figure 3.15: Illustration of ranging errors due to NLOS propagation in UWB for Types II and III at 2 m ground truth when a human subject is blocking.

In addition, Figure 3.15 also showed some spikes in the evaluation results, which occurred in the measurement due to the body movement of the human subject during the data collection process. The results indicated that both the AltDS-TWR and SDS-TWR provided identical performance in the special case (Type II), which was illustrated in the upper image of Figure 3.15. In this case, the outcomes of AltDS-TWR (blue color) were merged into the outcomes of SDS-TWR (green color). On the contrary, the diversified outcomes among the three TWR techniques can be seen in the typical case (Type III), as described in the bottom image of Figure 3.15.

3.5.2 Ranging Error due to Multi-path Scenario in TWR

For investigation of the ranging errors due to the MP effects in the TWR techniques, several measurements were carried out at static conditions. For the ground truth, various distances were used during measurement campaign, which were from 4 m up to 20 m for both the LOS and MP scenarios (Figure 3.16). For the LOS data, the measurement was conducted in a big hall of Center for Cognitive Interaction Technology (CITEC) building and for the MP data, the measurement was conducted in the narrow corridor of office environments, where the floor plan was given in Figure 3.9. Similar to Section 3.4, the data were collected for the special or symmetry case (Type II) and the typical or asymmetry case (Type III). For the asymmetry case, the applied reply times in the evaluation are $t_{\text{replyA}} = 836.8 \mu\text{s}$ and $t_{\text{replyB}} = 397.4 \mu\text{s}$.

In general, the UWB signals are inherently robust against the MP effects in wireless communications compared to its counterpart the narrow-band signals. However, the evaluation results from our comprehensive measurements showed that the reflected signals due to the MP effects in UWB communications still make apparent errors in the

3.5 Inspection of Ranging Error in TWR Techniques

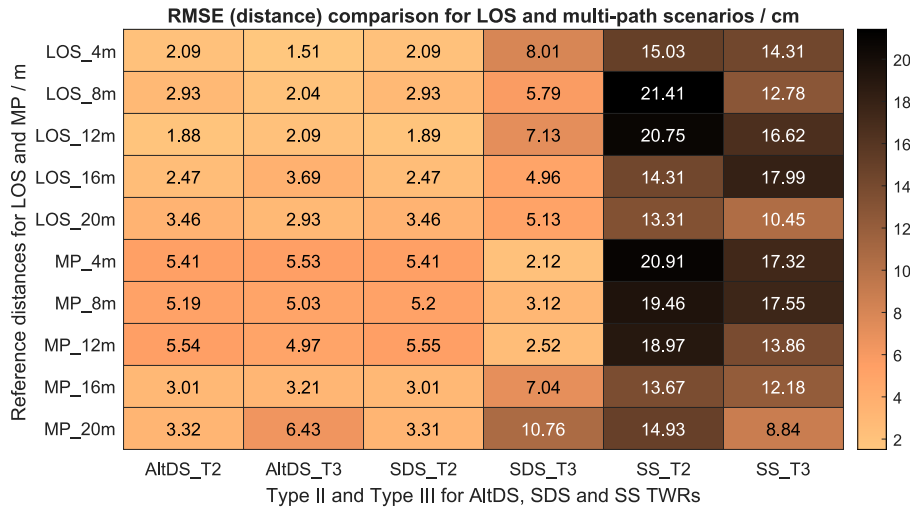


Figure 3.16: RMSE comparison of Types II and III for three TWRs in LOS and MP scenarios

estimation of distances using TWR techniques (Figure 3.16). Figure 3.16 showed the complete data-set of the measurement conducted at different ranges in two scenarios (LOS and MP) for both the special case (Type II) and typical case (Type III). The measurements were separately conducted for the three evaluated TWR (AltDS, SDS, and SS) at each different locations. The results were presented using RMSE as a performing score, which is the square root of the mean error (difference) between the measurement and the true reference.

Overall, the evaluation results showed that the distance error using AltDS was always less than 6.43 cm in all tested scenarios for both the special case (Type II) and the typical case (Type III) as reported in the first two columns of Figure 3.16. This implied that the performance of AltDS-TWR was better than other evaluated TWRs. Regarding the special case (Type II), it was observed that both the AltDS and SDS gave approximately equal distance errors in all of the tested locations in the evaluation (see the first and third columns in Figure 3.16). Moreover, the results reported that SS-TWR gave the largest distance errors in the measurement (Figure 3.16).

Regarding the MP scenarios, the distance errors for all TWRs were generally increased compared to the LOS conditions in the measurement results (compare the upper-half rows (LOS) and lower-half rows (MP) in Figure 3.16). In the MP conditions at Type III (esp. 4, 8, and 12 m), the reported results suggest that SDS-TWR gave the smallest error among the three TWR methods regarding the distance estimation (the fourth column in Figure 3.16). The occurrence of this conditions was due to the chosen fixed reply time for the typical case in this particular evaluation, i.e., $t_{replyA} = 836.8 \mu\text{s}$ and $t_{replyB} = 397.4 \mu\text{s}$. As already discussed in Section 3.4.2.4, the ranging errors due to SDS-TWR were more significant compared to AltDS when the asymmetry of the reply times were getting bigger. This scenario was demonstrated in Section 3.4.2 by varying the reply time of one device with different values.

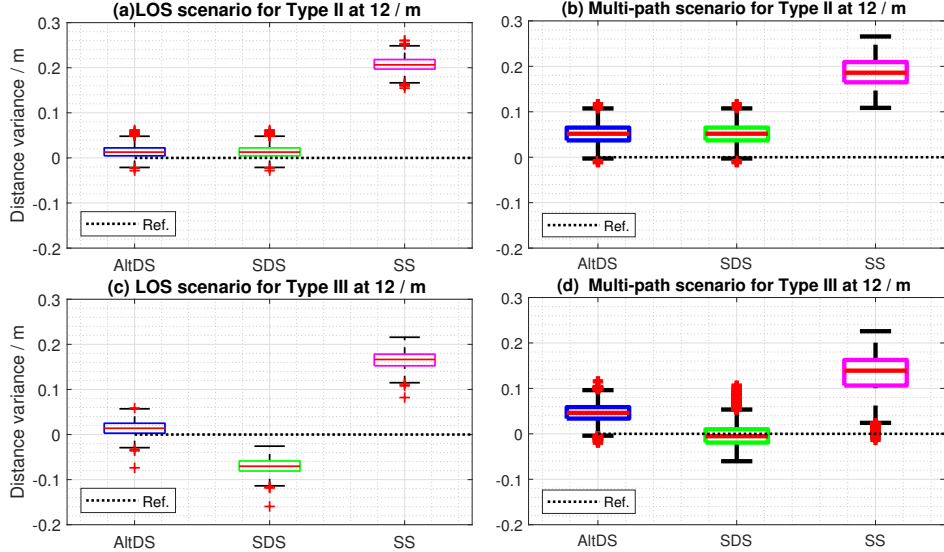


Figure 3.17: Comparison of the LOS and MP scenarios for Type II and Type III at a 12 m true reference. The images in a row represent the two types (II and III) and the images in columns represent the LOS and MP

For better visualization of the reported results, Figure 3.17 depicted the comparative experimental outcomes for the LOS and MP scenarios by specifically presenting the measurement conducted in true reference at 12 m. The outcomes were compared side by side in the figure. The first column in Figure 3.17 (a and c), showed the results achieved from the LOS condition (measured at a hall), and the second column in Figure 3.17(b and d), depicted the results achieved from the MP scenario. Furthermore, the measured outcomes from Type II and III are compared in the rows of Figure 3.17 to clearly identify the differentiation between the two cases.

It can be seen in the experiment result that SDS and AltDS have approximately the same performance level in the special case (Type II) as already stated in the simulation results (Section 3.4.1, see Figure 3.17a,b). However, a significant variation between SDS and AltDS can be observed in the typical case (Type III) as expected from the simulation results (Section 3.4.1, see Figure 3.17c,d). In addition, the results also showed that both SDS and AltDS always provided better performance scores compared to the SS-TWR in all the three cases (Figure 3.17).

Particularly for the LOS condition in Type II, the measured distance errors of both SDS and AltDS were very close to the reference value (Figure 3.17a). However, AltDS provided the smallest error in the typical case (Type III) among the three evaluated methods in LOS conditions (Figure 3.17b).

In the multi-path scenario at the special case (Type II), the distance error due to the SDS and AltDS were slightly increased compared with the LOS scenario (Figure 3.17a,b). Still, the mentioned distance errors caused by SDS and AltDS were relatively smaller than the SS-TWR technique (Figure 3.17b). In the typical case (Type

III), the evaluation results suggested that SDS provides the smallest error among the three methods (Figure 3.17e). This condition was caused by the applied reply times as already clarified in previous sections.

3.5.3 Ranging Error due to Closed LOS Scenario in TWR

The ranging errors in UWB due to the NLOS and MP conditions were widely discussed and examined in many papers [177]. However, the error due to close LOS scenarios was highly ignored. In this section, we examined the ranging error in close LOS scenarios by using different measured data collected at the static conditions starting from 0.25 up to 2 m. The experiments were carried out at one of the laboratories in CITEC, Bielefeld University (Figure 3.9). Again, the evaluation was conducted for both special case (Type II) and typical case (Type III).

The evaluation results using RMSE as a decisive score showed that all TWRs gave tremendous errors in close LOS scenarios when the ground truth reference was less than 0.75 m (first three rows in Figure 3.18). In specific, the RMSE was larger than 11 cm on average for all TWR methods at both Type II and Type III cases. Moreover, the evaluation results indicated that the errors due to the close LOS conditions in UWB were noticeably decreased when the ground truth references between the transceivers were set more than 1.5 m apart (last three rows in Figure 3.18). In this particular measurement results, the calculated RMSE for the AltDS (for both Type II and Type III) and the SDS (for Type II only) had been always less than 5 cm. Based on the evaluation results, the transitional phase that linked the gap between the worst-case scenario (i.e., RMSE greater than 10 cm) and the best case scenario (i.e., RMSE less than 5 cm) in the close LOS conditions was also spotted in the experiments. This region corresponds to the ground truth reference between 0.75 m and 1.5 m.

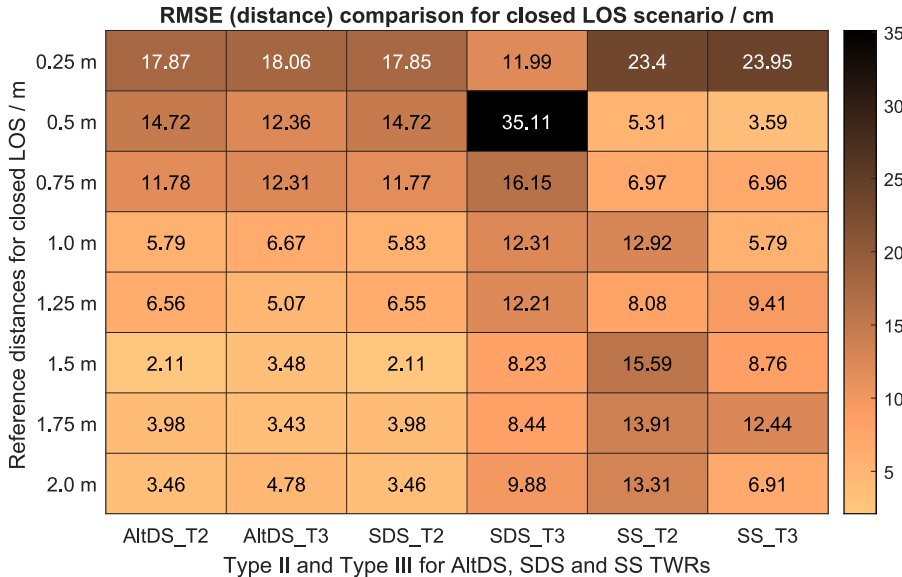


Figure 3.18: RMSE comparison of Types II and III for three TWRs in a close LOS scenario.

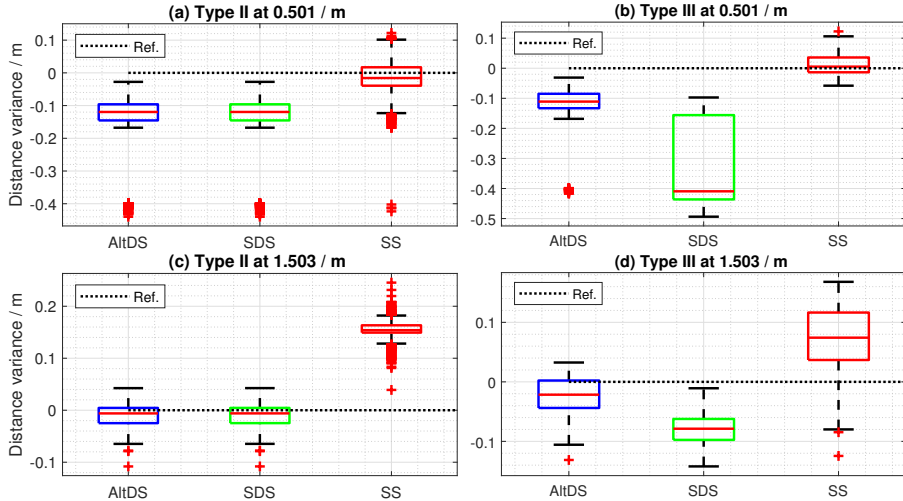


Figure 3.19: Results comparison of Types II and III for close LOS at true reference 0.25, 1.00, and 1.50 m. (a–c) measurement results for Type II (special case), and (d–f) corresponding results for Type III (typical case).

For a better visualization of the data, the evaluation results for close LOS scenario conducted at ground truth reference of 0.5 m and 1.5 m were presented in Figure 3.19. The results showed that a large extent of outliers (denoted in plus signs with red color in the figure) was evident in the measurements conducted at 0.5 m (Figure 3.19a,b). Figure 3.19b also illustrated that SDS-TWR was relatively skewed in the scenario where the measurement was conducted at 0.5 m. However, the presence of outliers in the measured data decreased substantially as previously given when we increased the distances between the two transceivers in the evaluation. This implied the scenarios of both the Type II and Type III cases as we can visualize the outcomes achieved from 1.5 m ground truth in Figure 3.19c, d respectively.

The major cause of distance error in close LOS scenario is due to the effect of PATD described in Section 3.2.1. The phenomenon of the PATD is more considerable in close LOS condition if the construction of the transceivers in the UWB hardware is based on a coherent receiver architecture [46]. This is because particular preamble sequence codes are required to initially transmit before the data communication between the transceivers for a coherent architecture so that the synchronization between devices in the physical layer could be done based on the perfect periodic auto-correlation procedure [46]. Additionally, the UWB hardware modules that are commercially available to buy in the market at the time of writing this paper are based only on the coherent receiver architecture. This includes the UWB hardware used in this evaluation, which is a DWM1000 module from Qorvo (Decawave).

Concerning this, there exist several preamble sequence codes for UWB data communication in literature. In this experiment, we used the preamble sequence code index no. 3 from the IEEE 502.15.4 standard [33, 96, 97]. Specifically, the pattern of the code sequence look like “ $- + 0 + + 0 0 0 - + - + + 0 0 + + 0 + 0 0 - 0 0 0 0 - 0 + 0 -$ ” according

to [33]. The mentioned sequence is classified as the shorter sequence in UWB configurations [33]. In principle, the longer the code sequence in the system implementation, the more likely to produce more severe errors in close LOS scenarios. This is due to the fact that the base symbol rate for the synchronization header is proportional to the preamble symbol transmission rate [33] (pp. 200–207). This corresponds to the longer time to detect the SFD during the accumulation time in the PHY layer of UWB according to IEEE 802.15.4 [33].

3.6 Chapter Discussion and Conclusion

In the past two decades, the most frequently highlighted TWR technique in the UWB-based localization system was the SDS-TWR method. The main reason was that SDS-TWR achieved remarkable outcomes regarding the accuracy score in the wireless distance estimation when the reply times (t_{replyA} and t_{replyB}) in the transceivers are symmetric. The renown of the SDS-TWR even makes the method become a de facto standard for TWR techniques in UWB localization. This implied that SDS-TWR was commonly used as the gold standard to benchmark the performance with newly discovered TWR techniques in literature [13, 114, 122, 127, 148, 149]. However, the robustness of the SDS-TWR was feasible only when the reply times are symmetric or uniformly equivalent throughout the measurement in all conditions as demonstrated in Section 3.4.1.2 and 3.4.2.3. In case the mentioned symmetry in the reply time was inaccessible, the evaluation results showed that SDS suffered severe errors in the estimation of distances in UWB localization (Section 3.4.1.2 and 3.4.2.4). This signifies that SDS-TWR is not the best candidate to be used as a baseline model (or) the reference method for benchmarking the performance of different TWR methods. Indeed, the evaluation results showed that the necessity of a strict symmetry in the reply time is not only the major drawback but also the pitfall of the SDS-TWR method. In other words, the mentioned constraint in SDS limits the flexibility of the method to be used in different areas. Moreover, the perfect symmetry cannot usually be achievable in practice. Indeed, the exact same issue regarding the constraint of strict symmetry in SDS-TWR was also discussed in [62, 114].

On the contrary, we demonstrated in this chapter using TEEM model that AltDS-TWR method was robust against clock drift and can perceived consistent outcomes in any tested condition (Section 3.4.1.3 and 3.4.2.4). Moreover, the results based on numerical simulation and experimental evaluation proved that the corrupting effect of the delay in different reply time does not affect the accuracy of AltDS-TWR (Figures 3.6, 3.8 and 3.13 and Table 3.5). The mentioned matter is crucial for typical applications in wireless communications and WSN, where both the location information and the sensor data are necessary to process in the application. The evaluation results revealed that AltDS-TWR was able to simultaneously provide both the location information and sensor data on the payload of its MAC layer without losing the ranging accuracy. In other words, AltDS-TWR is the only method in the evaluated four TWRs that can be used in typical WSN, where non-deterministic processing times for sensor data reading and transmitting are expected in the application.

The primary reason for stressing out the aforementioned nondeterministic scenario in WSN is that the current state-of-the-art system implementations in UWB-based wireless localization emphasize only the accuracy of the location information. Hence, the data payload section of MAC layer [33] (p. 57), where sensor data and other information can be transmitted on it depending on the available resource space, was commonly ignored and not used in most of the papers in literature. For instance, the implementation of UWB localization systems in [87, 126, 199, 229] solely addressed the accuracy of the positioning algorithms and generally assumed that no payload was sent during the data communication process. In exceptional cases, the data payload section of the MAC layer was used only for essential timestamps to be used in the positioning algorithm. Hence, a secondary wireless technology is usually mandatory in such a system if the sensor data are also important to obtain. However, AltDS-TWR reveals the ability to give the mentioned two information in one technology while keeping the same performance level of location accuracy. For instance, it can be considered the variation of reply time given in Table 3.5 (Section 3.4.2.2) as a representation of sensor data processing time in WSN. An example application of such scenarios includes a wireless body sensor network for sports analysis, where the location and other sensor data from a particular player are helpful for the central server (coach) to analyze the performance of each athlete and game strategy. It is worth noting that the processing time for reading and transmitting the data from the sensor in that scenario is generally unpredictable depending on several hardware and software constraints.

Moreover, the evaluation results given in Sections 3.4.1 and 3.4.2 suggested that AltDS-TWR is the preferred method for real-world scenarios compared to the rest of the evaluated TWR in this chapter since it is robust against the variation of reply time and clock drifts. The conclusion based on the results from numerical and experimental evaluations at different conditions is that the performance of AltDS-TWR is the most reliable technique among the four evaluated TWR methods. Therefore, AltDS-TWR should be preferred to be used as a baseline method for bench-marking TWR methods in contrast to the current commonly used SDS-TWR in many academic papers. In general, it is desirable for TWR in any conditions that the magnitude of the reply times (t_{replyA} and t_{replyB}) and relative delay errors of round-trip time (ξ_{ABA} and ξ_{BAB}) are as small as possible. This is because the smaller the magnitude of the mentioned time in the system is, the better the ranging accuracy (Section 3.4.1 and 3.4.2).

Regarding the simulation results given in Section 3.4.1, it should be noted that the relative error includes all delays namely PTD, PATD, TTD, and RTD introduced in Section 3.2.1. In contrast, the relative errors due to the TTD and RTD were excluded in the experimental evaluation results (Section 3.4.2). The reason is that it is possible to identify a certain approximately constant delay error in practice (upon the identical complete hardware setup). This is done by measuring the estimated distance between the two UWB transceivers in a pure LOS scenario and manipulating the reported values with the known ground-truth reference. The procedure of identifying and eliminating the mentioned constant is commonly termed in the community of UWB hardware implementation as the calibration of the aggregated antenna delay [43]. In brief, the mentioned identified constant is usually used to match the estimated TOF value measured by the transceivers with the ground truth reference distance. The mentioned

elimination of delays in UWB hardware correspond to the TTD and RTD delays given in Section 3.2.1 and we had calibrated them before the measurement was conducted in the experiments according to Section 3.4.2.1. Recently, a method that is capable of calibrating the above-mentioned antenna-related delay without the need for manual interventions was proposed in [184].

In addition, three scenarios that caused ranging errors in wireless communications, namely NLOS, MP and close LOS conditions, were experimentally examined in this chapter. The ranging errors due to NLOS in UWB and wireless communications were apparent. Hence, the effects of NLOS conditions were comprehensively studied in many papers especially for UWB systems [18, 82, 85, 113, 135, 138, 177, 181, 219]. The ranging error due to MP conditions were also seen as an essential aspect for precise localization systems in [38, 41, 130, 180]. However, the comprehensive evaluation of the MP effects is commonly neglected in the existing literature. Therefore, the identification and mitigation of the above mentioned NLOS and MP conditions in UWB localization was thoroughly addressed in chapter 5 using Machine Learning (ML) methods. Concerning the close LOS scenario, the issue is rarely expressed in literature except for some recommendations given from the manufacturer [46, 47]. Therefore, the error due to close LOS was also comprehensively analyzed in this chapter where part of the results was also published in our previous work [130].

Based on the evaluation results given in this chapter, we can draw a few recommendations for the UWB-based localization systems as follows: Firstly, the ranging distance between transceivers in the application should be larger than 0.75 m for the best performance. Regarding this, the anchor (fixed) nodes should be placed far away from the dedicated region so that the distance gap between the anchor and mobile nodes maintains at least 0.75 m. Secondly, the evaluation results suggest that both AltDS- and SDS-TWR will give a reasonably small errors in distance estimation (i.e., less than 10 cm) if the difference between the two reply times($|t_{replyA} - t_{replyB}|$) can be maintained under 400 μ s. Thirdly, the finding in this chapter reveals that AltDS-TWR is the only chosen method for real-world application, where the non-deterministic processing time (e.g. sensor-data reading) is expected in the system apart from the location data. Therefore, we can conclude upon this observation that AltDS-TWR is the preferred method for the baseline model when bench-marking the performance of different TWRs in contrast to the commonly used SDS-TWR in literature.

In summary, this chapter describes the novel TOF error estimation model for TWR methods namely TEEM, which was originally proposed in our previous works [130, 172]. TEEM is an extended version of the conventional clock-drift error model for TWR methods defined originally in IEEE 802.15.4-2011 standard [33]. Hence, TEEM completely holds the characteristics of the mentioned model defined in the IEEE 802.15.4-2011 standard. In addition, TEEM is capable of clarifying the performance difference between even similar TWRs, which is generally unfeasible in the conventional model. Using TEEM in the evaluation, we found that all the four TWR methods gave the exact same performance in the ideal case (Section 3.4.1.1). The evaluation results also proved that AltDS-TWR is the best TWRs for typical applications in UWB localization system (Sections 3.4.1 and 3.4.2). In contrast, we demonstrated that SDS-TWR produces small TOF error comparable to AltDS-TWR only when the reply times (t_{replyA}

and t_{replyB}) are symmetric. In other words, AltDS-TWR and SDS-TWR have the same level of accuracy in the symmetric case. However, AltDS-TWR is the only robust method among the three evaluated TWRs for the asymmetric case. Therefore, we recommend the AltDS-TWR as the baseline method when the comparison or bench-marking of different TWR is conducted for quality assessment. In other words, the evaluation results suggested that the AltDS-TWR should be used as a replacement for the commonly used SDS-TWR for bench-marking purposes in comparative analyses.

In short, the main contributions made in this chapter are in three folds: First, TEEM proposed in our previous work [130, 172] was clearly explained. Second, the systematic pitfall and misconception of SDS-TWR technique was demonstrated in the chapter using TEEM. Third, AltDS-TWR was suggested as the baseline model for benchmarking TWR techniques as well as the best TWR technique based on the evaluation results, which is in contrast to the commonly applied SDS-TWR method in the literature.

In this chapter, the ranging errors due to the NLOS and MP conditions were also examined using experimental data for the two transceivers under TWR methods. The result showed that the mentioned NLOS and MP errors are significant and early identification of the conditions to effectively mitigate the errors are crucial for high resolution UWB localization system. Therefore, the identification and mitigation of the NLOS and MP conditions in UWB localization were addressed in the Chapter 5 of this dissertation. Moreover, the evaluation results based on the complete positioning system, i.e., using multiple anchor nodes and a single mobile node on the test-bed system, were examined in Chapter 4.

4 Benchmarking Position Estimation Algorithms for UWB Localization

This chapter addresses the positioning phase regarding the overall system implementation of UWB-based localization system. The main focus is made by rigorously studying the comparative analyses or bench-marking of different positioning algorithms relevant for a bidirectional UWB system. In general, a localization platform for wireless communications is regarded as a usable system, if the ranging phase discussed in Chapter 3 and the positioning phase addressed in this chapter are established. Therefore, the implementation process for the evaluation of the positioning phase and the overall system evaluation is rarely conducted separately in literature because the process is usually regarded as the same [87, 198, 200, 204, 229]. In other words, the complete set of both ranging and positioning phases is necessary to evaluate the comparative analysis of location estimation algorithms. Hence, this chapter assumes that the ranging part of the UWB localization system (Chapter 3) is already established. Additionally, the supplementary filtering part of UWB-based localization, i.e. a pragmatic approach in many real-world solutions, is also discussed in this chapter. Figure 4.1 highlights the sectional focus of this chapter upon the overall system implementation process in bidirectional UWB-based positioning and navigation.

This chapter is a heavily revised and extended version of our workshop paper [171]. In addition, a subset of the data and source codes used for presenting the evaluation results given in this chapter were provided in the public domain as an open source,

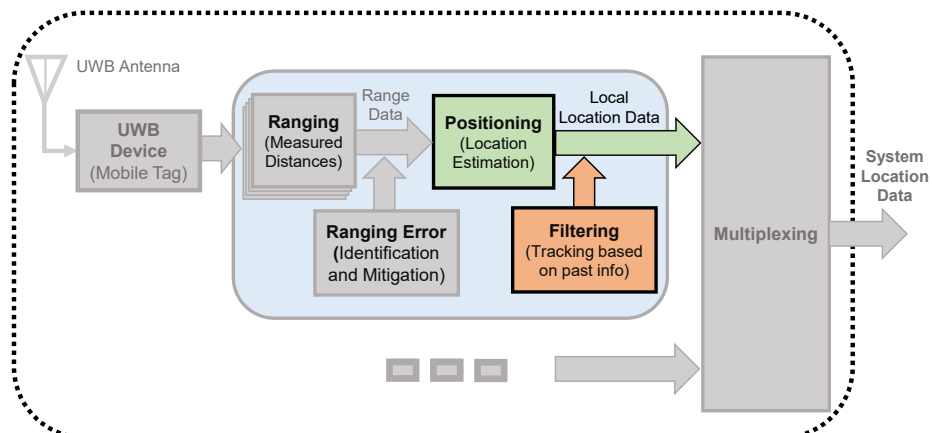


Figure 4.1: Illustration of the sectional focus for the bidirectional UWB system in this chapter, which includes the implementation of different positioning algorithms and filtering aspects.

which are available on Gitlab¹ and Github². This is in the hope that the given source code would be useful for other interested researchers and practitioners in the case of verifying the presented results as well as to proceed on further works that don't cover in this dissertation. The chapter is arranged as follows: Section 4.1 addressed the motivation behind the comparative study of different positioning algorithms, its background as well as the state of the art, and the contributions made in this chapter. Next, the fundamental theories of five positioning algorithms evaluated in the chapter are briefly introduced in Section 4.2. Then, it is followed by the implementation of the Bayesian-based system models and filtering process for the above-mentioned algorithms especially for UWB-based localization (Section 4.3). The comparative analyses of the positioning algorithms based on the evaluation results were provided in Section 4.4. And finally, the chapter conclusion and discussion are given in Section 4.5.

4.1 Background and Motivation

This subsection addresses four topics in short: (i) the brief background knowledge of the study (Section 4.1.1), (ii) the motivation by indicating why it is crucial to benchmark UWB positioning algorithms (Section 4.1.2), (iii) the state of the art in literature (Section 4.1.3), and (iv) the contributions made in this chapter (Section 4.1.4).

4.1.1 Brief Background Knowledge of the Study

UWB has been regarded as a promising technology for precise wireless localization systems in the indoor GNSS-denied environments compared to its counterpart the narrow-band wireless technologies [7, 175, 210]. Generally, the location estimation process in wireless communications needs at least two phases namely the ranging phase addressed in Chapter 3, and the positioning phase examined in this chapter. The ranging phase corresponds to measuring the distances between the fixed anchors (reference nodes) and the tag (the mobile node). Meanwhile, the positioning phase corresponds to resolving the location of the unknown target or mobile node using the information from the ranging phase and a positioning algorithm.

However, the complete integration of the system usually requires other methods and algorithms such as filtering or smoothing of the estimated outputs of the system in practice. Particularly for the bidirectional UWB system addressed in this dissertation, the multiplexing phase is also mandatory in addition to the above-mentioned two phases (see Section 2.4 in Chapter 2). That is the case when multiple objects are tracked simultaneously in the bidirectional system. However, it should be pointed out that the multiplexing phase is irrelevant for unidirectional TDoA based positioning systems, especially for a GNSS-like system integration. On those systems, the location information is calculated on the on-board mobile node for the purpose of self-localization or self-navigation [87, 229, 230]. In addition, range error identification and mitigation

¹<https://gitlab.ub.uni-bielefeld.de/csang/positioning-algorithms-for-uwb-localization-matlab>

²<https://github.com/cliansang/positioning-algorithms-for-uwb-matlab>

technique (Chapter 5) also play a crucial role in the complete system integration process of UWB-based positioning and navigation.

In this chapter, five positioning algorithms were evaluated under the assumption of the state-space approach. The state-space means that the state vector of the localization system relies on the motion model as addressed in Section 4.3.1. In general, the state vector contains all the information necessary for adequately describing the positioning and navigation system under the investigation. Regarding the measurements part, it is assumed that they are available at discrete times in all the algorithms under investigation in this chapter. That being said, there exist two models needed to be addressed by a localization system: (i) the system dynamic model, which describes the evolution of the state of the system with time, and (ii) the measurement model, which is typically responsible for relating the noisy measured data into the state vector. In UWB-based localization system, we assume that the state model is linear (Section 4.3.1) and the measurements can be regarded as either linear or nonlinear depending on the context and the algorithmic choice in the system integration [83, 230].

Moreover, the comparative analyses conducted in the chapter were based on the pragmatic system integration process in real-world applications. This means that filtering parts to smooth the raw outcomes from the applied algorithms were also accounted for in positioning methods such as Trilateration, Multilateration, and Taylor Series (TS). In addition, the five algorithms were intended to be used in a bidirectional UWB localization system, where a true-range measurement is feasible in the ranging phase (Chapter 3). In simple terms, true-range in this context refers to the accuracy of the measurement in the ranging phase (Chapter 3) is not influenced by the clock drift errors. That is in contrast to the pseudo-range in typical wireless communication systems, e.g., GNSS. The mentioned true-range measurement in wireless communication can generally be achieved by using TWR methods addressed in Chapter 3 [130, 172]. In this chapter, AltDS-TWR is applied as the ranging method for bidirectional UWB localization system, which was verified as the most reliable and optimized TWR method in our previous work [130, 172] and in Chapter 3. In other words, only one ranging technique is used for all evaluated positioning methods given in this chapter. This ensures that a consistent and fair comparative analysis was made among the evaluated algorithms.

4.1.2 Motivation

In a fundamental term, it can be stated that the backbone of any localization system/engine, regardless of its use cases and designs, is the positioning algorithm. This is because the main purpose of the localization system, i.e., calculating the target location of the mobile node (hereinafter referred to as a tag) based on the known references (hereinafter referred to as anchors), is predominantly performed by the positioning algorithm. In fact, this location information is usually the final goal of most localization systems in practice. Concerning this, there existed several positioning algorithms for wireless location estimation in the literature with different properties, advantages, and drawbacks. However, this enormous choice of algorithms leads to challenging and daunting experiences for the practitioners and researchers to determine the relevant methods for a particular localization platform. This is also particularly

true for newcomers in the field. In fact, it is time-consuming and tedious to evaluate every available method in the field, i.e. one at a time from scratch until the desired specifications are matched. Moreover, each algorithm encounters advantages and drawbacks in terms of performance scores and resource utilities depending on the use-case scenarios. Therefore, the comparative analyses (i.e., bench-marking results based on an evaluation) rigorously conducted by experts in the field are crucial for decision-making in many industrial and academic applied projects.

In the attempt to fulfill the aforementioned requirements, the performance of five true-range positioning algorithms for UWB-based localization systems were benchmarked in this chapter. The five positioning methods were specially chosen for a bidirectional UWB-based localization system. However, they are general enough to be used in any UWB-based localization system. Besides, the chosen methods are largely diversified in terms of complexity and usability starting from a simple geometry-based method called Trilateration to an advanced positioning algorithm based on a statistical approach like Unscented Kalman Filter (UKF). In particular, the evaluated algorithms in the chapter include: (i) a Trilateration method based on the conventional surveying technique using geometry, (ii) a closed-form Multilateration method that uses a least-squares technique, (iii) an iterative linearization of the non-linear process using first-order Taylor series, (iv) a recursive linearization solution based on the Extended Kalman Filter (EKF), and a recursive approach using a statistical method based on (v) the UKF. In essence, there are several other positioning algorithms for wireless localization systems proposed by researchers such as Particle Filter (PF) and its variants. Moreover, the authors in [220] recently introduced the non-convex optimization method as a positioning algorithm for wireless localization by using approximation methods similar to the min-max. However, the chosen five provided in this chapter is sufficiently adequate for the practical use-case of any UWB-based positioning and navigation processes. A few discussions regarding the exclusion of PF as position estimation algorithm for UWB system in this dissertation was also addressed in Section 4.5.

There are, indeed, comparative analyses of different position estimation algorithms for UWB-based localization systems in the literature. However, the existing comparative studies were solely based on the results achieved from simulation. Undoubtedly, the outcomes and analysis based on the computer simulation are crucial for the earlier development and system assessment of many wireless location-based services and applications. However, the simulation environment often does not represent the pragmatic problems concerning the realistic conditions of the actual world. This motivates the author to address the evaluation of the positioning algorithms for UWB using the on-ground data-sets so that the outcomes can be directly matched to the pragmatic concerns. Hence, the presented outcomes in this chapter regarding the comparative analysis of positioning algorithms for UWB technology were solely based on experimental data. This is in contrast to the simulation approaches commonly practiced in literature. In addition, the evaluated algorithms are highly diversified compared to the existing comparative analyses in the literature [7, 31, 81, 111, 171, 182, 227]. This implies that the evaluation includes the simplest positioning algorithm (i.e., Trilateration) up to one of the most advanced ones in the field based on statistical method (UKF).

4.1.3 State of The Art

When localization systems in wireless communications were implemented for a specific application, it is overwhelming for practitioners to decide the most appropriate algorithm for a certain design choice as already mentioned in the previous section. In light of this, researchers have attempted to provide comparative analyses of different wireless positioning algorithms for GNSS-denied indoor environments. Hence, there are several studies that conducted the performance comparison of different positioning algorithms in literature, especially for UWB-based localization systems [7, 31, 81, 111, 182, 227]. However, the majority of research works available in the literature lack pragmatic analysis. In fact, most of the research works available in the literature were solely based on the data produced by computer simulations. The outcomes from the simulation are, indeed, essential for the analysis of the behavior and effectiveness of the intended algorithms. However, the readers are often left with unanswered questions regarding the feasibility of the algorithms in real-world situations. For instance, it can't be identified that the best algorithm perceived in the simulation would actually outperform the other simpler counterparts in practice.

Moreover, the realistic conditions in pragmatic problems are usually overlooked by simplified assumptions in simulation environments. To put it in other words, many simulations were conducted on overly simplistic assumptions. Although the simulation study needs neither to use a complex model nor to explore every possible situation, the impact can cause real risks in the actual implementation, if overly simplified models are used. In some cases, the real-world scenario can not simply be modeled in the simulation environment. Moreover, the outcomes from the simulation could be volatile to errors during evaluation due to inevitable parameter choice by accident, which could lead to a misleading conclusion in the report.

Besides, an unfair judgment between two completely distinct algorithms was frequently performed in the simulation (e.g. Trilateration vs. EKF or particle filter as in [31]). In practice, geometric and closed-form methods are rarely used alone in system implementation and are typically coupled with a filter or smoother [175]. It should also be aware that the UWB research community acknowledges the limitations of simplifying assumptions in simulation and now shifting into the practical orientation approach. This is possible thanks to the availability of low cost UWB hardware from manufacturers such as Qorvo UWB Business Unit (former Decawave)³, Ubisense⁴, and other vendors. However, the positioning algorithms integrated into the state-of-the-art implementation of UWB localization in practice are limited to a few specific methods.

Concerning the general position estimation algorithms for wireless communications, an overview of indoor positioning technologies was addressed in [7]. Likewise, mathematical methods for indoor positioning algorithms were discussed in [182]. However, the location estimation algorithms were expressed in a generic way intended to be helpful for new researchers in the field as a general guideline. In [31], a comparative analysis of EKF, particle filter, Trilateration, and least squares approach were evaluated in a simulation. The results showed that the particle filter has the best performance

³<https://www.decawave.com/>

⁴<https://ubisense.com/>

while the EKF performed worst (especially when the target speed is increased) in most of the conducted scenarios. The latter case could be somewhat misleading as the motion model of EKF is, in general, expected to adapt the mobility of the target system. In other words, different motion models should be used and updated accordingly if the mobility of the tracking system is changed significantly in a short period of time.

Moreover, several UWB-based location estimation algorithms for both ToA- and TDoA-based system integration were addressed in [81] and [185]. In particular, the authors conducted five positioning methods for each ToA and TDoA namely: (i) analytical method, (ii) least squares approach, (iii) TS-based technique, (iv) maximum likelihood method, and (vi) genetic algorithm. However, the system setup in the simulation was specifically designed only for a LOS scenario. This means that the resultant outcomes from the simulation were based only on LOS condition and the NLOS situation was completely ignored. In the authors' simulation results, it was shown that the TS method has been dominantly preferred in most of the evaluated conditions with minimal average error and failure rate. The evaluation results based on real-world data verified that the concluding remarks were very likely (Section 4.4).

4.1.4 Chapter Contributions

In contrast to the simulation approaches discussed in the previous section, this chapter addresses the bench-marking of multiple position estimation algorithms based on experimental real-world data. The main purpose is to provide pragmatic comparative analyses to the practitioners in the field. Accordingly, five location estimation algorithms of range-based ToA localization have been addressed for the GNSS-denied indoor environments. Besides, the performance comparison was conducted based on the final outcomes of each method implemented on the pragmatic practices, i.e., filtering parts were accounted for in the system integration. This is in contrast to the typical simulation-based comparative analyses of UWB localization addressed in the literature. Figure 4.2 gave the overview of the five positioning algorithms evaluated in this chapter.

Moreover, the implementation process of the positioning algorithms for UWB localization system (Section 4.3) was given in a concise and clear way so that the presented results could easily be reproduced without the need for expert knowledge in the field. For this purpose, the exemplary source codes applied in the implementation of each algorithm in the chapter were made publicly available as already mentioned at the beginning of the chapter. In fact, most of the referenced literature in the field such as the ones given in [15, 166] provided great resources. However, they tend to provide one-dimensional cases only with excerpt information, which lacks the detail of the implementation process. Thus, this chapter attempts to minimize the mentioned gap by providing concise implementations for two motion models namely Constant Velocity (CV) and Constant Acceleration (CA) in 3D setup (see Section 4.3 for the details).

The UWB-based positioning algorithms were categorized into groups when comparative studies were conducted in the literature. By doing this, the trend and direction of the methods could be easily classified for later use-cases. Examples of such categories include parametric vs. non-parametric [31], iterative vs. optimization-based [111, 227], and geometric-based vs. Bayesian-based approaches [182]. Following a similar

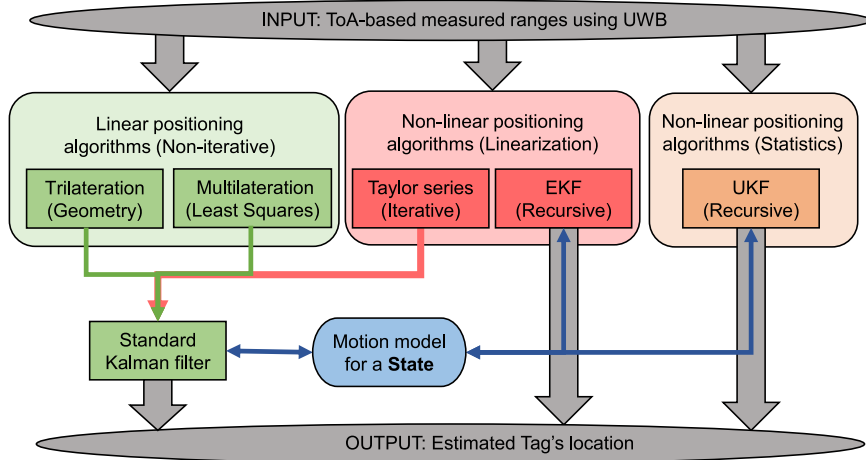


Figure 4.2: Overview of the implementation process for the evaluated five true-range positioning algorithms. The methods are categorized as linear systems (light green), non-linear systems based on linearization methods (light red), and non-linear systems based on statistical techniques (light orange). The motion model (blue) corresponds to the implementation requirements for Bayesian-based filters (Section 4.3). The image is a modified version from our previous work in [171].

practice in the literature, the evaluated positioning algorithms presented in this chapter are categorized into three parts: (i) linear positioning algorithms, (ii) the non-linear approach based on linearization techniques, and (iii) the non-linear approach based on statistical techniques as depicted in Figure 4.2.

4.2 True-range Positioning Algorithms in UWB

This section briefly presents the fundamental theory of five true-range positioning algorithms for UWB-based localization systems addressed in this chapter (Figure 4.2). Since the implementation of EKF and UKF are closely related to the basic understanding of the standard Kaman Filter (KF) as well as the use-case of KF as a continuous tracker in the linear positioning algorithms, the brief overview of the discrete KF is also tackled in Section 4.2.4. In specific, the brief positioning algorithm regarding the Trilateration method is given in Section 4.2.1, the closed-form Multilateration in 4.2.2, the TS method in 4.2.3, EKF in 4.2.5, and UKF in 4.2.6 respectively.

4.2.1 Trilateration: Geometric Technique

Trilateration is the most basic and straightforward positioning algorithm in UWB-based localization system. The method rooted from a conventional surveying approach using the geometric technique as depicted in Figure 4.3. In literature, the term Trilateration is interchangeably used with the true-range Multilateration method [170]. For the sake of clarity, the mentioned two terms are separated in this dissertation. In this regard, Trilateration specifically refers to the positioning algorithm that uses exactly three

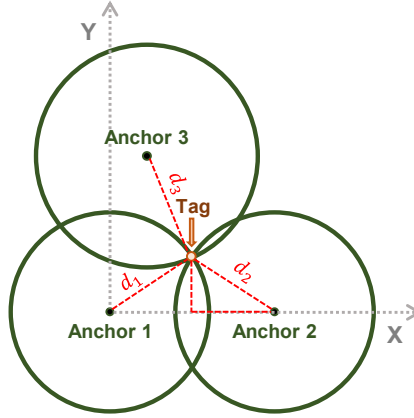


Figure 4.3: Illustration of Trilateration algorithms for positioning use-case in 2D. The image was reproduced with slight modification from [171] (©2019 IEEE. Reprinted, with permission.).

circles (i.e., three ranges) to compute the location of an unknown mobile node (tag) using an analytic geometry in 2D (Figure 4.3). In contrast, the Multilateration method uses multiple ranges, i.e., starting from three ranges up to an unlimited number of ranges in theory, for computing the location of a mobile node.

Accordingly, if we assume that the three known anchor nodes for Trilateration are A1, A2 and A3, and their corresponding Cartesian locations in 3D are $A1(0, 0, 0)$, $A2(U, 0, 0)$, $A3(V_x, V_y, 0)$ as depicted in Figure 4.3, the location of an unknown tag ($T(x_t, y_t, z_t)$) can be computed as follows, i.e Pythagoras theorem [55, 170]:

$$d_1^2 = x_t^2 + y_t^2 + z_t^2 \quad (4.1a)$$

$$d_2^2 = (U - x_t)^2 + y_t^2 + z_t^2 \quad (4.1b)$$

$$d_3^2 = (x_t - V_x)^2 + (y_t - V_y)^2 + z_t^2 \quad (4.1c)$$

where, d_i is the measured distance (radius of a circle or sphere) between the i th anchor node and the tag, (x_t, y_t, z_t) is the wanted unknown location of the tag.

Subtracting (4.1b) from (4.1a) provides

$$x_t = \frac{d_1^2 - d_2^2 + U^2}{2 \cdot U}$$

If we extract z_t^2 from (4.1a) and substitute it into (4.1c), we achieve

$$y_t = \frac{d_1^2 - d_3^2 + V_x^2 + V_y^2 - 2 \cdot x_t \cdot V_x}{2 \cdot V_y}$$

If we substitute the above computed x_t and y_t into (4.1a), it returns

$$z_t = \pm \sqrt{d_1^2 - x_t^2 - y_t^2} \quad (4.2)$$

Equation (4.2) shows that an ambiguous solution (i.e., $\pm z_t$) exists for the Z-axis. In order to eliminate the undesired one and determine the valid value between the two in 3D, the Trilateration algorithm needs the information from the fourth anchor.

In general, Trilateration algorithm encounters three major constraints: (i) the first anchor (*Anchor1* in Figure 4.3) must be on the origin of the coordinate system, i.e. the origin of 3D in Cartesian is $(0, 0, 0)$, (ii) the second anchor (*Anchor2* in Figure 4.3) must be on the horizontal line of the X-axis, and (iii) the height of all the anchors (Z-value) in the system must be exactly the same. Assigning different values on the height of the anchors in the Trilateration algorithm will degrade the accuracy of the system output.

Indeed, there are several ways to overcome the above-mentioned constraints regarding Trilateration in an arbitrary system setup. For instance, the first constraint, i.e., to put the *Anchor1* in Figure 4.3 to the origin, can be resolved by subtracting its coordinate values from all the available known anchors in the system including itself. There are three anchors in total for the Trilateration method as depicted in Figure 4.3. For the second constraint mentioned above, this can be resolved by projecting the coordinate values of the second anchor (*Anchor2* in Figure 4.3) onto the X-axis.

4.2.2 Multilateration: Closed-form Least Squares

A true-range Multilateration method, based on the Cartesian equation of a sphere, is slightly different from the typical Multilateration (based on the hyperbolic equation), which is widely used in TDoA-based systems [87, 126, 198, 229, 236]. The term true-range in the former case is used to distinguish it from the pseudo-range in the latter case and GNSS system. In this regard, true-range refers to the performance metric of the measurement that is more or less independent of the influence of clock drift errors. In other words, errors due to clock drifts in the ranging phase of true-range systems are negligible. This can be accomplished, for instance, by using AltDS-TWR [130, 149] in the bidirectional UWB localization system. In both cases of the mentioned Multilateration technique, the location of an object is determined by using multiple ranges (measured distances) between the anchors and tag as depicted in Figure 4.4.

Theoretically, the unknown location of a tag based on the known positions of the anchors can be determined by calculating the intersection of three circles in 2D (solid circles in Figure 4.4) and at least four spheres in 3D. However, the unavoidable deviations due to noise in the wireless channel corrupt the ranging measurement in practice (dotted circles in Figure 4.4) as explained in Chapter 2.4 as well. The core causes of noise in wireless channel of UWB includes the NLOS conditions, multi-path signals, hardware limitations, etc. Due to these measurement noises, the circles rarely intersect at a single location in practice. Rather, what we typically attain is an area of the estimated location. In Figure 4.4, the mentioned estimated area using three circles is shown in red color, and the areas using four circles in green. Based on the visual representation under the assumption of constant deviation, we can conclude that the estimated area is getting smaller if we increase the number of anchor nodes in the system (Figure 4.4).

For the demonstration purpose regarding the derivation of true-range Multilateration algorithm (Figure 4.4) [66], we can suppose that the tag in 3D is located at position $X_t = [x_t, y_t, z_t]^T$, and the anchors (centers of spheres) are at positions $X_i = [x_i, y_i, z_i]^T$,

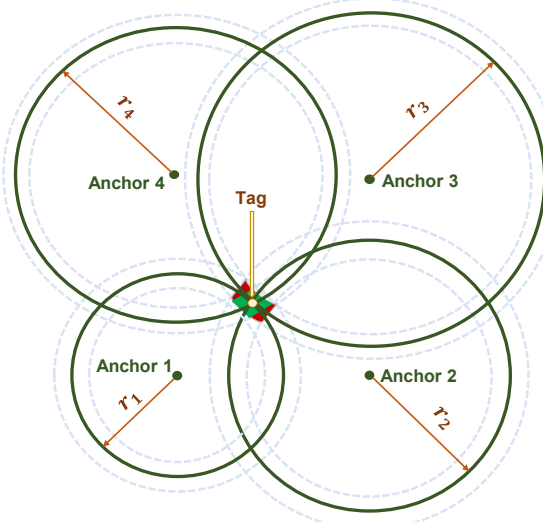


Figure 4.4: Illustration of positioning algorithms based on true-range Multilateration in 2D. The image was reproduced with minor changes from [175] (©2019 IEEE. Reprinted with permission).

where $i = 1, 2, \dots, N$ are the known anchors' IDs. Then, the generic spherical equation for the true-range Multilateration using the measured distances between anchors and tag (i.e., the radius of a sphere) can be written in 3D as follows (Figure 4.4):

$$d_i^2 = (x_i - x_t)^2 + (y_i - y_t)^2 + (z_i - z_t)^2 \quad (4.3)$$

where, d_i is the measured distance (range) between the anchor X_i and tag X_t .

For the sake of simplicity, the formula derivation of the true-range Multilateration for four anchors in 3D will be demonstrated in this section. It should be noted that the algorithm is not restricted to four anchors. Instead, it can be expanded to any number of anchors available in the system. That being said, the measured four distances between four anchors and a tag using (4.3) can be written as:

$$d_1^2 = (x_1 - x_t)^2 + (y_1 - y_t)^2 + (z_1 - z_t)^2 \quad (4.4)$$

$$d_2^2 = (x_2 - x_t)^2 + (y_2 - y_t)^2 + (z_2 - z_t)^2 \quad (4.5)$$

$$d_3^2 = (x_3 - x_t)^2 + (y_3 - y_t)^2 + (z_3 - z_t)^2 \quad (4.6)$$

$$d_4^2 = (x_4 - x_t)^2 + (y_4 - y_t)^2 + (z_4 - z_t)^2 \quad (4.7)$$

Subtracting (4.4) from (4.5) and simplifying yields:

$$\begin{aligned} & (x_2 - x_1) \cdot x_t + (y_2 - y_1) \cdot y_t + (z_2 - z_1) \cdot z_t \\ &= \frac{1}{2} \cdot [d_1^2 - d_2^2 + (x_2^2 + y_2^2 + z_2^2) - (x_1^2 + y_1^2 + z_1^2)] \end{aligned} \quad (4.8)$$

Similarly, by subtracting (4.4) from (4.6) and (4.7), we can achieve the system of equations in a matrix notation as:

$$Ax = b \quad (4.9)$$

where,

$$A = \begin{bmatrix} x_2 - x_1 & y_2 - y_1 & z_2 - z_1 \\ x_3 - x_1 & y_3 - y_1 & z_3 - z_1 \\ x_4 - x_1 & y_4 - y_1 & z_4 - z_1 \end{bmatrix}, \quad x = \begin{bmatrix} x_t \\ y_t \\ z_t \end{bmatrix},$$

$$b = \frac{1}{2} \cdot \begin{bmatrix} d_1^2 - d_2^2 + (x_2^2 + y_2^2 + z_2^2) - (x_1^2 + y_1^2 + z_1^2) \\ d_1^2 - d_3^2 + (x_3^2 + y_3^2 + z_3^2) - (x_1^2 + y_1^2 + z_1^2) \\ d_1^2 - d_4^2 + (x_4^2 + y_4^2 + z_4^2) - (x_1^2 + y_1^2 + z_1^2) \end{bmatrix}$$

In this regard, it is noteworthy that the elements of the matrix A in (4.9) come from the reference coordinates of the anchor nodes, i.e., the known coordinate values of the system. All elements in the vector b are also known to the system, i.e., the measured distances (ranges) and the coordinate of the anchors. Thus, the vector x is the only unknown term in (4.9) as well as the desired value to be estimated in the system, i.e., the location of the interested tag device.

As a matter of fact, we can address Equation (4.9) as a least squares problem if the square matrix $A^T A$ (e.g. in the case of more than four anchors in the system) is invertible [195]. Theoretically, the matrix $A^T A$ becomes a singular (or) non-invertible matrix if and only if all coordinates of the anchor nodes lie on a col-linear line (i.e. they all lie on a single straight line) in 2D and a co-planar plane (i.e., on the same plane) in 3D [15]. This manner can be checked easily by finding the column rank of the matrix A , i.e., the independent column vectors of the matrix [195]. In this regard, the column rank of the concerned matrix A should be exactly 2 for a 2D environment and 3 for the 3D. This can be accomplished by the careful deployment of the anchor nodes. When the required verification of the column rank is met, the estimated solution for (4.9) can be calculated as follows [15, 66, 195]:

$$x = (A^T A)^{-1} A^T b \quad (4.10)$$

where x is the estimated coordinate of a tag device. When the number of anchors in the system is more than three in 2D and more than 4 in 3D, the Ordinary Least Square (OLS) method defined in (4.10) is generally considered as the over-determined system. The term over-determined is used in the sense that there are more equations than unknowns in the problem to be solved.

4.2.3 First-order Taylor Series: Non-linear Iterative Method

TS method can be used as a UWB-based position estimation algorithm in a 3D environment for both TDoA-based and the ToA-based systems [65, 81, 94]. In literature, the modified version of TS method was also conducted and used as the location estimation algorithm for TDoA wireless positioning and navigation [226].

Based again on the generic spherical equation for UWB-based positioning and navigation given in Equation (4.3), a function that corresponds to the i th measured range between the i th anchor and a tag can also be defined as [65] (Figure 4.4):

$$\begin{aligned} f_i(x, y, z) &= \sqrt{(x_i - x)^2 + (y_i - y)^2 + (z_i - z)^2} \\ &= d_i + \varepsilon_i \quad (i = 1, 2, \dots, n) \end{aligned} \quad (4.11)$$

where, ε_i is the range estimation error between a tag and the i th anchor. In this regard, it is assumed that the errors (ε) are statically distributed, and its elements are independent to each other based on zero-mean Gaussian random variables [65]. Thus, the error covariance matrix can be written as:

$$R = E[\varepsilon \varepsilon^T] = \text{diag}[\sigma^2 \dots \sigma^2] \quad (4.12)$$

where, σ is the range estimation error.

If we suppose that (x_v, y_v, z_v) is an initial guess of the true tag's location (x_t, y_t, z_t) of the system, we can express it in the equation as:

$$x_t = x_v + \delta_x, y_t = y_v + \delta_y, z_t = z_v + \delta_z \quad (4.13)$$

where, δ_x , δ_y , and δ_z are the location errors related to the true location of a tag to be determined. In other words, it is the incremental error between the guess and the true position of the mobile node or tag.

If Equation (4.11) is expanded into the TS by keeping the first-order term, it is possible to achieve as in the following:

$$f_{i,v} + a_{i,1} \cdot \delta_x + a_{i,2} \cdot \delta_y + a_{i,3} \cdot \delta_z \approx d_i + \varepsilon_i \quad (4.14)$$

where,

$$\begin{aligned} f_{i,v} &= f_i(x_v, y_v, z_v), \quad a_{i,1} = \frac{\partial f_i}{\partial x} \Big|_{x_v, y_v, z_v} = \frac{x_v - x_i}{r_i}, \\ a_{i,2} &= \frac{\partial f_i}{\partial y} \Big|_{x_v, y_v, z_v} = \frac{y_v - y_i}{r_i}, \quad a_{i,3} = \frac{\partial f_i}{\partial z} \Big|_{x_v, y_v, z_v} = \frac{z_v - z_i}{r_i}, \\ r_i &= \sqrt{(x_i - x_v)^2 + (y_i - y_v)^2 + (z_i - z_v)^2} \end{aligned}$$

Equation (4.14) can be written in matrix notation as

$$H\delta = \Delta d + \varepsilon \quad (4.15)$$

where, $\Delta d = d_i - f_{i,v} = d_i - r_i$,

$$H = \begin{bmatrix} a_{1,1} & a_{1,2} & a_{1,3} \\ a_{2,1} & a_{2,2} & a_{2,3} \\ \dots & & \\ a_{n,1} & a_{n,2} & a_{n,3} \end{bmatrix}, \quad \delta = \begin{bmatrix} \delta_x \\ \delta_y \\ \delta_z \end{bmatrix}, \quad \varepsilon = \begin{bmatrix} \varepsilon_1 \\ \varepsilon_2 \\ \dots \\ \varepsilon_n \end{bmatrix}$$

Using the covariance of measurement error (R) in (4.12) as a weight, (4.15) can be solved using the over-determined weighted least square method [65] as:

$$\delta = (H^T R^{-1} H)^{-1} H^T R^{-1} \Delta d \quad (4.16)$$

If we substitute the initial guess (x_v, y_v, z_v) and the computed incremental error (δ) from (4.16) to (4.13), we can achieve the location estimation (x_t, y_t, z_t) of the tag or mobile node by continually refining the mentioned process using iterative approach.

In summary, positioning based on TS method starts with an initial guess. Then, it improves the estimate at each iteration step by determining the solution of the local linear least-squares parameters. The method is iterative because the beginning states of the TS will encounter some errors depending on how well the initial guess constitutes the actual ground truth. As the iteration continues, the method will eventually converge except for a few cases where realistic initial guesses are not available. In such a scenario, the method could take a long time to converge or fail to converge completely. However, such scenarios hardly happen especially in UWB-based position estimation process due to short-range environments (i.e., typically less than 100 m). Nevertheless, the realistic initial guess should be given within the mentioned coverage range.

4.2.4 Standard Kalman Filter: Continuous Tracking Mechanism

The positioning techniques described so far (from Section 4.2.1 to 4.2.3) are suitable for static location estimation of objects in wireless communications. The reason is that there is no guarantee that the estimate for two consecutive events at the same location would provide the same or nearby value in such algorithms. For instance, an added noise in UWB measurement due to NLOS condition introduces a location error that could cause to jump the estimated positioning data invariably. To address such a scenario, continuous object tracking algorithms are beneficial for many applications.

KF is widely used for continuous object tracking systems since the method take advantage of past information to predict the best estimate for the current state condition. As a matter of fact, the filter even supports estimations of past, present, and future states [17, 56]. In some cases, it is claimed in the literature that the filter still works fine in a situation where the precise nature of the system model is unknown [17]. This allows the KF to be a versatile method for many application domains including position estimation, filtering, and smoothing of noisy data. However, a defined system model is mandatory for the filter to be used as a location estimator for location estimation processes addressed in this chapter. The implementation process of KF for the purpose of location estimation is expressed in Section 4.3.3.1. In short, an appropriate motion model of the state and measurement function is necessary for the implementation.

In this chapter, standard KF was used as a continuous tracking mechanism for location estimation of UWB-based static algorithms as well as the data smoother for the resultant location output from the closed-form positioning algorithms. In particular, the standard KF is used for tracking purposes and refining process of the outcomes from three positioning algorithms namely Trilateration (Section 4.2.1), Multilateration (Section 4.2.2) and Taylor series (Section 4.2.3). Regarding this, the measurement function in the filter is simply the positioning outcome provided by the mentioned static algorithm. In contrast, the EKF (Section 4.2.5) and UKF (Section 4.2.6) are used as standalone positioning algorithms by taking the ranging equation in (4.3) as the measurement function, i.e., a nonlinear function.

Generally speaking, the standard KF gives a recursive solution to a linear filtering problem for estimating the state of a process governed by the difference equation and its measurement as formulated in the following [17]:

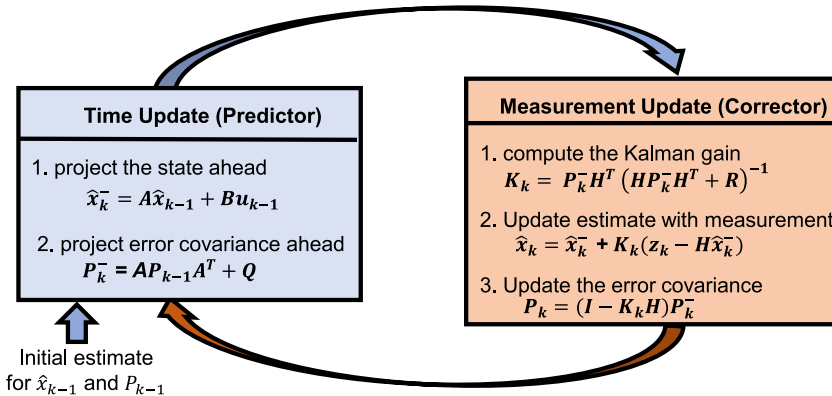


Figure 4.5: Illustration of Kalman Filter operation. P_k^- and P_k are the priori and posteriori estimate of error covariance matrices, and K_k is the $n \times m$ matrix Kalman gain. The representation of the concept depicted in the image was inspired by the work in [17].

$$x_k = Ax_{k-1} + Bu_{k-1} + w_{k-1}, w_k \sim N(0, Q) \quad (4.17)$$

$$z_k = Hx_k + v_k, v_k \sim N(0, R) \quad (4.18)$$

where, x_k is the state vector, A is the $n \times n$ state transition matrix, u_k is the input vector, B is the $n \times l$ input control matrix, z_k is the measurement vector, H is the $m \times n$ state to measurement transition matrix, w_k and v_k are the process and measurement noise respectively. Q and R are the process and measurement noise covariance respectively and m , n , and l are the number of available measurements, state variable, and inputs.

In general, the Kalman filter estimates a process by recursively resembling two sets of equations namely a predictor (time update) and corrector (measurement update) as illustrated in Figure 4.5 [17, 109]. To shorten the discussion of this well-established filter, the author would refer to the introductory theory of KF to [17, 56] for more details. In a simple term, the filter predicts the new possible outcome based on the previous data (i.e., the initial value if the filter is used for the first time) and process noises introduced by the system in the time update phase (predictor). In the measurement update phase (Corrector), the measurement data originated from the measuring device (e.g., UWB hardware) were taken into account. Then, the Kalman gain is applied to decide which portion of the data should be kept by taking the difference between the measured value and the predicted value. Using the Kalman gain, it is feasible to calculate a new predicted value of the state and its uncertainty (variance) by feeding back into the time update phase. This process repeats continuously in each cycle as depicted in Figure 4.5 until the filter eventually converges to the desired solution.

In this dissertation, the standard KF is used for the purpose of continuous positioning (or) tracking in location estimation algorithms for linear methods which do not have such capability naively within their standalone process. Such algorithms include Trilateration, Multilateration, and TS approach (Figure 4.2). Standard KF equip the mentioned simple algorithms to provide the optimal solution using basic linear arithmetic. Concurrently, standard KF acts as the output data filter for smoothing the

outcomes of linear positioning algorithms. The implementation of standard KF for the purpose of continuous positioning and tracking system is expressed in Section 4.3.3.1.

However, it should be noted that the standard KF assumes the processed data are in the form of Gaussian Distribution and its estimation is based only on linear equations. In pragmatic real-world situations, most of the conditions are in the form of non-linear functions. This is where the EKF comes into effect for solving the non-linearity in the system as described in Section 4.2.5.

4.2.5 Extended Kalman Filter: Recursive Positioning Technique

For solving non-linear problems, the extension of the standard KF called EKF is widely utilized in many systems [17, 191]. The operation of EKF is very similar to standard KF as depicted the functional diagram in Figure 4.6. In contrast to standard KF, EKF can be achieved by linearizing the state and measurement equations using the TS expansions. Thus, EKF can fundamentally be thought of as the combination of TS (Section 4.2.3) and standard KF (Section 4.2.4) [17, 90]. Accordingly, the non-linear functions are generally linearized by keeping either the first-order or the second-order of the TS expansion. The outcome achieved by the former case is usually called the Jacobian approximation, whereas the latter case is called the Hessian approximation.

The most crucial exception opposed to the TS is that the EKF is keeping track of the total quantities of the state variables whereas the incremental ones are keeping track in the TS approach [22]. However, it is possible that the performance of the EKF could be very poor (or) could be divergent in some cases if the underlying non-linearity of the problem is very high [191]. Principally, EKF assumes that the non-linearity of the given problem to be solved is within the scope of the Gaussian approximation. In other words, EKF will be likely to divergent if the process and measurement noises in the system cannot be modeled with Gaussian approximation.

Figure 4.6 highlights the core differences between EKF and the standard KF. In terms of application areas, there are several used cases of EKF in many fields such as

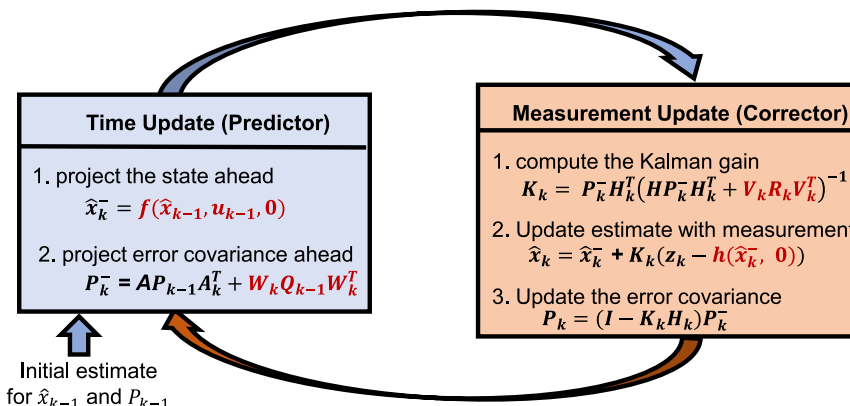


Figure 4.6: Illustration of Extended Kalman Filter Operation. The representation of the concept depicted in the image was inspired by the work in [17].

nonlinear state estimation, nonlinear dynamic systems, machine learning, etc [162, 186, 206]. Importantly, the EKF was also one of the primary position estimation algorithms in wireless localization systems [21, 22, 23, 26, 112, 198, 229, 230]. The main reason is that EKF is capable of serving as a standalone positioning algorithm with tracking capability based on past information. Thus, EKF was applied as the standalone positioning method for bidirectional UWB-based localization system in this chapter.

4.2.6 Unscented Kalman Filter: Statistical Positioning Method

The EKF expressed in the previous section was one of the most widely used estimation algorithms for nonlinear systems since its first use-case at the Apollo space mission in 1962 [155]. However, EKF tends to be difficult when implementing and tuning in practice due to the need of linearization based on Jacobian (or) Hessian [107]. It is mostly suitable for a system with easy to differentiate nonlinear functions. The UKF was developed with the intention of overcoming the mentioned difficulties encountered by the EKF using a statistical transformation called Unscented Transform [106, 108]. The Unscented Transform (UT) is a method to propagate the mean and covariance of the information in a system through nonlinear transformations. It has been proved that the UKF is more robust compared to EKF in terms of accuracy and ease of implementation while maintaining the same order of computing complexity [106, 107, 206]. The original paper of UKF can be found in [106].

In short, the UKF addresses the nonlinear problem using the so-called sigma points, which are deterministic sample points carefully chosen for the transformation [106, 206]. The transformed method is known as the unscented transformation. There are two steps in UKF. The first step involves the determination of the sigma points. The second step involves the update of errors related to the state and measurement functions similar to the standard KF and EKF. For the former case, it is supposed that a random variable x is propagated through a nonlinear function with a known mean \bar{x} and covariance P_x , which can be formulated as follow:

$$y = g(x) \quad (4.19)$$

The sigma points for (4.19) is determined in UKF as $\sigma = 2n + 1$, where σ is the dimension of the state [230]. From there, the mean related to the vector of sigma points X_i and its corresponding weight W_i can be formulated. Hence, the approximation of the mean of sigma points using UT yields:

$$X_i = \begin{cases} \bar{x}, & \text{when } i = 0 \\ \bar{x} + (\sqrt{(n + \lambda)P_x})_i, & \text{when } i = 1, 2, \dots, n \\ \bar{x} - (\sqrt{(n + \lambda)P_x})_i, & \text{when } i = n + 1, n + 2, \dots, 2n \end{cases} \quad (4.20)$$

where X_i is the sigma vectors of $2n + 1$ in which n is the dimension of the state, λ is the scaling parameter which is defined as $\lambda = \alpha^2(n + \kappa) - n$. α specifies the sigma points spreading around the mean \bar{x} which is usually set to a small positive value in practice (e.g. $1e^{-3}$). Additionally, κ is a secondary scaling parameter in addition to α and this κ value is usually set to zero in practical implementation.

The parameters for the weight correspond to two kinds, namely the weight related to the mean ($W_i^{(m)}$) and the weight related to the covariance ($W_i^{(c)}$). The said two weighted for UKF can be defined as follows:

$$W_i^{(m)} = \begin{cases} \frac{\lambda}{n+\lambda}, & \text{when } i = 0 \\ \frac{1}{2(n+\lambda)}, & \text{when } i = 1, 2, \dots, 2n \end{cases} \quad (4.21)$$

$$W_i^{(c)} = \begin{cases} \frac{\lambda}{n+\lambda} + (1 - \alpha^2 + \beta), & \text{when } i = 0 \\ \frac{1}{2(n+\lambda)}, & \text{when } i = 1, 2, \dots, 2n \end{cases} \quad (4.22)$$

where β corresponds to the prior knowledge of the distribution of the input random signal, which optimal value is $\beta = 2$ for Gaussian distribution [206]. The important characteristic to note here is that the normalized sum of the two mentioned weights ($W_i^{(m)}$ and $W_i^{(c)}$) should be 1.

Based on the above-mentioned sigma points, the approximation of the nonlinear function can be computed as:

$$Y_i = g(X_i) \quad \text{where } i = 0, 1, \dots, 2n \quad (4.23)$$

The posterior sigma points for the weighted sample mean and covariance are:

$$\bar{y} \approx \sum_{i=0}^{2n} W_i^{(m)} Y_i \quad (4.24)$$

$$P_y \approx \sum_{i=0}^{2n} W_i^{(c)} (Y_i - \bar{y})(Y_i - \bar{y})^T \quad (4.25)$$

The conceptual approximation process of the UT for the UKF is depicted in Figure 4.7, in which it is compared with the process applied in EKF. In a nutshell, the rest of

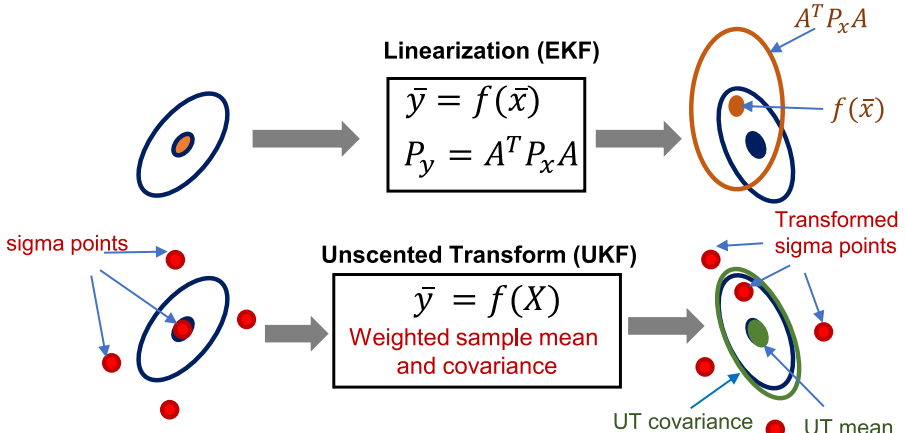


Figure 4.7: Conceptual illustration of the EKF (upper row) and the UKF (lower row) regarding the approximation over the nonlinear functions. The blue circles represent the actual transformation. The image was inspired by the work in [206] and it was modified from it.

the UKF operation is very similar to the EKF, apart from the approximation process of the nonlinear function with UT. Thus, it is also assumed in UKF that the distribution of the state and measurement functions are Gaussian Random Variable (GRV) akin to EKF. For a better understanding of the theory and applications of UKF other than position estimation purposes, the author would refer to the works in [107, 206]. The practical use-cases of UKF for wireless positioning system including the integration process for the UWB-based localization system was addressed in detail at the works in [74, 230].

In general, the algorithm of UKF can be accomplished in the following steps. For brevity, the procedure was outlined without giving any mathematical equations and the details can be found in [74, 206].

1. Select the sets of sigma points (X_i) and their corresponding weights ($W_i^{(m)}$ and $W_i^{(c)}$) for $0 \leq i \leq 2n + 1$ using (4.20), (4.21), and (4.22) based on the dimension of the system. If the state function is linear, the sigma point calculation can be skipped and use the linear model directly.
2. Calculate the time update state of UKF
3. Compute the Kalman gain for the UKF operation
4. Compute the predicted measurement mean and covariance of UKF

In summary, the general advantage of UKF over the EKF is in cases, where non-linear functions cannot be easily differentiated analytically by a method such as Jacobian or Hessian. In such particular cases, UKF is effective to propagate the nonlinear functions through its sigma point transformation since no analytical differentiation are necessary. However, the two methods gave comparable results for the use-case of UWB localization, where the nonlinear function is differentiable, as discussed in Section 4.4.

4.3 Implementation of Bayesian-based Filters for IPS

The bidirectional UWB localization system under investigation in this dissertation is assumed as a state-space model. In this regard, it is assumed that the target motion of the system and its measurements can be represented with some known mathematical models. In general, there are two models to represent a dynamic system in the state-space approach. The first model concerns about the evolution of the state with respect to time, which is typically called the dynamic or system model. The second model deals with the noisy measurement that relates its observation to the state of the system, which is typically called as a measurement model. In this dissertation, it is assumed that the mentioned noisy measurement data from the UWB localization system are available at a discrete time. Specifically, the measurement update rate of 10 Hz was used in all the presented evaluation results given in this dissertation (i.e., the discrete-time system as opposed to the continuous-time). The reason for using this update rate is that the UWB hardware used in the evaluations, which is manufactured by Decawave (Qorvo), is capable of extracting data at this rate in real-time.

The state model is one of the key discriminators for whether the filter would be used as a location estimation algorithm or other filtering processes in various applications. Based

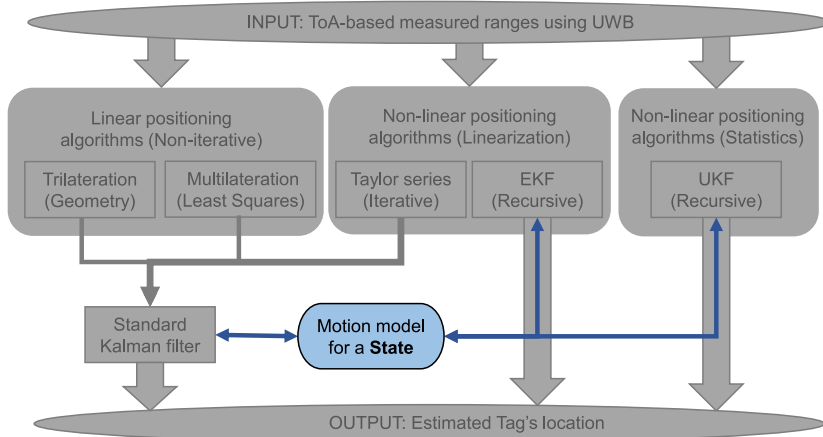


Figure 4.8: Highlight of the motion model commonly used in all position estimation algorithms

on the concerned problem, the state and measurement models could be either linear or nonlinear. As already specified in Equation (4.3) (Section 4.2.2), the measurement function of the ranging phase in UWB system is expressed in a quadratic equation. Therefore, the measurements in UWB-based localization systems are generally in the form of a non-linear function. However, the state function can be defined as linear mathematical equations based on Newton's law of motion. Indeed, the linear model for the state function is a common practice in point-based wireless navigation and positioning such as UWB, GNSS, etc [230]. The point-based system refers to modeling the moving targets as a point object without any shapes in location-based services such as target tracking, navigation, and localization [166]. KF is one example of among other available point-based localization schemes based on the state-space approach.

This section focuses on the maneuver/motion models (Section 4.3.1) used in the state-space model as well as its measurement concerns (Section 4.3.2). Accordingly, the concrete implementation process of the standard KF was discussed in Section 4.3.3.1, followed by the implementation of EKF in Section 4.3.3.2, and UKF in Section 4.3.3.3.

4.3.1 Dynamic or Motion Model for UWB Localization

A motion model relates the dynamic behavior of the system between measurements and the localization algorithms. As depicted in Figure 4.8, the motion model is a common block for all the location estimation algorithms evaluated in this dissertation. It is worth noting that localization systems can indeed be integrated without the need to use the state model (for instance, by using PF) [80]. Though, the use of motion models in wireless object tracking and navigation system generally provides better performance compared to the model-less approaches if the underlying model is designed to effectively represent the state [121]. This signifies that the right choice of motion model is crucial in some system implementations of UWB-based localization.

In multidimensional systems, e.g., in 3D Cartesian coordinate, the motion of an object along the x direction is theoretically independent of its motion along the Y and

Z directions. Thus, the motion model can be divided separately into three independent dimensions in 3D. This means, in principle, the motion of an object in the horizontal direction (e.g. in 2D) is unrelated to the motion in the vertical direction, and vice versa. For instance in 3Ds, the motion of an object in all three-dimensional directions can be computed by examining and combining each three one-dimensional axes separately.

In this regard, the most commonly used motion models for wireless positioning and navigation systems (i.e., UWB, GNSS, etc.) are the CV and CA motion models. In CV and CA models, the general assumption is that the derivatives of the position in the second-order (i.e, velocity) and the third-order (i.e., acceleration) terms are not zero, but a random process with zero-mean. By all means, there exist several other kinematic models in literature based on the behavior of maneuvers. For a comprehensive list of the motion models for the dynamic systems including the positioning and navigation use-cases, a great survey can be found in [166]. However, the author would stress out that many practical applications in target tracking and navigation systems for UWB as well as in other wireless positioning approaches rarely use the other models available in literature due to the increased complexity in implementation while the performance improvement is not significant compared to the CV and CA.

For the sake of approval, the evaluation of four motion models specifically for flight navigation was conducted in [121]. The experimental results based on real-world data show that CA motion model performed the best in a high dynamic maneuver scenario whereas the CV (or) decoupled state motion model provided reliably good outcomes in all test conditions, i.e., taking off, straight and level, dynamic maneuver, and landing phases of the flight. CV motion model was also examined in many application areas of positioning and navigation in conjunction with location estimation algorithms. To mention them a few, CV was chosen as a motion model for PF-based location estimation in [83], for the EKF-based position estimator in [213], and it integrated with the standard KF for smoothing the output location data in [175]. Similarly, CA model was also the common choice for many wireless positioning and navigation systems [198, 230] as well as in sensor fusion system [75]. Therefore, the CV and CA motion models are addressed within the context of UWB localization in the coming next two subsections. In short, the motion model corresponds to two matrices in the implementation of the Bayesian-based state-space model namely the state or dynamic model of the system and its corresponding process noise.

4.3.1.1 Constant Velocity Motion Model

Based on the Newtonian kinematic equation, we can express our 3D physical word, i.e., Cartesian Coordinate system, with its 3D position, velocity, acceleration vectors [224]. Concerning this, the location of a moving object to be examined in a system is usually assumed as a point-based target/tag (i.e., the estimated location is based on the center of the object). For such a point-based localization system, the state vector can be expressed in many ways. Among different available models, two widely used state vector implementation styles were concretely discussed in this section. Though the mentioned two state vectors are identical, the different implementation processes for the same information in literature could be confusing to the practitioners and

researchers who are new to this research field. The reason is that the order of the state vector defines slight implementation changes in the structure of the transition matrix, that relates the measurement and the state, as well as the matrices concerning the process and measurement noises.

A motion model for moving objects can generally be classified into two types namely maneuver and non-maneuver models [166]. The CV model addressed in this section can usually be put under the former category based on how the process noise is processed (for instance, it is assumed as white Gaussian noise). In contrast, the CA motion model addressed in Section 4.3.1.2 is one of the widely used models in the latter case. In literature, CV is also called as the uniform motion model, Position-Velocity (PV) model, and white-noise acceleration model.

In general, the order of a state vector in a state-space system at Cartesian coordinate regarding the CV model can be written as either $x_k = [x \dot{x} y \dot{y} z \dot{z}]^T$ or $x_k = [x y z \dot{x} \dot{y} \dot{z}]^T$. Here, $[x y z]$ is the vector related to the position of the moving target (i.e. a tag in UWB localization) whereas $[\dot{x} \dot{y} \dot{z}]$ is its corresponding velocity vector. Referring back to the state-space model for Kalman-based filters in Section 4.2.4, the dynamic state model implies the matrices A and the process noise Q . In some literature, the focus of the location estimation on the state vector is usually addressed on the 2D Cartesian coordinate. This means the velocity part for the Z-direction is omitted [166]. For the sake of clarity, the velocities for all three directions are addressed in this chapter.

For the state vector $x_k = [x \dot{x} y \dot{y} z \dot{z}]^T$, the corresponding state-space model can be described in a discrete-time system as [15]:

$$x_k = Ax_{k-1} + \Gamma w_{k-1} \quad (4.26)$$

where w_{k-1} is a zero-mean white random or Gaussian noise. For simplicity, we first assume a single coordinate case (i.e., the multi-coordinate system follows subsequently).

The transition matrix for (4.26) in a single coordinate is:

$$A = \begin{bmatrix} 1 & T \\ 0 & 1 \end{bmatrix}$$

The vector gain that multiplies the scalar process noise w_{k-1} becomes [15]:

$$\Gamma = \begin{bmatrix} \frac{1}{2}T^2 \\ T \end{bmatrix}$$

The covariance of the process noise for a single coordinate Q is:

$$Q = E[\Gamma w_{k-1} w_{k-1} \Gamma^T] = \Gamma \sigma_w^2 \Gamma^T = \begin{bmatrix} \frac{1}{4}T^4 & \frac{1}{2}T^3 \\ \frac{1}{2}T^3 & T^2 \end{bmatrix} \sigma_w^2 \quad (4.27)$$

σ_w^2 is the variance of the process noise in a single dimension, which is scalar. In CV model given above, it is assumed that the changes in the velocity over a discrete time interval (i.e., the value of $\sigma_w T$, are smaller than the actual velocity of the system.

For multidimensional or 3D, the motion model for the state-space can be written as:

$$x_k = \text{diag}[A_{cv}, A_{cv}, A_{cv}]x_{k-1} + w_{k-1} \quad (4.28)$$

$$Q = \text{diag}[\sigma_{wx}^2 \dot{Q}_{cv}, \sigma_{wy}^2 \dot{Q}_{cv}, \sigma_{wz}^2 \dot{Q}_{cv}] \quad (4.29)$$

where,

$$A_{cv} = \begin{bmatrix} 1 & T \\ 0 & 1 \end{bmatrix}, \quad Q_{cv} = \begin{bmatrix} \frac{1}{4}T^4 & \frac{1}{2}T^3 \\ \frac{1}{2}T^3 & T^2 \end{bmatrix}, \quad w_{k-1} = \begin{bmatrix} w_x \\ w_y \\ w_z \end{bmatrix}$$

From the above equations, w_k is the discrete-time white Gaussian noise sequence, T is the sampling interval or system update rate in many practical applications, and $\sigma^2(w)$ is the variance of the process noise. One of the core ideas to model the process noise in motion model as a random process is that it is unrealistic to assume that there are no disturbances in the system. Therefore, it is assumed that the random process is able to approximate the real-world system in discrete time if the right interval can be set. For the sake of completeness and clarity, the full matrices for state or dynamic model for CV and its corresponding covariance of the noise term can be described as:

$$A = \begin{bmatrix} 1 & T & 0 & 0 & 0 & 0 \\ 0 & 1 & 0 & 0 & 0 & 0 \\ 0 & 0 & 1 & T & 0 & 0 \\ 0 & 0 & 0 & 1 & 0 & 0 \\ 0 & 0 & 0 & 0 & 1 & T \\ 0 & 0 & 0 & 0 & 0 & 1 \end{bmatrix}, \quad Q = \begin{bmatrix} \frac{1}{4}T^4 & \frac{1}{2}T^3 & 0 & 0 & 0 & 0 \\ \frac{1}{2}T^3 & T^2 & 0 & 0 & 0 & 0 \\ 0 & 0 & \frac{1}{4}T^4 & \frac{1}{2}T^3 & 0 & 0 \\ 0 & 0 & \frac{1}{2}T^3 & T^2 & 0 & 0 \\ 0 & 0 & 0 & 0 & \frac{1}{4}T^4 & \frac{1}{2}T^3 \\ 0 & 0 & 0 & 0 & \frac{T^4}{2} & T^2 \end{bmatrix} \sigma_w^2$$

Here, it is assumed that the variances σ_w^2 of the process noise Q are in a scalar. The core significant feature within the matrices is that the parametric values regarding the motion model are ordered as blocks of data in the main diagonal of the matrices.

Alternatively, the matrices related to the state (dynamic) model and its corresponding covariance of the noise term for the CV become as in the following, if the state vector is organized as in the order of $x_k = [x \ y \ z \ \dot{x} \ \dot{y} \ \dot{z}]^T$.

$$A = \begin{bmatrix} 1 & 0 & 0 & T & 0 & 0 \\ 0 & 1 & 0 & 0 & T & 0 \\ 0 & 0 & 1 & 0 & 0 & T \\ 0 & 0 & 0 & 1 & 0 & 0 \\ 0 & 0 & 0 & 0 & 1 & 0 \\ 0 & 0 & 0 & 0 & 0 & 1 \end{bmatrix}, \quad Q = \begin{bmatrix} \frac{1}{4}T^4 & 0 & 0 & \frac{1}{2}T^3 & 0 & 0 \\ 0 & \frac{1}{4}T^4 & 0 & 0 & \frac{1}{2}T^3 & 0 \\ 0 & 0 & \frac{1}{4}T^4 & 0 & 0 & \frac{1}{2}T^3 \\ \frac{1}{2}T^3 & 0 & 0 & T^2 & 0 & 0 \\ 0 & \frac{1}{2}T^3 & 0 & 0 & T^2 & 0 \\ 0 & 0 & \frac{1}{2}T^3 & 0 & 0 & T^2 \end{bmatrix} \sigma_w^2$$

In summary, the final outcomes of the individual parameters in the state vector will be identical for both implementation styles presented in this section. The former one based on the state vector of $x_k = [x \ \dot{x} \ y \ \dot{y} \ z \ \dot{z}]^T$ deals with the computation of block diagonal matrices (i.e., blocks of values are presented on the diagonal of a matrix, which is different but similar to a single main diagonal line in typical matrix representation). On the other hand, the latter mainly deals with symmetric matrices, especially on the covariance of processes noise. Personally, the author prefers the implementation style of the latter. Therefore, the forthcoming sections in this chapter are based on the later state vector ordering approach specifically $x_k = [x \ y \ z \ \dot{x} \ \dot{y} \ \dot{z}]^T$.

4.3.1.2 Constant Acceleration Motion Model

In CA motion model, it is assumed that the acceleration, which is typically a white noise process if nothing is explicitly defined, is nearly constant and it is an independent process between two-time intervals in a discrete system. Similar to the CV in Section 4.3.1.1, the state vector of CA model add the acceleration terms in addition to the position and velocity terms. More precisely, the state vector of CV model includes the position, its corresponding velocity and acceleration, which can be represented as $x_k = [x \ y \ z \ \dot{x} \ \dot{y} \ \dot{z}]^T$. In simple terms, the velocity is the derivative of the position, and the acceleration is the derivative of its velocity term. Therefore, the CA model is also commonly called in literature as a Wiener-sequence acceleration model or a discrete-time Wiener-process model [166].

Similar to the CV model discussed in Section 4.3.1.1, the matrices related to the state mode (A) and covariance of process noise (Q) regarding CA model for a single coordinate can be represented as follows [15]:

$$A = \begin{bmatrix} 1 & T & \frac{1}{2}T^2 \\ 0 & 1 & T \\ 0 & 0 & 1 \end{bmatrix}, \quad \Gamma = \begin{bmatrix} \frac{1}{2}T^2 \\ T \\ 1 \end{bmatrix}, \quad Q = \Gamma \sigma_w^2 \Gamma^T = \begin{bmatrix} \frac{1}{4}T^4 & \frac{1}{2}T^3 & \frac{1}{2}T^2 \\ \frac{1}{2}T^3 & T^2 & T \\ \frac{1}{2}T^2 & T & 1 \end{bmatrix} \sigma_w^2$$

For multidimensional system with the state vector as $x_k = [x \ y \ z \ \dot{x} \ \dot{y} \ \dot{z}]^T$, the dynamic model (A) and its corresponding process noise (Q) are:

$$A = \begin{bmatrix} 1 & 0 & 0 & T & 0 & 0 & \frac{1}{2}T^2 & 0 & 0 \\ 0 & 1 & 0 & 0 & T & 0 & 0 & \frac{1}{2}T^2 & 0 \\ 0 & 0 & 1 & 0 & 0 & 0 & T & 0 & \frac{1}{2}T^2 \\ 0 & 0 & 0 & 1 & 0 & 0 & 0 & T & 0 \\ 0 & 0 & 0 & 0 & 1 & 0 & 0 & 0 & T \\ 0 & 0 & 0 & 0 & 0 & 0 & 1 & 0 & 0 \\ 0 & 0 & 0 & 0 & 0 & 0 & 0 & 0 & 1 \\ 0 & 0 & 0 & 0 & 0 & 0 & 0 & 1 & 0 \\ 0 & 0 & 0 & 0 & 0 & 0 & 0 & 0 & 0 \end{bmatrix} \quad (4.30)$$

$$Q = \begin{bmatrix} \frac{1}{4}T^4 & 0 & 0 & \frac{1}{2}T^3 & 0 & 0 & \frac{1}{2}T^2 & 0 & 0 \\ 0 & \frac{1}{4}T^4 & 0 & 0 & \frac{1}{2}T^3 & 0 & 0 & \frac{1}{2}T^2 & 0 \\ 0 & 0 & \frac{1}{4}T^4 & 0 & 0 & \frac{1}{2}T^3 & 0 & 0 & \frac{1}{2}T^2 \\ \frac{1}{2}T^3 & 0 & 0 & T^2 & 0 & 0 & T & 0 & 0 \\ 0 & \frac{1}{2}T^3 & 0 & 0 & T^2 & 0 & 0 & T & 0 \\ 0 & 0 & \frac{1}{2}T^3 & 0 & 0 & T^2 & 0 & 0 & T \\ \frac{1}{2}T^2 & 0 & 0 & T & 0 & 0 & 1 & 0 & 0 \\ 0 & \frac{1}{2}T^2 & 0 & 0 & T & 0 & 0 & 1 & 0 \\ 0 & 0 & \frac{1}{2}T^2 & 0 & 0 & T & 0 & 0 & 1 \end{bmatrix} \sigma_w^2 \quad (4.31)$$

In summary, the two motion models (i.e., CV and CA) addressed in this dissertation are simple, and yet very powerful kinematic models for many applications in navigation

and tracking-based localization systems. Moreover, the two models are mathematically traceable and they are the most commonly used dynamic model in diverse fields of academic and industrial application areas compared to other available motion models in literature [15, 166]. Compared to CV, CA model covers both the velocity and acceleration of the motion of the system under investigation. Therefore, CA motion model is usually regarded as the preferred model in many use-cases. The results from both models are addressed in this dissertation. Though, CA model will be used as the default for presenting results in this chapter if nothing is stated explicitly.

4.3.2 Measurement Model for UWB Localization

In Bayesian-based state-space systems specifically in Kalman-based approaches, the measurement model is mainly associated with the transition matrix (i.e., H in Kalman filter operation) that relates to the measurement and the system state vector as well as the measurement noise matrix (i.e., R). Based on the measurable input data for the mentioned state-space approach, the measurement model for a system under investigation differs significantly in wireless localization. Two forms of measurement model were applied in the evaluation results of UWB localization systems presented in this dissertation. The first measurement model concerns smoothing the outcomes, in which the inputs to the state-space model are already location data with a few noises in it. The main goal here is to smooth the noisy data to get better location estimation results typically in real-time at 3D. The second measurement model is related to estimating the location of unknown tags from the ranging data between anchors and tag in UWB localization. In this case, the measured inputs for the state-space model are the ranging data, i.e., the distances achieved from the UWB hardware, as opposed to the estimated positioning data in the first model. The measurement model designed particularly for a smoothing filter is simple to implement and yet relatively effective in practice. Regarding this, the complete integration of the measurement model, as well as its corresponding motion model for smoothing purposes, is addressed in Section 4.3.3.1.

To be specific, the standard KF applied in this dissertation falls under the first category (i.e. smoothing the measurement noise). This refers that the location estimation data fed into the standard KF were, indeed, the estimated location data with their position x , y , and z resulted from three evaluated algorithms namely Trilateration, Multilateration, and TS techniques. In this particular situation, standard KF is used to smooth out the outcomes from the above-mentioned algorithms as the final outputs for the system under investigation. To put it in simple terms, the standard KF was used as a smoothing filter for the Trilateration, Multilateration, and TS-based positioning algorithms, in which the mentioned methods already provide their estimated location data (i.e., x , y , and z in Cartesian coordinate).

By contrast, the EKF and UKF applied in this dissertation fall under the second category, which is a range-based measurement model. As such, the raw UWB ranging measurements, i.e., measured distances between tag and anchors, are used to get the location of the tag by using EKF and UKF as the standalone UWB positioning algorithms in this dissertation. In this case, a single algorithm acts not only as the position method but also as the task of filtering in one shot. This is also one of the

reasons why non-linear positioning algorithms such as EKF, UKF and PF are very popular for localization purposes. The complete integration of such a system for EKF is addressed in Section 4.3.3.2 and UKF in Section 4.3.3.3.

In summary, the measurement model needs to adapt the state vector of the system in order to apply it correctly in the applications. As it has already been shown in the previous sections, the arrangement of the elements in the state vector affects the matrices for the dynamic model and its corresponding process noises. The same is true for the measurement model as explained in the forthcoming subsections.

4.3.3 Integration of the Dynamic and Measurement Models

In the state-space approach, the motion model, the measurement model, and the location estimation algorithm are tied together. In other words, the target motion model needs to work jointly with both the location estimation algorithms and the measurement model. For the sake of a complete picture, this section addresses the implementation of the said joint motion and measurement models as well as the position algorithms for each of the evaluated techniques described in this dissertation.

4.3.3.1 Implementation of Standard KF for UWB Localization Systems

As already mentioned, the standard KF is used to smooth the location outputs achieved from three positioning algorithms namely Trilateration, Multilateration and TS methods. In fact, there are two advantages by using standard KF on top of the mentioned location estimation algorithms. Firstly, the filter lets the said localization algorithm the ability to provide a continuous location information provider. Secondly, the standard KF also acts as the smoothing filter in such a scenario so that the noisy outcomes resulting from the algorithms are smoothed out. For instance, the output of static algorithms could jump around even if the actual device is not moving at all in case there are measurement errors due to NLOS condition. In such a situation, the standard KF on top of the static algorithm smoothed out the noise to produce stable and reliable estimations. The high-level overview of the standard KF implementation is illustrated in Figure 4.9. Note that the input of the filter is a location data (e.g., x , y , and z in Cartesian coordinate) as opposed to EKF and UKF. Additionally, it is noteworthy that the control input of standard KF is usually omitted in practices, especially in the tracking scenario.

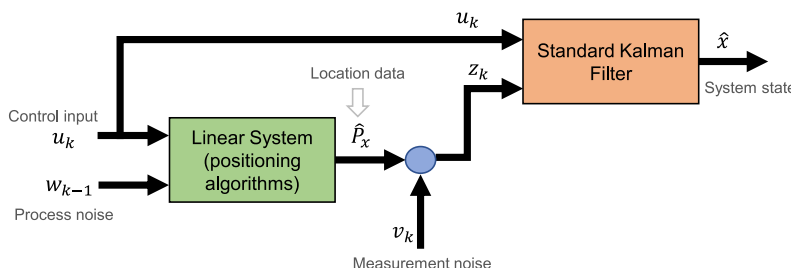


Figure 4.9: High-level overview of standard KF implementation for continuous tracking mechanism in UWB-based localization. The input of the KF filter is location data.

For a kinematic motion model of the state in standard KF, both a CV [15, 22], a.k.a *Position Velocity* model and CA, a.k.a *Position-Velocity-Acceleration*, are applied for the implementation in this dissertation. In specific, the same motion model (i.e., either CV or CA) were applied for all Kalman-based filters (i.e., standard KF, EKF and UKF) evaluated in this chapter. For the sake of brevity, the author will discuss the implementation process of the CA in this section, in which the process of CV has been more or less covered as well. Besides, the detailed implementation of CV model for UWB localization has been already addressed in our previous works in [171, 175].

As already mentioned in the earlier section, there are, indeed, several other target tracking motion models in literature based on the system requirements [166]. However, the CV and CA models are simple to implement, mathematically traceable, easy in spotting implementation errors, and most prominently, satisfy the necessity of many use-cases in UWB localization. Exemplary case studies were given in this chapter based on the data gathered from Cognitive Interaction Tracking (CITrack) [119] lab and the sport hall (see the results in Section 4.4).

For the sake of a clearer complete picture, the author would like to refrain from a few matrices already explained in the earlier sections once again for the implementation of the standard KF. The common part of all systems due to the uniform motion model applied in the algorithms, e.g., the matrices related to the state and its process noise covariance, will not be repeated again in the upcoming implementation of EKF and UKF. Hence, the necessary parameters of standard KF for UWB-localization can be expressed as in the following. The mentioned parameters are: the state vector (x), state transition matrix (A), measurement-to-state transition matrix (H), covariance of the process noise (Q), and covariance of the measurement noise (R) as defined below [15, 166]:

$$x_k = [x \ y \ z \ \dot{x} \ \dot{y} \ \dot{z} \ \ddot{x} \ \ddot{y} \ \ddot{z}]^T, R = \text{diag}([\sigma_{vx}^2 \ \sigma_{vy}^2 \ \sigma_{vz}^2])$$

$$A = \begin{bmatrix} 1 & 0 & 0 & T & 0 & 0 & \frac{1}{2}T^2 & 0 & 0 \\ 0 & 1 & 0 & 0 & T & 0 & 0 & \frac{1}{2}T^2 & 0 \\ 0 & 0 & 1 & 0 & 0 & T & 0 & 0 & \frac{1}{2}T^2 \\ 0 & 0 & 0 & 1 & 0 & 0 & T & 0 & 0 \\ 0 & 0 & 0 & 0 & 1 & 0 & 0 & T & 0 \\ 0 & 0 & 0 & 0 & 0 & 1 & 0 & 0 & T \\ 0 & 0 & 0 & 0 & 0 & 0 & 1 & 0 & 0 \\ 0 & 0 & 0 & 0 & 0 & 0 & 0 & 1 & 0 \\ 0 & 0 & 0 & 0 & 0 & 0 & 0 & 0 & 1 \end{bmatrix},$$

$$Q = \begin{bmatrix} \frac{1}{4}T^4 & 0 & 0 & \frac{1}{2}T^3 & 0 & 0 & \frac{1}{2}T^2 & 0 & 0 \\ 0 & \frac{1}{4}T^4 & 0 & 0 & \frac{1}{2}T^3 & 0 & 0 & \frac{1}{2}T^2 & 0 \\ 0 & 0 & \frac{1}{4}T^4 & 0 & 0 & \frac{1}{2}T^3 & 0 & 0 & \frac{1}{2}T^2 \\ \frac{1}{2}T^3 & 0 & 0 & T^2 & 0 & 0 & T & 0 & 0 \\ 0 & \frac{1}{2}T^3 & 0 & 0 & T^2 & 0 & 0 & T & 0 \\ 0 & 0 & \frac{1}{2}T^3 & 0 & 0 & T^2 & 0 & 0 & T \\ \frac{1}{2}T^2 & 0 & 0 & T & 0 & 0 & 1 & 0 & 0 \\ 0 & \frac{1}{2}T^2 & 0 & 0 & T & 0 & 0 & 1 & 0 \\ 0 & 0 & \frac{1}{2}T^2 & 0 & 0 & T & 0 & 0 & 1 \end{bmatrix} \sigma_w^2,$$

$$H = \begin{bmatrix} 1 & 0 & 0 & 0 & 0 & 0 & 0 & 0 & 0 \\ 0 & 1 & 0 & 0 & 0 & 0 & 0 & 0 & 0 \\ 0 & 0 & 1 & 0 & 0 & 0 & 0 & 0 & 0 \end{bmatrix}$$

where x, y and z are the position coordinates of the state in 3D, \dot{x}, \dot{y} and \dot{z} are their corresponding velocities (derivation of the position), \ddot{x}, \ddot{y} and \ddot{z} are their corresponding acceleration (derivation of the velocity), and T is the update rate of the system, which is expected to be quite small so that the changes in acceleration over this interval could be assumed as a constant (or) approximately constant [15].

For reference, the evaluation results given in this dissertation are based on the subsequent values during the data measurement processes. The system update rate (T) was 10 Hz, σ_w^2 in the process noise (Q) was 0.01 (i.e., this particular value was based on the manufacturer's precision rate of the UWB hardware used in the evaluation which is DWM1000 module from Decawave (Qorvo) [44]), and $[\sigma_{vx}^2, \sigma_{vy}^2, \sigma_{vz}^2]$ in the measurement noise (R) was $[0.015, 0.015, 0.025]$ (i.e., this particular value was drawn from our prior experimental measurement results).

4.3.3.2 Implementation of EKF for UWB Localization Systems

In this chapter, the EKF and UKF were used as a standalone positioning algorithm as well as the mechanism for continuous tracking and navigation of objects in UWB localization. Compared to the implementation of standard KF in Section 4.3.3.1, the core difference is that the input to the filter of EKF and UKF are the unprocessed ranging data as opposed to the processed position (or) location data in the former case. Figure 4.10 illustrates the high-level overview of the mentioned EKF and UKF implementation for the use-case of UWB localization systems. Note that the input of the filter is a ranging data as opposed to positioning data in standard KF. This implies that the filter also acts as a positioning algorithm. Similar to standard KF given above, the control input is usually omitted in practices.

It is noteworthy that the state model of the system still remains unchanged for both the linear and nonlinear location estimation algorithms addressed in this thesis. The reason is that the non-linearity in the context of UWB-based localization system occurred only in the measurement (i.e., based on the quadratic Equation (4.11)). In terms of the state-space model, the mentioned equation falls under the category of

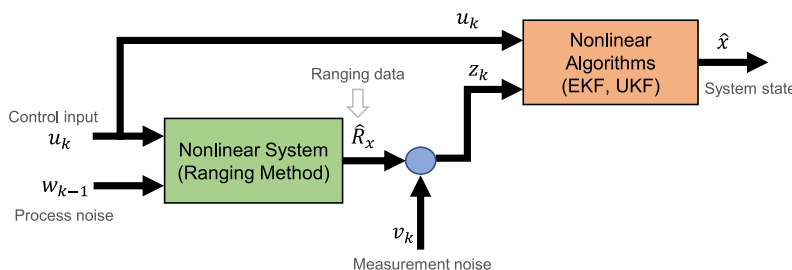


Figure 4.10: High level overview of nonlinear Bayesian-based filters (EKF and UKF) implementation for UWB-based localization. The input of the filter is a ranging data as opposed to the location data in standard KF.

measurement function. Therefore, the state or dynamic model is still the same for both linear and non-linear across all evaluated algorithms. In fact, the assumed linear endeavor model is directly related to Newton's second law of motion. Accordingly, the mentioned assumption is, indeed, in-line with the conventional wireless tracking and navigation scenarios widely practiced in several applications [15, 22]. Therefore, the state model defined in Section 4.3.1 were applied as before for both EKF and UKF without any modification. This shows that the state transition matrix (A) and covariance of the process noise (Q) related to the state are exactly the same as in the standard KF implementation (see Section 4.3.3.1). For the sake of brevity, this section addresses the implementation of the measurement model for EKF omitting the state model part.

Therefore, the observation vector (z) of the measurement update phase for the EKF as a standalone positioning algorithm in the state-space model can be written as [223]:

$$z_{i,k} = [d_{1,k} \quad d_{2,k} \quad \dots \quad d_{n,k}]^T \quad (4.32)$$

where, $d_{i,k}$ denotes the measured range (or) distance between a tag and the i th anchor at the current estimation time z_k . $i = 1, 2, \dots, n$ indicates the number of anchor nodes that have range/distance information with the targeted tag.

Referring back to the nonlinear range Equation (4.11), the measurement function for EKF can be expressed as $h(\hat{x}_{k/k-1}) \cdot h(\hat{x}_{k/k-1})$ is simply the measured distances between the tag and i th anchors at the estimation time t_k , which we can be defined as:

$$h(\hat{x}_{k/k-1}) = [f_1(t, A_1) \quad f_2(t, A_2) \quad \dots \quad f_n(t, A_n)]^T \quad (4.33)$$

where, $f_i(t, A_i) = \sqrt{(x_t - x_i)^2 + (y_t - y_i)^2 + (z_t - z_i)^2}$

Assuming that the applied state model is CA, the Jacobian matrix (H_k) for EKF (i.e., the approximation of first-order Taylor series) can be derived as:

$$H_k = \begin{bmatrix} \frac{x_t - x_1}{f_1(t, A_1)} & \frac{y_t - y_1}{f_1(t, A_1)} & \frac{z_t - z_1}{f_1(t, A_1)} & 0 & 0 & 0 & 0 & 0 & 0 \\ \dots & \dots \\ \frac{x_t - x_n}{f_n(t, A_n)} & \frac{y_t - y_n}{f_n(t, A_n)} & \frac{z_t - z_n}{f_n(t, A_n)} & 0 & 0 & 0 & 0 & 0 & 0 \end{bmatrix}$$

Similarly, the error covariance matrix (R_k) for the measurement function concerning the EKF can be achieved as follow:

$$R_k = \text{diag}([\sigma_{1,k}^2 \quad \sigma_{2,k}^2 \quad \dots \quad \sigma_{n,k}^2]) \quad (4.34)$$

In the author's implementation, i.e., based on four anchors in the system setup, the values used for the error covariance matrix R_k are ($\text{diag}([0.0016, 0.0014, 0.0014, 0.0014])$). These values came from the prior experimental evaluation results conducted in the intended application environments. To achieve the best performance for a certain deployment, the mentioned value may need to adapt or tune a bit upon the hardware setups and its intended scenarios other than the one provided in this dissertation.

4.3.3.3 Implementation UKF for UWB Localization Systems

From the high-level point of view, the implementation process of UKF for the use-case of UWB localization system is quite similar to EKF as described in Figure 4.10. The main difference between the EKF and UKF lies in how the non-linearity of a given system is handled. As already mentioned in Section 4.2, EKF uses either Jacobian or Hessen approximation to linearize the nonlinear functions whereas the UKF uses the sigma points (Section 4.2.6). From the perspective of UWB localization system, the nonlinear function occurs only at the measurement function due to the ranging equation defined in Equation (4.11). Therefore, the dynamic state function for UKF is again linear similar to EKF and the standard KF implementation. Consequently, the same motion model (Section 4.3.1) is usable for the UKF as well. Hence, the unscented transform (Section 4.2.6) using sigma points was applied only to the measurement model. In other words, the nonlinear function due to Equation (4.11) for UWB localization system was approximated by using sigma points in UKF implementation.

In the evaluation results presented in this chapter, the error covariance matrix (R_k) regarding the measurement noise for UKF was exactly the same for the one used in EKF due to the nonlinear Equation (4.34) (Section 4.3.3.2). Again, the mentioned value was extracted from prior measurement results. In UKF, the spread of the sigma points around the mean value of the state is controlled by the scaling parameter composed of α and κ (Section 4.2.6). In our implementation, the α value is set to 0.001, whereas the value of κ is assumed to be zero. In addition, the parameter related to the prior knowledge of the distribution in UKF (β) was chosen as 2, which is the standard choice for a non-linear system with Gaussian distribution [206].

For uniformity and consistency, the initial estimated locations for all the Bayesian-based filters examined in this chapter were set to (2, 1.5, 2) in the Cartesian coordinate. Though any arbitrary realistic position can be chosen for the initial condition, the convergence of the filter may suffer if implausible values are used.

4.4 Comparative Experimental Evaluation Results

In this section, the comparative analyses of five true-range position algorithms were evaluated in different scenarios and their corresponding results are reported. Specifically, performance comparisons conducted at three scenarios at two different locations were analyzed using the actual experimental data from the ground. The mentioned three scenarios were: a static condition (Section 4.4.2), a LOS situation (Section 4.4.3), and a NLOS scenario (Section 4.4.4). Moreover, the qualitative and computation complexity of the analyzed five algorithms were addressed in Section 4.4.5.

For the reproducible results and uniform process across the algorithms presented in this chapter, the outcomes described in this chapter were implemented on Matlab from Mathworks. The required data and Matlab scripts applied in the evaluation were also provided as an open source in the public domain as already mentioned at the beginning of the chapter. For the implementation of the EKF and UKF, the "state estimation library of the control system toolbox" from Matlab is used as a dependency for the sake of

simpler reproducible results. The rest of the source codes are self-implemented in-house at Cognitronics and Sensor Systems research group, CITEC, Bielefeld University. The experimental data were collected by using the UWB hardware manufactured by Decawave (<https://www.decawave.com/>), which is now become part of Qorvo.

4.4.1 Experimental Setup

The data collections of the measurements were conducted at two separate locations in order to evaluate small-scale and large-scale scenarios for the demonstration of practical use-case in UWB localization. Figure 4.11 depicted the mentioned two environments which were in the CITrack laboratory [119] and at the university's indoor sports hall. Two ground truth references were applied during the data collection for the mentioned two scenarios. In CITrack (left bounding box in Figure 4.11), the integration and evaluation of current tracking technologies in a controlled environment of 6x6x3.7 m can be evaluated in real-time. The Vicon's motion capturing system, which has an accuracy of millimeter range, was also integrated into CITrack. Therefore, the Vicon system in the CITrack was utilized as the ground truth reference for evaluations made in CITrack lab., which are denoted as the small-scale scenario in this dissertation. Regarding the ground truth reference for system evaluation in sport hall, there exist several designated lines (see right bounding box in Figure 4.11), which are dedicated for a specific sport category such as badminton, volleyball, etc. We used those lines as the ground truth reference to present the evaluation results, i.e., the measurements were conducted by following those lines during the data collection process.

In the experiment, we used the commercially available TREK1000 system [47] from Decawave (now Qorvo) as an UWB hardware for collecting the measurement data.



Figure 4.11: Set-up for the experimental evaluations conducted at the laboratory environment in CITrack [119] and University's indoor sport hall arena.

Four anchors, in total, were utilized during the data collection process and deployed in the four corners of each test environment, which were conducted at CITrack and sport hall (see Figure 4.11). For the sake of convenience, the measurement data of a single tag was recorded in the course of the data collection process to demonstrate the UWB-based tracking and navigation. The four measured ranges between every four anchors and the tag were logged during the measurements. This makes sure that the same ranging data was applied consistently to each algorithm in order to compare their performance. The mentioned logged ranging data were fed into each of the evaluated location estimation algorithms in the post-processing phase using Matlab. As already mentioned, the logged ranging data and its corresponding source code (Matlab scripts) were given as an open source for the purpose of result verification and further work.

Regarding the Vicon system as a reference in the small-scale scenario at CITrack Lab., it was necessary to transform the two separate systems (Vicon vs. UWB) into the common frame in order to quantify the measurement results. To accomplish this, the point cloud registration method Iterative Closest Point (ICP) algorithm was applied for registering the data between two systems. For the qualitative score of the performance comparison, RMSE value was used in the evaluation.

4.4.2 Performance Comparison based upon a Static Scenario

The scatter plot in Figure 4.12 demonstrated the visual representation of the performance comparison among five positioning algorithms at a static scenario in 2D. The static refers to the situation where the mobile tag was not moving and stayed stationary in the course of the whole data collection process. For better visualization, the reference location of the stationary tag was shifted to the origin of the coordinate (i.e., at 0,0). In this static scenario, it was observed that the precision of all the evaluated five location estimation algorithms were under 10cm (Figure 4.12). In terms of accuracy, the results showed that the RMSE was less than 0.1cm in reference to the Vicon system (Figure 4.12). More qualitative results using RMSE as the quantifying score for both CA and CV motion models were discussed in Section 4.4.5.

It was remarkable to see in the evaluation results that both EKF and UKF had comparable performances. Specifically in this particular evaluation data, the distinction between the two algorithms cannot be clearly identified and their difference can be seen only at the initial conditions when the two filters were not completely converged yet (Figure 4.12). Such occurrence was evident in all the evaluated scenarios expressed in this chapter (i.e., noticeable in the upcoming sections as well). Therefore, a conclusion can be drawn based on evaluation results that EKF and UKF have equivalent performance in terms of accuracy in UWB localization. This implies that the non-linear measurement function in the ranging phase was based on Equation (4.11) in the state space model.

Moreover, the scatter plot in Figure 4.12 showed that the TS technique happened to be the worst performance in a static scenario compared to the other four location estimation algorithms. Meanwhile, the linear positioning methods (namely Trilateration and Multilateration) were shine to be a better accuracy than the non-linear techniques (EKF, UKF, and TS) in static scenario (Figure 4.12). In general, a few outliers appeared in all evaluated five positioning estimation algorithms, especially in

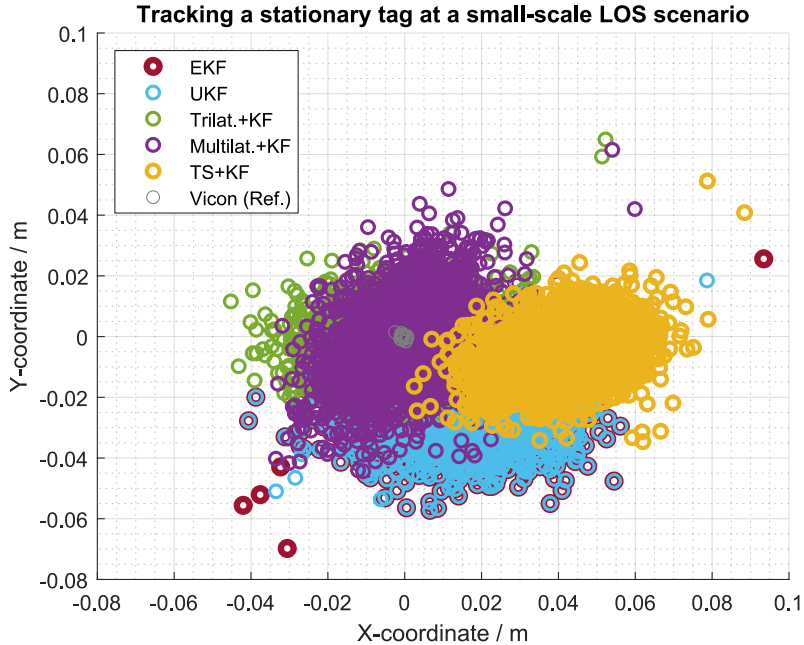


Figure 4.12: Performance comparison of five position estimation algorithms for the static scenario at CITrack, in which CA is used as a motion model for the state.

their initial conditions (Figure 4.12). Indeed, it is a very common situation in Bayesian-based filters due to its iterative nature and the impact doesn't play a crucial role in the real-world situation as long as the filter is converged eventually.

4.4.3 Performance Comparison based upon a pure LOS Scenario

For a pure LOS scenario, the performance comparison for five position estimation algorithms was conducted at two different environments marked as a small-scale scenario for the data gathered at CITrack (i.e., left image in Figure 4.11) and as a large-scale scenario for the data gathered at the university's indoor sport hall arena (i.e., the right image in Figure 4.11). The corresponding evaluation results of each test environment were given in Figure 4.13 and Figure 4.14 respectively. As already mentioned in the chapter, the Vicon camera system was used as the ground truth reference for the small-scale scenario (CITtrack) whereas the borderlines of the Badminton field were applied as the ground truth reference for the large-scale scenario (the indoor sport arena on the campus of Bielefeld University). CA motion model was utilized as the state model in the presented results provided in Figure 4.13 and Figure 4.14.

In the small-scale LOS scenario, the evaluation results revealed that the linear location estimation algorithms (Trilateration and Multilateration) closely followed our reference trajectory from the Vicon system (Figure 4.13) compared to the nonlinear ones. This claim can also be confirmed with the qualitative score using RMSE in Section 4.4.5. As previously noted in the static scenario, both EKF and UKF provided equivalent

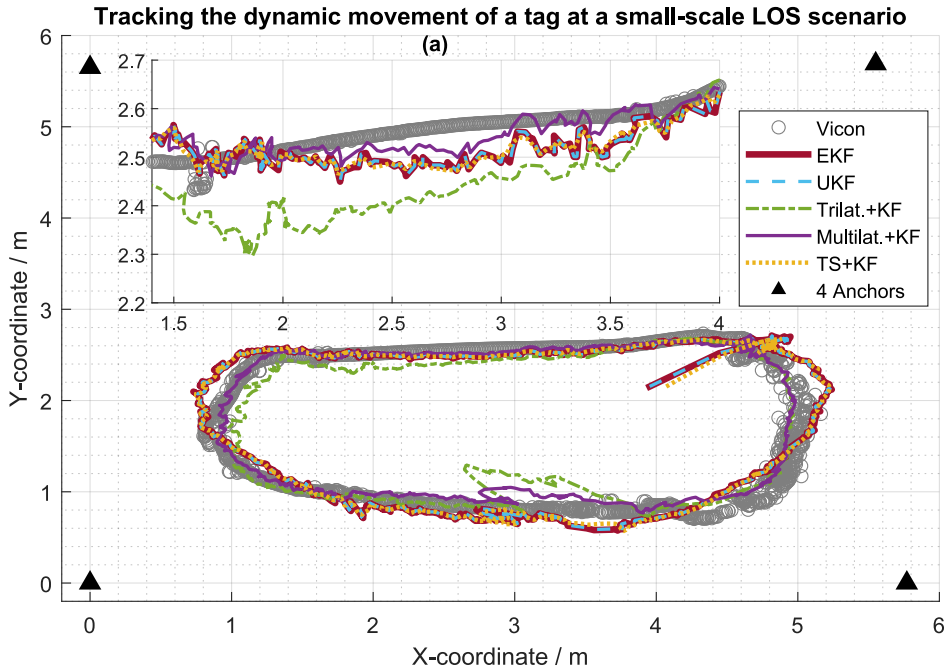


Figure 4.13: Performance comparison of five position estimation algorithms for tracking the movement of a mobile tag in the CITrack using CA as the motion model for the state.

results. Interestingly, the TS method showed outcomes similar to the EKF and UKF in this small-scale LOS scenario. For better visualization of the results, Figure 4.13 (a) provided the portion of the results in a zoom-out view in which all the trajectories from each location estimation algorithm seem closely followed to the reference. In addition, there was an accidental, but important occurrence, happened during the data collection process which can be seen in Figure 4.13 (i.e., roughly between 2.7 m and 3.7 m in X-axis). This unusual measurement had an impact on all the five evaluated location estimation algorithms. Importantly, such conditions can occur frequently in practice. The evaluation results showed that linear methods (Trilateration and Multilateration) were more sensitive to react negatively to this occurrence compared to their counterpart non-linear systems (TS, EKF, and UKF). It is worth mentioning that the ability to overcome such granular incidents naturally (or) algorithmic way could play important role in some UWB-based system implementations in practices.

During the data collection process for a large-scale scenario in sport hall presented in Figure 4.14, the UWB tag was put on top of the person's head in order to get the LOS view from all the four anchor nodes. The four anchors were allocated at the corners of 20x40m area in sport arena (Figure 4.14). The measurement was conducted when a person jogging (running) along the borderlines of the basketball field.

In general, the trajectory of the runner on the field was able to track correctly by all the evaluated position estimation algorithms in this LOS large-scale scenario in sport arena (Figure 4.14). As expected, all the algorithms gave a similar performance

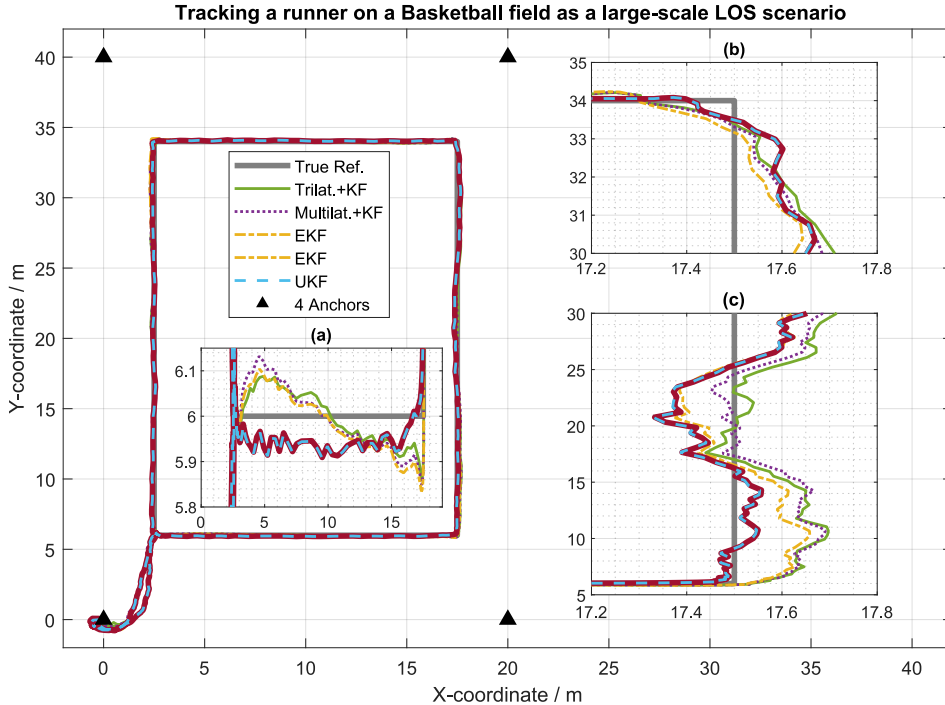


Figure 4.14: Performance comparison of five algorithms for tracking a moving UWB tag in a large-scale scenario (an indoor sports arena) at LOS. CA was used as the motion model.

from the aspect of bird eye view in 2D. The comparison of the five algorithms based on the RMSE as the qualitative score further confirmed the similarity between the five outcomes in LOS scenario (Section 4.4.5). In order to compare the five evaluated algorithms visually in this scenario, three subsets of the outcomes were enlarged in Figure 4.14. The optimum case of the evaluation results (Figure 4.14 (a)) showed that all the position estimation algorithms achieved an absolute error of less than 12 cm in reference to the ground truth when CA is used as the motion model. In a dilemma depicted in Figure 4.14 (b) and (c), the evaluation results revealed that an absolute error of up to 22 cm could be reached. As already witnessed in the small-scale scenario, the EKF and UKF gave the exact same performance in the LOS scenario whereas the TS method closely followed the trajectories of EKF and UKF in most cases. Moreover, the evaluation results showed that all the evaluated position estimation algorithms suffered from the abrupt changes in the corner of the field (Figure 4.14 (b)). In fact, we have shown in our previous work [171] that the corner impact in the evaluation was even worse if the CV motion model was applied as the state model. This signifies that the model choice for a specific system integration could have some significant impacts on the overall system performance. Therefore, Section 4.4.5 considered the impact of the motion model (CV vs. CA) in UWB localization for the four scenarios addressed in this chapter using RMSE as a qualitative score.

4.4.4 Performance Comparison based upon a NLOS scenario

For evaluating the comparative analysis of NLOS condition, a soft-NLOS scenarios were conducted in the indoor sports hall arena at different settings (Figure 4.15 and Figure 4.16). In each of these NLOS cases presented in this section, a person carried the UWB tag in front of his chest during the data collection period in order to block the direct LOS communication between some anchors and the tag. The mentioned UWB tag was at 0.3 m distance from the body of the person who carried it.

Figure 4.15 showed the evaluation results of five position estimation algorithms when the four anchors were placed at 20x20 m square area in sport hall. The data were collected during a runner took two consequent paths one after another (i.e., the first path included the border of a square whereas the second path was across the four corners in the shape of the letter 'X'). In general, the accuracy of all the evaluated position estimation algorithms degraded sharply due to the NLOS condition in reference to the ground truth (Figure 4.15). In specific, the two linear positioning estimation algorithms (Trilateration and Multilateration) performed poorly in the NLOS scenario whereas the two non-linear methods and statistical approach provided quite impressive performances (Figure 4.15). Similar result can also be seen in Figure 4.16. In terms of measurement function, this implied that the incremental correction in the iterative and/or recursive approach (i.e., TS, EKF, and UKF) plays a beneficial role in scenarios where abrupt disturbance in UWB signal could occur. The deviation due to NLOS can even be visualized in the best fraction of the measurements (Figure 4.15 (b) and (c)).

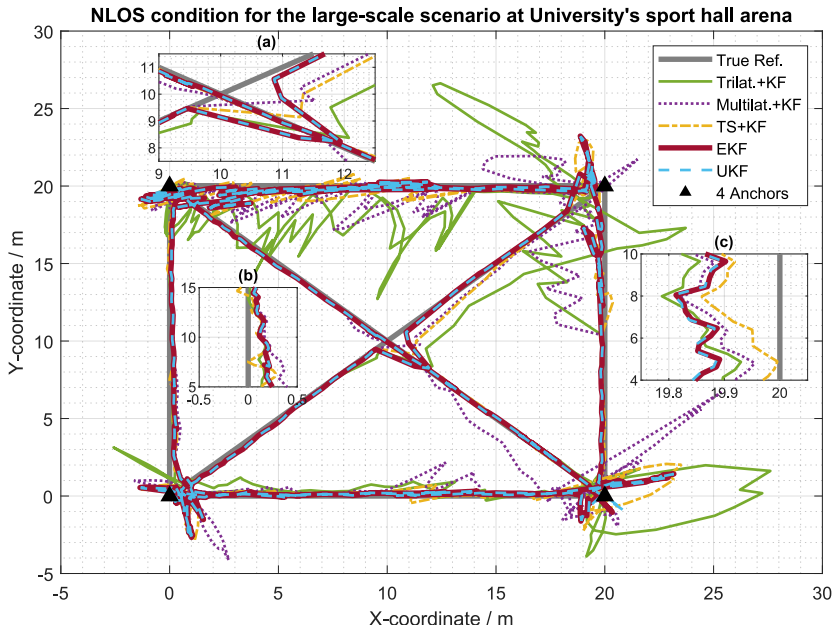


Figure 4.15: Comparison of five location estimation algorithms at a NLOS scenario in university's indoor sports hall (20x20 m arena). CA was utilized as the dynamic motion model.

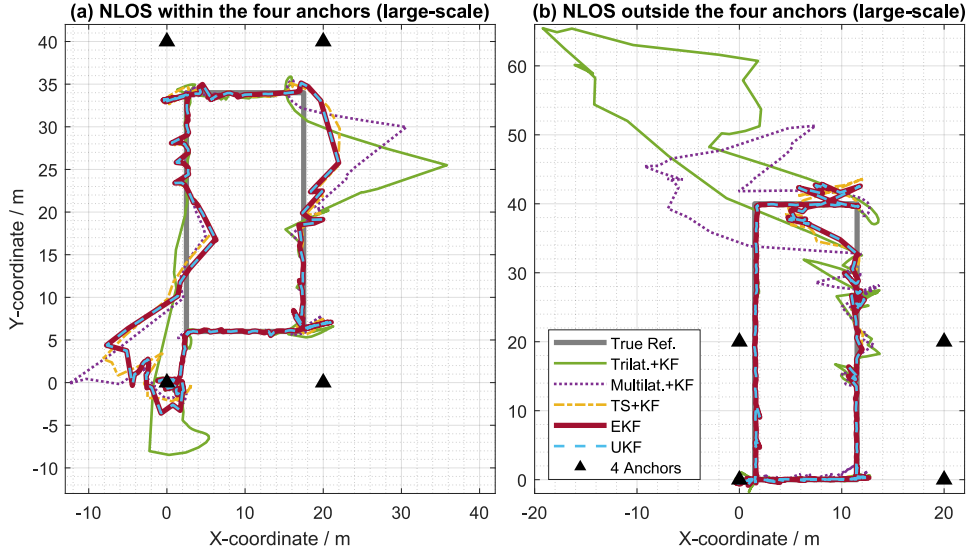


Figure 4.16: Evaluation of NLOS condition at two anchor settings and trajectory paths: (a) allocation of the four anchors at 20x40 m , (b) allocation of the four anchors at 20x20 m.

In addition, there was a drift from the reference in Figure 4.15 during measurements which occurred at the center when the person ran from the bottom left corner to the upper right corner (Figure 4.15 (a)). In fact, this drift was used as a good opportunity for comparing how well the evaluated algorithms can detect such occasions in this section. The results revealed that the mentioned drift was correctly detected by all the five algorithms (Figure 4.15 (a)). However, all the considered positioning methods provided different reactions to this occurrence in which EKF and UKF have the best response whereas Trilateration provided the worst (Figure 4.15 (a)).

Since NLOS condition in UWB localization is still an open and active research challenges in literature, the behavior of NLOS in terms of the location estimation algorithms were further explored in this Section (Figure 4.16). In the figure, two types of anchors' settings were conducted in sport hall arena, i.e., the four anchors were allocated at 20x40 m in the first set-up whereas they are put at 20x20 m in the second setup. Figure 4.16 (a) showed the evaluation results of the five algorithms regarding the NLOS condition, in which the movement of the UWB tag was limited to be inside the four anchors. In contrast, Figure 4.16 (b) allowed the moving UWB tag to be expended beyond the square area of the four anchors allocation. As observed previously, the abrupt changes due to NLOS had strong negative impacts on the two linear methods (Trilateration and Multilateration). In contrast, the three nonlinear methods followed quite adequately the trajectory of the ground truth. However, all the five algorithms suffered the impact of the NLOS condition in the measurements. Moreover, it was impressive to see that the bidirectional UWB system using TWR method has the ability to provide positioning data even when the moving tag was our of the square area of the anchors' allocations (Figure 4.16 (b)). This is one of the crucial and advantageous aspects of ToA-based system compared to its counterpart TDoA-based system, in which the location data are available only inside the anchors' allocations [198, 230].

4.4.5 Qualitative Score and Computational Aspect

For the qualitative score to discriminate the performance of the evaluated five positioning algorithms, the RMSE was applied as the decisive factor in this chapter. Figure 4.17 described the side by side RMSE comparison for CV and CA models regarding the four scenarios (i.e., static, small-scale LOS, large-scale LOS, and NLOS scenarios) addressed in this chapter. The evaluation results showed that there was no considerably large difference between CV and CA in terms of RMSE in all the evaluated location estimation algorithms in each scenario (Figure 4.17). Indeed, the use of CA as the state model did, in general, improve the RMSE score a bit in all the measured scenarios except in the static condition. This makes sense since the addition of acceleration in the CA compared to the CV doesn't have any influence on the static condition. Instead, it generally accumulated more noises into the state model.

For each evaluated positioning algorithm, the heatmap in Figure 4.17 summarized the four measurement scenarios by using RMSE as the decisive score. The figure showed a clear distinct line between the NLOS condition and all the LOS situations (i.e., static, small-scale, and large-scale) in terms of RMSE. The contrast between the two groups was indeed significantly large. This explained the challenges of NLOS condition in UWB localization, and the reason why it is still an active open research problem. In specific, the location error of EKF and UKF algorithms due to NLOS jumped into approximately 4 times compared to the LOS in the particular measurement data (Figure 4.17). Similarly, TS technique rose around 5 times due to NLOS condition whereas the Multilateration increased circa 6 times and the Trilateration up to 10 times. In terms of LOS data comparison, the large-scale scenario in the sport-hall arena provided a higher error rate than the static and small-scale scenario. In the small-scale scenario (the first to fourth columns in Figure 4.17), the linear positioning algorithms showed up pretty well with a smaller error rate compared to the nonlinear methods. Overall, the EKF

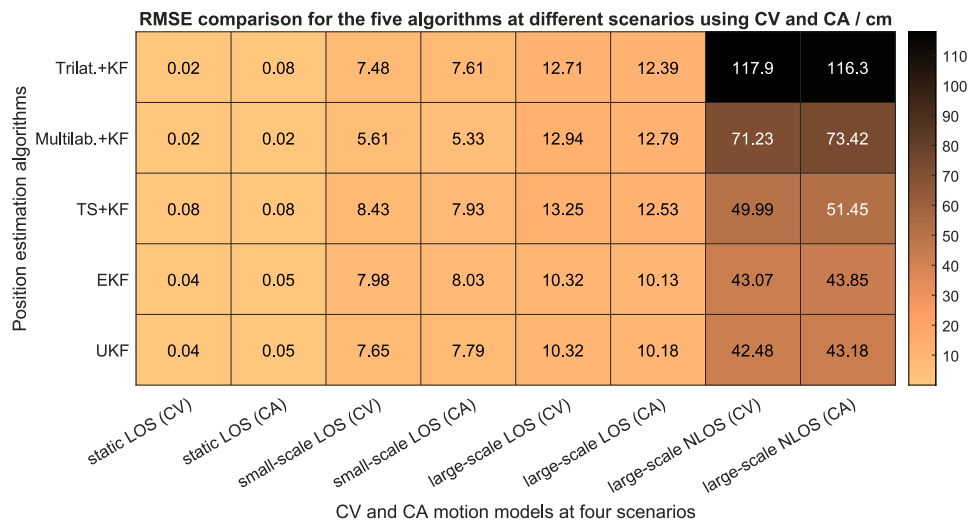


Figure 4.17: RMSE comparison for the evaluated five algorithms at four different scenarios

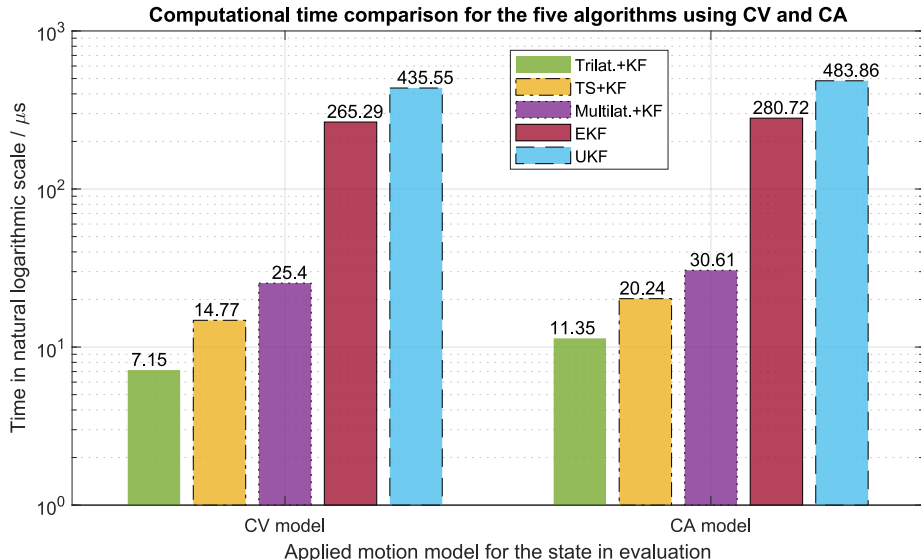


Figure 4.18: Computational time comparison of the evaluated five location estimation algorithms using CV and CA motion models. The presented time referred to the mean time required for a test-bed machine to compute a location by each algorithm in microseconds.

and UKF produced comparable results in all measured scenarios as already mentioned previously. Moreover, EKF and UKF consistently provided quite reliable outcomes even in the NLOS condition (the fourth and fifth row in Figure 4.17). Interestingly, the TS was able to produce comparable results to the EKF and UKF at both LOS and NLOS conditions. By contrast, the Trilateration and Multilateration performed extremely bad in NLOS condition compared to the other three algorithms.

Regarding the comparison of computational complexity for each algorithm, the time that the CPU (or) computational machine requires to run a given task was applied [63]. To accomplish this, the processing time was measured based upon the sample data size of 2400 for 10 iterations on the exact same machine (i.e., Intel Xeon CPU E3-1226 v3, which has 4 cores with 3.30 GHz and 16 GB RAM without external graphic). In this case, the start and end of each algorithm to accomplish the mentioned 2400 samples within a for loop were recorded, and computed the execution time for each sample. The recording was repeated 10 times. Figure 4.18 represented the mean computational time for each algorithm addressed in this chapter using two motion models namely CV and CA. It should be noted that the exact computational time may vary a bit depending on the specification of the machine. However, the trend of the data should be the same in any condition as the author has confirmed in at least three different machines.

The evaluation results showed that the CA model generally needs more computational time than the CV model in all the evaluated five algorithms (Figure 4.18). However, the gap between the two models was not that much. In specific, the processing time for CA model is roughly around 5 μs longer than CV model in TS and the two linear algorithms. On the contrary, it was roughly around 15 μs more in EKF and 50 μs in UKF. In terms of computational time for each five algorithms, the evaluation results uncovered that

the EKF and UKF were extremely worse than the rest of the three position estimation algorithms (Figure 4.18). On the contrary, Trilateration outperformed them all in the context of processing time in both CV and CA whereas the UKF was the worst. In addition, the evaluation results indicated that the EKF necessitated roughly around 10 times computational time than the Trilateration, TS, and Multilateration methods (Figure 4.18). Compared to the EKF, the UKF needs nearly double processing time in both CV and CA models. In contrast, the Trilateration, TS, and Multilateration gave quite a small processing time specifically 11.35 μ s, 20.24 μ s, and 30.61 μ s respectively when CA was applied as the motion model of the state.

It is remarkable to see that TS method required a quite short processing time compared to the other nonlinear methods. Interestingly, the results showed that TS provided even less computational time than the Multilateration technique. As can be seen in the previous section, TS also provided a rather appealing performance in terms of accuracy, i.e., comparable to the EKF and UKF. Therefore, the evaluation results suggested that TS is the most efficient and competent method among the five evaluated position estimation algorithms in terms of processing time and performance score.

In summary, EKF and UKF were able to produce impressive outcomes in terms of RMSE. Despite that, the evaluation results showed that they suffered considerably large computational time compared to the other three methods. On the one hand, the two linear algorithms needed relatively small processing time. On the other hand, they struggled to endure the abrupt changes, especially in the NLOS scenario. Moreover, the evaluation results revealed that TS-based positioning technique was not only capable of producing a performance score similar to the EKF and UKF but also very efficient in terms of the computational time (Figure 4.17 and Figure 4.18).

4.5 Chapter Discussion and Conclusion

UWB has been regarded as a promising technology for precise wireless localization systems, especially in indoor environments. Nowadays, the UWB hardware chips are available at low prices thanks to the leading manufacturers in the fields such as Decawave (now part of Qorvo), Bespoon, Ubisense, etc. Regarding this, the performance comparison of the commercially available UWB systems has been conducted by renounce researchers in the field [100, 103]. Moreover, Decawave, for instance, shipped the UWB evaluation kits called MDEK1001 and TREK1000, in which Trilateration algorithm was already implemented in it so that the intimidating development time of UWB technology could be shortened. By far, Trilateration is the simplest location estimation algorithm.

Fundamentally, location estimation algorithms are the backbone of any localization system including the UWB technology. Hence, many positioning algorithms were proposed for UWB and wireless communications in the literature. However, the detailed implementation process of the algorithms was usually overlooked. This leads to daunting experiences for practitioners and researchers who want to reproduce or use the defined system in literature for real-world problems. This is especially true for the newcomers in the field. In light of this, the concrete implementation process and their corresponding evaluation results of five commonly used location estimation algorithms

in UWB localization were addressed in this chapter namely Trilateration, Multilateration, TS, EKF, and UKF. The mentioned five positioning estimation algorithms have been designed, implemented, and evaluated using the experimental data extracted from the real UWB hardware. This is in contrast to a few comparative analyses available in the literature which are solely based on simulation. Moreover, the evaluation results came from the finalized implementation of each algorithm based upon the pragmatic integration approach. To the best of the author's knowledge, the first such pragmatic comparison was done by our previous work in [171] and this chapter is the heavily revised and extended version of the mentioned work.

The Bayesian framework of the state-space approach has been applied for the implementation of all the evaluated algorithms in order to confront with the pragmatic real-world system integration. For this reason, a standard KF has been coupled on top of Trilateration, Multilateration, and TS positioning methods so that a continuous tracking mechanism could be naturally applicable to those systems. Since the EKF and UKF are inherently capable of such continuous tracking mechanisms, they were applied as the standalone location estimation algorithms for UWB system in the chapter. For a state-space approach, dynamic state functions and measurement likelihood functions are necessary to provide to the system under investigation. In general, the mentioned two functions could be either linear or nonlinear. For the sake of brevity, the linear function based on Newton's law of motion was traditionally applied for the state function in wireless positioning and navigation system. Therefore, the non-linearity occurs only in the measurement function of the state-space model, especially for range-based wireless positioning systems including the UWB technology addressed in this thesis.

Accordingly, the dynamic model of the state was assumed as linear in this dissertation. Concerning this, two linear dynamic models (i.e., CV and CA models) were thoroughly explored for the UWB based localization system (Section 4.3.1). The detailed expression of the mentioned two motion models specifically for UWB localization was regarded as an important aspect of the dissertation because the literature is usually overlooked and expressed only in a general sense. For instance, the details of the implementation process for different system aspects were not given even in most referenced papers and books in the field [15, 66, 166]. This often the time leads to confusion in practice for user-specific system integrations (e.g., for UWB localization). Therefore, the integration process of the state and measurement function for each algorithm was thoroughly explained in the dissertation (Section 4.3) so that newcomers in the field can easily understand and implement it. For this purpose and further exploration, the basic source code and the experimental data used for presenting the results in this dissertation were given publicly as already stated at the beginning of the chapter.

Regarding the approximation of the nonlinear measurement function (i.e., Equation (4.3) for UWB localization system) in positioning and navigation, one of the most advanced and frequently used algorithm was PF [11]. In brief, EKF approximates the nonlinear function by using analytical linearization methods such as Jacobian or Hessian whereas UKF approximates the nonlinear function by using a statistical approach based on a set of deterministically chosen sample points called "sigma points". By contrast, the PF uses the Sequential Monte Carlo (SMC) methods to generate simulated particles for addressing the nonlinear functions in the system. This dissertation highly

acknowledges the prominence of PF as a location estimation algorithm in many application areas including in UWB technology [76, 84, 103, 213]. However, the method was excluded from the evaluation because the improvement of the performance score compared to EKF and UKF was insignificant in terms of the non-linear function applicable in UWB-based positioning and navigation. The perfection of PF compared to the more classic EKF and UKF will be noticeable only when the non-linearity of the measurement function cannot be analytically expressed. However, that is not the case in the UWB measurement function. Moreover, it was quite obvious that the computational cost of PF dramatically increases due to the increased number of particles to be applied compared to the sigma points requirement in UKF. If the readers are interested in a good understanding of the PF as either a location estimation algorithm or a general purpose approximation method, the author would refer to the tutorial in [11, 84], and the book in [52, 165]. For pragmatic exercises with a source code to understand general approximation methods, the author would refer to an intuitive open source book on interactive Jupyter notebook [124], in which the theory of both PF and the Kalman-based filters were examined in Python language.

In literature, the linear location estimation algorithms (namely Trilateration and Multilateration) are less valued and usually discriminated as poor performances in simulation results. However, either the quality of the ranging process (true-range) or the pragmatic integration of the method was normally neglected when the merits of performance scores are conducted in simulation environments [31, 81, 111, 182, 227]. The evaluation results given in this chapter were achieved upon both the pragmatic system integration and careful quality access of the ranging data extracted from the real UWB hardware. In terms of accuracy by using RMSE as a decisive score, our evaluation results indicated that the linear location estimation algorithms produced superior performance scores in static and small-scale LOS scenarios compared to the nonlinear positioning methods (Section 4.4.2 and 4.4.3). In contrast, the nonlinear positioning methods showed better resistance to abrupt changes of signal due to unintentional measurement errors or alike. Moreover, the three nonlinear methods appeared to be significantly superior performance scores than their counterpart linear algorithms at NLOS scenario. Overall, the evaluation results showed that the NLOS condition extremely degraded all the five evaluated algorithms. Therefore, we can conclude that this deterioration of performance score due to NLOS is independent of the algorithmic usage and needs to address from a different perspective. Moreover, the methods to overcome the mentioned impact of NLOS in UWB are challenging, and it is actively explored research problems in literature [138, 147, 177]. Regarding this, the identification and mitigation of the NLOS condition in UWB-based positioning and navigation was separately addressed in Chapter 5 in this dissertation. It should be noted that the results given in this Chapter 4 were based solely upon the measurement data without using any NLOS identification and mitigation techniques.

In terms of the motion model, our evaluation results suggested that there were no substantially large differences between the performance score of CV and CA motion models. In other words, the two motion models are more or less equivalent in terms of the accuracy or performance score. Likewise, it can be stated that the computation time required by the two models was rather comparable too even though a higher processing

time was necessary for the CA model across all the five algorithms. Therefore, we can conclude based on our observation given in this chapter that both of the two motion models are equally usable in any given location-based UWB application in practice if the constraint in processing time is not relatively strict.

Regarding the computational time, the evaluation results showed that EKF and UKF were terribly higher than the other three positioning algorithms. To express in other words, the processing time for EKF was roughly around 10 times higher than the other three algorithms whereas it was approximately 18 times higher in UKF. By contrast, the evaluation results revealed that the Trilateration algorithm needs the least computational time followed by the TS and Multilateration. From this observation, it can be concluded that Trilateration is the best whereas UKF is the worst among the evaluated five location estimation algorithms in terms of computational time. Moreover, the results showed that EKF and UKF provided nearly equal outcomes in all the tested scenarios in terms of the performance score. However, the computational time of UKF is almost double higher than the EKF. This fact leads to the conclusion that EKF and UKF can be equally usable as the location estimation algorithm for UWB-based localization systems in practice. However, EKF will be the preferred method if the processing time of the algorithm plays a crucial role in the intended system use-case in the application.

Moreover, the evaluation results revealed a crucial fact regarding the TS positioning technique. In all the evaluated scenarios, the experimental results constantly showed that TS method was capable of producing the performance score rather quite close to the EKF and UKF meanwhile its computational time was approximately as low as the Trilateration positioning method. Therefore, we can conclude based on the results that TS algorithm was the most efficient method among the five location estimation algorithms examined in this chapter in terms of both the computational time and performance score. In general, it should also be noted that the Kalman-based location estimation algorithms need a good approximation of the initial value unless it could diverge from the trajectory of the real path in rare cases. The general rule of thumb is to choose a value, which is located inside the coverage areas of all the anchor nodes as the initial value. In practice, the origin of the UWB-based coordinate system is also frequently used as the initial location information for the Kalman-based filter. Moreover, it should be highlighted that all the evaluated algorithms addressed in this chapter, except for the Trilateration method, can also be used as the location estimation algorithm for the TDoA-based UWB localization systems.

In this chapter, the evaluation results were presented in 2D so that the outcomes from the five positioning algorithms were easily visualized for better comparative analyses. Another reason was that the availability of the data was more appropriate for 2D setting by the time of writing this dissertation. However, it should be cleared and noted that all the presented location estimation algorithms in this chapter are capable of directly producing 3D output data without the need for further intervention. For future work, the evaluation results can be expressed on the 3D setting. Moreover, the evaluation results indicated that the extreme degradation of performance score in all algorithms due to the NLOS condition was a stumbling block for UWB localization. Therefore, the identification and mitigation process of the NLOS in the context of UWB localization system was addressed in the coming Chapter 5.

5 Identification and Error Mitigation of Non-direct Path Signals in UWB

The main location estimation errors in UWB localization are due to the non-direct path signals in the ranging phase (Chapter 3). Therefore, the identification and mitigation of the mentioned errors are vital for persistent quality assurance in UWB-based localization system. However, the identification and mitigation process of wireless signals such as IR-UWB are, in general, challenging and difficult to realize in practice due to the nature of fundamental limits in the physical radio propagation. Recently, machine learning methods are regarded as attractive solutions for overcoming the mentioned fundamental limits in wireless communications, e.g., the errors due to non-direct path signals [231, 235]. Therefore, this chapter addresses the feasibility of machine learning algorithms for the identification process of the non-direct path signals in UWB-based localization systems. Moreover, the identification process was considered as a multi-class problem, which is in contrast to the binary classification approaches commonly practiced in literature. Additionally, the mitigation technique for UWB localization was also proposed in the dissertation (Chapter 5.2). Figure 5.1 highlighted the sectional focus of the chapter from the big picture of the overall bidirectional UWB localization scheme, i.e., the identification and mitigation of the ranging errors sections.

Parts of the ideas presented in this chapter were published in our previous work [177], in which three classical machine learning methods were evaluated for the identification processes. Moreover, the research data and its corresponding source codes were given

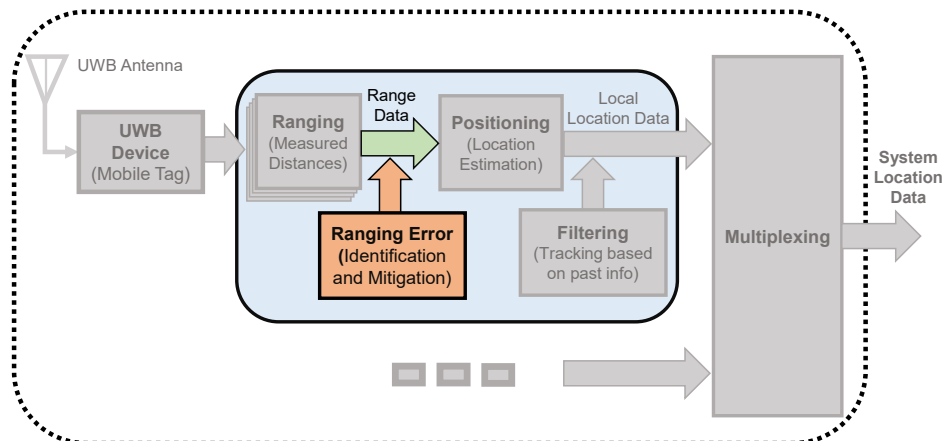


Figure 5.1: Illustration of the sectional focus addressed in this chapter, which is the identification and mitigation of ranging errors due to NLOS conditions in UWB localization systems.

as an open source in [176], which were also available on Gitlab¹ and Github². This chapter further extended the mentioned work by presenting the mitigation technique for the multi-class problem as well as the feasibility of additional two other ML methods on the identification process of non-direct path signals in UWB-based ranging systems.

Accordingly, the chapter is organized as follows: Section 5.1 describes the typical problems encountered in the radio-based ranging systems and the motivation behind the need for a multi-class identification process in UWB as well as the state-of-the-art approaches in the field. The mitigation technique applicable in any Lateration-based location estimation algorithm was introduced in Section 5.2. Then, the procedures of data preparation for the machine learning algorithms such as experimental setup, data measurement, feature extraction, and data preprocessing processes were addressed in Section 5.3. The overview of the ML models used in the evaluation are briefly reviewed in Section 5.4. The comparative results regarding the identification process of the non-direct path signals in UWB were discussed in Section 5.5. Finally, the chapter is wrapped up with the discussion and conclusion in Section 5.6.

5.1 Background and Motivation

This section discusses the problem regarding the main sources of errors in UWB-based ranging and localization system (Section 5.1.1) as well as the motivation behind the need for identification and mitigation process for the mentioned errors (Section 5.1.2). Then, the state-of-the-art methods regarding the identification process of non-direct path signals in UWB (Section 5.1.3) are addressed based on basic two approaches namely: (i) the classical techniques and (ii) the machine learning methods. Afterward, the main contribution made in the chapter are described in Section 5.1.4.

5.1.1 Problem Description

In a radio-based wireless ranging system, the distance between a transmitter and a receiver can generally be determined by multiplying the estimated TOF between the two transceivers by the speed of light (Chapter 3). In a nutshell, the ranging algorithm, especially in UWB-based localization system, basically assumes that the measured TOF signals are achieved from a direct LOS situation. Therefore, the non-direct path signals, i.e. the NLOS [16, 138, 208] and MP [41] conditions, cause a positive bias in the estimated distances of the typical ranging scheme. For the purpose of the conceptual illustration addressed in this chapter, an abstract view of the LOS, NLOS, and MP conditions in typical wireless communications are depicted in Figure 5.2. In the figure, it was illustrated that a signal sent from a tag device (green pyramid shape in the middle) can be arrived at its receiving anchor nodes (yellow pyramid shapes) in different forms based on the conditions of the scenarios.

The LOS in the figure refers to a propagation path of an UWB signal sending from a transmitter reaches to its intended receiver in a direct straight line path (Figure 5.2). On

¹<https://gitlab.ub.uni-bielefeld.de/csang/identification-of-nlos-and-mp-in-uwb-using-ml>

²<https://github.com/cliansang/Identification-of-NLOS-and-MP-in-UWB-using-ML>

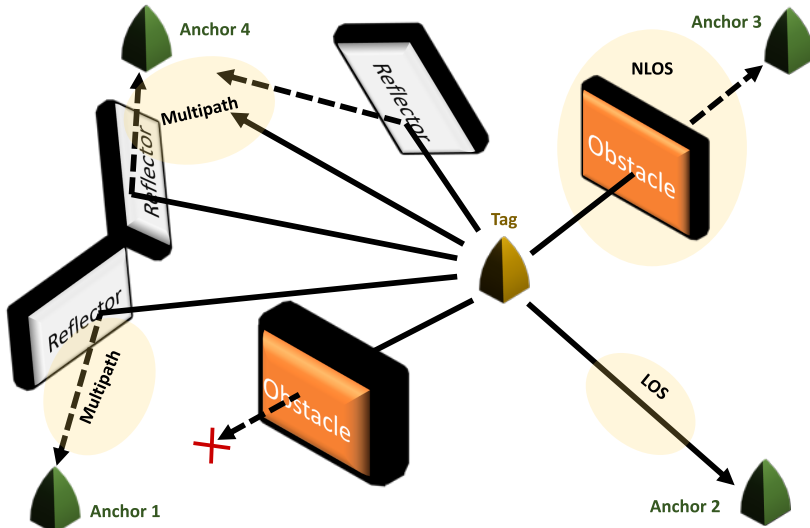


Figure 5.2: Illustration of LOS, NLOS and MP scenarios in a UWB-based ranging system. The image was a slightly decorated version from our previous work in [177].

the contrary, the NLOS corresponds to a propagation path of an UWB signal that needs to go through obstacles by penetrating them in order to reach its intended destination. Regarding MP scenario, two possible conditions in wireless ranging system was defined particularly in Figure 5.2. On the one hand, the first path signal is completely blocked by obstacles in the first MP scenario defined in the figure. In that case, it is very clear that the only arrival signal at the receiver during the measurement process is bounded from one or more of the reflectors (Figure 5.2). On the other hand, the measured signals in wireless communications are normally influenced and distorted by the simultaneous arrival of multiple signals from the same source at the receivers due to reflections such as walls and other materials in the environment (Figure 5.2). In such a scenario, the ranging errors similar to MP occurred even if there is no direct obstacle between the transceivers. Example scenarios in such wireless measurement include the data collected in a narrow corridor, tunnel, indoor factory areas that exist several metals in the environment, etc. The error caused by such MP conditions has been proved and confirmed for UWB-based localization system in our previous work in [172] and the work reported in [180]. Hence, the differentiation between LOS, NLOS, and MP conditions is important for the realization of precise UWB localization system for GNSS-denied indoor environments.

In this chapter, the multi-class classification of LOS, NLOS, and MP in UWB ranging process was evaluated using ML methods. By specifying the mentioned classes, a positioning algorithm addressed in chapter 4 is capable of mitigating the biases caused by NLOS and MP condition by using the mitigation technique addressed in Section 5.2. However, the identification of UWB measurement signals in practice is very challenging due to a variety of physical effects such as walls, furniture, humans, the orientation of the UWB antenna, etc are contributed as accumulated ranging errors. In turns, this error distorts the direct LOS signal in several different ways as illustrated in

Figure 5.2 [41, 93]. Therefore, machine learning techniques are regarded as attractive solutions for solving such complicated problems. Incidentally, the use of ML methods for the identification and mitigation process of the NLOS condition in UWB, or wireless communications in general, are not new. The interest on ML techniques for UWB localization has significantly increased in recent years [6, 38, 51, 93, 138, 153, 163, 179, 208, 217]. However, the majority of the contributions addressed in the literature viewed it as a binary classification problem, i.e., the identification between LOS and NLOS in UWB ranging system (Section 5.1.3).

In contrast, this chapter addresses the feasibility of machine learning algorithms as multi-class problem (LOS, NLOS, and MP) for the use-case of UWB indoor localization. The evaluations were conducted on the experimental data collected in different indoor scenarios. For the sake of reproducible results and further exploration, the core subsets of the experimental research data and the corresponding source codes are provided in the public domain. The evaluation of the algorithms was conducted using the open-source Python machine learning library dubbed scikit-learn [159] and Microsoft's Light Gradient Boosting Machine (LightGBM) library.

5.1.2 Motivation

The goal of the identification process in a wireless ranging system is to detect the present of NLOS and/or MP conditions during the data communication between transceivers. This procedure is critical because the MP effects and the NLOS conditions have generally significant impacts on the distance estimation produced by the UWB technology. To demonstrate the mentioned impact of NLOS and MP conditions in UWB measurements, comparison of the three situations (LOS, NLOS, and MP) based on the real-world experimental data was given in Figure 5.3 as an exemplary sample. The measured

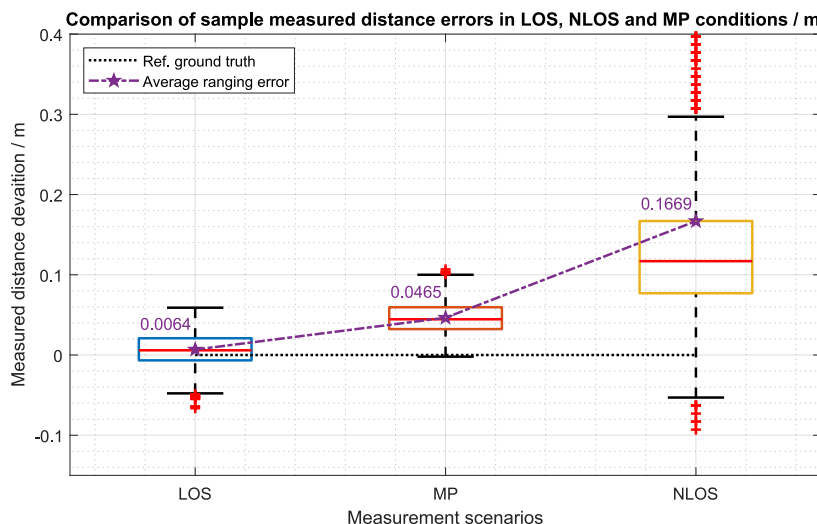


Figure 5.3: Comparison of the sample measured distance errors in the three conditions (LOS, NLOS, and MP) at static scenarios for motivational purposes.

errors given in the figure were based on a static scenario, where the ground truth between the anchor and a tag was put at a 6 m distance to each other.

The measured results in Figure 5.3 showed that the magnitude of errors produced by NLOS and MP conditions were substantially larger than the LOS condition when compared to the ground truth reference. In addition, the errors generated by the MP condition were remarkably lower than the NLOS condition, in which the UWB signal was completely blocked by obstacles and was necessary to penetrate through it in order to reach the intended receiver. Surely, the severity of the errors depends heavily on the materials made of the obstacles [41]. The NLOS error given in Figure 5.3 was based on a human as an obstacle during the experiment. The results showed that the NLOS condition introduces the highest impact on the measured distance errors (Figure 5.3). These motivational facts push the author to classify the UWB-based ranging system into three classes namely LOS, NLOS, and MP in the evaluations. The purpose is to enhance the location accuracy produced by the UWB localization system.

Moreover, the classified ranging information addressed in this chapter is applicable for the enhancement of the location service produced by any positioning algorithm (chapter 4). This can be accomplished by using the classified ranges to eliminate the biases caused by the NLOS [175, 217, 228] and MP conditions in the mitigation algorithm (see Section 5.2). It should be noted that the error deviations demonstrated in Figure 5.3 correspond only to a single range measurement. In general, at least three ranges (usually more in Multilateration) are mandatory for UWB-based location estimation systems [81, 171]. This implies that the accumulation of such several errors in the ranging process has a major impact on overall system performance.

5.1.3 State of the Art

The correction strategy of ranging errors in UWB due to the non-direct path signals (i.e., NLOS and MP) is typically accomplished in two steps [113, 138] namely (i) the identification phase of the non-direct path [18, 85, 181] and (ii) the mitigation phase of the error produced by the non-direct path [49, 85, 138]. This chapter gives the generic non-direct path mitigation technique (Section 5.2), which could be applicable in any Lateration-based positioning algorithms (chapter 4). As a matter of fact, there are indeed methods that accomplish both the identification and mitigation process within a single technique for instance using channel statistics as a feature for ML classifiers [215, 217]. However, those techniques limit the freedom of applicable positioning algorithms for the system under investigation in the latter case as the mitigation process can only be applied in a few compatible algorithms.

The common and more appropriate approach is detecting the non-direct path signal in the first stage. Then, the location errors can be corrected by the positioning algorithms in the second stage by using the detected information to mitigate the biased due to the NLOS as well as the MP conditions [93, 118, 138, 208, 215, 217, 228]. According in the research works in literature, the identification process can be put under two categories: (i) the conventional signal processing approaches (Section 5.1.3.1) and (ii) the modern ML-based approaches (Section 5.1.3.2). The evaluation results given in this chapter were based on the ML-based approach.

5.1.3.1 Conventional NLOS Identification Approaches in UWB

Conventionally, the NLOS recognition process in wireless communication systems including UWB technology is normally seen as a binary classification problem. Thus, the detection of MP condition is commonly regarded as unimportant in mainstream literature research. Indeed, there are a few papers that address and enlighten the crucial effects of the MP condition especially for UWB-based ranging system [41, 118, 172, 180]. For a summarized referencing purpose, the conventional NLOS identification techniques as a binary classification problem can be divided as follows:

1. Identification of NLOS using a binary hypothesis test [18]
2. Detection of NLOS upon the variation of Signal-to-Noise Ratio (SNR) [181]
3. Identifying NLOS based on the values in channel impulse response [135, 138]
4. NLOS detection techniques using multi-path channel statistics such as kurtosis, mean excess delay spread, and root mean squared delay spread [82, 85]
5. NLOS classification based on the RSS [82, 219]

In short, the identification process of NLOS condition in UWB using conventional techniques relied mainly on the statistical conditions of the received UWB signal. To demonstrate this situation, Figure 5.4 compares the received powers related to the First-Path (FP) and Channel Impulse Response (CIR) signals in UWB ranging for three conditions namely LOS, NLOS, and MP. In practice, the classification between LOS and NLOS using a dedicated threshold is the most commonly applied conventional technique [38, 46, 147]. The mentioned threshold is determined by subtracting the received power level of the FP signal from the total received power. Regarding this, the FP power level can be defined as follows [46] (Figure 5.4a–c):

$$FP \text{ Power Level} = 10 \cdot \log_{10}\left(\frac{F_1^2 + F_2^2 + F_3^2}{N^2}\right) - A \quad (5.1)$$

where F_1 , F_2 , and F_3 are the first, second, and third harmonics of the amplitude of the first-path signal at the UWB receivers [46, 147]. N is the reported value of the preamble accumulation count (e.g. measured by the DW1000 chip). A is a predefined constant value, that posses 133.77 using a Pulse Repetition Frequency (PRF) of 16 MHz and 121.74 for a PRF of 64 MHz.

The received (RX) power level for UWB signal can be defined as:

$$RX \text{ Power Level} = 10 \cdot \log_{10}\left(\frac{C \cdot 2^{17}}{N^2}\right) - A \quad (5.2)$$

where C is the reported value of the channel impulse response power (e.g. in DW1000 chip manufactured by Qorvo/Decawave).

Thus, the power level threshold [46], which is commonly used to discriminate the NLOS condition in conventional UWB ranging system, can be determined as:

$$Threshold \text{ Power} = RX \text{ Power Level} - FP \text{ Power Level} \quad (5.3)$$

In the mentioned conventional power threshold technique according to Equation (5.3), the measured range in UWB is defined as a LOS if the threshold power level is less

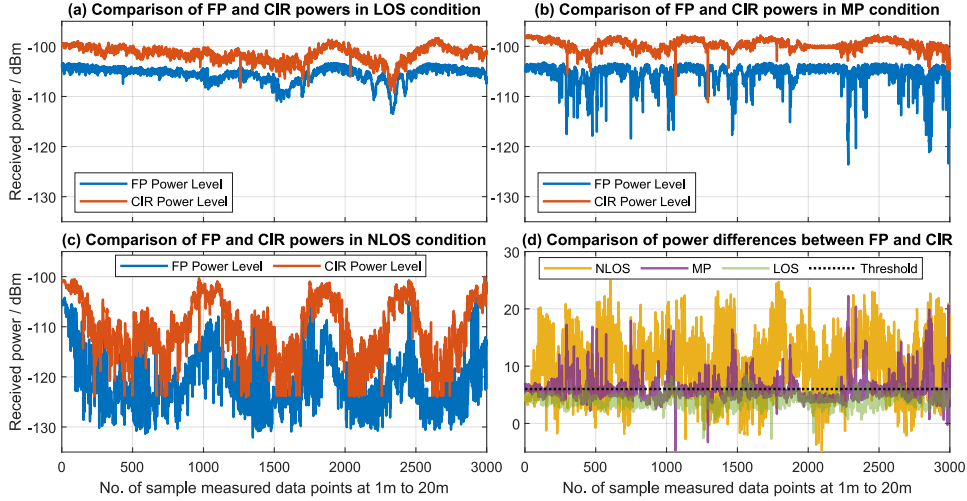


Figure 5.4: Illustration of the LOS, NLOS, and MP conditions in UWB ranging systems: (a–c) Comparison of the FP power, and the CIR power in three scenarios: (a) LOS, (b) NLOS, (c) MP conditions, and (d) the difference between the two power levels (FP and CIR powers) from (a) to (c). The measurement was conducted for the three scenarios at random movement between 1 m and 24 m distances in indoor environments.

than 6 dBm and recognized as a NLOS if it is more than 10 dBm [46]. Figure 5.4 (d) illustrates the power difference between the FP and CIR signals for LOS, NLOS, and MP conditions using the threshold power as 6 dBm. Each individual power level for the three classes was presented in Figure 5.4(a-c). The evaluation results were based on measured experimental data (Section 5.3.1). The results showed that the conventional power threshold technique can provide sub-optimal acceptable solutions for binary identification between LOS and NLOS conditions (Figure 5.4). To be more precise, the mean value of power threshold in LOS data based on Figure 5.4 (a) was 4.12 ± 1.13 dBm. Accordingly, the mean value for NLOS data based on Figure 5.4 (c) was 10.75 ± 5.51 dBm. However, the solution based on the power threshold technique is not optimal at all as a lot of overlapping areas between LOS and NLOS generally occurred, which can also be evident in the presented evaluation results (Figure 5.4 (d)). The situation is even tougher for the classification process of the MP conditions in UWB because the threshold power level usually lies within the central points of the measured MP data. Again, this process can be seen in the sample results given in Figure 5.4 (d).

It is apparent according to the evaluation results given in Figure 5.2 (d) that multi-class classification of UWB ranging measurement (i.e., LOS, NLOS, and MP) is not straightforward. Moreover, the indoor environment creates the mentioned complexity even harder due to the possession of different characteristics and refractive indexes in each individual material in the measured environments [41, 188]. This implied that the effects of MP and NLOS conditions are heavily dependent on factors such as the medium through which the signal travels (i.e. air or penetrating other materials such as wood, steel, etc.), the dimension of the measured environments (i.e. the size of rooms or places where the measurement is done), the present of objects with different

material characteristics within the measured environment, the orientation of the UWB antenna, etc. Therefore, ML-based techniques have been seen as engaging tactics for performing the identification process of NLOS signals in the mentioned complex environments in recent years (Section 5.1.3.2).

5.1.3.2 ML-based NLOS and MP Identification Processes in UWB

One of the earliest ML-based NLOS identification technique for UWB was conducted in [138], in which the Support Vector Machine (SVM) was used as a classifier. The paper considered the identification process as a binary classification problem (LOS vs. NLOS) and proved that ML-based approaches were superior to the traditional parametric techniques and signal processing technique. Subsequently, several ML-based studies were conducted regarding the NLOS identification process for UWB-based ranging and positioning system. For instance, SVM was utilized as the ML-based classifier for NLOS condition in [93, 118, 138, 208]. Similarly, the classification between LOS and NLOS for UWB was conducted using Multi-layer Perceptron (MLP) as a classifier in [19, 38, 120], Boosted Decision Tree (BDT) in [120], recursive decision tree in [147], kernel principal component analysis in [179], bagging based ensemble technique in [163], etc.

Recently, the unsupervised ML method called “expectation maximization for Gaussian mixture models” was utilized for the binary classification between LOS and NLOS in UWB [54]. Similarly, deep learning methods specifically Convolutional Neural Network (CNN)-based approaches were also widely used for binary classification between LOS and NLOS in UWB localization [153, 180]. In CNN-based techniques, the transfer learning technique are the norm by modifying the existing CNN network such as GoogLeNet [153], VGG-architecture (i.e., VGG-16 or VGG-19) [153, 180], AlexNet [153], etc. In all of the above mentioned approaches, the primary focus is to detect the NLOS measurement in UWB ranging. In short, the authors addressed only the binary classification between LOS and NLOS conditions within the measured data. By contrast, the binary classification between MP and LOS was also examined in [180].

In addition, comparative analyses of different ML techniques for the identification process of NLOS condition in UWB had been examined in [16, 93, 120]. The primary goals in those studies were to analyze the impact of ML-based classifiers under the same condition for the use-case in applications. In [120], two ML-based models (i.e., MLP and BDT) were evaluated for binary classification between LOS and NLOS in UWB and the authors concluded that the performance score of BDT is better than the MLP. Likewise, five ML-based classifiers (i.e., SVM, K-Nearest Neighbor (KNN), binary decision tree, Gaussian Process (GP), and generalized linear model) were addressed to discriminated the LOS and NLOS condition using MATLAB environment in [16]. The authors drew the conclusion that KNN and GP have better performance in general compared to the other three evaluated models. Lastly, three ML-based models (SVM, MLP, and Random Forest (RF)) were investigate to identify binary classes (LOS and NLOS) for a narrow-band wireless communications in [93]. The authors concluded that SVM poorly performed compared to the other two models in all of their evaluations. Meanwhile, MLP and RF showed comparable results.

5.1.4 Considered the Multi-class Approach and Contributions

The literature review described in the previous section showed that the non-direct path identification process in UWB has been regarded as a binary classification problem or hypothesis test (i.e., either LOS vs. NLOS or LOS vs. MP). To the best knowledge of the author, only two studies looked into the ranging errors identification in UWB as a multi-class problem [16, 118] except for the author's co-authored previous work in [177]. The first work [118] addressed the non-direct path identification process in UWB ranging as a two-step procedure and SVM was utilized as a ML-based classifier. In that work, the first step corresponds to identifying the NLOS from a LOS. Next, the second step proceeds for classification between NLOS and MP condition if the first step identification process resulted as a NLOS. The second work [16] subdivided the NLOS situation into two subcategories namely the soft-NLOS and the hard-NLOS conditions, i.e., in addition to the LOS condition. However, the mentioned work ignored the impact of MP effects. The categorization between the mentioned two NLOS types was conducted based upon the material of the obstacles that blocked the LOS condition and the UWB signal has to pass through by penetration. In their evaluation, the authors used two types of walls to distinguish a soft-NLOS and a hard-NLOS condition.

On the contrary, the authors' previous co-authored work [177] addressed a direct identification of the multi-class classification for UWB ranging signal. In that work, we defined three classes (LOS, NLOS, and MP conditions) and evaluated three classical machine learning methods namely SVM, RF, and MLP.

This chapter is the extension of our previous work in [177] by proposing a generic mitigation technique for multi-class problems in UWB (Section 5.2) as well as by addressing the comparative analysis of five ML methods in the identification process. The goal of exploring different models in the evaluation is to demonstrate the feasibility of the ML techniques as a multi-class classifier for UWB localization system. In total, five ML-based classifiers (Section 5.4) were evaluated to compare their performances for the identification process of the UWB ranging-based multi-class problem (Section 5.5). The evaluation results showed that even the simplest model namely NB can provide remarkable outcomes and generalize well on unseen data collected in different environments from the training process.

5.2 A Generic NLOS Mitigation Technique for UWB

A simple and yet very effective NLOS mitigation technique proposed in our previous work [175] is presented in this section. The proposal in our previous work was based solely on a binary class problem. In this section, the generic setting of the mentioned mitigation technique for a multi-class case was proposed as an extended version. Subsequently, two types of implementation processes for the considered mitigation techniques are briefly explained and demonstrated. Thus, this section was structured with the formulation of the mitigation technique (Section 5.2.1), the overall description of the integration process for the mitigation technique (Section 5.2.2), and the exemplary implementation on the closed-form methods (Section 5.2.3).

5.2.1 Formulation of the considered Mitigation Technique

This section addresses a very simple and effective NLOS mitigation technique which is applicable in the majority of the location estimation algorithms (see Chapter 4) utilized in UWB-based localization systems. For the motivational purpose, the effectiveness of the said mitigation method was demonstrated using the experimental real-world data in Figure 5.5. The figure described the comparison of two multilateral location estimation algorithms in NLOS scenario at static condition, in which one positioning method used the mitigation technique and the other used the regular one under the exact same setup and applied algorithm. The results showed that the regular positioning method produces several outliers data points due to NLOS condition. In contrast, the mentioned errors can nicely be mitigated by using the mitigation technique provided in this section (Figure 5.5). To be more specific, the positioning algorithm used in the figure was based on a true-range Multilateration method for both scenarios. The measurement was based on four anchors and a tag, in which the direct LOS condition between one anchor out of the four and a tag was blocked by a human as an obstacle.

In UWB-based positioning systems, outliers mainly occur due to the non-direct path signals, i.e., NLOS conditions (Fig. 5.5). For this reason, there are several NLOS identification techniques based on either ML methods addressed in this chapter or a conventional power threshold technique as discussed in Section 5.1.3. The mitigation technique presented in this section is a very generic one as it can flexibly be applied in any UWB-based location estimation algorithms (Chapter 4). The core idea is to generate a weighting matrix from the identifiable measured ranges and correct the measurement due to biases in the positioning phase. The pseudo-code of the algorithm regarding the

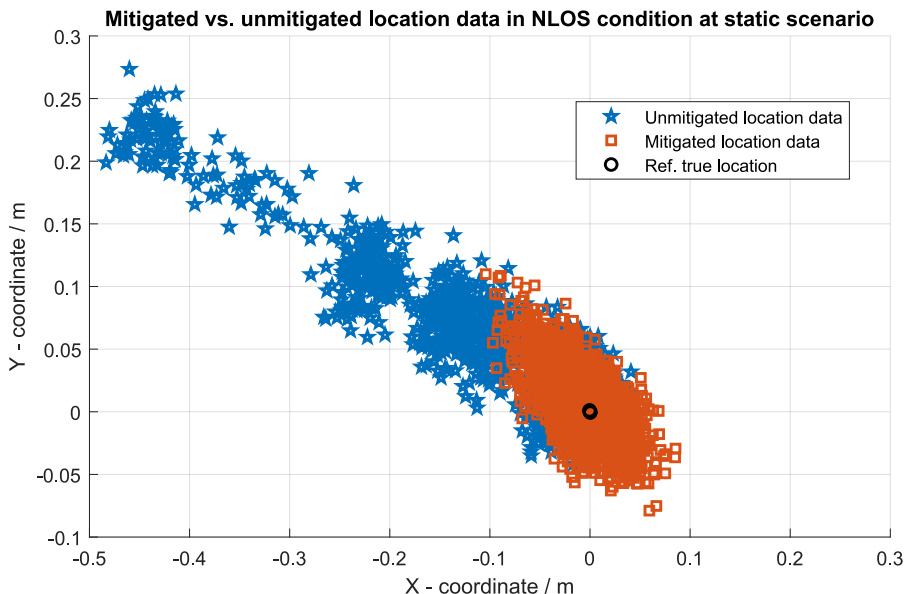


Figure 5.5: Comparison of the mitigated vs. unmitigated location outputs from Multilateration method at NLOS condition.

generation of the weighting matrix for mitigation of the NLOS condition in UWB-based localization system is expressed in Algorithm 1. For the multi-class problem, i.e., three classes in our evaluation, the pseudo-code for the weighting matrix, which is used to mitigate the non-direct path signals (i.e., both MP and NLOS conditions), is given in Algorithm 2. This implies that the given mitigation technique presented in this section can basically be utilized in both binary and multi-class problems as needed. In addition, two feasible implementation processes of the presented mitigation technique are briefly described in Section 5.2.3 and 5.2.2 respectively.

For the sake of brevity and clarity, the weighting algorithm for binary class scenario (Algorithm 1) regarding the mitigation technique of NLOS condition in UWB is concisely explained in this section. The weighting algorithm for the multi-class problem (Algorithm 2) is generally the extension of the explained binary class case and the idea can easily be grasped by understanding the binary problem expressed here. In general, the generation of the weighting matrix for the binary class problem firstly assigns equal weights to all the identifiable measured ranges. There are two inputs in the presented weighting algorithm for the binary class which are simply the total number of measurable ranges and the identifiable NLOS conditions in each measurement (Algorithm 1). It should be noted that the proposed technique requires more inputs for multi-class problems depending on its realizable categories, for instance, three inputs for three classes (Algorithm 2). Referring back to Algorithm 1, the weight of a specified range is relegated from its initially given value using a predefined weighting factor (e.g.,

Algorithm 1 Pseudo-code regarding generation of the weighting matrix for mitigation of the NLOS condition in UWB-based localization system for a binary class

Input: #nl {number of NLOS measurements}

Input: #r {total number of measurements}

```

1: iw  $\leftarrow \frac{1}{\#r}$  {initial equal weight value, scalar}
2: W  $\leftarrow \text{eye}(\#r)$  {initial weighting matrix (identity)}
3: if #nl = 0 then
4:   return W {return the identity, no weighting required}
5: else
6:   for i  $\leftarrow 1$  to #r do
7:     if measurement i is NLOS then
8:       W(i, i)  $\leftarrow \frac{\text{iw}}{2 \cdot \#r}$  {relegate the initial scalar weight with a factor  $\frac{1}{2 \cdot \#r}$ }
9:     else
10:      W(i, i)  $\leftarrow \text{iw} + \frac{(\text{iw} - \frac{\text{iw}}{2 \cdot \#r}) \cdot \#nl}{\#r - \#nl}$  {distribute the surplus from the relegated
           weight to the LOS}
11:    end if
12:   end for
13: end if
14: return W

```

Algorithm 2 Pseudo-code of non-direct path mitigation algorithm for multi-classes

```

Input: #mp {number of MP measurements}
Input: #nl {number of NLOS measurements}
Input: #r {total number of measurements}

1: iw  $\leftarrow \frac{1}{\#r}$  {initial equal weight value, scalar}
2: W  $\leftarrow \text{eye}(\#r)$  {initial weighting matrix}
3: if #nl = 0 and #mp=0 then
4:   return W {no weighting is required}
5: else
6:   for i  $\leftarrow 1$  to #r do
7:     if measurement i is NLOS then
8:       W(i,i)  $\leftarrow \frac{iw}{2 \cdot \#r}$  {a weighting factor  $\frac{1}{2 \cdot \#r}$  is used for NLOS condition}
9:     else if measurement i is MP then
10:    W(i,i)  $\leftarrow \frac{iw}{\#r}$  {here,  $\frac{1}{\#r}$  is used as a weighting factor for MP condition}
11:   else
12:     W(i,i)  $\leftarrow iw + \frac{(iw - \frac{iw}{2 \cdot \#r}) \cdot \#nl + (iw - \frac{iw}{\#r}) \cdot \#mp}{\#r - \#nl - \#mp}$  {each LOS portion}
13:   end if
14:   end for
15: end if
16: return W

```

$1/(2 \cdot \#r)$ in Algorithm 1) if a NLOS condition is identified in that specific measurement. Correspondingly, the surplus (excess) of the relegated weight is equally distributed to all the LOS conditions in the measurement (line no. 10 in Algorithm 1).

It can be realized in Algorithm 1 that the trace (the sum of elements of the main diagonal) of the generated weighting matrix is always 1 unless all the measured ranges are in either LOS or NLOS condition. In those extreme cases (all implies LOS or NLOS), no weighting (equal weight) will be applied to the measured ranges. Moreover, the weighting matrix W in Algorithm 1 and 2 is generally assumed as a diagonal matrix due to the fact that the measured ranges are normally independent of each other. Similar to typical generic algorithm, the predefined weighting factor (i.e., line 8 of Algorithm 1) can be tuned in order to give a specified weight to a NLOS data based on the system requirements (e.g. a factor of $1/3 \cdot \#r$, $1/\#r$, etc. can be used instead of $1/2 \cdot \#r$). In such a specific scenario, the formulation related to the distribution of surplus (i.e. line 10 in Algorithm 1) should be adjusted accordingly.

5.2.2 Explanatory Integration Process of the Mitigation Technique

The overview of the integration process for the proposed mitigation technique in UWB-based localization system was depicted as a block diagram in Figure 5.6. The core

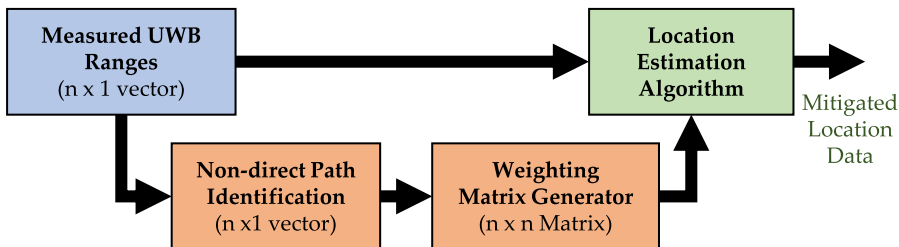


Figure 5.6: Block diagram of the implementation process regarding the mitigation technique given in this chapter for UWB localization.

Idea regarding the implementation of the proposed mitigation technique is that the information conveyed in the measured ranges shouldn't change its total quantity as a whole. In other words, the measured ranges should still pertain to their information fully in the mitigated process even after the multiplication with the weighting matrix has been made (Figure 5.6). In simple words, it can be supposed that the vector of the measured ranges is multiplied by a scalar 1, which should be resulted back to the same value in total even after the multiplication process. However, the weighting matrix in the presented algorithm does give priority to some measurements, e.g. more attention on LOS condition, and less to the others namely NLOS or MP conditions. This results in an effective and efficient solution for a scenario where the negative impacts of the non-direct path signals are necessary to be filtered out in a given problem.

Mathematically, this can be accomplished in the close-form least squares method by multiplying the basic formula with the weighting matrix generated by the proposed mitigation technique. Specifically, the Multilateration location estimation algorithm was, indeed, based on the least squares technique so as the first order TS approach addressed in Chapter 4. Fundamentally, the Kalman-based filters are also built upon the least squares method under the hood. Therefore, the proposed weighting matrix can literally be applied in all the considered positioning algorithms addressed in Chapter 4 except for the Trilateration method.

5.2.3 Exemplary Implementation on Closed-form Methods

This section describes the implementation process of the proposed mitigation technique on two close-form location estimation algorithms namely Multilateration and first-order TS techniques. In general, the major disadvantage of the OLS approach such as a typical Multilateration method given in Equation (4.9) from Chapter 4 is that the technique is very sensitive to outliers [195]. This implies that the estimation of the algorithm can easily be biased by a few outliers in OLS. In the context of UWB localization, the outliers in the measurements are mainly due to the NLOS condition in the ranging phase. To overcome the mentioned problem caused by the outliers, the Weighted Least Square (WLS) technique is commonly used in the applied mathematics [66]. WLS is similar to OLS in many ways, and it is, in reality, a more generic approach. For the Multilateration positioning algorithm, WLS can be derived from Equation (4.9) by

multiplying both sides of the equations with the weighting matrix generated by the proposed mitigation technique as follow [66, 195]:

$$\begin{aligned} Ax &= b \\ WAx &= Wb \\ x &= (A^T W^T WA)^{-1} A^T W^T Wb \\ x &= (A^T CA)^{-1} A^T Cb \end{aligned} \quad (5.4)$$

where, W is the weighting matrix produced by the proposed mitigation technique described in Section 5.2.1, and C is $W^T W$.

For the implementation process of the mitigation technique in TS-based location estimation algorithm, Equation (4.15) can be rewritten as follows akin to Multilateration:

$$\begin{aligned} H\delta &= \Delta d \\ WH\delta &= W\Delta d \\ \delta &= (H^T W^T WH)^{-1} H^T W^T Wb \\ \delta &= (H^T CH)^{-1} H^T Cb \end{aligned} \quad (5.5)$$

where, W is again the weighting matrix generated by the mitigation algorithm addressed in this section (Section 5.2.1), and C is $W^T W$.

5.3 Setup and Data Preparation for Identification Process

This section describes the experimental setup (Section 5.3.1), the data labeling and feature extraction (Section 5.3.2), the data collection processes (Section 5.3.3), and the data preprocessing process (Section 5.3.4) for the identification process of the non-direct path signals in UWB ranging system.

5.3.1 Experimental Setup

For the data collection process of UWB ranging in our experiments, a DWM1000 module [46] manufactured by Decawave was utilized as the UWB hardware and STM32 NUCLEO-L476RG [193] development board from STMicroelectronics was used as the MCU. Table 5.1 gave the hardware configurations used in the data collection and measurement process for the UWB technology in this chapter.

The evaluation results in chapter 3 showed that AltDS-TWR is the most reliable and efficient TWR technique in literature. Therefore, AltDS-TWR was applied as the ranging method for all the collected UWB-based data presented in this chapter. In addition, the built-in HSI clock source of 16 MHz from the MCU was utilized for time-stamping of the UWB ranging data because AltDS-TWR can provide accurate ranging without the need to use high precision external oscillators (Chapter 3). In accordance with the data-sheet [192] from the manufacturer, the applied built-in HSI clock source has an accuracy of $\pm 1\%$ using the factory-trimmed Resistor-Capacitor (RC) oscillator.

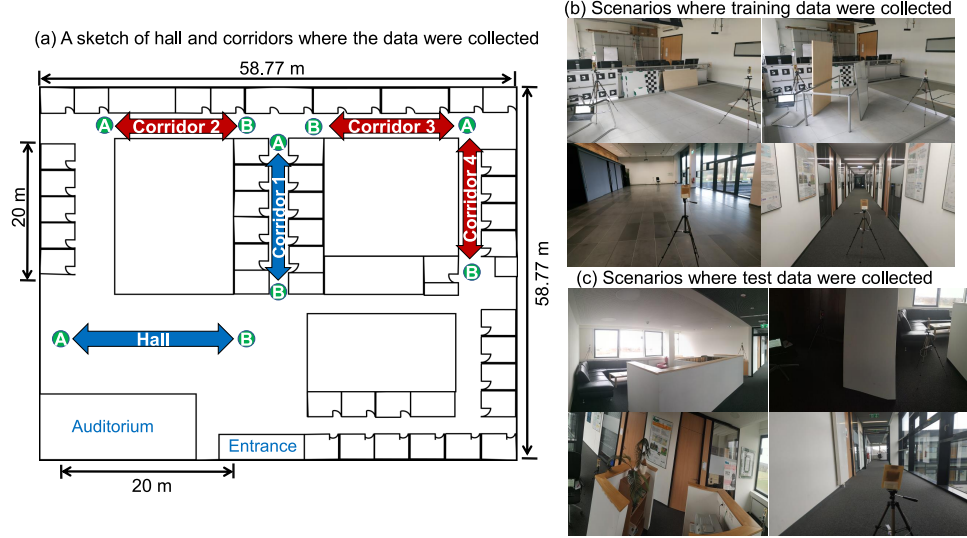


Figure 5.7: Illustration of the scenarios where training and test data were collected for evaluation: (a) A sketch of the building where the experimental data for training and test were collected. (b) Training data were collected for LOS, NLOS (including human blocking) and MP conditions in a laboratory, a large hall, and a corridor (blue color in (a)). (c) Similar to (b), test data were collected in a different room (including different types of furniture and NLOS human blocking) and a different corridor (red in (a)).

During measurement at the data collection process, one of the two transceivers was connected to a PC for logging the measured ranging data of UWB via a serial USART port. The logged data included the extracted features given in Section 5.3.2. Those logged data were saved into a file for each trial during the measurement campaign. In order to avoid the effect of Fresnel zones in the measurements, the antenna height was always maintained at 1.06 m in one of the UWB device under test, i.e., the static one that recorded the measurement data into the PC.

Table 5.1: Configurations of the primary hardware used in the experimental evaluation.

Types of Hardware	Properties	Settings
UWB module	Module name	DWM1000
	Data rate	6.8 Mbps
	Center frequency	3993.6 MHz
	Bandwidth	499.2 MHz
	Channel	2
	PRF	16 MHz
	Reported precision	10 cm
	Manufacturer	Decawave (Qorvo)
	MCU	STM32L476RG
	Development board	NUCLEO-L476RG
	Manufacturer	STMicroelectronics

Figure 5.7 illustrates the environments and scenarios where the experimental data were collected for the evaluation results presented in this chapter. In specific, the experimental data were collected in three scenarios (two small rooms, a hall, and four corridors) at seven different places in indoor environments (Figure 5.7). The two rooms where the data collection was conducted include the $6\text{ m} \times 6\text{ m}$ laboratory in CITEC and the $8\text{ m} \times 6\text{ m}$ communication room. In both of the mentioned two rooms, different items of typical furniture were in place during the measurement.

The data collected at the narrow corridors (Figure 5.7) were designated for the examination of the MP condition in the chapter. In this particular case, the direct LOS signal from the UWB transceivers were indistinguishable due to the multiple reflections from the narrow walls. In contrast, the NLOS data were achieved by blocking the communication between two transceivers using a human as an obstacle in all the measured scenarios depicted in Figure 5.7. Moreover, a thick concrete wall, pieces of concrete block, and a mixture of wood and metal were also utilized as parts of the obstacles for generating data regarding NLOS condition in the laboratory room. For the LOS scenario, the measurement was based simply on no obstacles between the two transceivers at different settings (i.e., static and dynamic scenarios).

The collected data included both the static and dynamic scenarios in all measurement campaigns. In the course of the dynamic case, the UWB device attached to the PC for data logging purposes stayed still as static whereas the other one held by a human was in motion with random walks. Moreover, the antenna of the UWB device held by a human was allowed to rotate between 0° and 180° during the data collection process for the dynamic case. On the contrary, both the UWB transceivers were at stationary positions in the static case, in which the antennas of both the transceivers were at 90° pointing to an upward or vertical position without any rotation.

5.3.2 Data Labeling and Feature Extraction

The multi-class labels (LOS, NLOS, and MP) predefined for evaluation of the ML-based classifier in this chapter were manually annotated in the preprocessing phase after the data measurement and collection processes has been finished. In order to be able to do this, a block of observed measured data for each trial in the collection process was saved individually as a separate file into the PC during the measurement campaign. Regarding this, the experimental data related to each multi-class category (LOS, NLOS, and MP) were separately collected in different scenarios and the whole block of data was stored under a unique file name. The block of data means a collection of data belonging to the same class in a specific environment, which were saved separately with a unique name in PC as a single file during the measurement campaign.

For instance, the measured data related to a motion of a random walk between 1 m to 20 m was collected in Corridor 2 (Figure 5.7) for five minutes using an update rate of 20 Hz. During the measurement, it was made certain that no obstacles were placed between the two transceivers as well as the measured data were solely based on the UWB antenna at 90° in the upward position. The mentioned block of recorded data was saved into the PC and annotated the whole measured data within that block as a MP class in preprocessing phase so that it can be used in ML-based multi-class classification

process. In the same manner, the LOS and NLOS data were annotated manually for each trial in the measurement campaign.

Regarding the feature extraction process, twelve features were specifically extracted from the UWB hardware module namely DWM1000, which was manufactured by Decawave (Qorvo) [46] (see the applied configuration settings in Table 5.1). Indeed, the mentioned extracted features were based upon the typical system parameters essential for identification of NLOS in conventional approach (see Section 5.1.3.1). This ensures that the use of the mentioned extracted features in ML-based application has no extra burdens in the identification process of the non-direct path signals in UWB localization system. For the sake of a complete picture allowable by the applied UWB hardware, two more features namely standard noise and maximum noise specifically produced by the DW1000 module were also included as features in the evaluations. Hence, the full twelve features extracted and saved during the data collection process and measurements can be categorized as follows:

1. the reported measured distance
2. the compound amplitudes of multiple harmonics in the FP signal
3. the amplitude of the first harmonic in the FP signal
4. the amplitude of the second harmonic in the FP signal
5. the amplitude of the third harmonic in the FP signal
6. the amplitude of the channel impulse response (CIR)
7. the preamble accumulation count reported in the DW1000 chip module
8. the estimated FP power level using (5.1)
9. the estimated RX power level using (5.2)
10. the difference between the FP and RX power level using (5.3)
11. the standard noise reported in the DW1000 chip module
12. the maximum noise reported in the DW1000 chip module

Concerning the above-mentioned twelve extracted features, it should be mentioned that the data extraction was conducted based solely on the DW1000 chip from Decawave (Qorvo) as the UWB hardware. It is expected that the mentioned features can also be able to extract in other UWB-based vendors in the market even though the author haven't tested it yet at the time of writing this dissertation.

5.3.3 Data Collection Process for Two Independent Test Scenarios

Two independent test data-sets based on two unrelated environments were utilized to present the experimental evaluation results given in Section 5.5. For this reason, the data collection process for test datasets can be divided into two scenarios. The mentioned two test scenarios for evaluating the multi-class classification of five ML models in this chapter can be categorized as follow:

- **Test Scenario I:** was based on the datasets split as unseen data for testing purposes from the data used in the training process. In other words, the test dataset from scenario I comes from the same environments (i.e, room, hall, corridors, etc) as the training data, in which a subset of it was split as unseen data.

- **Test Scenario II:** was based on the datasets separately collected at completely different environments (i.e., room, hall, corridors, etc) from the datasets used in the training process. The main goal here is to evaluate the generalization of the trained ML model in unseen environments.

In short, the evaluations using the data from test scenario I were designated for unseen datasets whereas the test scenario II was dedicated to the unseen environments. With this in mind, the collected UWB ranging data are partitioned into two groups. The data in the first group were used for both training and validation of the five ML-based classifiers addressed in this chapter as well as presentation of the classification results for test scenario I (i.e., model evaluation based on the unseen data). In contrast, the data in the second group were used only for the investigation of the model performance for the test scenario II (i.e., model evaluation based on the unseen environments).

Regarding this, the datasets for the first group were collected from the measurement environments at the laboratory, the hall, and the first corridor illustrated in Figure 5.7 (b). Specifically, 185.790 sample observations were gathered after equally balancing the considered three classes (LOS, NLOS, and MP) for model training and evaluation of the test scenario I. This implies that the three classes belonged to 61.930 data points each. For evaluation of test scenario I, thirty percent of the data points were left out as unseen datasets by random shuffling in each trial conducted in Section 5.5. The classification results achieved using the mentioned evaluation datasets are categorized as outcomes from test scenario I in the chapter (Section 5.5).

In fact, the process of evaluating the classification results based on test scenario I was a common practice for representing evaluation results in most UWB-based literature [16, 118, 208]. In some papers, the datasets used for testing purpose was differentiated by deliberately switching the subject of the experiment (for instance, a person who carried the UWB device in [16]). Nevertheless, the environment used in the data measurement process remained unchanged in those settings.

On the contrary, a test scenario II was created to examine the generalization of the trained ML-based models in this chapter. The measurement campaign specifically for test scenario II was conducted in different environments from the above-mentioned test scenario I, i.e., a different room with various items of furniture in three different corridors (Figure 5.7 c). The results achieved from the second environment were expressed as outcomes from the test scenario II in the chapter (Section 5.5). In total, 36.015 data points were gathered for test scenario II after balancing the data for the three considered classes (LOS, NLOS, and MP). Again, this implied that each class belongs to 12.005 data points for test scenario II.

5.3.4 Data Preprocessing

The raw UWB datasets obtained from the measurements and discussed in the previous subsection were imbalanced for the considered three classes (LOS, NLOS, and MP) in the initial states. In fact, this phenomenon is very common in real-world data collection processes for ML-based applications. Class imbalance is a term used in cases where the number of collected samples in classes is not the same. In other words, one or more

classes of the samples are considerably smaller or larger than those belonging to other classes. In such cases, a re-sampling technique [28] is one of the widely used methods to deal with imbalanced data in classification problems.

A random under-sampling technique [28] was applied to balance (i.e., making the three considered classes to possess an equal amount of data) the gathered UWB ranging data. In the under-sampling method, the class that belongs to the smallest number of sample observations is usually set as a base class. Then, the classes with higher samples of observation were lowered to balance with the total number of the base class by randomly selecting their member elements. This confirmed that there was no artificial data generation involved in the sampling process apart from real measured data.

Moreover, feature importance plays a crucial role in many ML-based applications especially when the use cases are intended for edge devices. Our previous work in [177] showed that three out of the twelve features have more impact on the identification of the non-direct path signal in UWB ranging data. Nevertheless, the evaluated results presented in this chapter were based on the full twelve features given in Section 5.3.2 for the sake of uniformity across all the evaluated ML-models.

In many ML models, feature scaling technique (i.e., scaling the data using standardization or normalization method) usually enables a faster training time and a better overall system performance. However, the impact of the mentioned feature scaling depends strongly on the applied ML-methods, and no effects were shown in some models (e.g., RF has no effects on the feature scaling process in UWB data [177]). For the sake of uniformity across the evaluated ML-models, standardization-based feature scaling was used in all the presented models in this chapter. Standardization refers to scaling the data into a mean of zero and a standard deviation of one (unit variance).

5.4 Machine Learning Models for Identification of the Non-direct Path Signals

Five machine learning models (NB, SVM, RF, LightGBM, and MLP) were evaluated for the identification process of non-direct path signals in this chapter. NB was considered as a baseline model for the evaluation. The brief description and setup used in the implementation of each classifier are given in the coming subsequent sections.

In general, several parameters are necessary to tune in ML-based classifiers to achieve the optimized results. In addition, every classifier has its own specific hyper-parameters, which cannot be directly comparable with other classifiers. Therefore, the comparative analysis under exactly the same parameters for all classifiers was implausible. Therefore, the comparative results given in this chapter were based on the chosen most relevant and influential characteristics in each classifier.

For the reproducible results, the parameters regarding each evaluated classifier (e.g., the activation function, optimizer, earlier stopping criteria for the training, learning rate, etc.) were based on the default setting of the scikit-learn [159] library (Version 1.1.1) and Microsoft's LightGBM library³ (Version 3.3.2) if nothing is explicitly described. In

³<https://github.com/microsoft/LightGBM>

addition, the descriptions of each presented ML model are given at an abstract level for the sake of brevity since their technical details are widely and openly available in the public domain. Instead, the systematical analyses of the evaluation results produced by each model were thoroughly discussed in a comparative manner (Section 5.5).

5.4.1 Naive Bayes Classifier

NB classifier is one of the simplest, most efficient, and effective machine learning algorithms, commonly used as a base model in many ML-based comparative analyses [232]. Theoretically, NB classifier is a subset of probabilistic classifiers that are capable of producing a probability distribution regarding its prediction in addition to outputting the most likely class in a given problem. In NB, it is assumed that all the features fed into the algorithm for the prediction of a class are independent, i.e., naive assumption. In general, the features in the real-world data are usually correlated to each other and the assumption is rarely true. However, it is evident in many applications that the performance of NB algorithms are surprisingly good, especially in classification problem. Regarding this, a systematic investigation of the main cause was also examined in [232].

In this dissertation, the NB classifier was regarded as the base model for contrasting and comparing the performance of the other evaluated four algorithms. The implementation of the NB classifier in this chapter was based on the Gaussian distribution [27] denoted as a Gaussian NB classifier in scikit-learn library.

5.4.2 Support Vector Machine Classifier

SVM is a type of classical ML algorithm that is widely used in classification and regression problems [37, 197]. SVM rooted strongly from the framework of statistical learning theory [189]. In the past, SVM was one of the most influential ML techniques in the ML community due to its robustness and superior performance while maintaining less adjustable parameters in comparison with the deep learning approaches [138]. In a nutshell, the data provided as an input into the classifier were separated by a hyper-plane in SVM and outputted back as predefined classes. The main task of the mentioned hyper-plane in SVM algorithm is to maximize the margin between separable classes in the input data as wide as possible.

In general, the choice of the kernel types in SVM has a strong influence on its outputted performance (e.g., overall accuracy) especially in UWB measurement data. Our previous work in [177] showed that the Radial Basis Function (RBF) kernel provided the highest performance compared to other available kernels in SVM whereas using the Sigmoid function as the kernel gave the poorest performance. Thus, all the presented results given in this chapter for SVM classifier were based on the RBF kernel.

5.4.3 Random Forrest Classifier

RF is one of the most widely used ensemble ML techniques for classification and regression tasks. In the nutshell, RF combines the predictions of numerous decision

trees in the forest to produce a more accurate and reliable outcome compared to its individual prediction [20]. Generally, the decision trees in the forest are grown using a random vector in which its values are assumed to be independently and identically distributed. The core advantages of RF include: (i) less likely to be over-fitted in the training data due to the outcomes of RF relying on the average of several decision trees, and (ii) the low rate of prediction errors as this occurrence happens only when more than half of the decision trees has made the wrong prediction in RF. By contrast, the disadvantage is that RF is basically a more complex and computationally expensive classifier than the simple decision tree algorithm.

In brief, the more trees in the forest, the better the prediction for RF algorithm. However, this flexibility comes with the cost of the processing time required for training and actual test scenario. Based on our previous work in [177], the prediction accuracy of RF increased steadily as the number of decision trees in the forest increased. Though, the improvement slowed down when the number of trees in the forest was more than 50, particularly for the evaluated UWB measurement data. Therefore, the evaluation results given in this chapter for RF are based on 50 decision trees.

5.4.4 Light Gradient Boosting Machine Classifier

LightGBM, a.k.a. Histogram-Based Gradient Boosting, is a class of decision trees-based ensemble ML algorithm which is originally proposed by Microsoft in [110]. LightGBM is primarily used for ranking, classification, and regression tasks of the tabular data. In fact, the LightGBM was designed to improve the efficiency, faster training speed, and scalability of the most widely used ensemble ML technique called Gradient Boosting Decision Tree (GBDT) [110] algorithm. Regarding this, LightGBM uses a histogram-based technique for improving the learning process of decision trees in contrast to the pre-sort-based algorithm in other variance of GBDT methods.

Moreover, LightGBM uses the leaf-wise tree growth approach in its ensemble method, which is in contrast to the depth-wise tree growth method typically used in many other popular ensemble ML-based algorithms. The experimental results carried out by the original authors showed that the leaf-wise growth algorithm had the ability to converge much faster than its counterpart depth-wise growth approach [110]. However, it should be noted that the leaf-wise growth approach may over-fit easily on the training data, if the appropriate parameters in the algorithm are not used.

Following the chosen parameters given in RF, the total number of boosted trees for LightGBM classifier was set as 50 for our evaluation in this chapter. The rest of the parameters are based on the default setting given in the LightGBM library, which is version 3.3.2 by the time of writing this dissertation.

5.4.5 Multilayer Perceptron Classifier

MLP is basically a deep feed-forward Artificial Neural Network (ANN) typically composed of at least three layers (an input layer, a hidden layer, and an output layer) in its structure [89]. In MLP, the neurons in the hidden and output layers are usually used

with the nonlinear activation functions such as Rectified Linear Unit (ReLU), leaky ReLU, Sigmoid, Softmax, etc. The term deep is generally used in the MLP if the network needs to be constructed with more than one hidden layer. Moreover, the back-propagation algorithm [167] is basically used for training the constructed network in MLP.

According to our previous work [177], there was a significant increase in the overall accuracy by adding a second and third hidden layer to the network. However, the improvement was meager when more than 3 hidden layers were used for a network. In terms of the number of neurons per layer in the network, the use of 128 neurons in three hidden layers for MLP network seems the optimal choice (see more detailed analyses on this matter specifically for UWB data in our previous work [177]).

Therefore, the MLP classifier applied in this chapter was composed of three hidden layers with 128 neurons in each layer. For the activation function, a ReLU was utilized for each hidden layer and the Softmax function was used in the output layer. Adaptive Moment Estimation (Adam) was utilized as the optimization algorithm in the network. During the training process, the maximum epoch was set to 500 with an early stopped condition if there is no improvement of training loss for 10 consecutive times.

5.5 Experimental Evaluation Results

This section examines the experimental evaluation results produced by five ML classifiers for the identification of non-direct path signals in UWB based on three quantifying metrics. Firstly, Section 5.5.1 quantifies and compares the performance of the evaluated five ML-based classifiers based on single score value metrics namely the overall accuracy and the macro or micro average F1-score. Likewise, Receiver Operating Characteristic (ROC) curve and Area Under Curve (AUC)-ROC were used as the second metric for validating the outcomes of classification results regarding the identification of non-direct path measured ranges in Section 5.5.2. Thirdly, a complete confusion matrix was used to analyze the insightful knowledge of performance (Section 5.5.3).

The classification results presented in this section are based on two test scenarios defined in Section 5.3.3. For the sake of clarifying the usage of terms, the two defined test scenarios are described again here in short as follows:

- **Test Scenario 1:** was designated for evaluating the trained ML- models based on the unseen datasets. Correspondingly, the data for test scenario 1 were separately split from training and validation datasets. However, the mentioned unseen test datasets come from the same environments as training.
- **Test Scenario 2:** was designated for evaluating the trained ML- models based on the unseen environments. The main purpose is to analyze the generalization of the evaluated ML-model in real-world settings. Accordingly, the data in test scenario 2 were gathered from environments different from the data used in the training process (i.e., a different room, corridor, etc.).

5.5.1 Performance Comparison based on Accuracy and F1-Score

Single score metrics namely an overall accuracy and a macro average F1-score were chosen as quantifying measures for the comparative analysis of five ML models addressed in this Section (Figure 5.8). As stated in Section 5.3.4, the training and test datasets were balanced in preprocessing phase. Hence, using the overall accuracy as a quantifying metric is simple, intuitive, easy to understand, and valid (Figure 5.8 (a)). However, it should be noted that the outcomes from highly populated classes will have more impact on the accuracy score in the case of imbalanced datasets [77]. Accuracy can be formulated by using the numerator as the sum of true positive and true negative (i.e., diagonal values in the confusion matrix) and the denominator as the sum of all elements in the confusion matrix.

To countercheck the classification results reported based on the accuracy as a decisive metric, a macro average F1-score has also been utilized in this section (Figure 5.8). In general, the F1-score takes both the precision and recall from the confusion metrics to produce a decisive single score [16, 190]. In fact, it is a harmonic mean or weighted average of the precision and recall, which can be formulated as:

$$F1 = 2 \cdot \frac{Precision \cdot Recall}{Precision + Recall} \quad (5.6)$$

For a multi-class problem, there are two common ways to calculate the overall single value F1-score for a classifier, i.e., the macro-average F1-score and the micro-average F1-score [190]. Macro-average F1-score treated all the classes equally to compute the average score whereas the micro-average F1-score computes the mentioned average metric by aggregating the individual contributions of all classes. In this chapter, macro-average F1-score was utilized (Figure 5.8 (b)) because the balanced datasets used in the

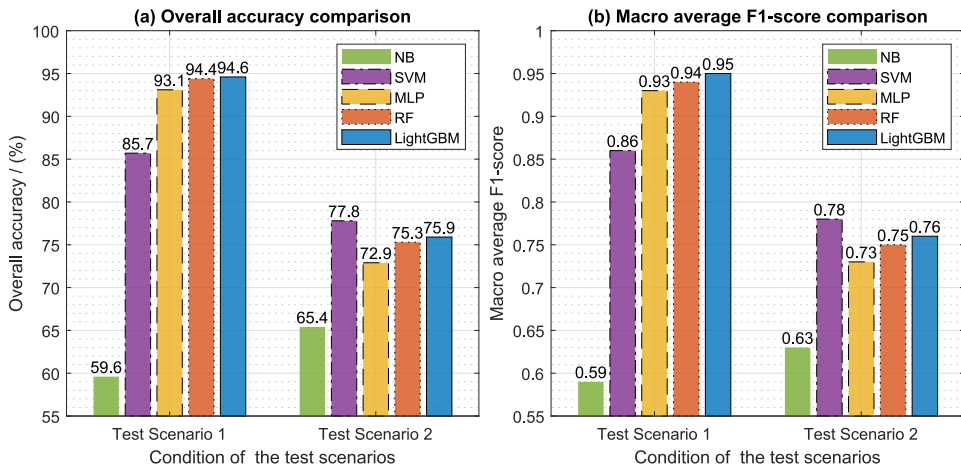


Figure 5.8: Performance comparison of five ML-based classifiers based on the overall accuracy and macro-average F1-score at two test scenarios: (i) test scenario 1 was designated for the unseen data, and (ii) test scenario 2 was intended for the unseen environments. The presented values were based on the average results of 10 experimental trials for each classifier.

evaluations showed that there were no significant differences between the mentioned two F1-scores in the results (see Figure C.11 in Appendix C for more details).

Using the mentioned accuracy and macro-average F1-score as decisive metrics, Figure 5.8 compares the experimental evaluation results of five classifiers in two test environments (test scenario 1 and 2 as previously defined in Section 5.3.3 and 5.5). The presented results in the figure were based on the average of 10 experimental trials for each considered five algorithms. Overall, the evaluation results showed that there were no considerable gaps between the defined two environments namely test scenario 1 and 2 in all classifiers in terms of accuracy and macro F1-score (Figure 5.8). Besides, Figure 5.8 revealed that the trend of the results in both considered metrics (accuracy vs. F1-score) are very similar in both environments (test scenario 1 and 2).

In short, all the classifiers (excepts for the base model NB) provided impressive outcomes in the environment of test scenario 1, in which RF, LightGBM, and MLP achieved more than 93 % in accuracy score and 0.93 in macro F1-score (Figure 5.8). The performance score of SVM was essentially higher than the baseline NB method though it is substantially lower than the scores produced by the rest of the three classifiers.

On the contrary, the performance scores (i.e., accuracy and macro F1-score) of all classifiers were notably degraded in test scenario 2 environments. To be more specific, the resultant mean of MLP classifier was reduced approximately more than 20 % in test scenario 2 compared to test scenario 1. Similarly, the outcome of RF was reduced roughly around 19 % whereas it was circa 18.5 % in LightGBM. Interestingly, the performance of SVM was reduced only circa 7.8 % in test scenario 2 as well as it was found to be the best classifier among the evaluated five models in this specific environment (Figure 5.8). Surprisingly, the results showed that the base model NB classifier was the only model that even improved its performance up to 5.8 percent in test scenario 2 based on both measuring metrics (accuracy and macro F1-score).

The evaluation results pointed out that drawing a conclusion based only on a single test scenario (e.g. using only test scenario 1) could be misleading in some cases. The main reason is that the measured UWB ranges can be affected by a variety of physical impacts in indoor environments [177]. However, it is kind of a common practice in presenting UWB-based classification results as described in Section 5.3.3. In a nutshell, the lowest F1-score was evident with 0.59 in the based model NB classifier at test scenario 1, and the highest score reached 0.95 using LightGBM in all the experiments. In this regard, the experimental results in Figure 5.8 proved that the ML-classifiers, regardless of the type of the models, can effectively identify the non-directly path signal of UWB-based ranging data in multi-class settings. Based on these results, it can be concluded that the ML-based classifiers are very promising and showed a potential to increase the performance of non-direct path signal identification processes in UWB compared to its counterpart traditional approaches explained in Section 5.1.2.

5.5.2 Comparative Analyses based on ROC Curve

One important performance measure for classification problems is the use of ROC-AUC curve, which is applicable in both balanced and imbalanced datasets. The ROC is a 2D plot, in which the True Positive Rate (TPR) is usually utilized on the Y-axis and

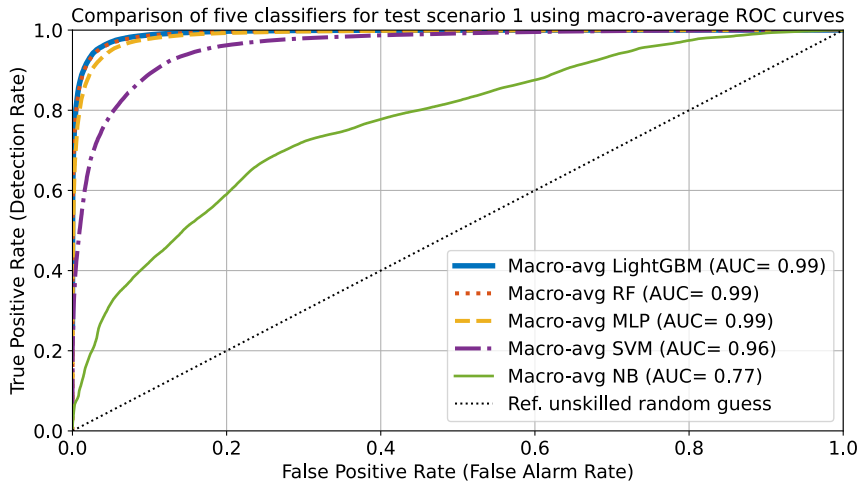


Figure 5.9: Comparison of the evaluated five ML-based classifiers at test-scenario 1 using macro-average ROC curves and their corresponding AUC values.

False Positive Rate (FPR) on the X-axis. The AUC part represents a summary of the model skill, which is convenient to compare multiple models on the same datasets. In this section, ROC curves and their corresponding AUC scores were used to compare the performance of five classifiers for identification of the non-direct path signals in UWB-based ranging system (Figure 5.9 and Figure 5.10). The aim of ROC curve is for analyzing the detection or sensitivity rate of a ML-based predictor while minimizing the false alarm rate as low as possible. As such a good performing model will be drawn with its ROC curve closed to the top left of the graph. In ROC curve, the diagonal line in the middle of the graph represents the baseline unskilled random guess classifier. Thus, the ROC curve of the less powerful model will be closer to that mentioned diagonal line. Similarly, the greater the AUC score in the graph, the better the classifier is.

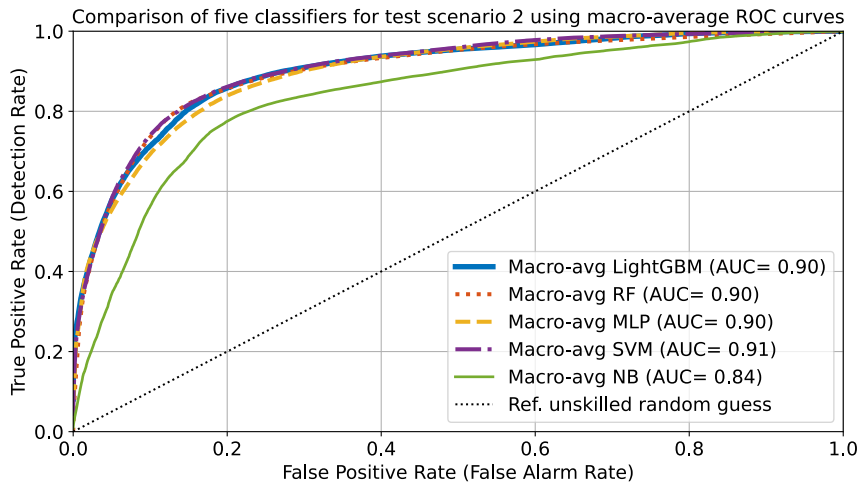


Figure 5.10: Comparison of the evaluated five ML-based classifiers at test-scenario 1 using macro-average ROC curves and their corresponding AUC values.

For the sake of clarity and better visualization, this section compared the ROC curves for five evaluated classifiers based on the macro-average score. For individual models, the detailed ROC curves for each classifier at two test environments (test scenario 1 and 2) were given in Appendix C (i.e. Figure C.4, C.5, C.6, C.7, C.8, and C.9). Regarding test scenario 1 using macro-average ROC curves, Figure 5.9 gave the comparison of five classifiers as well as their respective AUC values. The trend of the outcomes in the experiments was very similar to the results produced by the single value accuracy and F1-score addressed in the previous section. In specific, the LightGBM, RF, and MLP classifiers produced comparable results using ROC curves and the same AUC values of 0.99 within two decimal point precision.

Similar to the result produced by accuracy and macro F1-score, the ROC-AUC showed that all the evaluated models were degraded their performance except for NB classifier in test scenario 2 (Figure 5.10). However, the experimental results revealed that it is hard to distinguish the performance differences among four classifiers excluding the base NB model in ROC curves. Moreover, the AUC values of the mentioned four models were comparable to each other as well (Figure 5.10).

Overall, the ROC-AUC curves reported the same story of results with different metrics compared to the outcomes from accuracy and macro F1-score (Section 5.5.1). However, the value provided by the AUC in ROC curves tends to be larger than the accuracy and macro F1-score. Moreover, the ability to separate the performance differences between a few classifiers were a bit harder using AUC values in ROC curves compared to the accuracy and macro F-1 score (i.e., LightGBM, RF, MLP in Figure 5.9 and 5.10).

5.5.3 Evaluation of the Results Using Confusion Matrix

The considered single score metrics (i.e., accuracy, F1-score, and characteristics in the ROC curve) discussed in the previous sections were, indeed, based on parts of the element from the confusion matrix. The single score metrics are good for evaluating and visualization of the performance differences among ML-based models. However, the details of how the classifier produces the said metrics were usually hidden under the hood and the insightful details of the actual conditions are usually hard to understand in most cases. To examine the mentioned classification results more extensively, the outcomes of the complete confusion matrices were given in this section. For the sake of brevity, two classifiers namely LightGBM and NB (the base model) were chosen as a representative in this section. The detailed classification results for the rest of the classifiers were depicted and can be found in Appendix C.

For confusion matrix discussed in this Section (Figure 5.11 and Figure 5.12) as well as Figure C.2, C.3 and C.1 in Appendix C, the output class in the Y-axis refers to the prediction of the classifier. On the contrary, the target class in the X-axis refers to the true reference class of the classifier. The overall accuracy, as well as the macro average F1-score of the classifier, were provided at the bottom of each confusion matrix as a single score value in order to see the overall results. The correct predictions for each class (LOS, NLOS, and MP) were displayed in the diagonal of the realized confusion matrix. The off-diagonal values in the confusion matrix represented the Type-I error (i.e., False Positive) and Type-II error (i.e., False Negative).

5.5 Experimental Evaluation Results

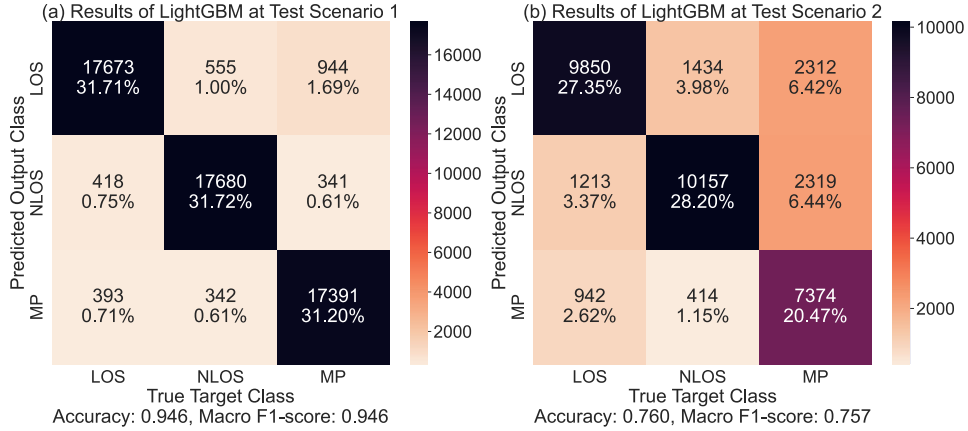


Figure 5.11: Comparison of confusion matrices for LightGBM classifier at two test scenarios: (a) test scenario 1 (i.e., evaluation of the trained model on the unseen datasets), (b) test scenario 2 (i.e., evaluation of the trained model on the unobserved environments).

Concretely, Figure 5.11 depicted the confusion matrices for both test scenario 1 and 2 produced by the LightGBM classifier. In the test scenario 1, LightGBM was able to classify all the realized three classes (LOS, NLOS, and MP) with equal amount of separation (see the diagonal of confusion matrix in Figure 5.11 (a)). The results also showed that both Type I and Type II errors were relatively small (the off-diagonal values in the matrix). In specific, the correct predictions of LightGBM in test scenario 1 were quite high and wellly distributed, i.e., approximately around 31 % for each considered three classes. At the same time, the miss-classification rate was also pretty small, i.e., less than 1.7 % for all the three classes. In fact, the equivalent results and comparable conditions were produced by the RF and MLP classifiers in the test scenario 1 (see the details confusion matrices for the mentioned two classifiers in Appendix C).

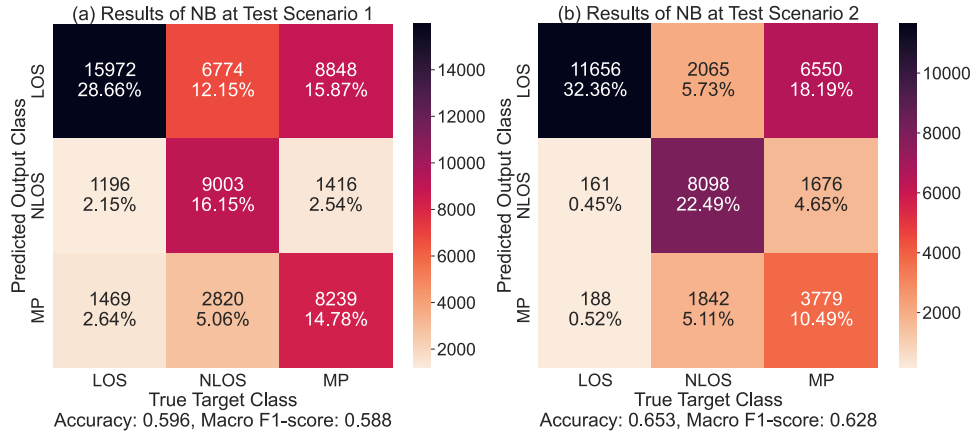


Figure 5.12: Comparison of confusion matrices for NB classifier at two test scenarios: (a) test scenario 1 (i.e., evaluation of the trained model on the unseen datasets), (b) test scenario 2 (i.e., evaluation of the trained model on the unobserved environments).

In contrast, the significant performance degradation was evident in test scenario 2 using LightGBM classifier (see the changes of color palette in the off-diagonal of the confusion matrix in Figure 5.11 (b)) as already observed previously using accuracy and F1-score. The great thing about using the confusion matrix as a decisive metric was that it precisely showed us which class was the core responsible for the decrease in performance. In this specific UWB-based classification problem, the evaluation results clearly showed that the identifiable condition of MP situation was the main cause of the decay in the classifier's overall system performance (Figure 5.11 (b)). Indeed, the correct prediction rate of LOS and NLOS conditions was decreased as well in test scenario 2. However, the mentioned two rates were circa 3 times lower than the MP condition. Again, the similar trends regarding test scenario 2 was observed in the rest of the evaluated classifiers in this chapter namely RF, MLP, and SVM (see Figure C.1 (b), Figure C.2 (b), and Figure C.3 (b) in Appendix C).

It is exciting to realize that all the considered classifiers were capable of correctly predicting the NLOS condition in test scenario 2 with pretty high accuracy (see the image on the right site of Figure 5.11, C.1, C.2, and C.3). Moreover, the false negative rate of the NLOS (i.e., a classifier falsely classifies a NLOS condition as either a LOS or MP) was considerably low in all the experimental results produced by the four classifiers (excluding the base model) in test scenario 2. In UWB ranging system, the false negative rate especially for the NLOS condition is crucial because the highest error in the localization system was due to this specific condition as discussed in Section 5.1.1. On the contrary, the false positive rate of NLOS condition (i.e., a classifier incorrectly classifies either a LOS or MP condition as a NLOS) in UWB localization system is less important compared to false negative rate because the impact on the mitigation technique as a result of this incorrectness is insignificant. For instance, a mitigation technique (Section 5.2) gives less weight to the NLOS condition and the false classification of the LOS as the NLOS in this example doesn't hurt the overall system performance that much. This is because the location algorithm can still rely on other correctly classified data supposing that multiple ranges are available in the system. Conversely, the false negative rate (e.g. classifying the NLOS condition as a LOS) in the above-mentioned example is problematic as the mitigation technique will give more weight to the NLOS condition, which is falsely classified in this case. Consequently, the overall system performance will be directly affected in the mentioned situation.

For reference, the confusion matrix for the two test scenarios regarding the base model NB classifier was also given in Figure 5.12. The confusion matrix showed that the impressive improvement of the classification results in test scenario 2 was due to the ability to correctly identify the LOS and NLOS conditions (Cf. Figure 5.12 (a) and (b)). Akin to the rest of the four classifiers, the results showed that there was a decrease in correctly identifying the MP situation using NB classifier in test scenario 2 as well (Figure 5.12 (b)). Similar results were evident in SVM (Figure C.3 in Appendix C).

5.5.4 Computational Time Comparison

For evaluating the computation cost of the considered five ML-based classifiers, the processing time during training and testing of the ML-model were measured on a test-

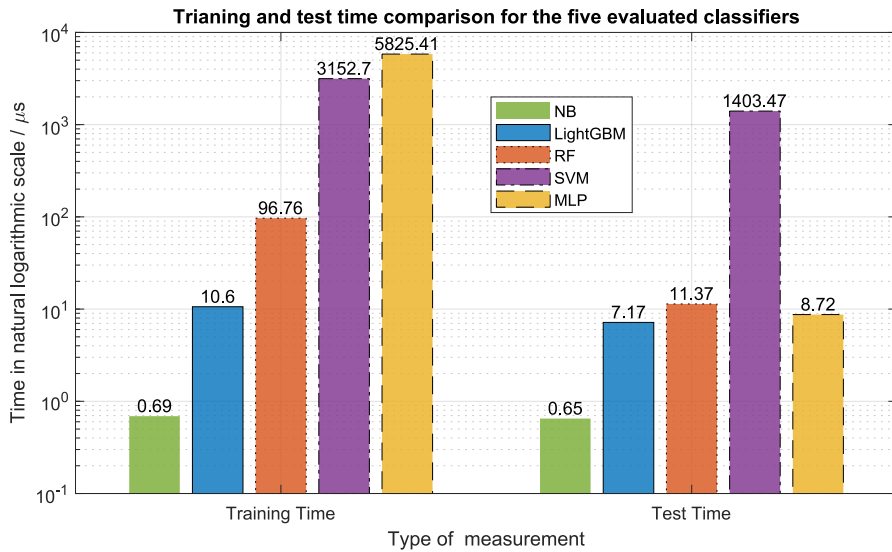


Figure 5.13: Comparison of training and testing time for the five evaluated classifiers. The described numbers in the image refer to the processing time per sample for each ML model. The values were based on the mean of 10 experimental trials using a test-bed machine.

bed machine. The test-bed machine was configured to use a single core CPU for each classifier during the process with the aim of uniformity. Ten experimental trials (i.e., generating 10 ML models in total) using the same datasets were evaluated and the presented results given in Figure 5.13 were based on the mean processing time in microseconds per a single sample for the test-bed machine to accomplish the given task (i.e., training or testing the model using the provided data). Overall, the lower the processing time, the better the performance of the classifier.

For the sake of better visualization, the training time required for the test-bed machine in each classifier was sorted in an ascending order (Figure 5.13). The results showed that NB is extremely fast to train compared to the other four classifiers. It was also evident in the evaluation results that the training time required for the two ensemble-based ML methods (RF and LightGBM) were pretty fast compared to the SVM and MLP (Figure 5.13). Within the two ensemble methods, LightGBM was approximately 10 times faster than the RF under the same level of applied decision trees in the evaluation (i.e. 50 for each ensemble method as described in Section 5.4). The evaluation results revealed that MLP has the worst performance in terms of training time which was followed by the SVM. Both SVM and MLP required the training time in the order of several milliseconds per sample (i.e. circa 3 ms in SVM and 6 ms in MLP). In contrast, the training time per sample in the ensemble methods was in the order of microseconds whereas the same task can be accomplished within a few hundreds of nanoseconds using NB classifier (Figure 5.13).

In terms of the test time, the evaluation results indicated that SVM had the worst performance among the evaluated five classifiers reaching up to 1.4 ms per sample (Figure 5.13). Meanwhile, the average test time per sample required by a test-bed machine

for the rest of the four classifiers was under 12 μ s. Appealingly, the test time required for the MLP was quite low (i.e., 8.72 μ s in the test-bed machine) and its performance was even better than the RF classifier. Overall, the experimental results suggested that the test time for LightGBM, RF, and MLP were comparable to each other, in which LightGBM gave a slightly better performance. Again, the NB appeared to be the fastest among the five classifiers giving the best performance in terms of test time.

In a nutshell, the experimental evaluation results showed that NB classifier is remarkably fast in both training and test time (Figure 5.13). This ability reflects one of the reasons why the NB classifier was quite popular as a baseline model in many ML-based applications. In addition, it was also evident in the previous section that the generalization of the NB model is quite impressive even in test scenario 2. Though the overall performance of NB, in general, was lower than the other ML classifiers. Likewise, the results disclosed that the training and test time required by the test-bed machine for LightGBM classifier was impressively fast (Figure 5.13). Moreover, the LightGBM scored the highest performance in terms of overall accuracy and F1-score in test scenario 1. Notably, the test time of MLP was also quite fast, which again reflect its widely used cases in many ML-related applications [16, 28, 190] even though the training time is the slowest among the evaluated classifiers (Figure 5.13). Interestingly, the evaluation results revealed that the SVM, which showed the best performance in terms of accuracy and F1-score in test scenario 2, was extremely slower than the rest of the classifiers with regard to test time as depicted in Figure 5.13.

5.5.5 Detailed Summary of the Classification Results

In summary, the multi-label classification of the UWB-based ranging data was addressed in this chapter (Section 5.5) and the results were quantified by using single score matrices as well as the complete confusion matrix. In fact, single score metrics are convenient, easy to understand, and truly useful in comparative analyses of different models. How-

Table 5.2: Summary of the results based on the F1-scores and overall accuracy. The presented results were based on the average of 10 individual trials for each classifier.

Scenarios	Classifiers	F1-Scores			Macro avg.	Micro avg.	Accuracy
		LOS	NLOS	MP			
Test Scenario I	NB	0.63	0.60	0.53	0.59 ± 0.0014	0.60 ± 0.0012	59.58 ± 0.12
	SVM	0.85	0.84	0.88	0.86 ± 0.0010	0.86 ± 0.0010	85.69 ± 0.10
	MLP	0.93	0.94	0.93	0.93 ± 0.0020	0.93 ± 0.0020	93.13 ± 0.20
	RF	0.94	0.95	0.94	0.94 ± 0.0009	0.94 ± 0.0009	94.39 ± 0.09
	LightGBM	0.94	0.96	0.94	0.95 ± 0.0006	0.95 ± 0.0006	94.60 ± 0.09
Test Scenario II	NB	0.72	0.74	0.43	0.63 ± 0.0009	0.65 ± 0.0007	65.41 ± 0.07
	SVM	0.79	0.82	0.71	0.78 ± 0.0009	0.78 ± 0.0009	77.81 ± 0.09
	MLP	0.69	0.78	0.70	0.73 ± 0.0127	0.73 ± 0.0119	72.85 ± 1.19
	RF	0.77	0.79	0.68	0.75 ± 0.0021	0.75 ± 0.0021	75.91 ± 0.21
	LightGBM	0.77	0.79	0.71	0.76 ± 0.0037	0.76 ± 0.0039	75.91 ± 0.39

The bold numbers refer to the best performance scores for each class (LOS, NLOS, and MP) and each classifier based on the metrics and scenarios.

ever, the insightful information of the prediction provided by each classifier is usually inaccessible. Concerning this, the confusion matrix revealed the more insightful details of the prediction results provided by a certain classifier.

For reference informational purposes, the detailed summary of single score metrics (i.e., the accuracy and F1-scores) used in this chapter were given in Table 5.2. In addition, the table also included the individual F1-score for the three classes (LOS, NLOS, and MP) defined for UWB ranging data in this chapter. Based on the data given in Table 5.2, it is hard to clarify that the correct perdition of MP condition is generally low in all considered ML models in this chapter. Conversely, the mentioned phenomenon can be disclosed clearly in Section 5.5.3 by using confusion matrix.

5.6 Chapter Discussion and Conclusion

The primary challenge for persistent quality assurance in UWB-based localization system is dealing with the NLOS conditions, i.e. non-direct path signal propagation in UWB-based measurement, because it deteriorates the overall system performance. Therefore, the differentiation between the LOS, and the non-direct path signals is crucial in the enhancement of the location services provided by the UWB system. This chapter addressed the identification of the non-direct path signals in UWB ranging systems as a multi-class problem (i.e., by defining three classes namely LOS, NLOS, and MP). In addition, the mitigation technique for multi-class settings to overcome the error caused by the mentioned non-direct path signals in UWB was also introduced (Section 5.2). The consideration of UWB ranging data as a multi-class problem was opposed to the binary classification approach (i.e., LOS vs. NLOS) commonly practiced in literature.

In general, the main errors during measurement in UWB-based ranging systems are due to the non-direct path signals as stated previously at the beginning of the chapter. Therefore, the identification and mitigation of that error are crucial for UWB localization system. For that specific reason, there are many approaches regarding the identification processes in literature as discussed in Section 5.1.3. In this chapter, ML-based techniques were addressed by defining the identification process as a multi-class problem (i.e., LOS, NLOS, and MP). In the evaluation, five ML-based algorithms (NB, SVM, ML, RF, and LightGBM) were examined as a classifier (Section 5.4). Several quantifying metrics (i.e., accuracy, F1-score, ROC curves, and confusion matrix) were used to evaluate and compare the performance of the mentioned five ML classifiers.

Overall, the experimental results showed that the environments where the measurement was conducted had a strong impact on the quality of all the ML-based classifiers for identification of the non-direct path signals addressed in this chapter. This implied that the notable degradation in all the classifiers' outputs at test scenario 2 in contrast to the test scenario 1 (Section 5.5). Regarding this, one can argue that this phenomenon occurred due to the over-fitting of examined classifiers during the training phase. However, the same behavior was discovered in all the five ML models even when different hyper-parameters were tuned accordingly. Concerning this, more details can be observed in our previous work [177]. Moreover, the mentioned phenomenon occurred due to parts of the generalization problem caused by the incapability of adequate data

that fully represented the conditions defined in the three classes. As a consequence, the trained model performed relatively well using the data from the same environment (i.e., test scenario 1) dropped its performance drastically when fed with the data gathered from different environments (i.e., test scenario 2). As a matter of fact, judging the performance of ML models based on test scenario 1 (i.e., unseen data gathered from the same environments as training) is the typical practice in reporting the results of UWB related data in literature [16, 118, 208]. In this chapter, the elaboration was further made by examining the results in test scenario 2 (i.e., evaluating the trained ML-models on the unseen environments).

Moreover, it is worth mentioning that collecting the UWB-related data for the defined three classes (LOS, NLOS, MP) in this chapter was not straightforward, time-consuming, and complex because of the very nature of wireless signal propagation. This implied that the measured UWB signal could be affected differently by the environment where the measurement was conducted due to the conditions and types of materials, walls, furniture, etc. The main attempt in this chapter was to examine the feasibility of the ML approaches on the identification of the non-direct path signals as a multi-class problem, which is basically in contrast to the conventional methods and techniques described in Section 5.1.3. Based on the experimental evaluation results using single score metrics (Section 5.5.1), it can be concluded with high confidence that the ML approaches to identification of non-direct path signals in UWB ranging system are very promising, and the outcomes achieved in the evaluations were also quite satisfying. In brief, the experimental results showed that even the simplest ML classifier namely NB was capable of producing more than 59 % in terms of overall accuracy, which is, indeed, the worst case scenario observed in the experiments. On the contrary, the best case scenario showed up to 94.6 % during the experimental evaluation (Section 5.5.1).

In addition, the evaluation results showed that both the macro average F1-score and micro average F1-score had comparable outcomes based on the balanced UWB ranging datasets examined in the chapter. Interestingly, the mentioned F1-scores were more or less identical in values produced by the overall accuracy score in both test scenario 1 and 2. Moreover, the comparative analysis of the outcomes produced by each classifier was evaluated in Section 5.5.2 using ROC curves and the evaluation results were consistent as given by the single value metrics. Generally speaking, the AUC valued produced by the ROC curves are typically higher than the single value metrics (accuracy and F1-score). However, the trend of the results (i.e. which classifier performs best or worst in certain test conditions) observed in ROC curves remained pretty much the same as the single score values (i.e., accuracy and F1-score).

In general, the single score metrics discussed in the previous paragraph are particularly useful for a comparative analysis for benchmarking multiple classifiers. However, the insightful details regarding the performance and contribution of the individual class in the classifier are not accessible by single score metrics. In order to examine the states of each unique class of a classifier, a complex confusion matrix was utilized in the chapter (Section 5.5.3). The evaluation results using the confusion matrix showed that the prediction score of MP condition was notably dropped in all the five classifiers in the test scenario 2 (i.e., evaluating the generalization of ML model at unseen environments). In other words, the results indicated that the identification process of MP

condition-related class in UWB was challenging and harder to detect compared to the other two classes (LOS and NLOS). The said phenomenon cannot clearly be pinpointed using single score metrics and using macro/micro average ROC curves.

Moreover, it can be concluded from the observations based on the confusion matrices (Section 5.5.3) that the prediction rate of the class regarding NLOS condition was quite high in all the evaluated five classifiers. Meanwhile, the results expressed that the false negative rate of the NLOS condition (i.e., predicting NLOS as either a LOS or MP) was relatively low. This fact is crucial because the highest errors in UWB localization were generally rooted from this specific NLOS condition as mentioned several times in the chapter. Conversely, falsely identifying the LOS condition as a NLOS typically doesn't hurt, in general, the overall system performance of UWB localization system. This is because a mitigation algorithm simply provides less weight to the falsely identified NLOS conditions. Accordingly, the positioning algorithm in UWB localization will still provide reliable location data by using other correctly classified ranging data.

Aside from the quantifying metrics and scores used in classification problems, the computation time (i.e., training and test times) required by each evaluated ML model was also examined in this chapter. Surprisingly, the computational time taken by the ML classifiers were generally overlooked and ignored completely in many comparative reports in the literature. Undeniably, the test time necessary by a certain classifier plays a crucial role in many applications in practice. For instance, the experimental evaluation results showed that SVM took the longest test time (i.e. the poorest performance) among the five models. However, SVM can be highlighted as the best performing classifiers in terms of the single scores metrics at test scenario 2 (Section 5.5.1). The two contrasting metrics (i.e., computational time vs. performance-based measures such as accuracy, F-score, etc.) showed the choice of the method based on one metric could have a negative impact on the other measures. This phenomenon could be an important factor in prioritizing the system implementation process in some applications.

In this chapter, the identification of the non-direct path signals for UWB ranging data was conducted using five classical ML algorithms, and the results related to the Deep Learning (DL) approaches were excluded. Indeed, the preliminary evaluation of DL-based models, namely the deep transfer learning method and one-dimensional CNN approach, were examined based on our open source data given in [176]. The preliminary results suggested that the DL methods were not feasible on the mentioned data for two reasons. Firstly, the provided datasets were not a time-series data type as the random shuffling was made during the preprocessing process. Therefore, pseudo-images were necessary to create from the feature columns of the UWB data in order to be usable as input images in the DL model. The preliminary results based on pseudo-images as inputs using transfer learning methods showed that the outcomes were sufficiently high in terms of overall accuracy in test scenario 1. However, the score was drastically dropped at the level which was even worse than the baseline NB model in test scenario 2. The improvement was hardly conceivable even if different hyper-parameters tuning were made. One core reason could be the generation of pseudo-images that are very similar to each other. As a result, the over-fitting of the training data was likely to occur. Secondly, the evaluation outcomes based on the one-directional approaches seemed encouraging compared to the transfer learning approach. However, a substan-

tial dropped in the overall accuracy was observed again similar to the pseudo-image based transfer learning approach. Therefore, the evaluation results suggested that new datasets specifically structured during the measurement campaign for DL models should be separately gathered for UWB ranging data (for instance, by extracting the whole CIR related data from the UWB hardware as investigated in [153]). It should be noted that extracting the whole data intended to be used only for signal diagnostic purposes could have a strong impact on the performance of the UWB hardware itself in terms of processing time, efficiency, the latency on prediction rate, etc.

In conclusion, it was evident in the experimental evaluation results based on several metrics that ML-based classifiers are very promising for the identification of non-direct path signals in UWB ranging data under the multi-class settings (i.e., LOS, NLOS, and MP). In specific, the evaluation results showed that more than 59.6 % in terms of overall accuracy were observed in the worst-case scenario (i.e., using one of the simplest and fastest ML models namely NB), whereas it reached up to 94.6 % in the best case scenario. The given number can also be verified using another single score metric namely macro-/micro- average F1-score as well as the ROC-AUC curves. Among the five evaluated ML-based classifiers, LightGBM was very efficient in terms of both the metrics typically used in classification problem (accuracy, F1-score, ROC, etc.) as well as the computational time. Nevertheless, the evaluation results revealed that LightGBM cannot outperform SVM in test scenario 2 in terms of single score metrics. This concludes that claiming one specific classifier as the best one was unreasonable without stating the quantifying metrics. Furthermore, it was interesting to see that the computational time (both training and test time) occupied by the NB classified is pretty short compared to the rest of the classifiers. Besides, the generalization of NB classifier was really good as well even though its performance scores were generally lower than the others. Likewise, the experimental results based on the confusion matrix and individual ROC curves suggested that the most challenging class (i.e., out of the three defined classes) to correctly identify in UWB ranging system is the MP condition. Another fact brought by the results from the confusion matrix was that the prediction rate of the class regarding NLOS condition was competently high in all the evaluated ML models at both test scenario 1 and 2 respectively.

For future work, the above-mentioned DL approach for UWB ranging data is, indeed, worth exploring. Moreover, the severity of the completely blocked NLOS scenario can be defined into further classes based on the materials the UWB signal has to be penetrated as conducted in the preliminary experimental setup in [16]. Supposing two completely blocked NLOS were defined as soft-NLOS and hard-NLOS based upon the materials or scenario, the multi-class process to identify would be in four classes (namely LOS, MP, soft-NLOS, and hard-NLOS). Surely, the data collection process for the mentioned four classes would be more complex as different materials possessed unique refractive indexes. In addition, the experimental results discussed in this chapter were based on the evaluation of the ML performed on a PC. A lot of application areas in UWB localization systems are nowadays on the edge devices. Therefore, the evaluation of the considered multi-class identification process directly on the edge device such as MCU would be worthwhile and of great value as well.

6 Conclusion and Outlook

In this dissertation, a bidirectional scheme of UWB-based localization system was specifically addressed, which is generally overlooked in the literature. The central characteristic of the bidirectional UWB localization scheme is that it has the ability to act as both navigation and tracking perspectives within a single localization scheme. Conventionally, the navigation and tracking scenarios of wireless localization systems were viewed as different perspectives because distinct methodologies were generally needed in the implementation process. The ability to possess two unique positioning perspectives (i.e., navigation and tracking) in a single system is indeed a paradigm shift in location-based services. The reason is that it opens up several application areas in diversified indoor environments. This dissertation pinpointed the potentials of the bidirectional UWB localization system by comparing its counterparts two widely studied unidirectional systems. Moreover, there are no well-documented books or research articles regarding the bidirectional UWB localization system. This dissertation attempts to serve as a compliment to the mentioned gaps in the literature.

Regarding this, the implementation process of the bidirectional UWB localization system was divided into several sectors (i.e., ranging, positioning, filtering, error identification and mitigation parts, etc.). Then, the comparative analyses of the applicable methodologies in each sector were examined with rigorous evaluations in order to clarify the practitioners in the fields with insightful knowledge as well as to provide the recommended methodologies in each sector. From this perspective, each sectional part of a bidirectional UWB localization system was addressed with dedicated chapters in this thesis. The findings, conclusion, and summary of each chapter addressed in the dissertation were presented in the following.

In Chapter 2, the state-of-the-art localization technologies for IPS were shortly explained and the role of UWB technology for the use-case of GNSS-deprived environments was spotlighted. Subsequently, the core features of UWB technology required for the implementation process of indoor localization system was described (Chapter 2.2). It was particularly focused on the basic understanding of the UWB technology regarding the general regulations of UWB in different countries, typical modulation schemes applicable in UWB, and the main standardization bodies that drive the current success of UWB technology into the commercial market and academic research areas. Specifically, the data communication flow in PHY and MAC of the IEEE 802.15.4 standard, i.e. the basic frame format for currently all available UWB-related standards, was also concisely explained. Afterwards, the three types of UWB-based topology were compared and the potentials of a bidirectional scheme was highlighted (Chapter 2.3). Accordingly, the implementation process of a bidirectional UWB localization system was briefly described (Chapter 2.4). It was followed by the block diagram expression of the bidirectional UWB localization system addressed in this dissertation.

Regarding the ranging sector of a bidirectional UWB localization system (Chapter 3), TEEM model proposed in our previous work [130, 172] for TWR methods was examined in order to demonstrate the misconception (i.e. the use of SDS-TWR as a de facto standard for quantifying the performance of other TWR [13, 114, 122, 127, 148, 149]) widely practiced in literature. In this regard, the experimental results produced by the analytical formulation (Chapter 3.2) as well as the numerical simulation and experimental evaluations (Chapter 3.4) using TEEM model showed that the pitfalls or systematic flaws of the SDS-TWR in this dissertation. On the contrary, the evaluation results suggested that there existed a better TWR technique, namely AltDS-TWR, to be used for quantifying different TWRs than the commonly used SDS-TWR. In total, four basic TWR schemes were rigorously evaluated at different conditions (ideal, symmetric and asymmetric cases) using TEEM model. The evaluation results revealed that all the four TWR methods gave the exact same performance in the ideal case. It was also evident in the results that AltDS-TWR and SDS-TWR were on the same performance level in the symmetric case. Interestingly, the results indicated that AltDS-TWR is the only robust method among the four evaluated TWRs in the asymmetric case. Generally speaking, the symmetric case is a very special condition, in which it is assumed that the two reply times used in the calculation of the range between two transceivers are exactly equal (see more details in Chapter 3.3.1). In practice, this assumption does not hold and the typical scenario in UWB-based ranging condition is the asymmetric case. Therefore, it can be concluded based on the evaluation results that AltDS-TWR is the most robust TWR among the four in all tested conditions, and the recommended method for quantifying different TWR instead of the commonly used SDS-TWR.

Chapter 4 corresponded to the sectional evaluations of position estimation process in bidirectional UWB localization system in this dissertation. Fundamentally, location estimation algorithms are the backbone of any localization system. Accordingly, five location estimation algorithms commonly used in wireless localization systems including UWB were rigorously bench-marked in this dissertation. Specifically, the implementation of all five algorithms was built upon the Bayesian framework in order to meet the pragmatic system integration procedure in the field. The detailed expression regarding the implementation of the Bayesian framework for UWB-based localization (Chapter 4.3) was regarded as an important aspect of this dissertation because the literature generally overlooked it. Regarding this, two motion models namely CV and CA were comprehensively explored for the UWB based localization system and the evaluation results showed that the performance of both models was rather comparable in terms of RMSE and computational time. Besides, the evaluation results revealed that TS method is able to produce the performance score very close to the EKF and UKF meanwhile the computational time was relatively low compared to them. Therefore, it can be concluded that TS algorithm was the most efficient method among the five examined algorithms in terms of the computational time and RMSE scores. In terms of accuracy by using RMSE as a decisive score, the experimental results proved that the linear location estimation algorithms (Trilateration and Multilateration) produced superior performance scores in static and small-scale LOS scenario compared to the nonlinear positioning methods (section 4.4.2 and 4.4.3). In contrast, the nonlinear positioning methods showed better resistance to abrupt changes of signal due to unintentional

measurement errors or alike. Moreover, the three nonlinear methods appeared to be significantly superior performance in terms of RMSE than their counterpart linear algorithms at NLOS scenario.

Chapter 5 addressed the sectional evaluations of bidirectional UWB system regarding the identification and mitigation process of non-direct path signals. Concerning the error mitigation part of the system, a novel mitigation technique under the multi-class settings for UWB has been proposed (Chapter 5.2). Likewise, the identification of the non-direct path signals in UWB ranging systems was considered as a multi-class problem, which was opposed to the binary approach ordinarily studied in the literature. In addition, the feasibility of the ML-based techniques for the identification process of non-direct path signals under the multi-class settings in UWB were particularly explored. In total, five ML-based classifiers (NB, SVM, ML, RF, and LightGBM) were studied in this dissertation. The experimental results based on several metrics showed that the use of ML techniques for identification of non-direct path signals in UWB was quite promising under the multi-class settings (i.e., LOS, NLOS, and MP). To be more specific, the worst-case scenario was evident in the results with more than 59 % accuracy using NB, i.e., one of the simplest ML classifiers. By contrast, the best case scenario using LightGBM algorithm reached up to 94.6 % in terms of overall accuracy score. The experimental results also indicated that the test data gathered in environments different from the training process produced significant performance degradation in all the evaluated models. This showed that it is crucial to be tested the trained ML model with data from different environments before deployment in production. Moreover, the results revealed that the identification process of MP condition in UWB was more challenging and harder to detect than the other two classes (LOS and NLOS). Furthermore, the results also uncovered that the prediction rate of the NLOS class was effectively high in all the evaluated ML models in all test scenarios. This fact is crucial because the highest errors in UWB localization system were generally rooted from this specific NLOS condition. In terms of test time, the results signified that SVM took notably the longest time (i.e. the poorest performance) among the five models. The rest of the four classifiers gave comparable test times. Arguably, SVM performed the best in terms of the single scores metrics in test scenario 2, which was circa 2 % better than LightGBM.

As a future perspective, UWB technology can be seen as the most prominent and viable solutions providers for indoor environments compared to the other existing technologies (c.f., Chapter 2.1.2). Moreover, the recent incorporation of the UWB chip into smartphones pioneered by Apple and followed by other vendors will definitely boost the rise of UWB technology in diverse application areas in the near future. To date, many companies from different industries are in the progress of integrating the UWB technology into their products [35]. However, one of the main stumbling blocks in the widespread adaptation of UWB technology for IPS is the regulations defined in different countries. At the current state, the frequency between 7.25 GHz and 8.5 GHz is the only common permissible band for UWB with maximum EIRP across the world (see more details about the frequency band in Figure 2.4). Therefore, one of the main challenges is the necessity to find a common ground for the technology across all regulatory bodies around the world, which is very demanding and tough at the same time.

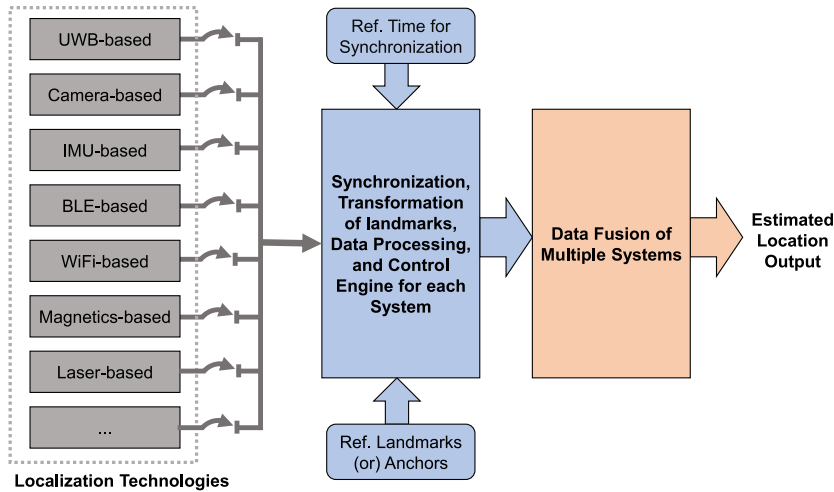


Figure 6.1: Block diagram representation of the future perspective regarding the versatile IPS for GNSS-denied indoor environments.

Regarding the generalized IPS as a whole, the author's perspective is that no single technology meets or will meet the needs of all use cases in indoor environments. In other words, there will not be one technology that is versatile or general enough to be used as a de facto standard for IPS similar to GNSS-based system in outdoor environments. In contrast, such a generic IPS for GNSS-deprived indoor environments will emerge from the combination of multiple localization systems. Toward this concept, Omlox open standard structure (<https://omlox.com/home>), which uses the concept of middle-ware Hub, was introduced by PROFIBUS and backed by many leading companies in the field [105]. However, the current structure of omlox is simply providing the ability to store and extract the demanded location data from multiple technologies using user or application interfaces. To accomplish this, the mentioned middle-ware hub, possibly based on the MQTT framework (<https://mqtt.org/>) or similar messaging protocols, is responsible for storing and extracting the location data. There is no fusion of location data achieved from different IPS-based technologies in omlox framework.

The more versatile IPS to the perspective of the author is illustrated in Figure 6.1. The figure depicts the block diagram of a versatile IPS that has the ability to combine multiple IPS-based technologies under the same umbrella (Figure 6.1). The core idea is to map the location data achieved from multiple positioning technologies within the same environments into a unified framework, in which the time for each technology is synchronized and the reference landmarks are matched. Then, the system-wide data fusion will be performed in the next step in order to produce the most accurate location data based on all available technologies. One starting point regarding the implementation of the author's proposed approach as the future perspective of IPS (Figure 6.1) could be the use of Robot Operating System (ROS) (<https://www.ros.org/>). This is because the time synchronization of different technologies can be accomplished based on the arrival time of location data at the ROS core as well as the coordinate transformation available in ROS could be used as landmarks matching problem.

List of Abbreviations

2D	two-dimensional
3D	three-dimensional
5G	Fifth Generation
6G	Sixth Generation
AAS	Active Anchor System
Adam	Adaptive Moment Estimation
ADS-TWR	Assymmetric Double-Sided Two-Way Ranging
AltDS	Alternative Double-Sided
AltDS-TWR	Alternative Double Sided Two-Way Ranging
ANN	Artificial Neural Network
AoA	Angle-of-Arrival
ATS	Active Tag System
AUC	Area Under Curve
BAATS	Bidirection Active Anchor-Tag System
BDT	Boosted Decision Tree
BLE	Bluetooth Low Energy
BPSK	Binary Phase Shift Keying
CA	Constant Acceleration
CDF	Cumulative Distribution Function
CIR	Channel Impulse Response
CITEC	Center for Cognitive Interaction Technology
CNN	Convolutional Neural Network
CRC	Cyclic Redundancy Check
CSI	Channel State Information
CV	Constant Velocity
D-TWR	Double Two-Way Ranging
DL	Deep Learning
DR	Dead Reckoning
DS-TWR	Double-Sided Two-Way Ranging
EIRP	Effective Isotropic Radiated Power
EKF	Extended Kalman Filter
ETSI	European Telecommunications Standards Institute
EU	European Union
FCC	Federal Communications Commission
FCS	Frame Checking Sequence
FoV	Field of View

FP	First-Path
FPR	False Positive Rate
GBDT	Gradient Boosting Decision Tree
GNSS	Global Navigation Satellite System
GP	Gaussian Process
GPS	Global Positioning System
GRV	Gaussian Random Variable
HSI	High Speed Internal
IEEE	Institute of Electrical and Electronics Engineers
IMU	Inertial Measurement Unit
IPS	Indoor Positioning System
IR	Infra-red
IR-UWB	Impulse Radio Ultra-Wideband
KF	Kaman Filter
KNN	K-Nearest Neighbor
LED	Light-Emitting Diode
LightGBM	Light Gradient Boosting Machine
LOS	Line-of-Sight
MAC	Medium Access Control
MCU	Microcontroller Unit
ML	Machine Learning
MLP	Multi-layer Perceptron
MP	Multi-path
NB	Narrow-band
NLOS	Non-Line-of-Sight
OFDM	Orthogonal Frequency Division Multiplexing
OOK	On-Off Keying
OSI model	Open Systems Interconnection model
PAM	Pulse Amplitude Modulation
PAN	Personal Area Network
PATD	Preamble Accumulation Time Delay
PC	Personal Computer
PCB	Printed Circuit Board
PDR	Padestrian Dead Reckoning
PDS-TWR	Parallel Double-Sided Two-Way Ranging
PF	Particle Filter

PHY	Physical Layer
PPM	Pulse Position Modulation
PRF	Pulse Repetition Frequency
PSD	Power Spectrum Density
PTD	Propagation Time Delay
PV	Position-Velocity
RBF	Radial Basis Function
RC	Resistor-Capacitor
ReLU	Rectified Linear Unit
RF	Random Forest
RFID	Radio-frequency identification
RMSE	Root Mean Square Error
ROC	Receiver Operating Characteristic
ROS	Robot Operating System
RSS	Received Signal Strength
RTD	Receiving Time Delay
RTLS	Real-time locating system
RToA	Round-trip Time of Arrival
SDS	Symmetric Doubled-Sided
SDS-TWR	Symmetric Double-Sided Two-Way Ranging
SFD	Start of Frame Delimiter
SLAM	Simultaneous Localization and Mapping
SMC	Sequential Monte Carlo
SNR	Signal-to-Noise Ratio
SS	Single-Sided
SS-TWR	Single-Sided Two-Way Ranging
SVM	Support Vector Machine
TDMA	Time Division Multiple Access
TDoA	Time Difference of Arrival
TEEM	Time-of-flight Error Estimation Model
ToA	Time-of-Arrival
TOF	Time-Of-Flight
TPR	True Positive Rate
TS	Taylor Series
TTD	Transmission Time Delay
TWR	Two-Way Ranging
UAV	Unmanned Arial Vehicle
UKF	Unscented Kalman Filter
USART	Universal Synchronous/Asynchronous Receiver/-Transmitter
UT	Unscented Transform

List of Abbreviations

UWB	Ultra-Wideband
VLC	Visible light communication
WLAN	Wireless Local Area Network
WoS	Web of Science
WPAN	Wireless Personal Area Network
WSN	Wireless Sensor Network

List of Figures

2.1	Block diagram regarding the overview of the signal measurement and positioning techniques in Indoor Positioning System (IPS). The image was inspired by the work in [222] and it was modified from it.	7
2.2	Illustration of the trend of technologies in academic publications: (a) comparison of Ultra-Wideband (UWB), WiFi, and Bluetooth Low Energy (BLE) in academic publications during the last decade based on the Web of Science (WoS) database, (b) UWB technology in academic publications from 2000 to 2020.	12
2.3	Spider chart comparison for four radio frequency-based positioning technologies in terms of eight core features. The information score represented with 1 (worst) to 5 (best) on the image are based on the typical reported data in survey papers and data-sheets of the vendors.	13
2.4	Illustration of UWB spectrum mask regulation in US, EU, Japan, and China. The representation style of four regulatory bodies on an image was inspired by the work in [230].	14
2.5	Power Spectrum density of UWB vs. Narrow-band (NB) signals in frequency domain [30, 50]. UWB is defined as absolute bandwidth $BW \geq 500$ MHz or fractional bandwidth $B_f > 0.2$. The representation of the image was inspired by the one depicted in [164].	16
2.6	Demonstration of four typical modulation techniques used in UWB system. The UWB pulse shape used in the Figure is based on the Gaussian doublet waveform.	18
2.7	Overview of the PHY and MAC layers frame structure in IEEE 802.15.4 standard specifically defined for wireless personal area networks including UWB technology [45, 97].	21
2.8	Illustration of visual comparison among the three topologies for UWB-based system integration namely the AAS, ATS, and BAATS.	25
2.9	Illustration of the coverage areas comparison for the Time Difference of Arrival (TDoA)- vs. Time-of-Arrival (ToA)-based UWB localization systems for accurate positioning under the same anchors' setup.	29
2.10	Block diagram representation of a bidirectional UWB-based localization system	30
2.11	Illustration of two-way ranging method usable for both distance measurement phase in Bidirection Active Anchor-Tag System (BAATS) as well as node synchronization process in TDMA scheme (shaded area). The image was reproduced with minor changes from [175] (©2019 IEEE. Reprinted, with permission.).	31
2.12	Demonstration of location estimation procedure in UWB-based localization system by using measured ranges between anchors and tags in two-dimensional (2D) space.	33
2.13	Highlight of the addressed thematic aspect in this dissertation.	36
3.1	Description of the sectional focus in the chapter which is the ranging phase	37

3.2 Illustration of measuring a signal's Time-Of-Flight (TOF) in wireless communications.	39
3.3 Illustration of single- and double-sided Two-Way Ranging (TWR) methods. The image was reproduced with slight modification from [175] (©2019 IEEE. Reprinted, with permission.).	41
3.4 Illustration of the asymmetric double-sided TWR method.	43
3.5 TOF error comparison using a Type I assumption (ideal case) as in Equation (3.24) and (3.25) (©2018 IEEE. Reprinted, with permission). .	57
3.6 Comparison of TOF errors in Type II, (i.e., special case) assumption based on Equations (3.26)–(3.29). (a) TOF error vs. delay (ξ) for four TWRs; and (b) TOF error only for Symmetric Double-Sided Two-Way Ranging (SDS-TWR) and Alternative Double Sided Two-Way Ranging (AltDS-TWR). .	57
3.7 3D representation of TOF error comparison for Single-Sided Two-Way Ranging (SS-TWR) and SDS-TWR using 65 sample point of parameters defined in Table 3.2.	58
3.8 TOF error comparison between TWR methods using Type III assumption (typical case) as in Equations (3.30)–(3.33). (a) TOF error when $t_{replyA} > t_{replyB}$, (b) TOF error when $t_{replyA} < t_{replyB}$, (c) TOF error when $t_{replyA} = 1640\mu s$ and $t_{replyB} = 400\mu s$, and (d) TOF error for AltDS-TWR method in (a)–(c).	59
3.9 Test environments of the experimental evaluations: (a) overview of office floor plan for the LOS experiment in hall (green arrow) and the multi-path experiment in a corridor (sky-blue arrow), (b) fixed-distance experiment in the laboratory, LOS experiment in a hall (office environment), and multi-path experiment in a corridor (office environment). .	61
3.10 Sample measured data for the symmetry in the special case (Type II) .	62
3.11 Sample measured data for the asymmetry in the typical case (Type III) .	63
3.12 Evaluation results of three TWRs for the special case (Type II) using box plots and empirical Cumulative Distribution Function (CDF) measured at a static distance of 5.494 m	65
3.13 Variable reply times at fixed distance measurement.	66
3.14 Variable reply times at fixed distance measurement.	67
3.15 Illustration of ranging errors due to Non-Line-of-Sight (NLOS) propagation in UWB for Types II and III at 2 m ground truth when a human subject is blocking.	70
3.16 Root Mean Square Error (RMSE) comparison of Types II and III for three TWRs in Line-of-Sight (LOS) and Multi-path (MP) scenarios . . .	71
3.17 Comparison of the LOS and MP scenarios for Type II and Type III at a 12 m true reference. The images in a row represent the two types (II and III) and the images in columns represent the LOS and MP . . .	72
3.18 RMSE comparison of Types II and III for three TWRs in a close LOS scenario.	73
3.19 Results comparison of Types II and III for close LOS at true reference 0.25, 1.00, and 1.50 m. (a–c) measurement results for Type II (special case), and (d–f) corresponding results for Type III (typical case). . .	74

4.1	Illustration of the sectional focus for the bidirectional UWB system in this chapter, which includes the implementation of different positioning algorithms and filtering aspects.	79
4.2	Overview of the implementation process for the evaluated five true-range positioning algorithms. The methods are categorized as linear systems (light green), non-linear systems based on linearization methods (light red), and non-linear systems based on statistical techniques (light orange). The motion model (blue) corresponds to the implementation requirements for Bayesian-based filters (Section 4.3). The image is a modified version from our previous work in [171].	85
4.3	Illustration of Trilateration algorithms for positioning use-case in 2D. The image was reproduced with slight modification from [171] (©2019 IEEE. Reprinted, with permission.).	86
4.4	Illustration of positioning algorithms based on true-range Multilateration in 2D. The image was reproduced with minor changes from [175] (©2019 IEEE. Reprinted with permission).	88
4.5	Illustration of Kalman Filter operation. P_k^- and P_k are the priori and posteriori estimate of error covariance matrices, and K_k is the $n \times m$ matrix Kalman gain. The representation of the concept depicted in the image was inspired by the work in [17].	92
4.6	Illustration of Extended Kalman Filter Operation. The representation of the concept depicted in the image was inspired by the work in [17].	93
4.7	Conceptual illustration of the EKF (upper row) and the UKF (lower row) regarding the approximation over the nonlinear functions. The blue circles represent the actual transformation. The image was inspired by the work in [206] and it was modified from it.	95
4.8	Highlight of the motion model commonly used in all position estimation algorithms	97
4.9	High-level overview of standard KF implementation for continuous tracking mechanism in UWB-based localization. The input of the Kaman Filter (KF) filter is location data.	103
4.10	High level overview of nonlinear Bayesian-based filters (Extended Kalman Filter (EKF) and Unscented Kalman Filter (UKF)) implementation for UWB-based localization. The input of the filter is a ranging data as opposed to the location data in standard KF.	105
4.11	Set-up for the experimental evaluations conducted at the laboratory environment in CITrack [119] and University's indoor sport hall arena.	108
4.12	Performance comparison of five position estimation algorithms for the static scenario at CITrack, in which CA is used as a motion model for the state.	110
4.13	Performance comparison of five position estimation algorithms for tracking the movement of a mobile tag in the CITrack using CA as the motion model for the state.	111

4.14 Performance comparison of five algorithms for tracking a moving UWB tag in a large-scale scenario (an indoor sports arena) at LOS. CA was used as the motion model.	112
4.15 Comparison of five location estimation algorithms at a NLOS scenario in university's indoor sports hall (20x20 m arena). Constant Acceleration (CA) was utilized as the dynamic motion model.	113
4.16 Evaluation of NLOS condition at two anchor settings and trajectory paths: (a) allocation of the four anchors at 20x40 m , (b) allocation of the four anchors at 20x20 m.	114
4.17 RMSE comparison for the evaluated five algorithms at four different scenarios	115
4.18 Computational time comparison of the evaluated five location estimation algorithms using Constant Velocity (CV) and CA motion models. The presented time referred to the mean time required for a test-bed machine to compute a location by each algorithm in microseconds.	116
5.1 Illustration of the sectional focus addressed in this chapter, which is the identification and mitigation of ranging errors due to NLOS conditions in UWB localization systems.	121
5.2 Illustration of LOS, NLOS and MP scenarios in a UWB-based ranging system. The image was a slightly decorated version from our previous work in [177].	123
5.3 Comparison of the sample measured distance errors in the three conditions (LOS, NLOS, and MP) at static scenarios for motivational purposes.	124
5.4 Illustration of the LOS, NLOS, and MP conditions in UWB ranging systems: (a–c) Comparison of the First-Path (FP) power, and the Channel Impulse Response (CIR) power in three scenarios: (a) LOS, (b) NLOS, (c) MP conditions, and (d) the difference between the two power levels (FP and CIR powers) from (a) to (c). The measurement was conducted for the three scenarios at random movement between 1 m and 24 m distances in indoor environments.	127
5.5 Comparison of the mitigated vs. unmitigated location outputs from Multilateration method at NLOS condition.	130
5.6 Block diagram of the implementation process regarding the mitigation technique given in this chapter for UWB localization.	133
5.7 Illustration of the scenarios where training and test data were collected for evaluation: (a) A sketch of the building where the experimental data for training and test were collected. (b) Training data were collected for LOS, NLOS (including human blocking) and MP conditions in a laboratory, a large hall, and a corridor (blue color in (a)). (c) Similar to (b), test data were collected in a different room (including different types of furniture and NLOS human blocking) and a different corridor (red in (a)).	135

5.8 Performance comparison of five Machine Learning (ML)-based classifiers based on the overall accuracy and macro-average F1-score at two test scenarios: (i) test scenario 1 was designated for the unseen data, and (ii) test scenario 2 was intended for the unseen environments. The presented values were based on the average results of 10 experimental trials for each classifier.	143
5.9 Comparison of the evaluated five ML-based classifiers at test-scenario 1 using macro-average ROC curves and their corresponding AUC values.	145
5.10 Comparison of the evaluated five ML-based classifiers at test-scenario 1 using macro-average ROC curves and their corresponding AUC values.	145
5.11 Comparison of confusion matrices for Light Gradient Boosting Machine (LightGBM) classifier at two test scenarios: (a) test scenario 1 (i.e., evaluation of the trained model on the unseen datasets), (b) test scenario 2 (i.e., evaluation of the trained model on the unobserved environments).	147
5.12 Comparison of confusion matrices for NB classifier at two test scenarios: (a) test scenario 1 (i.e., evaluation of the trained model on the unseen datasets), (b) test scenario 2 (i.e., evaluation of the trained model on the unobserved environments).	147
5.13 Comparison of training and testing time for the five evaluated classifiers. The described numbers in the image refer to the processing time per sample for each ML model. The values were based on the mean of 10 experimental trials using a test-bed machine.	149
6.1 Block diagram representation of the future perspective regarding the versatile IPS for Global Navigation Satellite System (GNSS)-denied indoor environments.	158
C.1 Comparison of confusion matrices for Multi-layer Perceptron (MLP) classifier at two test scenarios.	194
C.2 Comparison of confusion matrices for Random Forest (RF) classifier at two test scenarios.	194
C.3 Comparison of confusion matrices for Support Vector Machine (SVM) classifier at two test scenarios.	194
C.4 Multi-class results for LightGBM at test scenario 1 based on individual Receiver Operating Characteristic (ROC) curves.	195
C.5 Multi-class results for LightGBM at test scenario 2 based on individual ROC curves.	195
C.6 Multi-class results for NB at test scenario 2 on individual ROC curves.	195
C.7 Multi-class results for SVM at test scenario 2 on individual ROC curves.	196
C.8 Multi-class results for RF at test scenario 2 on individual ROC curves.	196
C.9 Multi-class results for MLP at test scenario 2 on individual ROC curves.	196
C.10 Performance comparison of five ML-based classifiers based on the overall accuracy at two specific test scenarios.	197
C.11 Performance comparison of five ML-based classifiers based on the macro average F1-score and the micro average F1-score at two specific test scenarios.	197

List of Tables

2.1	Summarized list of UWB related standards in IEEE	20
2.2	Summarized feature comparison of three UWB-based localization topologies	27
3.1	Three types of assumption for TOF Errors Classification (©2018 IEEE. Reprinted, with permission, from [172]).	53
3.2	Sample Values of the parameters used in the Numerical Simulations (©2018 IEEE. Reprinted, with permission, from [172]).	56
3.3	The configuration of UWB used in the evaluations.	62
3.4	Sample reply time drawn randomly from each category (LOS, close LOS, and MP).	63
3.5	Evaluation results for variable reply times at fixed reference distance (5.494 m).	64
5.1	Configurations of the primary hardware used in the experimental evaluation.	135
5.2	Summary of the results based on the F1-scores and overall accuracy. The presented results were based on the average of 10 individual trials for each classifier.	150
A.1	Evaluation results for the special case (Type II) in different scenarios. . .	192
A.2	Evaluation results for the typical case (Type III) in different scenarios. .	193

Bibliography

- [1] M. Adams, M. Hesse, T. Hörmann, and U. Rückert. “Visuelles Sensorsystem für die Trainings- und Spielunterstützung im Leistungshandball”. In: *Technologien im Leistungssport 3: Tagungsband zur 19. Frühjahrsschule am 14./15. Mai 2018 in Leipzig*. Ed. by I. Fichtner. Vol. 3. Meyer & Meyer Verlag, 2018, pp. 106–115. ISBN: 978-3-8403-7628-3.
- [2] M. Afzalan and F. Jazizadeh. “Indoor Positioning Based on Visible Light Communication: A Performance-Based Survey of Real-World Prototypes”. In: *ACM Comput. Surv.* 52.2 (May 2019). doi: 10.1145/3299769.
- [3] D. B. Ahmed, E. M. Diaz, and J. A. C. Minguez. “Exploiting wearable devices for the calibration of inertial navigation systems”. In: *2017 International Conference on Indoor Positioning and Indoor Navigation (IPIN)*. 2017, pp. 1–5. doi: 10.1109/IPIN.2017.8115931.
- [4] E. Aitenbichler and M. Muhlhauser. “An IR local positioning system for smart items and devices”. In: *23rd International Conference on Distributed Computing Systems Workshops, 2003. Proceedings*. 2003, pp. 334–339. doi: 10.1109/ICDCSW.2003.1203576.
- [5] M. A. Al-Ammar, S. Alhadhrami, A. Al-Salman, A. Alarifi, H. S. Al-Khalifa, A. Alnafessah, and M. Alsaleh. “Comparative Survey of Indoor Positioning Technologies, Techniques, and Algorithms”. In: *2014 International Conference on Cyberworlds*. 2014, pp. 245–252. doi: 10.1109/CW.2014.41.
- [6] A. Al-Habashna, G. Wainer, and M. Aloqaily. “Machine learning-based indoor localization and occupancy estimation using 5G ultra-dense networks”. In: *Simulation Modelling Practice and Theory* 118 (2022), p. 102543. doi: 10.1016/j.smpat.2022.102543.
- [7] A. Alarifi, A. Al-Salman, M. Alsaleh, A. Alnafessah, S. Al-Hadhrami, M. Al-Ammar, and H. Al-Khalifa. “Ultra Wideband Indoor Positioning Technologies: Analysis and Recent Advances”. In: *Sensors* 16.5 (May 2016), p. 707. doi: 10.3390/s16050707.
- [8] N. Antigny, M. Servières, and V. Renaudin. “Pedestrian track estimation with handheld monocular camera and inertial-magnetic sensor for urban augmented reality”. In: *2017 International Conference on Indoor Positioning and Indoor Navigation (IPIN)*. 2017, pp. 1–8. doi: 10.1109/IPIN.2017.8115934.
- [9] M. O. A. Aqel, M. H. Marhaban, M. I. Saripan, and N. B. Ismail. “Review of visual odometry: types, approaches, challenges, and applications”. In: *SpringerPlus* 5.1 (Oct. 2016), p. 1897. doi: 10.1186/s40064-016-3573-7.
- [10] J. Armstrong, Y. A. Sekercioglu, and A. Neild. “Visible light positioning: a roadmap for international standardization”. In: *IEEE Communications Magazine* 51.12 (Dec. 2013), pp. 68–73. doi: 10.1109/MCOM.2013.6685759.
- [11] M. Arulampalam, S. Maskell, N. Gordon, and T. Clapp. “A tutorial on particle filters for online nonlinear/non-Gaussian Bayesian tracking”. In: *IEEE Transactions on Signal Processing* 50.2 (2002), pp. 174–188. doi: 10.1109/78.978374.
- [12] A. I. Baba. “Calibrating Time of Flight in Two Way Ranging”. In: *2011 Seventh International Conference on Mobile Ad-hoc and Sensor Networks*. 2011, pp. 393–397. doi: 10.1109/MSN.2011.23.
- [13] A. I. Baba and M. M. Atia. “Burst mode symmetric double sided two way ranging”. In: *2011 IFIP Wireless Days (WD)*. 2011, pp. 1–3. doi: 10.1109/WD.2011.6098183.

Bibliography

- [14] P. Bahl and V. N. Padmanabhan. "RADAR: an in-building RF-based user location and tracking system". In: *Proceedings IEEE INFOCOM 2000. Conference on Computer Communications. Nineteenth Annual Joint Conference of the IEEE Computer and Communications Societies (Cat. No.00CH37064)*. Vol. 2. 2000, 775–784 vol.2. doi: 10.1109/INFCOM.2000.832252.
- [15] Y. Bar-Shalom, X. R. Li, and T. Kirubarajan. *Estimation with applications to tracking and navigation: theory algorithms and software*. John Wiley & Sons, 2004. ISBN: 0-471-41655-X.
- [16] V. Barral, C. J. Escudero, J. A. García-Naya, and R. Maneiro-Catoira. "NLOS Identification and Mitigation Using Low-Cost UWB Devices". In: *Sensors* 19.16 (Aug. 2019), p. 3464. doi: 10.3390/s19163464.
- [17] G. Bishop, G. Welch, et al. "An introduction to the kalman filter". In: *Proc of SIGGRAPH, Course 8.27599-23175* (2001), p. 41.
- [18] J. Borras, P. Hatrack, and N. B. Mandayam. "Decision theoretic framework for NLOS identification". In: *VTC '98. 48th IEEE Vehicular Technology Conference. Pathway to Global Wireless Revolution (Cat. No.98CH36151)*. Vol. 2. 1998, 1583–1587 vol.2. doi: 10.1109/VETEC.1998.686556.
- [19] K. Bregar, A. Hrovat, and M. Mohorcic. "NLOS Channel Detection with Multilayer Perceptron in Low-Rate Personal Area Networks for Indoor Localization Accuracy Improvement". In: *Proceedings of the 8th Jožef Stefan International Postgraduate School Students Conference, Ljubljana, Slovenia*. Vol. 31. 2016.
- [20] L. Breiman. "Random Forests". In: *Machine Learning* 45.1 (Oct. 2001), pp. 5–32. doi: 10.1023/A:1010933404324.
- [21] R. G. BROWN. "Integrated Navigation Systems and Kalman Filtering: A Perspective". In: *NAVIGATION* 19.4 (1972), pp. 355–362. doi: 10.1002/j.2161-4296.1972.tb01706.x. eprint: <https://onlinelibrary.wiley.com/doi/pdf/10.1002/j.2161-4296.1972.tb01706.x>.
- [22] R. Brown and P. Hwang. *Introduction to Random Signals and Applied Kalman Filtering with Matlab Exercises*. CourseSmart Series. Wiley, 2012. ISBN: 9780470609699.
- [23] R. G. Brown, P. Y. Hwang, et al. *Introduction to random signals and applied Kalman filtering*. Vol. 3. Wiley New York, 1992.
- [24] N. Bulusu, J. Heidemann, and D. Estrin. "GPS-less low-cost outdoor localization for very small devices". In: *IEEE Personal Communications* 7.5 (Oct. 2000), pp. 28–34. doi: 10.1109/98.878533.
- [25] J. J. Caffery and G. L. Stuber. "Overview of radiolocation in CDMA cellular systems". In: *IEEE Communications Magazine* 36.4 (Apr. 1998), pp. 38–45. doi: 10.1109/35.667411.
- [26] Y. Cao, C. Yang, R. Li, A. Knoll, and G. Beltrame. "Accurate position tracking with a single UWB anchor". In: *2020 IEEE International Conference on Robotics and Automation (ICRA)*. 2020, pp. 2344–2350. doi: 10.1109/ICRA40945.2020.9197345.
- [27] T. F. Chan, G. H. Golub, and R. J. LeVeque. "Updating Formulae and a Pairwise Algorithm for Computing Sample Variances". In: *COMPSTAT 1982 5th Symposium held at Toulouse 1982*. Ed. by H. Caussinus, P. Ettinger, and R. Tomassone. Physica-Verlag HD, 1982, pp. 30–41. ISBN: 978-3-642-51461-6.

- [28] F. Charte, A. J. Rivera, M. J. del Jesus, and F. Herrera. “Addressing imbalance in multilabel classification: Measures and random resampling algorithms”. In: *Neurocomputing* 163 (2015). Recent Advancements in Hybrid Artificial Intelligence Systems and its Application to Real-World Problems Progress in Intelligent Systems Mining Humanistic Data, pp. 3–16. doi: 10.1016/j.neucom.2014.08.091.
- [29] Q. M. Chaudhari, E. Serpedin, and K. Qaraqe. “On Maximum Likelihood Estimation of Clock Offset and Skew in Networks With Exponential Delays”. In: *IEEE Transactions on Signal Processing* 56.4 (Apr. 2008), pp. 1685–1697. doi: 10.1109/TSP.2007.910536.
- [30] M. Chiani and A. Giorgetti. “Coexistence Between UWB and Narrow-Band Wireless Communication Systems”. In: *Proceedings of the IEEE* 97.2 (2009), pp. 231–254. doi: 10.1109/JPROC.2008.2008778.
- [31] J. Choliz, M. Eguizabal, A. Hernandez-Solana, and A. Valdovinos. “Comparison of Algorithms for UWB Indoor Location and Tracking Systems”. In: *2011 IEEE 73rd Vehicular Technology Conference (VTC Spring)*. 2011, pp. 1–5. doi: 10.1109/VETECS.2011.5956174.
- [32] E. technical committee. *Short Range Devices (SRD) using Ultra Wide Band (UWB); Part 3: Worldwide UWB regulations between 3,1 and 10,6 GHz*. ETSI, 2019. URL: https://www.etsi.org/deliver/etsi_TR/103100_103199/10318103/02.01.01_60/tr_10318103v020101p.pdf.
- [33] I. L. S. Committee. *IEEE Standard for Local and Metropolitan Area Networks—Part 15.4: Low-Rate Wireless Personal Area Networks (LR-WPANs)*. IEEE Std 802.15.4-2011 (Revision of IEEE Std 802.15.4-2006). IEEE, Sept. 2011. doi: 10.1109/IEEESTD.2011.6012487.
- [34] A. Conti, D. Dardari, M. Guerra, L. Mucci, and M. Z. Win. “Experimental Characterization of Diversity Navigation”. In: *IEEE Systems Journal* 8.1 (Mar. 2014), pp. 115–124. doi: 10.1109/JSYST.2013.2260638.
- [35] D. Coppens, E. De Poorter, A. Shahid, S. Lemey, and C. Marshall. *An Overview of Ultra-WideBand (UWB) Standards(IEEE 802.15.4, FiRa, Apple): Interoperability Aspects and Future Research Directions*. 2022. doi: 10.48550/ARXIV.2202.02190.
- [36] P. Corbalán, G. P. Picco, and S. Palipana. “Chorus: UWB Concurrent Transmissions for GPS-like Passive Localization of Countless Targets”. In: *2019 18th ACM/IEEE International Conference on Information Processing in Sensor Networks (IPSN)*. 2019, pp. 133–144. doi: 10.1145/3302506.3310395.
- [37] C. Cortes and V. Vapnik. “Support-vector networks”. In: *Machine Learning* 20.3 (Sept. 1995), pp. 273–297. doi: 10.1007/BF00994018.
- [38] K. K. Cwalina, P. Rajchowski, O. Blaszkiewicz, A. Olejniczak, and J. Sadowski. “Deep Learning-Based LOS and NLOS Identification in Wireless Body Area Networks”. In: *Sensors* 19.19 (Sept. 2019), p. 4229. doi: 10.3390/s19194229.
- [39] R. Dalce, A. van den Bossche, and T. Val. “A Study of the Ranging Error for Parallel Double Sided-Two Way Ranging Protocol”. In: *2016 IEEE 84th Vehicular Technology Conference (VTC-Fall)*. 2016, pp. 1–5. doi: 10.1109/VTCFall.2016.7880884.
- [40] D. Dardari, P. Closas, and P. M. Djurić. “Indoor Tracking: Theory, Methods, and Technologies”. In: *IEEE Transactions on Vehicular Technology* 64.4 (Apr. 2015), pp. 1263–1278. doi: 10.1109/TVT.2015.2403868.

Bibliography

- [41] D. Dardari, A. Conti, U. Ferner, A. Giorgetti, and M. Z. Win. “Ranging With Ultrawide Bandwidth Signals in Multipath Environments”. In: *Proceedings of the IEEE* 97.2 (Feb. 2009), pp. 404–426. doi: 10.1109/JPROC.2008.2008846.
- [42] G. De Angelis, V. Pasku, A. De Angelis, M. Dionigi, M. Mongiardo, A. Moschitta, and P. Carbone. “An Indoor AC Magnetic Positioning System”. In: *IEEE Transactions on Instrumentation and Measurement* 64.5 (May 2015), pp. 1267–1275. doi: 10.1109/TIM.2014.2381353.
- [43] Decawave. *Application Note - Antenna Delay Calibration of DW1000-Based Products and Systems*. 2018. URL: <https://www.decawave.com/product-documentation/>.
- [44] Decawave. *DW1000 Datasheet - DW1000 15.4-2011 UWB Transceiver (Datasheet for DW1000)*. 2018. URL: <https://www.decawave.com/product-documentation/>.
- [45] Decawave. *DW1000 User Manual - How to Use, Configure and Program the DW1000 UWB Transceiver*. 2017. URL: <https://www.decawave.com/product-documentation/>.
- [46] Decawave. *DW1000 User Manual: how to use, configure and program the DW1000 UWB transceiver*. 2017. URL: <https://www.decawave.com/product-documentation/>.
- [47] Decawave. *TREK1000 user manual*. 2017. URL: <https://www.decawave.com/product-documentation/>.
- [48] Decawave. *UWB Regulations - A Summary of Worldwide Telecommunications Regulations governing the use of Ultra-Wideband radio*. 2015. URL: https://www.decawave.com/sites/default/files/apr001_uwb_worldwide_regulations_summaryrev1.2.pdf.
- [49] B. Denis and N. Daniele. “NLOS ranging error mitigation in a distributed positioning algorithm for indoor UWB ad-hoc networks”. In: *International Workshop on Wireless Ad-Hoc Networks, 2004*. 2004, pp. 356–360. doi: 10.1109/IWAN.2004.1525602.
- [50] M.-G. Di Benedetto, T. Kaiser, A. F. Molisch, I. Oppermann, C. Politano, and D. Porcino. *UWB communication systems: a comprehensive overview*. Hindawi Publishing Corporation, 2006. ISBN: 977-5945-10-0.
- [51] S. Djosic, I. Stojanovic, M. Jovanovic, and G. L. Djordjevic. “Multi-algorithm UWB-based localization method for mixed LOS/NLOS environments”. In: *Computer Communications* 181 (2022), pp. 365–373. doi: 10.1016/j.comcom.2021.10.031.
- [52] A. Doucet, S. Godsill, and C. Andrieu. “On sequential Monte Carlo sampling methods for Bayesian filtering”. In: *Statistics and Computing* 10.3 (July 2000), pp. 197–208. doi: 10.1023/A:1008935410038.
- [53] S. Dwivedi, A. De Angelis, D. Zachariah, and P. Händel. “Joint Ranging and Clock Parameter Estimation by Wireless Round Trip Time Measurements”. In: *IEEE Journal on Selected Areas in Communications* 33.11 (Nov. 2015), pp. 2379–2390. doi: 10.1109/JSAC.2015.2430521.
- [54] J. Fan and A. S. Awan. “Non-Line-of-Sight Identification Based on Unsupervised Machine Learning in Ultra Wideband Systems”. In: *IEEE Access* 7 (2019), pp. 32464–32471. doi: 10.1109/ACCESS.2019.2903236.
- [55] B. T. Fang. “Trilateration and extension to global positioning system navigation”. In: *Journal of Guidance, Control, and Dynamics* 9.6 (1986), pp. 715–717. doi: 10.2514/3.20169.

- [56] R. Faragher. “Understanding the Basis of the Kalman Filter Via a Simple and Intuitive Derivation [Lecture Notes]”. In: *IEEE Signal Processing Magazine* 29.5 (2012), pp. 128–132. doi: 10.1109/MSP.2012.2203621.
- [57] R. Faragher and R. Harle. “Location Fingerprinting With Bluetooth Low Energy Beacons”. In: *IEEE Journal on Selected Areas in Communications* 33.11 (Nov. 2015), pp. 2418–2428. doi: 10.1109/JSAC.2015.2430281.
- [58] Z. Farid, R. Nordin, and M. Ismail. “Recent Advances in Wireless Indoor Localization Techniques and System”. In: *Journal of Computer Networks and Communications* 2013 (Sept. 2013), p. 185138. doi: 10.1155/2013/185138.
- [59] C. Feng, W. S. A. Au, S. Valaee, and Z. Tan. “Received-Signal-Strength-Based Indoor Positioning Using Compressive Sensing”. In: *IEEE Transactions on Mobile Computing* 11.12 (2012), pp. 1983–1993. doi: 10.1109/TMC.2011.216.
- [60] A. Fleureau, M. Lacome, M. Buchheit, A. Couturier, and G. Rabita. “Validity of an ultra-wideband local positioning system to assess specific movements in handball”. eng. In: *Biology of sport* 37.4 (Dec. 2020), pp. 351–357. doi: 10.5114/biolsport.2020.96850.
- [61] J. R. Foerster, M. Pendergrass, and A. F. Molisch. “A channel model for ultrawideband indoor communication”. In: *International Symposium on Wireless Personal Multimedia Communication*. Vol. 15. 2003.
- [62] N. I. Fofana, A. van den Bossche, R. Dalcé, and T. Val. “An Original Correction Method for Indoor Ultra Wide Band Ranging-Based Localisation System”. In: *Ad-hoc, Mobile, and Wireless Networks*. Ed. by N. Mitton, V. Loscri, and A. Mouradian. Springer International Publishing, 2016, pp. 79–92. isbn: 978-3-319-40509-4.
- [63] L. Fortnow and S. Homer. “A short history of computational complexity”. In: *Bulletin of the EATCS* 80.01 (2003). url: <https://open.bu.edu/handle/2144/1674>.
- [64] V. Fox, J. Hightower, L. Liao, D. Schulz, and G. Borriello. “Bayesian filtering for location estimation”. In: *IEEE Pervasive Computing* 2.3 (2003), pp. 24–33. doi: 10.1109/MPRV.2003.1228524.
- [65] W. H. FOY. “Position-Location Solutions by Taylor-Series Estimation”. In: *IEEE Transactions on Aerospace and Electronic Systems* AES-12.2 (Mar. 1976), pp. 187–194. doi: 10.1109/TAES.1976.308294.
- [66] S. Frattasi and F. Della Rosa. *Mobile positioning and tracking: from conventional to cooperative techniques*. 2nd Ed. John Wiley & Sons, 2017. isbn: 978-1-119-06881-5.
- [67] S. Ganeriwal, R. Kumar, and M. B. Srivastava. “Timing-Sync Protocol for Sensor Networks”. In: *Proceedings of the 1st International Conference on Embedded Networked Sensor Systems* (New York, NY, USA). SenSys 03. Association for Computing Machinery, 2003, pp. 138–149. doi: 10.1145/958491.958508.
- [68] C. Gao, G. Zhao, and H. Fourati. *Cooperative Localization and Navigation: Theory, Research, and Practice*. CRC Press, 2019. isbn: 978-1-138-58061-9.
- [69] F. Geyer and D. Schupke. *Precise Onboard Aircraft Cabin Localization using UWB and ML*. 2022. doi: 10.48550/ARXIV.2203.08403.
- [70] S. Gezici, Zhi Tian, G. B. Giannakis, H. Kobayashi, A. F. Molisch, H. V. Poor, and Z. Sahinoglu. “Localization via ultra-wideband radios: a look at positioning aspects for future sensor networks”. In: *IEEE Signal Processing Magazine* 22.4 (July 2005), pp. 70–84. doi: 10.1109/MSP.2005.1458289.

Bibliography

- [71] V. Gharat, E. Colin, G. Baudoin, and D. Richard. “Indoor performance analysis of LF-RFID based positioning system: Comparison with UHF-RFID and UWB”. In: *2017 International Conference on Indoor Positioning and Indoor Navigation (IPIN)*. 2017, pp. 1–8. doi: [10.1109/IPIN.2017.8115901](https://doi.org/10.1109/IPIN.2017.8115901).
- [72] M. Ghavami, L. Michael, and R. Kohno. *Ultra wideband signals and systems in communication engineering*. John Wiley & Sons, 2007. isbn: 978-0-470-02763-9.
- [73] D. Ghosh and P. K. Sahu. “UWB in healthcare”. In: *2016 International Conference on Electromagnetics in Advanced Applications (ICEAA)*. 2016, pp. 679–682. doi: [10.1109/ICEAA.2016.7731489](https://doi.org/10.1109/ICEAA.2016.7731489).
- [74] B. P. Gibbs. *Advanced Kalman filtering, least-squares and modeling: a practical handbook*. John Wiley & Sons, 2011. isbn: 978-0-470-52970-6.
- [75] D. Göhring, M. Wang, M. Schnürmacher, and T. Ganjineh. “Radar/Lidar sensor fusion for car-following on highways”. In: *The 5th International Conference on Automation, Robotics and Applications*. 2011, pp. 407–412. doi: [10.1109/ICARA.2011.6144918](https://doi.org/10.1109/ICARA.2011.6144918).
- [76] J. González, J. Blanco, C. Galindo, A. O. de Galisteo, J. Fernández-Madrigal, F. Moreno, and J. Martínez. “Mobile robot localization based on Ultra-Wide-Band ranging: A particle filter approach”. In: *Robotics and Autonomous Systems* 57.5 (2009), pp. 496–507. doi: [10.1016/j.robot.2008.10.022](https://doi.org/10.1016/j.robot.2008.10.022).
- [77] M. Grandini, E. Bagli, and G. Visani. *Metrics for Multi-Class Classification: an Overview*. 2020. doi: [10.48550/ARXIV.2008.05756](https://doi.org/10.48550/ARXIV.2008.05756).
- [78] B. Großwindhager, M. Stocker, M. Rath, C. A. Boano, and K. Römer. “SnapLoc: An Ultra-Fast UWB-Based Indoor Localization System for an Unlimited Number of Tags”. In: *2019 18th ACM/IEEE International Conference on Information Processing in Sensor Networks (IPSN)*. 2019, pp. 61–72. doi: [10.1145/3302506.3310389](https://doi.org/10.1145/3302506.3310389).
- [79] P. D. Groves. *Principles of GNSS, inertial, and multisensor integrated navigation systems*. Artech house, 2013. isbn: 978-1-60807-005-3.
- [80] X. Guo, D. Zhang, and L. M. Ni. “Localizing Multiple Objects in an RF-based Dynamic Environment”. In: *2012 IEEE 32nd International Conference on Distributed Computing Systems*. 2012, pp. 576–585. doi: [10.1109/ICDCS.2012.49](https://doi.org/10.1109/ICDCS.2012.49).
- [81] Guowei Shen, R. Zetik, and R. S. Thoma. “Performance comparison of TOA and TDOA based location estimation algorithms in LOS environment”. In: *2008 5th Workshop on Positioning, Navigation and Communication*. 2008, pp. 71–78. doi: [10.1109/WPNC.2008.4510359](https://doi.org/10.1109/WPNC.2008.4510359).
- [82] K. Gururaj, A. K. Rajendra, Y. Song, C. L. Law, and G. Cai. “Real-time identification of NLOS range measurements for enhanced UWB localization”. In: *2017 International Conference on Indoor Positioning and Indoor Navigation (IPIN)*. 2017, pp. 1–7. doi: [10.1109/IPIN.2017.8115877](https://doi.org/10.1109/IPIN.2017.8115877).
- [83] F. Gustafsson, F. Gunnarsson, N. Bergman, U. Forssell, J. Jansson, R. Karlsson, and P.-J. Nordlund. “Particle filters for positioning, navigation, and tracking”. In: *IEEE Transactions on Signal Processing* 50.2 (2002), pp. 425–437. doi: [10.1109/78.978396](https://doi.org/10.1109/78.978396).
- [84] F. Gustafsson. “Particle filter theory and practice with positioning applications”. In: *IEEE Aerospace and Electronic Systems Magazine* 25.7 (2010), pp. 53–82. doi: [10.1109/MAES.2010.5546308](https://doi.org/10.1109/MAES.2010.5546308).

- [85] I. Guvenc, C. Chong, and F. Watanabe. “NLOS Identification and Mitigation for UWB Localization Systems”. In: *2007 IEEE Wireless Communications and Networking Conference*. 2007, pp. 1571–1576. doi: 10.1109/WCNC.2007.296.
- [86] R. Hach. “Symmetric double side two way ranging”. In: *IEEE 802.15 WPAN Documents*, 15-05-0334-r00 (2005).
- [87] M. Hamer and R. D’Andrea. “Self-Calibrating Ultra-Wideband Network Supporting Multi-Robot Localization”. In: *IEEE Access* 6 (2018), pp. 22292–22304. doi: 10.1109/ACCESS.2018.2829020.
- [88] D. Hanley, A. B. Faustino, S. D. Zelman, D. A. Degenhardt, and T. Bretl. “MagPIE: A dataset for indoor positioning with magnetic anomalies”. In: *2017 International Conference on Indoor Positioning and Indoor Navigation (IPIN)*. 2017, pp. 1–8. doi: 10.1109/IPIN.2017.8115961.
- [89] T. Hastie, R. Tibshirani, and J. Friedman. *The Elements of Statistical Learning*. Springer Series in Statistics. Springer New York Inc., 2001. isbn: 978-0-387-21606-5.
- [90] S. Haykin. *Adaptive Filter Theory* (3rd Ed.) Prentice-Hall, Inc., 1996. isbn: 013322760X.
- [91] J. D. Hoffman and S. Frankel. *Numerical methods for engineers and scientists*. 2nd Ed. CRC press, 2018. isbn: 978-0-8247-0443-8.
- [92] K. A. Horváth, G. Ill, and Á. Milánkovich. “Passive extended double-sided two-way ranging algorithm for UWB positioning”. In: *2017 Ninth International Conference on Ubiquitous and Future Networks (ICUFN)*. 2017, pp. 482–487. doi: 10.1109/ICUFN.2017.7993831.
- [93] C. Huang, A. F. Molisch, R. He, R. Wang, P. Tang, B. Ai, and Z. Zhong. “Machine Learning-Enabled LOS/NLOS Identification for MIMO System in Dynamic Environment”. In: *IEEE Transactions on Wireless Communications* (2020), pp. 1–1. doi: 10.1109/TWC.2020.2967726.
- [94] Q. Huang and J. Liu. “Mobile Tracking Using Hybrid Measurements in NLOS Environments”. In: *2006 6th International Conference on ITS Telecommunications*. 2006, pp. 1075–1078. doi: 10.1109/ITST.2006.288773.
- [95] O. W. Ibraheem, A. Irwansyah, J. Hagemeier, M. Porrmann, and U. Rückert. “Reconfigurable vision processing system for player tracking in indoor sports”. In: *2017 Conference on Design and Architectures for Signal and Image Processing (DASIP)*. 2017, pp. 1–6. doi: 10.1109/DASIP.2017.8122114.
- [96] “IEEE Standard for Low-Rate Wireless Networks”. In: *IEEE Std 802.15.4-2015 (Revision of IEEE Std 802.15.4-2011)* (Apr. 2016), pp. 1–709. doi: 10.1109/IEEESTD.2016.7460875.
- [97] “IEEE Standard for Low-Rate Wireless Networks”. In: *IEEE Std 802.15.4-2020 (Revision of IEEE Std 802.15.4-2015)* (July 2020), pp. 1–800. doi: 10.1109/IEEESTD.2020.9144691.
- [98] “IEEE Standard for Low-Rate Wireless Networks—Amendment 1: Enhanced Ultra Wideband (UWB) Physical Layers (PHYs) and Associated Ranging Techniques”. In: *IEEE Std 802.15.4z-2020 (Amendment to IEEE Std 802.15.4-2020)* (Aug. 2020), pp. 1–174. doi: 10.1109/IEEESTD.2020.9179124.
- [99] Y. Jiang and V. C. M. Leung. “An Asymmetric Double Sided Two-Way Ranging for Crystal Offset”. In: *2007 International Symposium on Signals, Systems and Electronics*. 2007, pp. 525–528. doi: 10.1109/ISSSE.2007.4294528.

Bibliography

- [100] A. R. Jiménez and F. Seco. "Comparing Decawave and Bespoon UWB location systems: Indoor/outdoor performance analysis". In: *2016 International Conference on Indoor Positioning and Indoor Navigation (IPIN)*. 2016, pp. 1–8. doi: [10.1109/IPIN.2016.7743686](https://doi.org/10.1109/IPIN.2016.7743686).
- [101] A. R. Jiménez and F. Seco. "Finding objects using UWB or BLE localization technology: A museum-like use case". In: *2017 International Conference on Indoor Positioning and Indoor Navigation (IPIN)*. 2017, pp. 1–8. doi: [10.1109/IPIN.2017.8115865](https://doi.org/10.1109/IPIN.2017.8115865).
- [102] A. R. Jiménez, F. Seco, F. Zampella, J. C. Prieto, and J. Guevara. "PDR with a Foot-Mounted IMU and Ramp Detection". In: *Sensors* 11.10 (Sept. 2011), 9393–9410. doi: [10.3390/s111009393](https://doi.org/10.3390/s111009393).
- [103] A. R. Jiménez Ruiz and F. Seco Granja. "Comparing Ubisense, BeSpoon, and DecaWave UWB Location Systems: Indoor Performance Analysis". In: *IEEE Transactions on Instrumentation and Measurement* 66.8 (Aug. 2017), pp. 2106–2117. doi: [10.1109/TIM.2017.2681398](https://doi.org/10.1109/TIM.2017.2681398).
- [104] A. R. Jiménez Ruiz, F. Seco Granja, J. Carlos Prieto Honorato, and J. I. Guevara Rosas. "Pedestrian indoor navigation by aiding a foot-mounted IMU with RFID Signal Strength measurements". In: *2010 International Conference on Indoor Positioning and Indoor Navigation*. 2010, pp. 1–7. doi: [10.1109/IPIN.2010.5646885](https://doi.org/10.1109/IPIN.2010.5646885).
- [105] M. Jöst. "Standardisierte Ortungsdaten für die Produktion und Logistik". In: *ATZproduktion* 7.3 (Nov. 2020), pp. 66–66. doi: [10.1007/s35726-020-0094-z](https://doi.org/10.1007/s35726-020-0094-z).
- [106] S. J. Julier and J. K. Uhlmann. "New extension of the Kalman filter to nonlinear systems". In: *Signal Processing, Sensor Fusion, and Target Recognition VI*. Ed. by I. Kadar. Vol. 3068. International Society for Optics and Photonics. SPIE, 1997, pp. 182 –193. doi: [10.1117/12.280797](https://doi.org/10.1117/12.280797).
- [107] S. Julier and J. Uhlmann. "Unscented filtering and nonlinear estimation". In: *Proceedings of the IEEE* 92.3 (2004), pp. 401–422. doi: [10.1109/JPROC.2003.823141](https://doi.org/10.1109/JPROC.2003.823141).
- [108] S. Julier, J. Uhlmann, and H. Durrant-Whyte. "A new approach for filtering nonlinear systems". In: *Proceedings of 1995 American Control Conference - ACC'95*. Vol. 3. 1995, 1628–1632 vol.3. doi: [10.1109/ACC.1995.529783](https://doi.org/10.1109/ACC.1995.529783).
- [109] R. E. Kalman. "A New Approach to Linear Filtering and Prediction Problems". In: *Journal of Basic Engineering* 82.1 (Mar. 1960), pp. 35–45. doi: [10.1115/1.3662552](https://doi.org/10.1115/1.3662552).
- [110] G. Ke, Q. Meng, T. Finley, T. Wang, W. Chen, W. Ma, Q. Ye, and T.-Y. Liu. "LightGBM: A Highly Efficient Gradient Boosting Decision Tree". In: *Proceedings of the 31st International Conference on Neural Information Processing Systems*. NIPS'17. Curran Associates Inc., 2017, pp. 3149–3157. ISBN: 9781510860964.
- [111] Kegen Yu and I. Oppermann. "UWB positioning for wireless embedded networks". In: *Proceedings. 2004 IEEE Radio and Wireless Conference (IEEE Cat. No.04TH8746)*. 2004, pp. 459–462. doi: [10.1109/RWCON.2004.1389176](https://doi.org/10.1109/RWCON.2004.1389176).
- [112] R. Khan, F. Sottile, and M. A. Spirito. "Hybrid positioning through extended Kalman filter with inertial data fusion". In: *International journal of information and electronics engineering* 3.1 (2013), pp. 127–131. doi: [10.7763/IJIEE.2013.V3.281](https://doi.org/10.7763/IJIEE.2013.V3.281).
- [113] J. Khodjaev, Y. Park, and A. Saeed Malik. "Survey of NLOS identification and error mitigation problems in UWB-based positioning algorithms for dense environments". In: *annals of telecommunications - annales des télécommunications* 65.5 (June 2010), pp. 301–311. doi: [10.1007/s12243-009-0124-z](https://doi.org/10.1007/s12243-009-0124-z).

- [114] H. Kim. “Double-sided two-way ranging algorithm to reduce ranging time”. In: *IEEE Communications Letters* 13.7 (July 2009), pp. 486–488. doi: 10.1109/LCOMM.2009.090093.
- [115] J. Kim and H. Jun. “Vision-based location positioning using augmented reality for indoor navigation”. In: *IEEE Transactions on Consumer Electronics* 54.3 (Aug. 2008), pp. 954–962. doi: 10.1109/TCE.2008.4637573.
- [116] T. Kim Geok, K. Zar Aung, M. Sandar Aung, M. Thu Soe, A. Abdaziz, C. Pao Liew, F. Hossain, C. P. Tso, and W. H. Yong. “Review of Indoor Positioning: Radio Wave Technology”. In: *Applied Sciences* 11.1 (2021). doi: 10.3390/app11010279.
- [117] N. E. KLEPEIS, W. C. NELSON, W. R. OTT, J. P. ROBINSON, A. M. TSANG, P. SWITZER, J. V. BEHAR, S. C. HERN, and W. H. ENGELMANN. “The National Human Activity Pattern Survey (NHAPS): a resource for assessing exposure to environmental pollutants”. In: *Journal of Exposure Science & Environmental Epidemiology* 11.3 (July 2001), pp. 231–252. doi: 10.1038/sj.jea.7500165.
- [118] M. Kolakowski and J. Modelska. “Detection of direct path component absence in NLOS UWB channel”. In: *2018 22nd International Microwave and Radar Conference (MIKON)*. 2018, pp. 247–250. doi: 10.23919/MIKON.2018.8405190.
- [119] T. Korthals, D. Wolf, D. Rudolph, M. Hesse, and U. Rückert. “Fiducial Marker based Extrinsic Camera Calibration for a Robot Benchmarking Platform”. In: *2019 European Conference on Mobile Robots (ECMR)*. 2019, pp. 1–6. doi: 10.1109/ECMR.2019.8870969.
- [120] S. Krishnan, R. Xenia Mendoza Santos, E. Ranier Yap, and M. Thu Zin. “Improving UWB Based Indoor Positioning in Industrial Environments Through Machine Learning”. In: *2018 15th International Conference on Control, Automation, Robotics and Vision (ICARCV)*. 2018, pp. 1484–1488. doi: 10.1109/ICARCV.2018.8581305.
- [121] D. Kulemann, A. Jain, and S. Schön. “Evaluation and Comparison of Different Motion Models for Flight Navigation”. In: *2021 15th European Conference on Antennas and Propagation (EuCAP)*. 2021, pp. 1–5. doi: 10.23919/EuCAP51087.2021.9411080.
- [122] M. Kwak and J. Chong. “A new Double Two-Way Ranging algorithm for ranging system”. In: *2010 2nd IEEE International Conference on Network Infrastructure and Digital Content*. 2010, pp. 470–473. doi: 10.1109/ICNIDC.2010.5657814.
- [123] S.-G. Kwon, O.-J. Kwon, K.-R. Kwon, and S.-H. Lee. “UWB and MEMS IMU Integrated Positioning Algorithm for a Work-Tool Tracking System”. In: *Applied Sciences* 11.19 (2021). doi: 10.3390/app11198826.
- [124] R. R. Labbe. *Kalman and bayesian filters in python*. Roger R. Labbe, 2020. URL: <https://github.com/rlabbe/Kalman-and-Bayesian-Filters-in-Python>.
- [125] R. Lahouli, M. H. Chaudhary, S. Basak, and B. Scheers. “Tracking of Rescue Workers in Harsh Indoor and Outdoor Environments”. In: *Ad-Hoc, Mobile, and Wireless Networks*. Ed. by M. R. Palattella, S. Scanzio, and S. Coleri Ergen. Springer International Publishing, 2019, pp. 48–61. ISBN: 978-3-030-31831-4.
- [126] A. Ledgergerber, M. Hamer, and R. D’Andrea. “A robot self-localization system using one-way ultra-wideband communication”. In: *2015 IEEE/RSJ International Conference on Intelligent Robots and Systems (IROS)*. 2015, pp. 3131–3137. doi: 10.1109/IROS.2015.7353810.

Bibliography

- [127] J. X. Lee, Z. Lin, and C. P. S. Francois. “Symmetric Double Side Two Way Ranging with Unequal Reply Time”. In: *2007 IEEE 66th Vehicular Technology Conference*. 2007, pp. 1980–1983. doi: [10.1109/VETECF.2007.416](https://doi.org/10.1109/VETECF.2007.416).
- [128] M. Leng and Y. Wu. “On Clock Synchronization Algorithms for Wireless Sensor Networks Under Unknown Delay”. In: *IEEE Transactions on Vehicular Technology* 59.1 (Jan. 2010), pp. 182–190. doi: [10.1109/TVT.2009.2028147](https://doi.org/10.1109/TVT.2009.2028147).
- [129] B. Li, T. Gallagher, A. G. Dempster, and C. Rizos. “How feasible is the use of magnetic field alone for indoor positioning?” In: *2012 International Conference on Indoor Positioning and Indoor Navigation (IPIN)*. 2012, pp. 1–9. doi: [10.1109/IPIN.2012.6418880](https://doi.org/10.1109/IPIN.2012.6418880).
- [130] C. Lian Sang, M. Adams, T. Hörmann, M. Hesse, M. Porrmann, and U. Rückert. “Numerical and Experimental Evaluation of Error Estimation for Two-Way Ranging Methods”. In: *Sensors* 19.3 (2019). doi: [10.3390/s19030616](https://doi.org/10.3390/s19030616).
- [131] C. Lian Sang, M. Hesse, S. Zehe, M. Adams, T. Hörmann, and U. Rückert. “An Adaptive Acknowledgement On-demand Protocol for Wireless Sensor Networks”. In: *Proceedings of the 6th International Conference on Sensor Networks - Volume 1: SENORNETS*, INSTICC. SciTePress, 2017, pp. 174–181. doi: [10.5220/0006208501740181](https://doi.org/10.5220/0006208501740181).
- [132] J. Lim, S. Yoo, J. Park, T. Sung, J. Oh, S. Jeong, and K. Lee. “Error analysis of cooperative positioning system using two-way ranging measurements”. In: *2014 8th International Conference on Signal Processing and Communication Systems (ICSPCS)*. 2014, pp. 1–4. doi: [10.1109/ICSPCS.2014.7021104](https://doi.org/10.1109/ICSPCS.2014.7021104).
- [133] R. Liu. *Deep Learning-based Multi-class Classification for UWB Ranging*. Master Project. Bielefeld University, 2021.
- [134] Liuqing Yang and G. B. Giannakis. “Ultra-wideband communications: an idea whose time has come”. In: *IEEE Signal Processing Magazine* 21.6 (2004), pp. 26–54.
- [135] A. Maali, H. Mimoun, G. Baudoin, and A. Ouldali. “A new low complexity NLOS identification approach based on UWB energy detection”. In: *2009 IEEE Radio and Wireless Symposium*. 2009, pp. 675–678. doi: [10.1109/RWS.2009.4957442](https://doi.org/10.1109/RWS.2009.4957442).
- [136] M. Maheepala, A. Z. Kouzani, and M. A. Joordens. “Light-Based Indoor Positioning Systems: A Review”. In: *IEEE Sensors Journal* 20.8 (2020), pp. 3971–3995. doi: [10.1109/JSEN.2020.2964380](https://doi.org/10.1109/JSEN.2020.2964380).
- [137] S. N. Malek. *Accuracy of DW1000 in Game-Sports Tracking*. Master Project. Bielefeld University, 2019.
- [138] S. Maranó, W. M. Gifford, H. Wymeersch, and M. Z. Win. “NLOS identification and mitigation for localization based on UWB experimental data”. In: *IEEE Journal on Selected Areas in Communications* 28.7 (Sept. 2010), pp. 1026–1035. doi: [10.1109/JSAC.2010.100907](https://doi.org/10.1109/JSAC.2010.100907).
- [139] R. Mautz and S. Tilch. “Survey of optical indoor positioning systems”. In: *2011 International Conference on Indoor Positioning and Indoor Navigation*. 2011, pp. 1–7. doi: [10.1109/IPIN.2011.6071925](https://doi.org/10.1109/IPIN.2011.6071925).
- [140] R. Mautz. “Indoor positioning technologies”. Habilitation Thesis. ETH Zurich, Department of Civil, Environmental and Geomatic Engineering, 2012. doi: [10.3929/ethz-a-007313554](https://doi.org/10.3929/ethz-a-007313554).

- [141] C. McElroy, D. Neirynck, and M. McLaughlin. “Comparison of wireless clock synchronization algorithms for indoor location systems”. In: *2014 IEEE International Conference on Communications Workshops (ICC)*. 2014, pp. 157–162. doi: [10.1109/ICCW.2014.6881189](https://doi.org/10.1109/ICCW.2014.6881189).
- [142] G. M. Mendoza-Silva, J. Torres-Sospedra, and J. Huerta. “A Meta-Review of Indoor Positioning Systems”. In: *Sensors* 19.20 (2019). doi: [10.3390/s19204507](https://doi.org/10.3390/s19204507).
- [143] V. Moghtadaiee, A. G. Dempster, and S. Lim. “Indoor localization using FM radio signals: A fingerprinting approach”. In: *2011 International Conference on Indoor Positioning and Indoor Navigation*. 2011, pp. 1–7. doi: [10.1109/IPIN.2011.6071932](https://doi.org/10.1109/IPIN.2011.6071932).
- [144] A. Moreira, I. Silva, F. Meneses, M. J. Nicolau, C. Pendao, and J. Torres-Sospedra. “Multiple simultaneous Wi-Fi measurements in fingerprinting indoor positioning”. In: *2017 International Conference on Indoor Positioning and Indoor Navigation (IPIN)*. 2017, pp. 1–8. doi: [10.1109/IPIN.2017.8115914](https://doi.org/10.1109/IPIN.2017.8115914).
- [145] A. Morrison, V. Renaudin, J. B. Bancroft, and G. Lachapelle. “Design and Testing of a Multi-Sensor Pedestrian Location and Navigation Platform”. In: *Sensors* 12.3 (Apr. 2012), 3720–3738. doi: [10.3390/s120303720](https://doi.org/10.3390/s120303720).
- [146] D. Munoz, F. B. Lara, C. Vargas, and R. Enriquez-Caldera. *Position location techniques and applications*. Academic Press, 2009.
- [147] A. Musa, G. D. Nugraha, H. Han, D. Choi, S. Seo, and J. Kim. “A decision tree-based NLOS detection method for the UWB indoor location tracking accuracy improvement”. In: *International Journal of Communication Systems* 32.13 (2019). e3997 dac.3997, e3997. doi: [10.1002/dac.3997](https://doi.org/10.1002/dac.3997).
- [148] Y. Nam, H. Lee, J. Kim, and K. Park. “Two-Way Ranging Algorithms Using Estimated Frequency Offsets in WPAN and WBAN”. In: *2008 Third International Conference on Convergence and Hybrid Information Technology*. Vol. 1. 2008, pp. 842–847. doi: [10.1109/ICCIIT.2008.296](https://doi.org/10.1109/ICCIIT.2008.296).
- [149] D. Neirynck, E. Luk, and M. McLaughlin. “An alternative double-sided two-way ranging method”. In: *2016 13th Workshop on Positioning, Navigation and Communications (WPNC)*. 2016, pp. 1–4. doi: [10.1109/WPNC.2016.7822844](https://doi.org/10.1109/WPNC.2016.7822844).
- [150] C. T. Nguyen, Y. M. Saputra, N. V. Huynh, N.-T. Nguyen, T. V. Khoa, B. M. Tuan, D. N. Nguyen, D. T. Hoang, T. X. Vu, E. Dutkiewicz, S. Chatzinotas, and B. Ottersten. “A Comprehensive Survey of Enabling and Emerging Technologies for Social Distancing—Part I: Fundamentals and Enabling Technologies”. In: *IEEE Access* 8 (2020), pp. 153479–153507. doi: [10.1109/ACCESS.2020.3018140](https://doi.org/10.1109/ACCESS.2020.3018140).
- [151] K. A. Nguyen, C. Watkins, and Z. Luo. “Co-location epidemic tracking on London public transports using low power mobile magnetometer”. In: *2017 International Conference on Indoor Positioning and Indoor Navigation (IPIN)*. 2017, pp. 1–8. doi: [10.1109/IPIN.2017.8115963](https://doi.org/10.1109/IPIN.2017.8115963).
- [152] V. Niculescu, D. Palossi, M. Magno, and L. Benini. “Fly, Wake-up, Find: UAV-based Energy-efficient Localization for Distributed Sensor Nodes”. In: *Sustainable Computing: Informatics and Systems* 34 (2022), p. 100666. doi: [10.1016/j.suscom.2022.100666](https://doi.org/10.1016/j.suscom.2022.100666).
- [153] A. Niitsoo, T. Edelhäusser, and C. Mutschler. “Convolutional Neural Networks for Position Estimation in TDoA-Based Locating Systems”. In: *2018 International Conference on Indoor Positioning and Indoor Navigation (IPIN)*. 2018, pp. 1–8. doi: [10.1109/IPIN.2018.8533766](https://doi.org/10.1109/IPIN.2018.8533766).

Bibliography

- [154] H. Nikookar and R. Prasad. *Introduction to ultra wideband for wireless communications*. Springer Science & Business Media, 2008. ISBN: 978-1-4020-6632-0.
- [155] F. O'Brien. *The Apollo guidance computer: Architecture and operation*. Springer Science & Business Media, 2010. ISBN: 978-1-4419-0876-6.
- [156] I. Oppermann, M. Hämäläinen, and J. Iinatti. *UWB: theory and applications*. John Wiley & Sons, 2004. ISBN: 0-470-86917-8.
- [157] M. Ortiz, M. De Sousa, and V. Renaudin. “A New PDR Navigation Device for Challenging Urban Environments”. In: *Journal of Sensors* 2017 (Nov. 2017), p. 4080479. doi: 10.1155/2017/4080479.
- [158] V. Pasku, A. De Angelis, G. De Angelis, D. D. Arumugam, M. Dionigi, P. Carbone, A. Moschitta, and D. S. Ricketts. “Magnetic Field-Based Positioning Systems”. In: *IEEE Communications Surveys Tutorials* 19.3 (2017), pp. 2003–2017. doi: 10.1109/COMST.2017.2684087.
- [159] F. Pedregosa, G. Varoquaux, A. Gramfort, V. Michel, B. Thirion, O. Grisel, M. Blondel, P. Prettenhofer, R. Weiss, V. Dubourg, J. Vanderplas, A. Passos, D. Cournapeau, M. Brucher, M. Perrot, and E. Duchesnay. “Scikit-learn: Machine Learning in Python”. In: *Journal of Machine Learning Research* 12 (2011), pp. 2825–2830.
- [160] N. Pirzada, M. Y. Nayan, F. Subhan, M. F. Hassan, and M. A. Khan. “Comparative Analysis of Active and Passive Indoor Localization Systems”. In: *AASRI Procedia* 5 (2013). 2013 AASRI Conference on Parallel and Distributed Computing and Systems, pp. 92–97. doi: 10.1016/j.aasri.2013.10.063.
- [161] J. Powar, C. Gao, and R. Harle. “Assessing the impact of multi-channel BLE beacons on fingerprint-based positioning”. In: *2017 International Conference on Indoor Positioning and Indoor Navigation (IPIN)*. 2017, pp. 1–8. doi: 10.1109/IPIN.2017.8115871.
- [162] G. V. Puskorius and L. A. Feldkamp. “Decoupled extended Kalman filter training of feedforward layered networks”. In: *IJCNN-91-Seattle International Joint Conference on Neural Networks*. Vol. 1. IEEE. 1991, pp. 771–777. doi: 10.1109/IJCNN.1991.155276.
- [163] V. C. S. R. Rayavarapu and A. Mahapatro. “NLOS identification and mitigation in UWB positioning with bagging-based ensembled classifiers”. In: *Annals of Telecommunications* (Oct. 2021). doi: 10.1007/s12243-021-00884-6.
- [164] J. Reed. *An Introduction to Ultra Wideband Communication Systems*. First Ed. Prentice Hall Press, 2005. ISBN: 0131481037.
- [165] B. Ristic, S. Arulampalam, and N. Gordon. *Beyond the Kalman Filter: Particle Filters for Tracking Applications*. Artech House radar library. Artech House, 2004. ISBN: 9781580536318.
- [166] X. Rong Li and V. P. Jilkov. “Survey of maneuvering target tracking. Part I. Dynamic models”. In: *IEEE Transactions on Aerospace and Electronic Systems* 39.4 (Oct. 2003), pp. 1333–1364. doi: 10.1109/TAES.2003.1261132.
- [167] D. E. Rumelhart, G. E. Hinton, and R. J. Williams. “Learning representations by back-propagating errors”. In: *Nature* 323.6088 (1986), pp. 533–536. doi: 10.1038/323533a0.
- [168] C. Runde, J. Gröpl, V. Coors, F. Haspinger, S. Knauth, D. Uckelmann, and W. Eberhard. *Standardisierte Indoor-Ortung mit omlox*. 2022. doi: 10.6084/m9.figshare.19095539.v1.

- [169] A. Safaei and I. Sharf. “Velocity estimation for UAVs using ultra wide-band system”. In: *2021 International Conference on Unmanned Aircraft Systems (ICUAS)*. 2021, pp. 202–209. doi: [10.1109/ICUAS51884.2021.9476831](https://doi.org/10.1109/ICUAS51884.2021.9476831).
- [170] Z. Sahinoglu, S. Gezici, and I. Güvenc. *Ultra-wideband Positioning Systems: Theoretical Limits, Ranging Algorithms, and Protocols*. Cambridge University Press, 2008. doi: [10.1017/CBO9780511541056](https://doi.org/10.1017/CBO9780511541056).
- [171] C. L. Sang, M. Adams, M. Hesse, T. Hörmann, T. Korthals, and U. Rückert. “A Comparative Study of UWB-based True-Range Positioning Algorithms using Experimental Data”. In: *2019 16th Workshop on Positioning, Navigation and Communications (WPNC)*. 2019, pp. 1–6. doi: [10.1109/WPNC47567.2019.8970249](https://doi.org/10.1109/WPNC47567.2019.8970249).
- [172] C. L. Sang, M. Adams, T. Hörmann, M. Hesse, M. Porrmann, and U. Rückert. “An Analytical Study of Time of Flight Error Estimation in Two-Way Ranging Methods”. In: *2018 International Conference on Indoor Positioning and Indoor Navigation (IPIN)*. 2018, pp. 1–8. doi: [10.1109/IPIN.2018.8533697](https://doi.org/10.1109/IPIN.2018.8533697).
- [173] C. L. Sang, M. Adams, T. Hörmann, M. Hesse, M. Porrmann, and U. Rückert. *Supplementary Data for the Paper entitled “An Analytical Study of Time of Flight Error Estimation in Two-Way Ranging Methods”*. Bielefeld University, 2018. doi: [10.4119/unibi/2919795](https://doi.org/10.4119/unibi/2919795).
- [174] C. L. Sang, M. Adams, T. Hörmann, M. Hesse, M. Porrmann, and U. Rückert. *Supplementary Experimental Data for the Paper entitled Numerical and Experimental Evaluation of Error Estimation for Two-Way Ranging Methods*. Bielefeld University, 2019. doi: [10.4119/unibi/2939390](https://doi.org/10.4119/unibi/2939390).
- [175] C. L. Sang, M. Adams, T. Korthals, T. Hörmann, M. Hesse, and U. Rückert. “A Bidirectional Object Tracking and Navigation System using a True-Range Multilateration Method”. In: *2019 International Conference on Indoor Positioning and Indoor Navigation (IPIN)*. 2019, pp. 1–8. doi: [10.1109/IPIN.2019.8911811](https://doi.org/10.1109/IPIN.2019.8911811).
- [176] C. L. Sang, B. Steinhagen, J. D. Homburg, M. Adams, M. Hesse, and U. Rückert. *Supplementary Research Data for the Paper entitled Identification of NLOS and Multi-path Conditions in UWB Localization using Machine Learning Methods*. Bielefeld University, 2020. doi: [10.4119/unibi/2943719](https://doi.org/10.4119/unibi/2943719).
- [177] C. L. Sang, B. Steinhagen, J. D. Homburg, M. Adams, M. Hesse, and U. Rückert. “Identification of NLOS and Multi-Path Conditions in UWB Localization Using Machine Learning Methods”. In: *Applied Sciences* 10.11 (June 2020), p. 3980. doi: [10.3390/app10113980](https://doi.org/10.3390/app10113980).
- [178] L. Santoro, M. Nardello, D. Brunelli, and D. Fontanelli. “Scale up to infinity: the UWB Indoor Global Positioning System”. In: *2021 IEEE International Symposium on Robotic and Sensors Environments (ROSE)*. 2021, pp. 1–8. doi: [10.1109/ROSE52750.2021.9611770](https://doi.org/10.1109/ROSE52750.2021.9611770).
- [179] V. Savic, E. G. Larsson, J. Ferrer-Coll, and P. Stenumgaard. “Kernel Methods for Accurate UWB-Based Ranging With Reduced Complexity”. In: *IEEE Transactions on Wireless Communications* 15.3 (Mar. 2016), pp. 1783–1793. doi: [10.1109/TWC.2015.2496584](https://doi.org/10.1109/TWC.2015.2496584).
- [180] L. Schmid, D. Salido-Monzú, and A. Wieser. “Accuracy Assessment and Learned Error Mitigation of UWB ToF Ranging”. In: *2019 International Conference on Indoor Positioning and Indoor Navigation (IPIN)*. 2019, pp. 1–8. doi: [10.1109/IPIN.2019.8911769](https://doi.org/10.1109/IPIN.2019.8911769).
- [181] J. Schroeder, S. Galler, K. Kyamakya, and K. Jobmann. “NLOS detection algorithms for Ultra-Wideband localization”. In: *2007 4th Workshop on Positioning, Navigation and Communication*. 2007, pp. 159–166. doi: [10.1109/WPNC.2007.353628](https://doi.org/10.1109/WPNC.2007.353628).

Bibliography

- [182] F. Seco, A. R. Jimenez, C. Prieto, J. Roa, and K. Koutsou. “A survey of mathematical methods for indoor localization”. In: *2009 IEEE International Symposium on Intelligent Signal Processing*. 2009, pp. 9–14. doi: 10.1109/WISP.2009.5286582.
- [183] F. Seco, A. R. Jiménez, and F. Zampella. “Fine-grained acoustic positioning with compensation of CDMA interference”. In: *2015 IEEE International Conference on Industrial Technology (ICIT)*. 2015, pp. 3418–3423. doi: 10.1109/ICIT.2015.7125606.
- [184] S. Shah, L.-o. Kovavisaruch, K. Kaemarungsi, and T. Demeechai. “Node Calibration in UWB-Based RTLSs Using Multiple Simultaneous Ranging”. In: *Sensors* 22.3 (2022). doi: 10.3390/s22030864.
- [185] G. Shen. “Localization of Active Nodes within Distributed Ultra-Wideband Sensor Networks in Multipath Environments”. PhD thesis. Ilmenau University of Technology, Ilmenau, Germany, 2011.
- [186] S. Singhal and L. Wu. “Training Multilayer Perceptrons with the Extended Kalman Algorithm”. In: *Proceedings of the 1st International Conference on Neural Information Processing Systems*. NIPS’88. MIT Press, 1988, 133–140.
- [187] B. Sklar. *Digital Communications: Fundamentals and Applications*. Vol. 2. Prentice-Hall PRT, 2001. ISBN: 9780130847881.
- [188] D. R. Smith, J. B. Pendry, and M. C. K. Wiltshire. “Metamaterials and Negative Refractive Index”. In: *Science* 305.5685 (2004), pp. 788–792. doi: 10.1126/science.1096796.
- [189] A. J. Smola and B. Schölkopf. “A tutorial on support vector regression”. In: *Statistics and Computing* 14.3 (2004), pp. 199–222. doi: 10.1023/B:STCO.0000035301.49549.88.
- [190] M. Sokolova and G. Lapalme. “A systematic analysis of performance measures for classification tasks”. In: *Information Processing & Management* 45.4 (2009), pp. 427–437. doi: 10.1016/j.ipm.2009.03.002.
- [191] M. St-Pierre and D. Gingras. “Comparison between the unscented Kalman filter and the extended Kalman filter for the position estimation module of an integrated navigation information system”. In: *IEEE Intelligent Vehicles Symposium, 2004*. 2004, pp. 831–835. doi: 10.1109/IVS.2004.1336492.
- [192] STMicroelectronics. *STM32L476xx Datasheet - Ultra-low-power Arm Cortex-M4 32-bit MCU+FPU, 100DMIPS, up to 1MB Flash, 128 KB SRAM, USB OTG FS, LCD, ext. SMPS*. 2019. URL: <https://www.st.com/resource/en/datasheet/stm32l476je.pdf>.
- [193] STMicroelectronics. *UM1724 User manual: STM32 Nucleo-64 boards (MB1136)*. 2019. URL: https://www.st.com/resource/en/user_manual/dm00105823-stm32-nucleo-64-boards-mb1136-stmicroelectronics.pdf.
- [194] D. Stöber. *Konzeption und Entwicklung eines 3D Echtzeitlokalisierungssystems auf Basis der Funktechnologie Ultrabreitband*. Bachelor Thesis. Bielefeld University, 2018.
- [195] G. Strang. *Introduction to linear algebra*. Vol. 3. Wellesley-Cambridge Press Wellesley, MA, 1993. ISBN: 9780961408824.
- [196] M. Sugano, T. Kawazoe, Y. Ohta, and M. Murata. “Indoor Localization System using RSSI Measurement of Wireless Sensor Network based on ZigBee Standard”. In: *Wireless and Optical Communications* 538 (2006), pp. 1–6.
- [197] J. Suykens and J. Vandewalle. “Least Squares Support Vector Machine Classifiers”. In: *Neural Processing Letters* 9.3 (June 1999). doi: 10.1023/A:1018628609742.

- [198] J. Tiemann, F. Eckermann, and C. Wietfeld. “ATLAS - an open-source TDOA-based Ultra-wideband localization system”. In: *2016 International Conference on Indoor Positioning and Indoor Navigation (IPIN)*. 2016, pp. 1–6. doi: [10.1109/IPIN.2016.7743707](https://doi.org/10.1109/IPIN.2016.7743707).
- [199] J. Tiemann, F. Eckermann, and C. Wietfeld. “Multi-user interference and wireless clock synchronization in TDOA-based UWB localization”. In: *2016 International Conference on Indoor Positioning and Indoor Navigation (IPIN)*. 2016, pp. 1–6. doi: [10.1109/IPIN.2016.7743696](https://doi.org/10.1109/IPIN.2016.7743696).
- [200] J. Tiemann, Y. Elmasry, L. Koring, and C. Wietfeld. “ATLAS FaST: Fast and Simple Scheduled TDOA for Reliable Ultra-Wideband Localization”. In: *2019 International Conference on Robotics and Automation (ICRA)*. 2019, pp. 2554–2560. doi: [10.1109/ICRA.2019.8793737](https://doi.org/10.1109/ICRA.2019.8793737).
- [201] J. Tiemann and C. Wietfeld. “Scalable and precise multi-UAV indoor navigation using TDOA-based UWB localization”. In: *2017 International Conference on Indoor Positioning and Indoor Navigation (IPIN)*. 2017, pp. 1–7. doi: [10.1109/IPIN.2017.8115937](https://doi.org/10.1109/IPIN.2017.8115937).
- [202] I. Tomkos, D. Klonidis, E. Pikasis, and S. Theodoridis. “Toward the 6G Network Era: Opportunities and Challenges”. In: *IT Professional* 22.1 (2020), pp. 34–38. doi: [10.1109/MITP.2019.2963491](https://doi.org/10.1109/MITP.2019.2963491).
- [203] J. Torres-Sospedra, A. Jiménez, A. Moreira, T. Lungenstrass, W.-C. Lu, S. Knauth, G. Mendoza-Silva, F. Seco, A. Pérez-Navarro, M. Nicolau, and et al. “Off-Line Evaluation of Mobile-Centric Indoor Positioning Systems: The Experiences from the 2017 IPIN Competition”. In: *Sensors* 18.2 (Feb. 2018), p. 487. doi: [10.3390/s18020487](https://doi.org/10.3390/s18020487).
- [204] D. Vecchia, P. Corbalán, T. Istomin, and G. P. Picco. “TALLA: Large-scale TDoA Localization with Ultra-wideband Radios”. In: *2019 International Conference on Indoor Positioning and Indoor Navigation (IPIN)*. 2019, pp. 1–8. doi: [10.1109/IPIN.2019.8911790](https://doi.org/10.1109/IPIN.2019.8911790).
- [205] K. Vickery. “Acoustic positioning systems. A practical overview of current systems”. In: *Proceedings of the 1998 Workshop on Autonomous Underwater Vehicles*. 1998, pp. 5–17. doi: [10.1109/AUV.1998.744434](https://doi.org/10.1109/AUV.1998.744434).
- [206] E. A. Wan and R. Van Der Merwe. “The unscented Kalman filter for nonlinear estimation”. In: *Proceedings of the IEEE 2000 Adaptive Systems for Signal Processing, Communications, and Control Symposium (Cat. No.00EX373)*. 2000, pp. 153–158. doi: [10.1109/ASSPCC.2000.882463](https://doi.org/10.1109/ASSPCC.2000.882463).
- [207] J. Wang, M. Bell, X. Liu, and G. Liu. “Machine-Learning Techniques Can Enhance Dairy Cow Estrus Detection Using Location and Acceleration Data”. In: *Animals* 10.7 (2020). doi: [10.3390/ani10071160](https://doi.org/10.3390/ani10071160).
- [208] Weijie Li, Tingting Zhang, and Qinyu Zhang. “Experimental researches on an UWB NLOS identification method based on machine learning”. In: *2013 15th IEEE International Conference on Communication Technology*. 2013, pp. 473–477. doi: [10.1109/ICCT.2013.6820422](https://doi.org/10.1109/ICCT.2013.6820422).
- [209] M. Z. Win, R. M. Buehrer, G. Chrisikos, A. Conti, and H. V. Poor. “Foundations and Trends in Localization Technologies - Part I [Scanning the Issue]”. In: *Proceedings of the IEEE* 106.6 (June 2018), pp. 1019–1021. doi: [10.1109/JPROC.2018.2837342](https://doi.org/10.1109/JPROC.2018.2837342).
- [210] M. Z. Win, D. Dardari, A. F. Molisch, W. Wiesbeck, and J. Zhang. “History and Applications of UWB [Scanning the Issue]”. In: *Proceedings of the IEEE* 97.2 (Feb. 2009), pp. 198–204. doi: [10.1109/JPROC.2008.2008762](https://doi.org/10.1109/JPROC.2008.2008762).

Bibliography

- [211] M. Z. Win and R. A. Scholtz. “Impulse radio: how it works”. In: *IEEE Communications Letters* 2.2 (Feb. 1998), pp. 36–38. doi: [10.1109/4234.660796](https://doi.org/10.1109/4234.660796).
- [212] M. Z. Win and R. A. Scholtz. “Ultra-wide bandwidth time-hopping spread-spectrum impulse radio for wireless multiple-access communications”. In: *IEEE Transactions on Communications* 48.4 (Apr. 2000), pp. 679–689. doi: [10.1109/26.843135](https://doi.org/10.1109/26.843135).
- [213] J. Woo, Y.-j. Kim, J.-o. Lee, and M.-t. Lim. “Localization of Mobile Robot using Particle Filter”. In: *2006 SICE-ICASE International Joint Conference*. 2006, pp. 3031–3034. doi: [10.1109/SICE.2006.315151](https://doi.org/10.1109/SICE.2006.315151).
- [214] Q. Wu, Z. Wei, C. Pan, J. Liu, J. Wang, and A. Wang. “Joint Neighbor Discovery and Positioning for Unmanned Aerial Vehicle Networks”. In: *2021 IEEE 94th Vehicular Technology Conference (VTC2021-Fall)*. 2021, pp. 1–5. doi: [10.1109/VTC2021-Fall152928.2021.9625219](https://doi.org/10.1109/VTC2021-Fall152928.2021.9625219).
- [215] S. Wu, S. Zhang, K. Xu, and D. Huang. “Neural Network Localization With TOA Measurements Based on Error Learning and Matching”. In: *IEEE Access* 7 (2019), pp. 19089–19099. doi: [10.1109/ACCESS.2019.2897153](https://doi.org/10.1109/ACCESS.2019.2897153).
- [216] Y. Wu, Q. Chaudhari, and E. Serpedin. “Clock Synchronization of Wireless Sensor Networks”. In: *IEEE Signal Processing Magazine* 28.1 (Jan. 2011), pp. 124–138. doi: [10.1109/MSP.2010.938757](https://doi.org/10.1109/MSP.2010.938757).
- [217] H. Wyneersch, S. Marano, W. M. Gifford, and M. Z. Win. “A Machine Learning Approach to Ranging Error Mitigation for UWB Localization”. In: *IEEE Transactions on Communications* 60.6 (June 2012), pp. 1719–1728. doi: [10.1109/TCOMM.2012.042712.110035](https://doi.org/10.1109/TCOMM.2012.042712.110035).
- [218] S. Xia, Y. Liu, G. Yuan, M. Zhu, and Z. Wang. “Indoor Fingerprint Positioning Based on Wi-Fi: An Overview”. In: *ISPRS International Journal of Geo-Information* 6.5 (Apr. 2017), p. 135. doi: [10.3390/ijgi6050135](https://doi.org/10.3390/ijgi6050135).
- [219] Z. Xiao, H. Wen, A. Markham, N. Trigoni, P. Blunsom, and J. Frolik. “Non-Line-of-Sight Identification and Mitigation Using Received Signal Strength”. In: *IEEE Transactions on Wireless Communications* 14.3 (Mar. 2015), pp. 1689–1702. doi: [10.1109/TWC.2014.2372341](https://doi.org/10.1109/TWC.2014.2372341).
- [220] W. Xiong, H. C. So, C. Schindelhauer, and J. Wendeberg. “Robust Elliptic Localization Using Worst-Case Formulation and Convex Approximation”. In: *2019 16th Workshop on Positioning, Navigation and Communications (WPNC)*. 2019, pp. 1–6. doi: [10.1109/WPNC47567.2019.8970258](https://doi.org/10.1109/WPNC47567.2019.8970258).
- [221] T. Yang, A. Cabani, and H. Chafouk. “A Survey of Recent Indoor Localization Scenarios and Methodologies”. In: *Sensors* 21.23 (2021). doi: [10.3390/s21238086](https://doi.org/10.3390/s21238086).
- [222] A. Yassin, Y. Nasser, M. Awad, A. Al-Dubai, R. Liu, C. Yuen, R. Raulefs, and E. Aboutanios. “Recent Advances in Indoor Localization: A Survey on Theoretical Approaches and Applications”. In: *IEEE Communications Surveys Tutorials* 19.2 (2017), pp. 1327–1346. doi: [10.1109/COMST.2016.2632427](https://doi.org/10.1109/COMST.2016.2632427).
- [223] J. Yim, C. Park, J. Joo, and S. Jeong. “Extended Kalman Filter for wireless LAN based indoor positioning”. In: *Decision Support Systems* 45.4 (2008). Information Technology and Systems in the Internet-Era, pp. 960 –971. doi: [10.1016/j.dss.2008.03.004](https://doi.org/10.1016/j.dss.2008.03.004).
- [224] H. Young and R. Freedman. *University Physics*. Addison-Wesley series in physics. Addison-Wesley, 1996. ISBN: 9780201640441.

- [225] M. Youssef and A. Agrawala. “The Horus WLAN Location Determination System”. In: *Proceedings of the 3rd International Conference on Mobile Systems, Applications, and Services* (Seattle, Washington). MobiSys '05. ACM, 2005, pp. 205–218. doi: 10.1145/1067170.1067193.
- [226] K. Yu, Y. J. Guo, and I. Oppermann. “Modified Taylor Series Expansion Based Positioning Algorithms”. In: *VTC Spring 2008 - IEEE Vehicular Technology Conference*. 2008, pp. 2656–2660. doi: 10.1109/VETECS.2008.582.
- [227] K. Yu, J. philippe Montillet, A. Rabbachin, P. Cheong, and I. Oppermann. “UWB location and tracking for wireless embedded networks”. In: *Signal Processing* 86.9 (2006). Special Section: Signal Processing in UWB Communications, pp. 2153 –2171. doi: 10.1016/j.sigpro.2005.07.042.
- [228] R. Zandian and U. Witkowski. “NLOS Detection and Mitigation in Differential Localization Topologies Based on UWB Devices”. In: *2018 International Conference on Indoor Positioning and Indoor Navigation (IPIN)*. 2018, pp. 1–8. doi: 10.1109/IPIN.2018.8533781.
- [229] R. Zandian and U. Witkowski. “Robot self-localization in ultra-wideband large scale multi-node setups”. In: *2017 14th Workshop on Positioning, Navigation and Communications (WPNC)*. 2017, pp. 1–6. doi: 10.1109/WPNC.2017.8250062.
- [230] R. Zandian. “Ultra-wideband based indoor localization of mobile nodes in ToA and TDoA configurations”. PhD thesis. Universität Bielefeld, 2019. doi: 10.4119/unibi/2934897.
- [231] C. Zhang, P. Patras, and H. Haddadi. “Deep Learning in Mobile and Wireless Networking: A Survey”. In: *IEEE Communications Surveys & Tutorials* 21.3 (2019), pp. 2224–2287. doi: 10.1109/COMST.2019.2904897.
- [232] H. Zhang. “The Optimality of Naive Bayes”. In: *Proceedings of the Seventeenth International Florida Artificial Intelligence Research Society Conference (FLAIRS 2004)*. Ed. by V. Barr and Z. Markov. AAAI Press, 2004. URL: <https://www.aaai.org/Papers/FLAIRS/2004/Flairs04-097.pdf>.
- [233] Z. Zhang, H. Zhao, and Y. Shen. “High-Efficient Ranging Algorithms for Wireless Sensor Network”. In: *2019 11th International Conference on Wireless Communications and Signal Processing (WCSP)*. 2019, pp. 1–6. doi: 10.1109/WCSP.2019.8928120.
- [234] Z. Zhang, H. Zhao, J. Wang, and Y. Shen. “Signal-Multiplexing Ranging for Network Localization”. In: *IEEE Transactions on Wireless Communications* 21.3 (2022), pp. 1694–1709. doi: 10.1109/TWC.2021.3106172.
- [235] G. Zhu, D. Liu, Y. Du, C. You, J. Zhang, and K. Huang. “Toward an Intelligent Edge: Wireless Communication Meets Machine Learning”. In: *IEEE Communications Magazine* 58.1 (2020), pp. 19–25. doi: 10.1109/MCOM.001.1900103.
- [236] L. Zwirello, T. Schipper, M. Harter, and T. Zwick. “UWB localization system for indoor applications: Concept, realization and analysis”. In: *Journal of Electrical and Computer Engineering* 2012 (2012). doi: 10.1155/2012/849638.

Author's Publications

- [130] C. Lian Sang, M. Adams, T. Hörmann, M. Hesse, M. Porrmann, and U. Rückert. "Numerical and Experimental Evaluation of Error Estimation for Two-Way Ranging Methods". In: *Sensors* 19.3 (2019). doi: [10.3390/s19030616](https://doi.org/10.3390/s19030616).
- [131] C. Lian Sang, M. Hesse, S. Zehe, M. Adams, T. Hörmann, and U. Rückert. "An Adaptive Acknowledgement On-demand Protocol for Wireless Sensor Networks". In: *Proceedings of the 6th International Conference on Sensor Networks - Volume 1: SENORNETS*, INSTICC. SciTePress, 2017, pp. 174–181. doi: [10.5220/0006208501740181](https://doi.org/10.5220/0006208501740181).
- [171] C. L. Sang, M. Adams, M. Hesse, T. Hörmann, T. Korthals, and U. Rückert. "A Comparative Study of UWB-based True-Range Positioning Algorithms using Experimental Data". In: *2019 16th Workshop on Positioning, Navigation and Communications (WPNC)*. 2019, pp. 1–6. doi: [10.1109/WPNC47567.2019.8970249](https://doi.org/10.1109/WPNC47567.2019.8970249).
- [172] C. L. Sang, M. Adams, T. Hörmann, M. Hesse, M. Porrmann, and U. Rückert. "An Analytical Study of Time of Flight Error Estimation in Two-Way Ranging Methods". In: *2018 International Conference on Indoor Positioning and Indoor Navigation (IPIN)*. 2018, pp. 1–8. doi: [10.1109/IPIN.2018.8533697](https://doi.org/10.1109/IPIN.2018.8533697).
- [175] C. L. Sang, M. Adams, T. Korthals, T. Hörmann, M. Hesse, and U. Rückert. "A Bidirectional Object Tracking and Navigation System using a True-Range Multilateration Method". In: *2019 International Conference on Indoor Positioning and Indoor Navigation (IPIN)*. 2019, pp. 1–8. doi: [10.1109/IPIN.2019.8911811](https://doi.org/10.1109/IPIN.2019.8911811).
- [177] C. L. Sang, B. Steinhagen, J. D. Homburg, M. Adams, M. Hesse, and U. Rückert. "Identification of NLOS and Multi-Path Conditions in UWB Localization Using Machine Learning Methods". In: *Applied Sciences* 10.11 (June 2020), p. 3980. doi: [10.3390/app10113980](https://doi.org/10.3390/app10113980).

Research Data

- [173] C. L. Sang, M. Adams, T. Hörmann, M. Hesse, M. Porrmann, and U. Rückert. *Supplementary Data for the Paper entitled "An Analytical Study of Time of Flight Error Estimation in Two-Way Ranging Methods"*. Bielefeld University, 2018. doi: [10.4119/unibi/2919795](https://doi.org/10.4119/unibi/2919795).
- [174] C. L. Sang, M. Adams, T. Hörmann, M. Hesse, M. Porrmann, and U. Rückert. *Supplementary Experimental Data for the Paper entitled Numerical and Experimental Evaluation of Error Estimation for Two-Way Ranging Methods*. Bielefeld University, 2019. doi: [10.4119/unibi/2939390](https://doi.org/10.4119/unibi/2939390).
- [176] C. L. Sang, B. Steinhagen, J. D. Homburg, M. Adams, M. Hesse, and U. Rückert. *Supplementary Research Data for the Paper entitled Identification of NLOS and Multi-path Conditions in UWB Localization using Machine Learning Methods*. Bielefeld University, 2020. doi: [10.4119/unibi/2943719](https://doi.org/10.4119/unibi/2943719).

Co-supervised Work

- [133] R. Liu. *Deep Learning-based Multi-class Classification for UWB Ranging*. Master Project. Bielefeld University, 2021.

- [137] S. N. Malek. *Accuracy of DW1000 in Game-Sports Tracking*. Master Project. Bielefeld University, 2019.
- [194] D. Stöber. *Konzeption und Entwicklung eines 3D Echtzeitlokalisierungssystems auf Basis der Funktechnologie Ultrabreitband*. Bachelor Thesis. Bielefeld University, 2018.

A Derivations of AltDS-TWR in TEEM

A.1 Derivation of AltDS-TWR in TEEM for Type I Case

According to Type I assumption defined in Chapter 3.3 and originally described in our previous works [130, 172], the equation (3.3a) and (3.3b) becomes:

$$t_{roundA} \approx t_{replyB} \quad (\text{A.1a})$$

$$t_{roundB} \approx t_{replyA} \quad (\text{A.1b})$$

and the proposed model from (3.14a) to (3.14d) becomes:

$$\hat{t}_{roundA} \approx (1 + e + \xi)t_{roundA} \approx C_A t_{roundA}$$

$$\hat{t}_{replyA} \approx (1 + e)t_{replyA} \approx C_B t_{replyA}$$

$$\hat{t}_{roundB} \approx (1 + e + \xi)t_{roundB} \approx C_A t_{roundB}$$

$$\hat{t}_{replyB} \approx (1 + e)t_{replyB} \approx C_B t_{replyB}$$

Where, $C_A = 1 + e + \xi$ and $C_B = 1 + e$.

Therefore, the TOF error between the estimated and true value introduced by AltDS-TWR method in (3.19) becomes:

$$\begin{aligned} \hat{T}_{t0f} - T_{t0f} &\approx \frac{C_A^2 t_{roundA} \cdot t_{roundB} - C_B^2 t_{replyA} \cdot t_{replyB}}{(C_A(t_{roundA} + t_{roundB}) + C_B(t_{replyA} + t_{replyB}))} \\ &- \frac{t_{roundA} \cdot t_{roundB} - t_{replyA} \cdot t_{replyB}}{t_{roundA} + t_{replyA} + t_{roundB} + t_{replyB}} \end{aligned}$$

Substituting (A.1a) and (A.1b) in the equation and assuming $t_{replyA} = t_{replyB} = t_{reply}$ yields:

$$\hat{T}_{t0f} - T_{t0f} \approx \frac{(C_A + C_B)(C_A - C_B)t_{reply}^2}{2(C_A + C_B)t_{reply}}$$

$$\hat{T}_{t0f} - T_{t0f} \approx \frac{1}{2}(C_A - C_B)t_{reply}$$

Substituting C_A and C_B in the equation becomes:

$$\hat{T}_{t0f} - T_{t0f} \approx \frac{1}{2}\xi t_{reply} \quad (\text{A.3})$$

A.2 Derivation of AltDS-TWR in TEEM for Type II Case

According to Type II assumption defined in Chapter 3.3 and originally given in our previous works [130, 172], the equation (3.3a) and (3.3b) will now become:

$$t_{roundA} \approx t_{replyB} \quad (\text{A.4a})$$

$$t_{roundB} \approx t_{replyA} \quad (\text{A.4b})$$

and the proposed model from (3.14a) to (3.14d) will become:

$$\hat{t}_{roundA} \approx (1 + e_A + \xi_{ABA}) t_{roundA} \approx C_A + \xi_{ABA} t_{reply}$$

$$\hat{t}_{replyA} \approx (1 + e_A) t_{replyA} \approx C_A$$

$$\hat{t}_{roundB} \approx (1 + e_B + \xi_{BAB}) t_{roundB} \approx C_B + \xi_{BAB} t_{reply}$$

$$\hat{t}_{replyB} \approx (1 + e_B) t_{reply} \approx C_B$$

Where, $C_A = (1 + e_A) t_{reply}$ and $C_B = (1 + e_B) t_{reply}$.

Therefore, the TOF error between the estimated and true value introduced by AltDS-TWR method in (3.19) becomes:

$$\begin{aligned} \hat{T}_{t_{tof}} - T_{t_{tof}} &\approx \frac{(C_A + \xi_{ABA} t_{reply}) \cdot (C_B + \xi_{BAB} t_{reply}) - C_A C_B}{2C_A + 2C_B + \xi_{BAB} t_{reply} + \xi_{ABA} t_{reply}} \\ &\quad - \frac{t_{reply}^2 - t_{reply}^2}{4t_{reply}} \\ \hat{T}_{t_{tof}} - T_{t_{tof}} &\approx \frac{C_A \xi_{BAB} t_{reply} + C_B \xi_{ABA} t_{reply} + \xi_{BAB} \xi_{ABA} t_{reply}^2}{2(C_A + C_B) + (\xi_{BAB} + \xi_{ABA}) t_{reply}} \end{aligned}$$

Substituting C_A and C_B in the equation yields:

$$\begin{aligned} \hat{T}_{t_{tof}} - T_{t_{tof}} &\approx \\ \frac{[e_A \xi_{BAB} + e_B \xi_{ABA} + (\xi_{BAB} + \xi_{ABA} + \xi_{BAB} \xi_{ABA})] t_{reply}^2}{(2e_A + 2e_B + 4 + \xi_{BAB} + \xi_{ABA}) t_{reply}} \\ \hat{T}_{t_{tof}} - T_{t_{tof}} &\approx \frac{K_A}{K_B} t_{reply} \end{aligned} \quad (\text{A.6})$$

Where, $K_A = \xi_{BAB}(1 + e_A) + \xi_{ABA}(1 + e_B) + \xi_{BAB} \xi_{ABA}$ and $K_B = 4 + 2(e_A + e_B) + \xi_{BAB} + \xi_{ABA}$ respectively.

A.3 Derivation of AltDS-TWR in TEEM for Type III Case

According to Type III assumption defined in Chapter 3.3 and originally described in our previous works [130, 172], the equation (3.3a) and (3.3b) in Chapter 3 will now become:

$$t_{roundA} \approx t_{replyB} \quad (\text{A.7a})$$

$$t_{roundB} \approx t_{replyA} \quad (\text{A.7b})$$

and the proposed model from (3.14a) to (3.14d) will become:

$$\hat{t}_{roundA} \approx (1 + e_A + \xi_{ABA})t_{roundA} \approx (C_A + \xi_{ABA})t_{replyB}$$

$$\hat{t}_{replyA} \approx (1 + e_A)t_{replyA} \approx C_A t_{replyA}$$

$$\hat{t}_{roundB} \approx (1 + e_B + \xi_{BAB})t_{roundB} \approx (C_B + \xi_{BAB})t_{replyA}$$

$$\hat{t}_{replyB} \approx (1 + e_B)t_{replyB} \approx C_B t_{replyB}$$

Where, $C_A = (1 + e_A)$ and $C_B = (1 + e_B)$.

Therefore, the TOF error between the estimated and true value introduced by AltDS-TWR method in (3.19) becomes:

$$\hat{T}_{t_{of}} - T_{t_{of}} \approx$$

$$\frac{(C_A + \xi_{ABA})t_{replyB} \cdot (C_B + \xi_{BAB})t_{replyA} - C_A t_{replyA} \cdot C_B t_{replyB}}{(C_A + \xi_{ABA})t_{replyB} + (C_B + \xi_{BAB})t_{replyA} + C_A t_{replyA} + C_B t_{replyB}} \\ - \frac{t_{replyB} \cdot t_{replyA} - t_{replyA} \cdot t_{replyB}}{2(t_{replyA} + t_{replyB})}$$

$$\hat{T}_{t_{of}} - T_{t_{of}} \approx$$

$$\frac{[(C_A + \xi_{ABA}) \cdot (C_B + \xi_{BAB}) - C_A C_B]t_{replyA} \cdot t_{replyB}}{(C_A + \xi_{ABA})t_{replyB} + (C_B + \xi_{BAB})t_{replyA} + C_A t_{replyA} + C_B t_{replyB}}$$

Substituting $C_A = (1 + e_A)$ and $C_B = (1 + e_B)$ in the equation and simplifying it yields:

$$\hat{T}_{t_{of}} - T_{t_{of}} \approx$$

$$\frac{(\xi_{BAB} + e_A \xi_{BAB} + \xi_{ABA} + e_B \xi_{ABA} + \xi_{BAB} \xi_{ABA})t_{replyA} t_{replyB}}{(2 + e_A + e_B + \xi_{BAB})t_{replyA} + (2 + e_A + e_B + \xi_{ABA})t_{replyB}}$$

$$\hat{T}_{t_{of}} - T_{t_{of}} \approx \frac{C_1 t_{replyA} t_{replyB}}{C_2 t_{replyA} + C_3 t_{replyB}} \quad (\text{A.9})$$

Where $C_1 = \xi_{BAB}(1 + e_A) + \xi_{ABA}(1 + e_B) + \xi_{BAB} \xi_{ABA}$, $C_2 = 2 + e_A + e_B + \xi_{BAB}$ and $C_3 = 2 + e_A + e_B + \xi_{ABA}$ respectively.

B Detailed Tables: Ranging Errors due to close LOS and MP Conditions

As a summary of the reported evaluation results presented in Chapter 3.5, Table A.1 gave the detailed outcomes related to the special case (Type II) in all experiments conducted at LOS, close LOS and MP conditions. Similarly, Table A.2 gave the corresponding detailed of experimental evaluations results regarding the typical case (Type III). In Table A.1 (Type II) and Table A.2 (Type III), the smallest value achieved from the evaluated three TWR methods are symbolized with bold letters. In this regard, we considered the values of two numbers are equal or marked them as equal with bold if their difference is smaller than 0.02 cm.

Regarding the spread of the data in the measurement, we observed in the special case that it was less than 10 cm in both Symmetric Doubled-Sided (SDS) and Alternative Double-Sided (AltDS) for the experiments in the LOS scenario (rows of “LOS” and columns of “Spread of data” in Table A.1). The spread of the data in this context refers to the difference between maximum and minimum values of data points in the recorded experiments. Indeed, the mentioned specific data was the best-case scenario observed in the measurement during the experiments. As a matter of fact, the spotted measurement results matches with the precision range of the manufacturer reported in the data-sheet which is 10 cm [44, 46]. However, the spread of the data in the experiments reached up to 41.23 cm for AltDS and SDS TWRs and up to 54.54 cm for SS-TWR as the worst-case scenario spotted in the recorded data during experiments. Overall, the spread of data in the measurement generally got broader or larger in the typical case (Type III)

Table A.1: Evaluation results for the special case (Type II) in different scenarios.

Cases	Ref. (cm)	RMSE			STD (cm)			Spread of Data (cm)			Sample
		AltDS	SDS	SS	AltDS	SDS	SS	AltDS	SDS	SS	
Close LOS	25.63	17.87	17.85	23.40	3.41	3.41	2.00	30.56	30.56	9.85	2000
	50.08	14.72	14.72	5.30	6.85	6.85	5.19	41.23	41.23	54.54	2000
	75.44	11.78	11.77	6.95	2.34	2.34	5.05	13.19	13.19	20.06	2000
	103.90	5.79	5.83	12.92	2.79	2.79	3.59	14.19	14.19	16.89	2000
	125.18	6.56	6.55	8.08	2.80	2.80	4.96	15.95	15.95	24.62	2000
	150.30	2.11	2.11	15.59	1.84	1.84	1.59	15.06	15.06	20.64	2000
	175.27	3.98	3.98	13.91	3.88	3.88	4.09	16.18	16.18	17.53	2000
	200.77	3.46	3.46	13.31	2.19	2.19	2.40	15.71	15.71	14.71	2000
LOS (Hall)	399.82	2.09	2.09	15.03	2.08	2.08	4.13	14.30	14.31	24.33	2450
	806.70	2.93	2.93	21.41	1.33	1.33	1.34	8.44	8.44	11.73	2450
	1206.20	1.88	1.89	20.75	1.32	1.32	1.53	9.03	9.03	10.55	2450
	1600.20	2.47	2.47	14.30	2.15	2.15	9.29	13.59	13.60	40.34	2450
	2002.00	2.00	2.00	14.56	1.97	1.97	6.16	16.17	16.18	34.94	2450
Multipath (Corridor)	402.12	5.41	5.41	20.91	1.87	1.87	2.96	11.43	11.43	15.95	2350
	802.05	5.19	5.20	19.46	2.37	2.37	2.60	11.84	11.84	14.07	2350
	1200.44	5.54	5.55	18.97	2.05	2.05	2.93	12.78	12.78	15.71	2350
	1601.58	3.00	3.00	13.67	2.88	2.88	6.80	16.53	16.53	35.41	2350
	2003.24	3.32	3.31	14.93	1.86	1.86	1.79	11.96	11.96	12.66	2350

Table A.2: Evaluation results for the typical case (Type III) in different scenarios.

Cases	Ref. (cm)	RMSE (cm)			STD (cm)			Spread of Data (cm)			Sample Size
		AltDS	SDS	SS	AltDS	SDS	SS	AltDS	SDS	SS	
Close LOS	25.63	18.06	11.99	23.95	3.32	11.96	1.26	31.26	30.86	33.79	2000
	50.08	12.36	35.11	3.59	4.79	13.96	3.39	38.60	39.65	18.06	2000
	75.44	12.31	16.15	6.96	2.49	3.00	4.80	14.13	17.88	30.31	2000
	103.90	6.67	12.31	5.79	2.41	2.49	4.05	16.57	15.42	25.80	2000
	125.18	5.07	12.21	9.40	2.17	1.89	2.89	13.13	13.25	16.65	2000
	150.30	3.48	8.23	8.76	2.74	2.51	4.74	16.38	13.13	29.25	2000
	175.27	3.43	8.44	12.44	3.39	3.20	3.67	14.32	14.54	15.89	2000
	200.77	4.78	9.88	6.90	2.34	2.41	4.01	14.44	14.42	22.75	2000
LOS (Hall)	399.82	1.50	8.01	14.31	1.46	1.45	1.74	10.79	9.97	12.37	2450
	806.70	2.04	5.79	12.78	1.92	1.87	4.87	12.53	13.84	26.27	2450
	1206.20	2.09	7.13	16.62	1.55	1.53	1.73	13.25	13.37	13.37	2450
	1600.20	3.69	4.96	17.99	1.55	1.57	1.84	11.28	10.44	16.18	2450
	2002.00	2.93	5.13	10.45	2.74	2.89	9.28	26.34	22.40	48.48	2450
Multipath (Corridor)	402.12	5.53	2.12	17.32	1.58	1.80	2.68	13.55	12.13	17.12	2350
	802.05	5.03	3.12	17.55	1.93	1.98	2.12	10.88	10.20	13.84	2350
	1200.44	4.97	2.52	13.86	1.87	2.51	4.21	13.50	16.65	23.84	2350
	1601.58	3.20	7.04	12.18	3.02	3.55	5.93	18.38	23.80	35.88	2350
	2003.24	6.43	10.76	8.84	3.00	4.83	8.84	17.69	26.97	40.10	2350

compared to the special case (Type II) as can be verified in Tables A.1 (Type II) and A.2 (Type III). Moreover, the spread of the recorded data were larger in the MP and close LOS scenarios as a whole compared to the LOS condition (Tables A.1 and A.2). It should be noted that all presented data in the two tables are rounded off to two decimal points (the nearest hundredth).

C Detailed Classification Results: Confusion Matrices and ROC curves

As defined and discussed in chapter 5.5, the two test scenarios for the classification results presented in the dissertation are as follows:

- **Test Scenario 1:** the test datasets in this scenario were based on the split data for testing purpose and the data come from the same environments (i.e, room, hall, corridors, etc) as the training data. This test datasets were split as unseen data during training.
- **Test Scenario 2:** the test datasets in this scenario were based on the completely different environments (i.e, room, hall, corridors, etc) of the training process. The main goal here is to evaluate the generalization of the trained ML model in unseen or unobserved environments.

Appendix

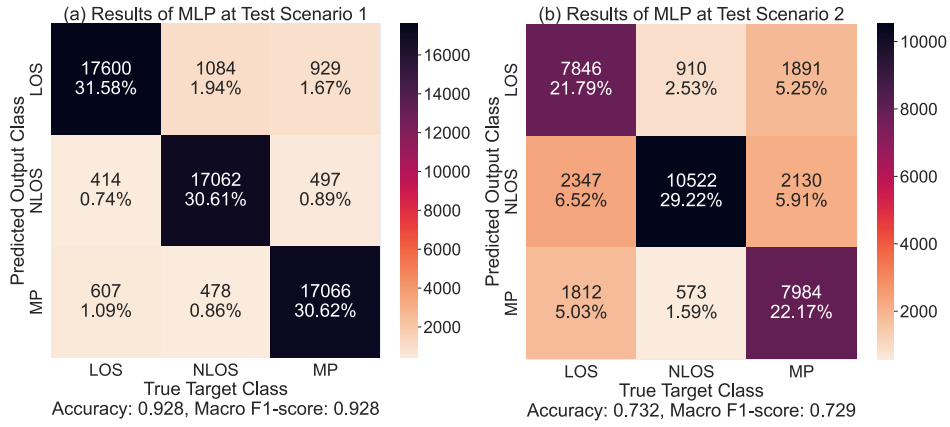


Figure C.1: Comparison of confusion matrices for MLP classifier at two test scenarios.

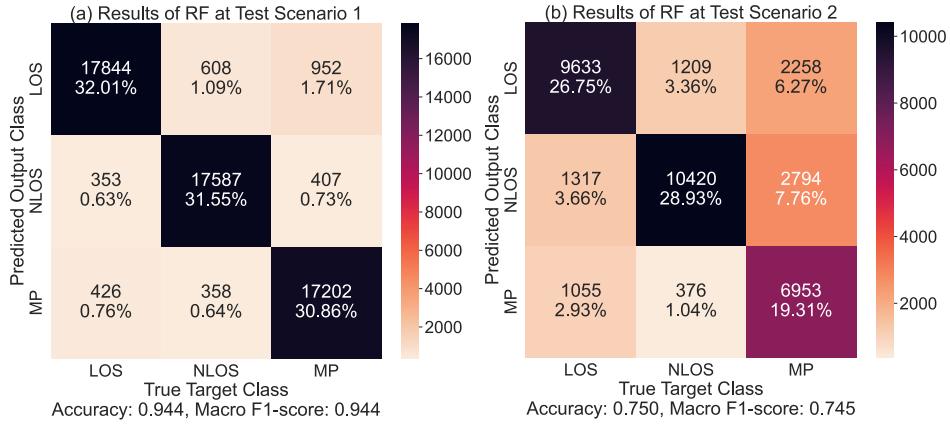


Figure C.2: Comparison of confusion matrices for RF classifier at two test scenarios.

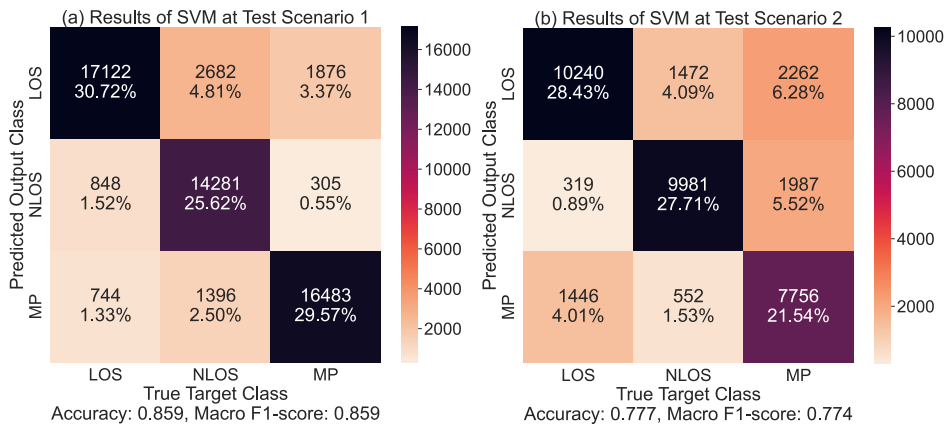


Figure C.3: Comparison of confusion matrices for SVM classifier at two test scenarios.

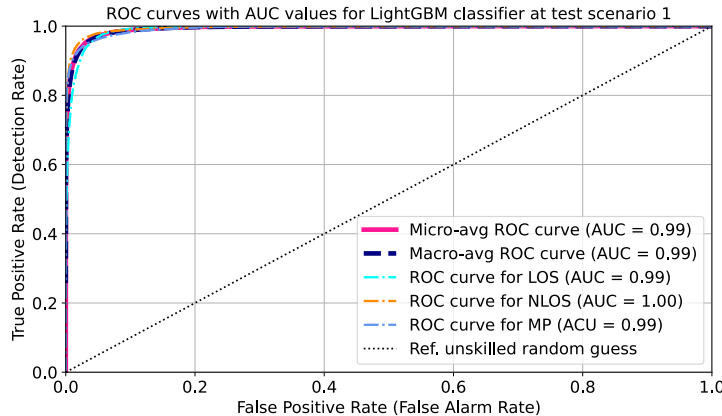


Figure C.4: Multi-class results for LightGBM at test scenario 1 based on individual ROC curves.

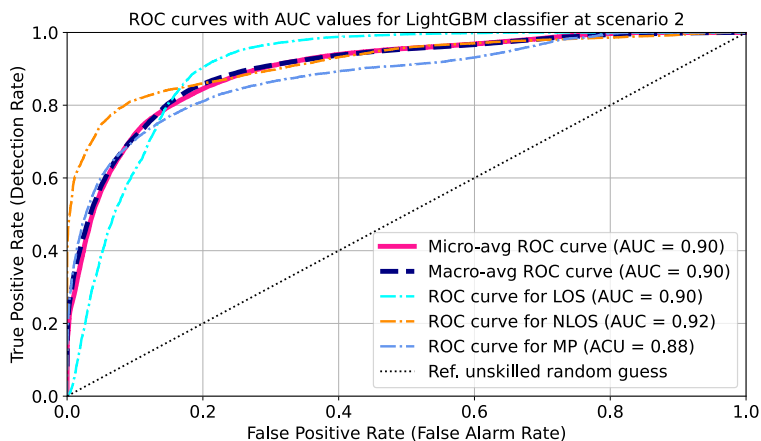


Figure C.5: Multi-class results for LightGBM at test scenario 2 based on individual ROC curves.

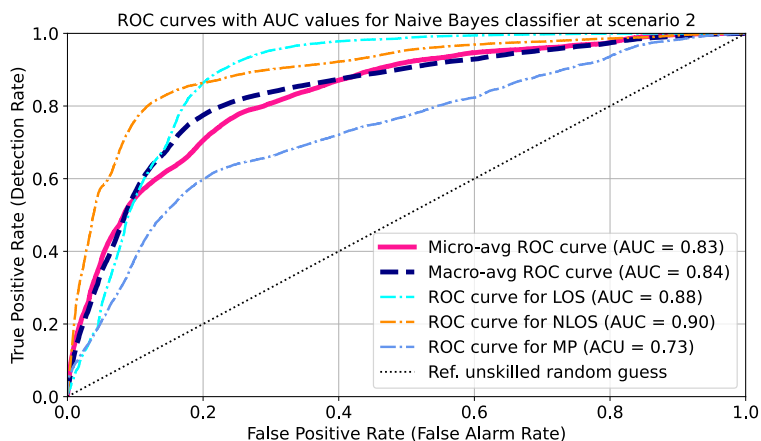


Figure C.6: Multi-class results for NB at test scenario 2 on individual ROC curves.

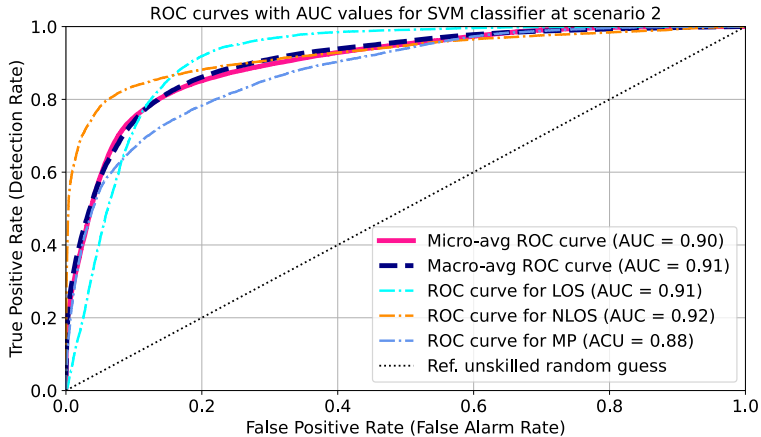


Figure C.7: Multi-class results for SVM at test scenario 2 on individual ROC curves.

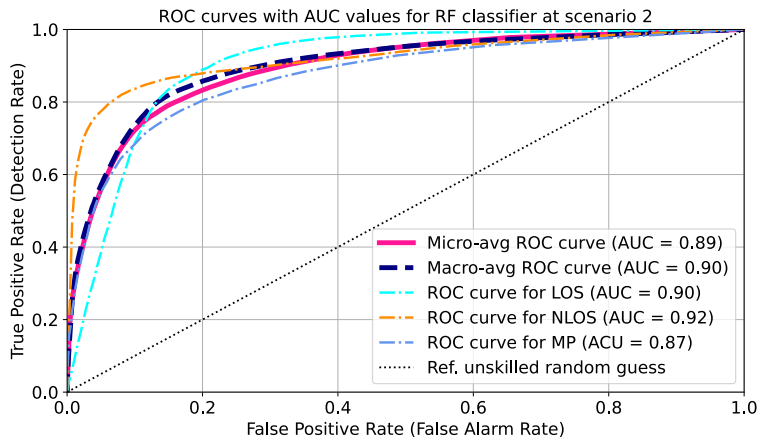


Figure C.8: Multi-class results for RF at test scenario 2 on individual ROC curves.

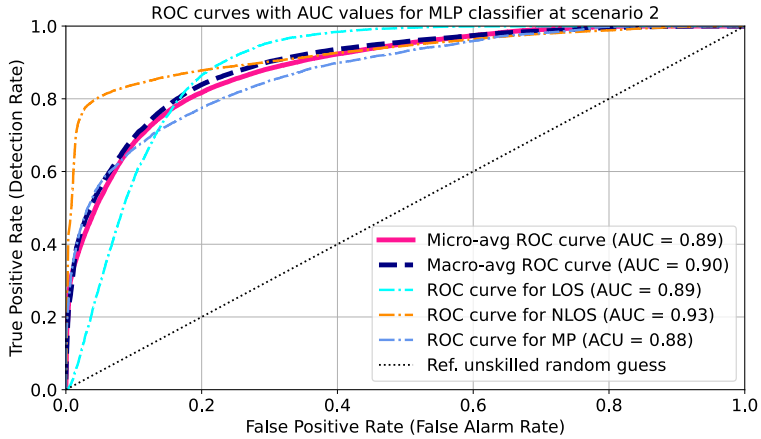


Figure C.9: Multi-class results for MLP at test scenario 2 on individual ROC curves.

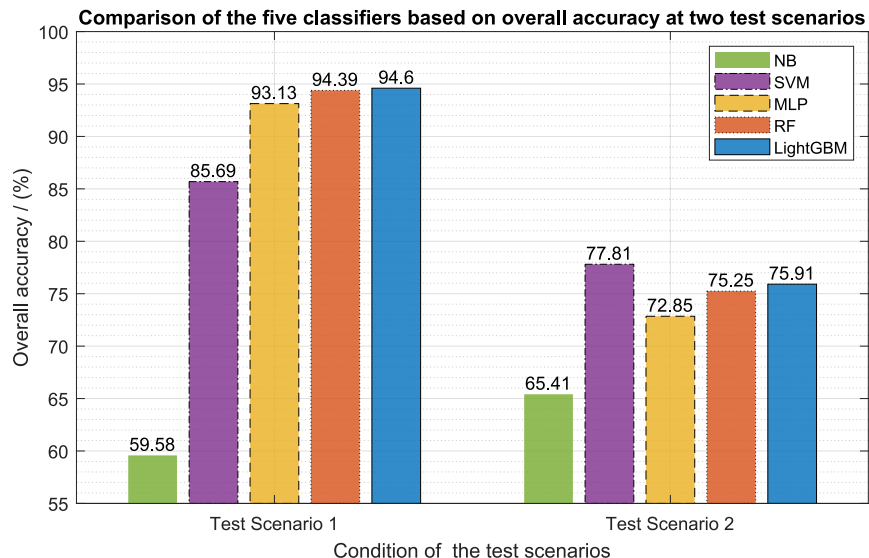


Figure C.10: Performance comparison of five ML-based classifiers based on the overall accuracy at two specific test scenarios.

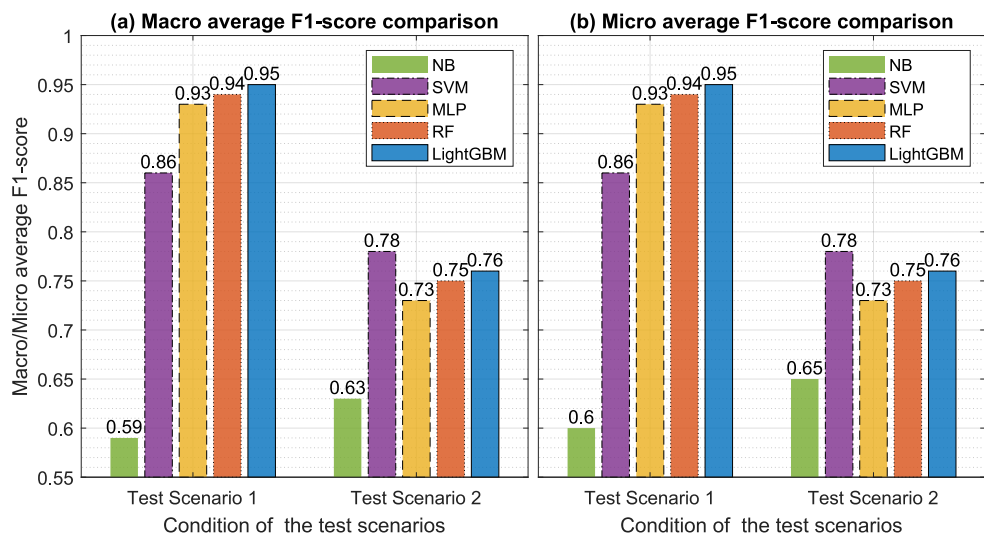


Figure C.11: Performance comparison of five ML-based classifiers based on the macro average F1-score and the micro average F1-score at two specific test scenarios.